Combined solar and pellet heating systems

Improvement of energy efficiency by advanced heat storage techniques, hydraulics, and control

Doctoral Thesis in Engineering Sciences
Michel Y. Haller

Institute of Thermal Engineering
Graz University of Technology

TU Graz

Supervisor:

Ao.Univ.-Prof. Dipl.-Ing. Dr.techn.
Wolfgang Streicher
Institute of Thermal Engineering
Graz University of Technology

Opponent:

Associate Prof.
Simon Furbo
Department of Civil Engineering
Technical University of Denmark

May, 2010

"We need to increase the use of renewable energy sources and improve energy efficiency. And we must not flinch from addressing the issue of over consumption - the fact that people in the developed countries use far more energy per capita than those in the developing world"

Kofi Annan, Secretary General, United Nations, cited from (World Energy Council 2007)

Acknowledgements

STATUTORY DECLARATION

I declare that I have authored this thesis independently, that I have not used other than the declared sources / resources, and that I have explicitly marked all material which has been quoted either literally or by content from the used sources.

11. 5. 2010

M. Hall

....

Date   **(signature)**

Contents

APPENDIX A: SIMULATION OF A TES INTEGRATED PELLET BURNER

APPENDIX B: DOCUMENTATION OF TRNSYS TYPES

PART II: ARTICLES INCLUDED IN THIS WORK

PAPER I:

METHODS TO DETERMINE STRATIFICATION EFFICIENCY OF THERMAL ENERGY STORAGE PROCESSES – REVIEW AND THEORETICAL COMPARISON (2009). SOLAR ENERGY 83(10), 1847-1860.

PAPER II:

A METHOD TO DETERMINE STRATIFICATION EFFICIENCY OF THERMAL ENERGY STORAGE PROCESSES INDEPENDENTLY FROM STORAGE HEAT LOSSES (2010). SOLAR ENERGY 84(6), 997-1007.

PAPER III:

A UNIFIED MODEL FOR THE SIMULATION OF OIL, GAS, AND BIOMASS SPACE HEATING BOILERS FOR ENERGY ESTIMATING PURPOSES - PART I: MODEL DEVELOPMENT. ACCEPTED FOR PUBLICATION IN THE IBPSA JOURNAL OF BUILDING PERFORMANCE SIMULATION IN FEBRUARY 2010.

PAPER IV:

A UNIFIED MODEL FOR THE SIMULATION OF OIL, GAS, AND BIOMASS SPACE HEATING BOILERS FOR ENERGY ESTIMATING PURPOSES - PART II: PARAMETERIZATION AND COMPARISON WITH MEASUREMENTS. ACCEPTED FOR PUBLICATION IN THE IBPSA JOURNAL OF BUILDING PERFORMANCE SIMULATION IN JANUARY 2010.

PART III: LIST OF PAPERS NOT INCLUDED IN THIS WORK

ABSTRACT

This work deals with the improvement of energy efficiency of combined solar and pellet heating systems for space heating and domestic hot water preparation by advanced heat storage techniques, hydraulics, and control.

For these studies a boiler model has been developed based on measurements performed on a pellet boiler, a wood chip boiler and a solar storage integrated pellet burner. Additionally, the work has been based on the analysis of data measured by cooperation partners on two pellet boilers, two oil boilers and two gas-boilers. A collector model has been adapted for the simulation of small time steps. Based on measurements performed on the storage tank with the integrated pellet burner, a storage model has been parameterized and used for subsequent system simulations. Methods for the determination of the stratification efficiency of themal energy storage processes have been reviewed and tested, and a new method has been developed. This new method has been evaluated both theoretically and practically with own measurements performed on a thermal energy storage with direct charging and discharging and with measurements performed by a cooperation partner on a tank-in-tank storage unit. Data from field measurements performed on five solar and biomass micro heating nets has been evaluated and analyzed.

Simulations have been performed for three principally different solutions for solar and pellet heating systems for a single family house. The first system was based on the solar storage tank with the integrated pellet burner that has also been tested in the laboratory, the second system was based on an external pellet boiler connected to a solar storage tank with an immersed heat exchanger spiral for domestic hot water preparation, and the third system was an external boiler connected to a solar storage of the tank-in-tank type. Starting with simulations parameterized based on the results of the laboratory measurements on existing components, a large potential for improvements has been detected for all these systems that may lead to an additional 10% - 20% of pellet fuel savings. The main potentials for improvements were:

- Better insulation of the storage tank and the boiler.

- Higher heat transfer rate to the domestic hot water in order to be able to keep the storage tank temperatures low without reducing comfort.

- Improvement of the combustion process in order to be able to keep a low excess air ratio (lambda) also at reduced combustion power.

It has further been found that the currently implemented control strategies for charging a thermal energy storage with a pellet boiler were not able to effectively use the possibility of combustion power modulation to match the heat demand. Different control strategies have been tested with simulation studies and a control strategy has been found that reduces the number of burner starts by a factor of three and at the same time increases the energy efficiency significantly.

Keywords: Solar thermal, pellet boiler, thermal energy storage

KURZFASSUNG

Diese Arbeit befasst sich mit der Steigerung der Energieeffizienz durch fortschrittliche Wärmespeicherung, Hydraulik und Regelung von Heizsystemen, welche Raumwärme und Brauch-Warmwasser auf der Basis von Solarthermie und Holzpellets bereitstellen.

Ein Modell wurde entwickelt für die Simulation von Heizkesseln, basierend auf Messungen welche an einem Pelletkessel, einem Hackgutkessel, und einem Solarspeicher-integrierten Pellets-Brenner durchgeführt wurden. Messdaten von weiteren Pellets-, Öl- und Gaskesseln wurden ausgwertet und mit dem Modell verglichen. Messungen wurden durchgeführt an einem Speicher mit integriertem Pelletbrenner und ein Speichermodell wurde mit Hilfe dieser Messdaten parametriert für die anschliessende Verwendung in Simulationsrechnungen. Methoden für das Bestimmen der Schichtungseffizienz von Wärmespeichern wurden evaluiert, getestet und miteinander verglichen, und eine neue Methode wurde entwickelt für die Berechnung der Schichtungseffizienz von Wärmespeicherprozessen. Diese neue Methode wurde theoretisch validiert und sowohl auf eigene Messungen an einem Wärmespeicher mit direkter Be- und Entladung als auch auf Messdaten von einem Tank-in-Tank Speicher an angewendet. Feldmessungen an fünf Pellet-Solar Systemen welche jeweils ein Mikro-Wärmenetz versorgen wurden ausgewertet und analysiert.

Drei unterschiedliche Pellet-Solar-Heizsysteme für Einfamilienhäuser wurden simuliert und miteinander verglichen. Das erste System ist ein Solarspeicher mit integriertem Pelletbrenner welcher im Labor ausgemessen wurde. Das zweite System ist ein frei stehender Pelletkessel welcher an einen Solarspeicher angebunden ist. Sowohl dieser als auch der erste Solarspeicher verfügen über einen internen Wärmetauscher für die Aufbereitung von Brauch-Warmwasser. Das dritte System besteht aus einem externen Pelletkessel, welcher an einen Solarspeicher mit einem innen liegenden Warmwasserspeicher (Tank in Tank) angebunden ist. Die Simulationen welche mit Hilfe der Messungen aus dem Labor parametrisiert wurden zeigen grosse Verbesserungspotenziale für alle System-Varianten auf, welche zu zusätzlichen Brennstoff-Einsparungen von 10% - 20% führen. Die Haupt-Einflussgrössen sind dabei:

– Eine bessere Isolation von Kessel und Speicher.

– Eine grössere Wärmeübertragungsrate vom Speicher ans Brauch-Warmwasser, welche es erlaubt die Solltemperaturen im oberen Speicherbereich tiefer zu setzen.

– Eine Verbesserung des Verbrennungsprozesses welche es erlaubt, auch bei reduzierter Feuerungsleistung den Luftüberschuss auf konstant tiefem Niveau zu halten.

Verschiedene Regelstrategien für das Beladen eines Solarspeichers durch einen Pelletkessel wurden simuliert und eine Lösung gefunden, welche sowohl die Anzahl Start-Vorgänge des Kessels um den Faktor drei reduziert als auch die Energieeffizienz des Systems signifikant erhöht.

Stichworte: Solarthermie, Pelletkessel, Wärmespeicher

Part I

Nomenclature, Abbreviations and Symbols

Nomenclature, abbreviations and symbols that are used repetitively throughout this work are listed here, whereas nomenclature and symbols that are only used within a short section of this work are explained only in the text of the respective section.

Energy loss / energy consumption

According to the first law of thermodynamics energy cannot be lost, destroyed or consumed, but only transferred into another state. The terms "energy loss" and "energy consumption" are used in common speech to refer to the loss of "useful energy". Likewise, in this work, the terms "energy loss" or "energy consumption" will be used to address energy that is transferred into a state that can not be used to serve the specified demand of the given application.

Fractional thermal energy savings

The main goal of using solar energy is usually to save as much as possible other energy resources. To compare the benefit of different solar thermal systems that cover the same heat demand, fractional thermal energy savings have been defined within the Task 26 of the International Energy Agency's Solar Heating and Cooling Program (IEA-SHC) (Jordan et al. 2003). A fractional thermal energy saving of 30% means that 30% less conventional fuel (usually oil, natural gas or biomass) is used by a system that includes the use of solar energy, than would be used in a comparative standard system without the use of solar energy (compare Section 5.3.1).

Minimum turndown ratio

The minimum turndown ratio is the ratio of minimum continuous combustion power to maximum continuous combustion power that a boiler is able to run automatically, i.e. the boiler is able to change its combustion power from the maximum to the minimum value automatically.

Power modulation

Power modulation is the ability of a boiler to change the combustion rate in order to match the heat output to the heat demand without having to stop and restart the burning process.

Solar combisystem

A solar combisystem is a system that provides both, domestic hot water (DHW) and space heat, using solar thermal collectors. An auxiliary heater is usually necessary to provide enough heat during times where the solar thermal system does not cover the whole heat demand.

Solar combistore

A solar combistore is a thermal energy storage (TES) device that provides both, domestic hot water (DHW) and space heat, from one storage unit. It is thus always part of a solar combisystem.

Abbreviations

CO	Carbon monoxide
DHW	Domestic Hot Water
IEA-SHC	International Energy Agency Solar Heating and Cooling Programme
TES	Thermal Energy Storage
FGWHX	Flue Gas to Water Heat EXchanger
FGAHX	Flue Gas to combustion Air Heat EXchanger
HX	Heat EXchanger
VOC	Volatile Organic Compounds

Greek Symbols

α	heat transfer coefficient, W/m^{2}K
δ	logical switch (0 or 1), -
γ_X	mass fraction of the elements (X = C,H,O,S,N) of ash (X = ash) and of water (X = H$_2$O) in the fuel per kg dry fuel, kg/kg
Γ	height, m
Δ	difference, variable unit
η	efficiency, -
λ	air ratio of the combustion process (1 = stoichiometric ratio), -
μ	dynamic viscosity, kg/ms
ξ	exergy, J
ρ	density, kg/m^2
τ	time, s

Latin Symbols

A	area, m^2
C	thermal capacitance, J/kg
cp	isobaric specific heat, J/kgK
d	diameter, m
E	energy, J
fr	fraction, -
g	acceleration of the earth's gravitational field, 9.81 m/s^2
GHV	gross heating value of the fuel (reference temperature 25°C, all H$_2$O in flue gas in liquid state), J/kg
h	specific enthalpy, J/kg
H	enthalpy, J

6

I	irradiance, W/m^2
k	conductivity, thermal diffusivity, W/mK
K	incident angle modifier, -
l	length, m
m	mass, kg
$\dot{m}$	mass flow rate, kg/h
N	Integer number, -
NHV	net heating value of the fuel (reference temperature of 25 °C, all H_2O in flue gas as vapour), J/kg
Nu	Nusselt number, -
O_{min}	stoichiometric oxygen demand for the combustion / oxidation of the fuel, kg O_2/kg fuel
P	power, W
Pr	Prandtl number, -
p	pressure, Pa
Q	thermal energy or chemical energy, J
$\dot{Q}$	heat transfer power, W
ppm	volumetric concentration in parts per million, ppm
pts	number of measured points, -
RH	relative humidity, -
Re	Reynolds number, -
S	entropy, J/K
t	temperature, °C
T	thermodynamic temperature, K
UA	overall heat transfer coefficient area product (UA-value), W/K
V	volume, m^3
$\dot{V}$	volume flow rate, m^3/s
W	work, electric energy, J
z	relative height / dimensionless height, -

Sub- or Superscripts

air	air; combustion air
amb	ambient
aux	auxiliary (backup) heating
B	boiler
b	beam
$burn$	burner
C	combustion (efficiency)
d	diffuse
cc	combustion chamber
ch	chimney or flue gas duct
$chem$	chemical (losses)

CO	carbon monoxide
coll	collector
cond	condensate
Ctherm	effective thermal capacitance
cw	cold water from the mains
da	draught air
dry	dry
d.b.	based on the dry mass (dry base)
eff	effective
el	electricity
evap	evaporation / condensation
exp	experimental
fg	flue gas
flow	flow (of water)
fuel	fuel
H	hydrogen
H_2O	water
hl	heat losses
hx	heat exchanger
in	at the inlet of the fluid
inf	after infinite time
int	internal
irr	irreversible
lam	laminar
lat	latent heat
loss	energy losses
max	maximum
min	minimum
mix	fully mixed reference
ms	measured value or value derived from measurements
nom	under nominal conditions
OFF	burner not in operation, standby
ON	burner operation
out	at the outlet of the fluid
pi	pipe
ref	reference condition
rt	return
sens	sensible heat
sh	space heating
sim	calculated value based on model assumptions or simulation
sol	solar collector loop
spec	specific
st	stratification

start	burner start
stag	stagnation
str	stratified reference
store	thermal energy storage tank (TES)
su	supply
tot	total
turb	turbulent
wat	water
w.b.	based on the wet mass (wet base)
wet	wet
ww	warm water (domestic hot water)
0	reference state
3*el*	electricity counted with a factor of three

Energy unit conversions

Gtoe	Giga-ton of oil equivalent, 1 Gtoe $\triangleq$ 41.9 EJ
kWh	kilo-Watt-hour, 1 kWh = 3600 kJ
J	Joule, 1 J = 1 Ws

Metric prefixes

E	Exa, 10^{18}
P	Peta, 10^{15}
T	Tera, 10^{12}
G	Giga, 10^{9}
M	Mega, 10^{6}
k	kilo, 10^{3}

1 Introduction

1.1 Background

1.1.1 World energy use and CO_2 emissions today

Total primary energy supply serving the worldwide needs of humanity for energy increased from 6.1 Gt (256 EJ) of oil equivalent (Gtoe) in 1973 to over 11.4 Gtoe (478 EJ) in 2005 (IEA 2007). The share of carbon-rich fossil fuels decreased only slightly from 87% of the energy supply in 1973 to 81% in 2005. This decrease has been accompanied by an increase of - equally non renewable – nuclear energy share from 1% to 6% within the same time-frame. The International Energy Agency (IEA) forecasts that primary energy use will increase to 15.4 – 17.1 Gtoe (645 – 716 EJ) until 2030, with 0 – 2% decrease in the share of carbon-rich fossil fuels.

As humanity's energy needs of today are largely met by extraction of fossil fuels from limited reservoirs within the crust of the earth, there can be no doubt that this way of covering the energy demand is not sustainable on a long term and cannot go on forever. Without changes in the energy consumption of humanity, the question is not whether peak oil – as well as peak natural gas and peak coal – are reality or not, the only question is when they will occur. Whereas most authors agree that peak oil occurs within the first half of the 21st century, the precise time is highly disputed and ranges from "has already occurred" to "not before 2025" or "not in sight" (Hirsch et al. 2005). According to the World Energy Council (World Energy Council 2007), the depletion mid-point for the estimated ultimate recovery of crude oil will be reached within the next 10 to 20 years. Peak natural gas is most likely to occur later within this century, whereas peak coal is expected to be some 150 years ahead still. Therefore, the only way of meeting a growing energy demand of humanity on a medium time scale of 10 – 150 years, without substitution by equally non-renewable nuclear fuels, is to change the energy supply for an increased share of renewable energy sources and to become more efficient in the use of energy.

The finiteness of non-renewable energetic resources are but one of the reasons why their use is not sustainable. The use of carbon rich fuels is also the most important contributor to the increase of the effect of green house gases (GHG) in the atmosphere of the earth. Today's atmospheric concentrations of CO_2 and CH_4 "...exceed by far the natural range over the last 650'000 years" (IPCC 2007). Emissions of carbon dioxide due to energy use increased from 15.6 Gt CO_2 in 1973 to 27.1 Gt CO_2 in 2005 (IEA 2007), and the concentration of CO_2 in the atmosphere rose from about 280 ppm in pre-industrial times to 379 ppm in 2005.

According to the International Panel on Climate Change, "most of the observed increase in globally-averaged temperatures since the mid-20th century is very

likely[1] due to the observed increase in anthropogenic green house gas concentrations." (IPCC 2007). The evidence for global warming as a result of human activities is striking, and, in contrast to previous decades, there are now only marginal doubts left about the causal relationship in general. Observed and anticipated consequences of the current global warming include rising sea level, decrease in snow and ice extent, changes in precipitation, increased frequencies of heavy precipitation, increase in cyclone activities, and many more that are mentioned in the Fourth Assessment Report of the IPCC. Humankind is currently changing the global climate quite significantly, without proper knowledge about the ultimate consequences that this will have for the one and only global environment we live in.

Providing energy with efficient solar and biomass heating systems instead of heating systems based on carbon rich fuels promises to be an effective way for reducing CO_2 emissions, given that the biomass originates from a sustainably exploited source.

1.1.2 Energy use in Austria and Switzerland

Energy use in Austria as well as in Switzerland today is considered far above the assumed sustainable level of 2000 Watt per person (Jochem et al. 2002) as well as highly dependent on non-renewables, above all on fossil fuels (Figure 1.1). In Austria as well as in Switzerland, energy use for room heating and domestic hot water (DHW) preparation accounts for about one third of total primary energy consumption (EVA 2002; BFE 2005).
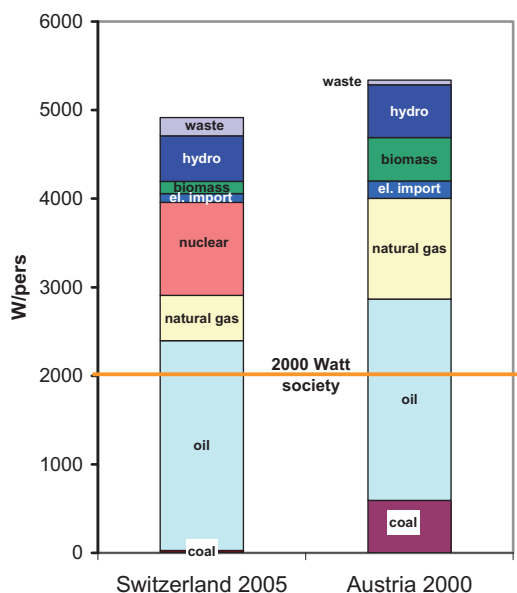
Figure 1.1: Primary energy use per person in Switzerland and in Austria, source of data: (EVA 2002; BFE 2005).

---

[1] The term "very likely" is used in the ICCP report for an estimated likelihood of > 90%.

It is estimated that currently (2006-2008) 4.1 PJ or about 0.8% of energy for room heating and DHW is produced from solar thermal collectors in Austria (Faninger 2007; Statistik Austria 2009). The growth rate of the total installed collector area was about 9.5% in 2006. In 2007/2008, about 25% of the household energy was covered by log wood, wood chips or wood pellets (Statistik Austria 2009).

1.2   Solar combisystems

Solar thermal systems for DHW preparation have been used extensively around the globe. In climates with space heating requirements, solar thermal systems for DHW and space heating – so called solar combisystems – are also used widely. The share of combisystems was 35% and 29% of total installed collector area for Austria and Switzerland, respectively, in 2006 (Faninger 2007; Jauch 2007). For a reasonable sized and well designed solar thermal system in Central Europe, the heat price for solar energy is currently estimated to be 0.10 - 0.40 €/kWh (Drück et al. 2004; Kaltschmitt & Streicher 2009), which is in the best cases not much above current prices for energy from oil or natural gas boilers, and may be even well below the price for electricity.

In central European climates, a heating system based on solar energy alone is usually not able to cover the whole demand for DHW and/or space heating of a residential building[2]. Therefore, only a fraction of the heating demand is normally covered by solar energy. Fractional thermal energy savings have therefore been introduced to measure the performance of solar combisystems in the IEA-SHC Task 26 (Streicher et al. 2002; Jordan et al. 2003; see also Nomenclature). These performance indicators will also be used in this work.

The performance of solar combisystems has been evaluated in the past both in the laboratory and in the field. With economical and practical limits for the collector area and the heat storage size of 15 m^2 and 1 m^3, respectively, fractional thermal energy savings of existing systems on the market have been measured and simulated to be in the range of 20 – 40% (Haller & Vogelsanger 2005a). These figures have been obtained for the case of a heating energy demand of 18.5 MWh/a (67 GJ/a), which corresponds to a DHW demand of 200 l/d (2.9 MWh/a or 10.4 GJ/a) and a house with a heated floor area of 200 m^2 and a specific space heating demand of 63 kWh/m^{2}a (227 MJ/m^{2}a). For a given solar combisystem, the solar fraction increases as the insulation of the house gets better. At the same time the specific collector yield and the absolute quantity of energy saved decreases because of the decreased total demand, and therefore the system may become less economical despite the increasing fractional thermal energy savings.

---
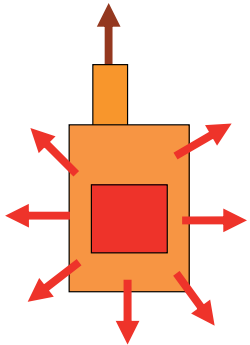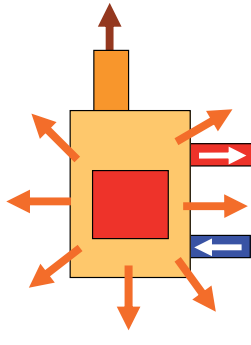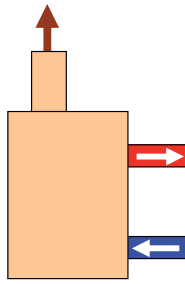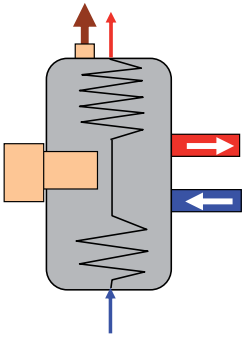
[2] Although it is possible to provide enough thermal energy only from solar for single family and for multifamily houses in a Central European climate, the collector area and storage size for such systems are quite large. As the ratio of performance over price decreases dramatically above a certain system size, these systems are not very common.

1.3 Biomass heating systems

Biomass heating systems have been the most important source for room heating for centuries, before other fuels such as coal, oil and natural gas became available. As concerns have arisen about the use of fossil fuels (see Section 1.1.1), biomass heating systems become popular again. For small scale systems, e.g. in single family houses, automatic wood pellet boilers are being used increasingly, since they offer the same comfort that people have got used to through automatic oil, natural gas or electric heating. For larger systems, wood chips are usually a more economic alternative.

Table 1.1: Different types of biomass heating units and their possibilities for DHW preparation, room heating and combination with solar energy.

pellet or wood stove	pellet or wood stove with water jacket	boiler	burner integrated into storage tank
heat delivery			
only through radiation and convection to the surroundings	both, by radiation and convection to the surrounding as well as by a hot water circuit	DHW and space heating only by hot water circuit	heating directly a solar combistore for hot water preparation and space heating
room heating			
for one warmer room and adjacent colder rooms only	for one warmer room and a number of other rooms, depending on the split of energy	to any number of rooms, near and far, limited by the nominal power of the boiler	to any number of rooms, near and far, limited by the nominal power of the boiler
DHW preparation			
not possible	possible, although during summer inconvenient	possible, although lower efficiency for hot water preparation in summer	possible, solar hot water in summer
combination with solar thermal			
Two separate systems with no direct interactions	Solar thermal for hot water preparation in summer is an ideal complementary heat source	Combination with solar for both, hot water preparation and space heating	The main purpose is the combination with solar for hot water preparation and space heating
⇨ ⇦ supply and return lines of the heat load; ➡ radiative and convective heat; ➡ exhaust / flue gas; → → cold water inlet and DHW outlet.			

The units used to convert biomass into heat can be divided into stoves, stoves with water jackets, and central heating boilers (see Table 1.1). Stoves are designed to deliver a medium to large amount of energy directly to their surroundings by heat radiation. Boilers are designed to deliver the heat to a water circuit that serves as a heat transportation system to the building. Consequently, stoves are installed in the rooms that shall be heated, and boilers are usually installed in a separate utility room. Since heat losses to this separate room are of little or no benefit for the user, they should usually not be higher than necessary to prevent the pipes in the room from freezing in winter.

Boilers can be designed for almost any size and deliver heat to as many rooms as desired via hot water pipes. Thus, they can serve single- and multi-family houses as well as district or industrial heating. Stoves are limited for heating the room of installation and some adjacent colder rooms at the most (Table 1.1).

1.4   Potential of combined solar and biomass heating systems

The potential for combined solar and biomass heating systems for DHW preparation and room heating in Austria is large. The Austrian Ministry of Agriculture, Forestry, Environment and Water Management mentions the goal to increase biomass heating from 81 PJ in 2000 to 130 PJ in 2020 (BMLFUW 2006). Assuming the same heat demand for DHW and room heating in 2020 as for today, about 29% could be covered by biomass heating alone[3]. Following the trend of recent years, the largest increase is expected to be for pellet heating systems, whereas the use of log wood heating systems is not expected to increase at all. If all biomass heating systems would be combined with solar thermal systems with fractional thermal energy savings of about 30%, achievable with less than 15 m^2 collector area and less than 1 m^3 of energy storage volume for a single family house (Konersmann et al. 2007; Persson et al. 2006), the share of combined solar and pellet heating systems could be more than 40% of the total energy needed for DHW and space heating in residential buildings (Figure 1.2). This figure could be far higher in the case of a lower total need for space heating due to better insulation standards and energy saving measures.

---

[3] Since the 130 PJ for heating in 2020 include other heat needs too, heat for residential buildings is lower than this figure. On the other hand, the total amount needed for domestic hot water preparation and room heating in the year 2020 is very uncertain too. As the insulation standard increases, the need for heating per meter square will certainly decrease. Whether this will lead to a decreased total heat demand for residential buildings in Austria depends on the counteracting effect of population growth and increasing demand of living area and comfort per person.
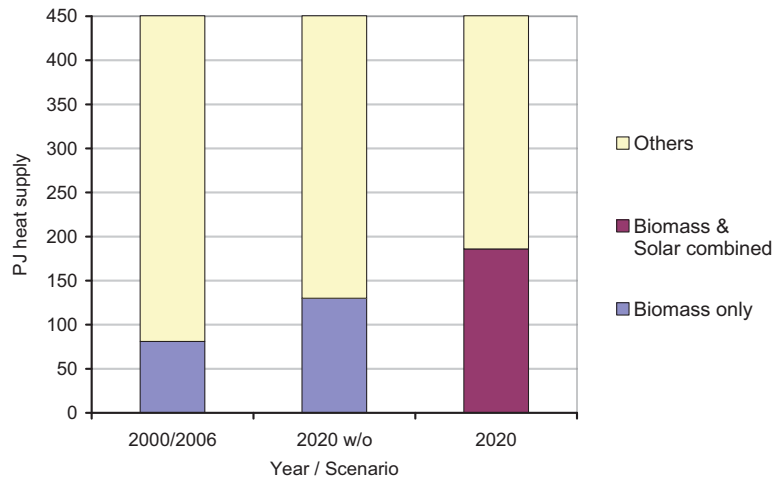
Figure 1.2: Assumed potential of combined solar and biomass heating for residential houses. "Others" includes also non-biomass energy sources combined with solar heat. The current share of combined solar and biomass heating is unknown. For "2020 w/o" it is assumed that all biomass heating is not combined with solar, for "2020" it is assumed that all biomass heating is combined with solar. Based on data from BMLFUW (2006) and Statistik Austria (2009).

1.5   Motivation and Objectives

Combined solar and pellets heating systems are already sold on the market. Although most of these systems work in a reliable way, their performance in terms of energy-efficiency is usually far from optimal (Bemmann et al. 2006). Especially control, hydraulics and energy storage usually show a large potential for improvements. Most laboratory and field measurements that have been reported have been conducted with installations for single family houses (Fiedler et al. 2006; Heinz 2007; Persson 2006). Dependency of results from different load profiles was not an issue in these investigations. Investigations showed that the energy efficiency of the studied combined solar and pellet heating systems could be increased from 62% to 75%. Furthermore, the number of start and stop cycles of a pellet heating system may be reduced by 75% if the pellet boiler is combined with a solar thermal system including a storage tank, and the overall system is controlled in a smart way (Persson et al. 2006). A detailed investigation on these control strategies has not been found. The reduction of start and stop cycles is of particular importance because the emissions of carbon monoxide and hydrocarbons are usually orders of magnitudes higher during these phases than during steady state combustion (Heinz 2007; Klippel & Nussbaumer 2007a) and emissions of particulate matter are usually considerably higher during the start-phase, but not during the stop phase of a wood burning process (Klippel & Nussbaumer 2007a).

16

> **The principle objective of this work is to assess possible improvements of the energy efficiency of combined solar and pellet heating systems for single family houses by advanced heat storage techniques, hydraulics and control.**

As energy system simulation programs, e.g. TRNSYS (SEL et al. 2006), are usually used for the optimization of these systems, it is important that the components or models that are used in these programs to simulate important parts of the system such as the pellet boiler, the energy storage and the solar collector are accurate and capable of showing dependencies of the efficiency on the influencing system parameters. Within the solar thermal research community, many efforts have been made to develop good models for the simulation of collectors and thermal energy stores, but only little investigation or validation of models has been undertaken for fuel fired boilers. As a result, the models used today for the simulation of oil, natural gas and pellet boilers show a considerable lack of validation and might not be capable of reflecting the boilers real response to changing system parameters such as reduced energy demand of a building, changes in return temperature, modulation of combustion power or change in mass flow rates of the heated water. A solar combisystem usually depends more than 70% on the auxiliary heat it gets from a fuel fired boiler. Thus, an efficiency improvement of 5% of the boiler has more than double the effect on total energy savings than an efficiency improvement of 5% on the solar part. Therefore, the qualities of the boiler model are of an equal or even higher importance than the qualities of the model for the solar collector or the thermal energy storage.

Previous investigations have shown that a high fraction of the energy demand of single family houses built today is in the lower range (below one third) of the nominal power of currently manufactured biomass boilers (Könighofer et al. 2001). Therefore special attention has to be paid to the start and stop behaviour of the boiler.

1.6   Outline of the Thesis

Chapter 2 of this Thesis deals with the development and validation of a model to simulate the thermal efficiency as well as the start and stop behaviour of small scale fuel fired boilers. The model shall be suitable to simulate not only pellet boilers, but also oil and natural gas boilers that might include condensation of flue gas vapour. The decision to include also oil and natural gas fired boilers for the development of the boiler model was made first of all because the principle equations for the calculation of flue gas composition and heat transfer are the same, and second because for these boilers condensation of water vapour in the flue gas is already a standard (natural gas) or about to become a standard (oil), whereas for small scale pellet boilers condensation of water vapour might become important in the future.

Chapter 3 presents measurements performed on a thermal energy storage (TES) of a solar combisystem with immersed heat exchangers for solar charging and DHW discharging. The measurement results were used for the parameterization of a storage tank model that was used in Chapter 5 for the simulation of the combined solar and pellet heating systems. Chapter 3 also includes a literature review and a theoretical evaluation of methods for the determination of stratification efficiency of TES. Based on this analysis, a new method for the determination of stratification efficiency that reduces the biasing influence of heat losses is presented.

In Chapter 4, the collector model used for the system simulations is discussed. In particular, changes that have been introduced into the existing model to solve problems, which occurred when the model was used with small time steps of calculation and high thermal capacitance, are explained.

Chapter 5 finally contains results from measurements performed on combined solar and pellet heating micro-nets as well as simulation results of combined solar and pellet heating systems for single family houses.

2 The boiler

This chapter presents a summary of work that has been presented on international conferences (Haller et al. 2008; Haller et al. 2009a; Haller et al. 2009b) and has been accepted for publication in the IBPSA Journal of Building Performance Simulation (Haller et al. 2010b; Haller et al. 2010c). The full journal articles are included in Part II, Paper III and Paper IV.

For the simulation of combined solar and pellets heating systems, it is important to have good models for the main components of the energy production and storage system which includes the collector, the heat store and the pellet boiler. Since the efficiency of residential boilers varies depending on the load and operating conditions within a wide range from far below 50% (Furbo et al. 2004) to above 100% with respect to the net heating value, it is important to simulate the overall heating system with a boiler model that reflects accurately dependencies of the boiler efficiency on load, return temperatures and control of the operation and modulation. Without a sufficiently accurate boiler model, comparison of fuel consumption derived from simulations of solar combisystems with different control strategies will remain questionable.

2.1 State of the art of boiler models

Boiler models can be classified into three different types according to their modelling approach (Bourdouxhe et al. 1994):

– **White box models:** Fundamental (physical) models with a detailed description of all heat transfer processes. These models require detailed data about the geometry and materials of the boiler and a different model is needed for every type of boiler. CFD is quite commonly used for these models.

– **Black box models:** Empirical models where the physical description of heat transfer processes are replaced by curve-fits.

– **Grey box models:** Hybrid models that include (usually simplified) physical models for heat transfer processes as well as empirical or measured data for tuning.

Based on literature studies as well as on own measurements, the following are proposed as requirements that a universal space heating[4] boiler model should meet:

– Possibility to simulate modern oil, natural gas and biomass boilers.

– Distinction between losses to the flue gas and thermal losses through the boiler envelope to the ambient.

– Possibility to calculate condensation gains.

– Effect of return water temperature on flue gas losses and condensation gains.

---

[4] The term „space heating boiler" is used here for a device that burns fuel in order to produce hot water for space heat and domestic hot water preparation. It does not include steam boilers or stoves.

- Effect of power modulation on flue gas losses and condensation gains.

- Cooling out of the thermal capacitance of the boiler with and without water mass flow.

- Electricity consumption.

- On-Off Cycling of the burner.

Although a large number of boiler models for energy estimating purposes are described in literature (Table 2.1), a well documented unified model for biomass, oil and gas boilers that includes all significant influences on the steady state and ON/OFF cycling efficiency was not found.

Table 2.1: Features of boiler models based on a literature review.

	black (B) or grey (G) box	fuels			influence of			thermal capacitance			start/stop, standby, and electricity			
		oil	natural gas	wood	return temp.	power mod.	cond. gains	loss separation[a]	Thermal capacitance modes	combi-boilers[b]	pilot flame	separate draught losses	other start/stop losses[c]	electricity use
Spreadsheet methods														
BoilSim (Paulsen 1999)	B	?	√	?	√	√	√	√	0	√	√	√	O	O
EN 15316-4-1 (2008) [d]	G	√	√	√	√	√	√	√	0	?	?	√	O	√
Eco-Boiler (Kemna et al. 2007)	G	√	√	O	√	√	√	√	1	?	√	O	√	√
TRNSYS														
TRNSYS standard Type 6 (SEL et al. 2006)	B	N/A[f]	N/A[f]	N/A[f]	O	O	O	√	0	N/A	O	O	O	O
TESS Type 751 (TESS n.d.)	B	N/A[g]	N/A[g]	N/A[g]	√	√	N/A	√	0	N/A	O	O	O	O
HVAC 1 Primary Toolkit (Lebrun et al. 1993; Bourdouxhe et al. 1994)	G	√	√	O	√	√	O	√	0	N/A	O	O	O	O
IEA ECBCS Annex 10 (Dachelet 1987; Laret 1989)	G	N/A[h]	N/A[h]	N/A[h]	√	√	O	√	0	N/A	O	O	O	O
TRANSSOLAR Type 370 (Koschak et al. 1998)	G	O	√	√	√	O	√	√	1[i]	N/A	O	O	O	O
SERC Type 210 (Nordlander 2003; Persson et al. 2009)	G	O	O	√	√	√	O	√	2	(√)[k]	O	√	√[m]	√
Other simulation tools														
ESP-r (Hensen 1991)[e]	B	O	√	O	√	O	√	√	2	O	O	?	√	O
ESP-r (Beausoleil-Morrison & Haddad 2003)	B	O	√	O	O	O	O	√	1	√	O	O	O	O
EnergyPlus (University of Illinois & University of California 2007)	B	N/A[n]	N/A[n]	N/A[n]	O	√	O	O	0	N/A	O	O	O	√
EMPA NNG model (Remund 1999)	G	√	√	O	√	O	√	√	N	O	O	?	O	O
Claus & Stephan (1985)	G	√	√	O	√	√	O	√	1	O	O	√	O	O

√: included; O: not included; ?: unknown; N/A: not applicable; [a] separation of flue gas losses and thermal losses; [b] boiler used for domestic hot water and space heating fluid in one unit; [c] other than draught losses; [d] boiler cycling method, pp. 29-38; [e] two node & on/off control, pp. 5.31-5.34; [f] constant combustion efficiency; [g] performance map; [h] fuel defined by its heating value only; [i] multi-node version has also been reported; [k] possibility shown in combination with a storage tank model; [m] by means of additional CO emissions; [n] part load ratio efficiency calculation.

2.2   Energy Balance

Energy balances of boiler units are described e.g. in the European standard EN 15316-4-1:2008 for hot water space heating boilers, in the German Industry Standard DIN 1942:1994 for steam boilers, and in Baehr (2005). A sankey-diagram for the energy balance of a boiler unit is shown in Figure 2.1. It is common practice for wood fuels to specify values for the wet fuel per kg of wet fuel (wet base, w.b.) and values given for the dry fuel per kg of dry fuel (dry base, d.b.). The conversion from gross heating value (GHV) to net heating value (NHV) and from wet base (w.b.) to dry base (d.b.) can be done if the hydrogen content of the fuel (γ_H) and the moisture content of the fuel (γ_{H_2O}) in kg per kg dry fuel are known:

Eq. 2.1 $NHV^{dry,d.b.} = GHV^{d.b.} - \Delta h_{evap} \cdot 9.079 \cdot \gamma_H$

Eq. 2.2 $NHV^{wet,d.b.} = GHV^{d.b.} - \Delta h_{evap} \cdot \left(9.079 \cdot \gamma_H + \gamma_{H_2O} \right)$

Eq. 2.3 $NHV^{wet,w.b.} = \left[GHV^{d.b.} - \Delta h_{evap} \cdot \left(9.079 \cdot \gamma_H + \gamma_{H_2O} \right) \right] \cdot \dfrac{1}{1+\gamma_{H2O}}$

The boiler model as shown schematically in Figure 2.1 has been divided into the three processes combustion chamber (1), heat exchanger(s) (2), and heat storage in the thermal capacitance (3). The enthalpy of the fuel, represented by ΔH_{fuel}^{GHV}, is the main energy input into the combustion chamber. It can be divided into the energy input according to its net heating value (ΔH_{fuel}^{NHV}) and two latent parts corresponding to the enthalpy of condensation of water formed from hydrogen in the dry fuel (ΔH_{evap}^{H}) and from the moisture content in the case of e.g. a biomass fuel ($\Delta H_{evap}^{H_2O}$). Further energy inputs result from the sensible and latent parts of the enthalpy of the combustion air ($\Delta H_{air,sens}$ and $\Delta H_{air,lat}$), and the sensible heat of the fuel itself ($\Delta H_{fuel,sens}$). Also electric energy consumed by a boiler (E_{el}) may be converted into thermal energy and contribute to the energy balance of the combustion chamber, e.g. in the case of electric ignition of biomass fuels or in the case of fuel oil preheating by electricity during burner start ($Q_{el,start}$). Losses of the combustion chamber on the other hand may be due to unburned residues in the ashes (Q_{ash}) and heat losses from the combustion chamber to the ambient ($Q_{cc,amb}$). Hot flue gas produced in the combustion chamber is entering the flue gas to water heat exchanger (FGWHX) (2) with its enthalpy ($\Delta H_{fg,hot}$) and chemical energy contained in unburned components, ($Q_{fg,chem}$). In the heat exchanger process, heat (Q_{hx}) is transferred to water (Q_{wat}) and the thermal capacitance of the boiler (Q_{Ctherm}), whereas the chemical energy ($Q_{fg,chem}$) is lost to the ambient together with the sensible enthalpy ($\Delta H_{fg,sens}$) and the latent enthalpy ($\Delta H_{fg,lat}$) of the flue gas.

Sensible and latent flue gas losses ($Q_{fg,sens}$ and $Q_{fg,lat}$) are defined by the difference between the sensible and latent enthalpies associated with the mass streams entering the combustion chamber and leaving the boiler with the flue gas:

Eq. 2.4 $Q_{fg,sens} = \Delta H_{fg,sens} - \Delta H_{air,sens} - \Delta H_{fuel,sens}$

Eq. 2.5 $Q_{fg,lat} = \Delta H_{fg,lat} - \Delta H_{air,lat}$

The total flue gas losses also include the chemical losses ($Q_{fg,chem}$):

Eq. 2.6 $\quad Q_{fg} = Q_{fg,sens} + Q_{fg,lat} + Q_{fg,chem}$

Finally, the useful heat leaving the boiler (Q_{wat}) equals the energy transferred by the FGWHX (Q_{hx}), reduced by the energy lost to the ambient ($Q_{hx,amb}$), lost to the boiler draught in standby (Q_{draft}), or stored in the thermal mass (Q_{Ctherm}).
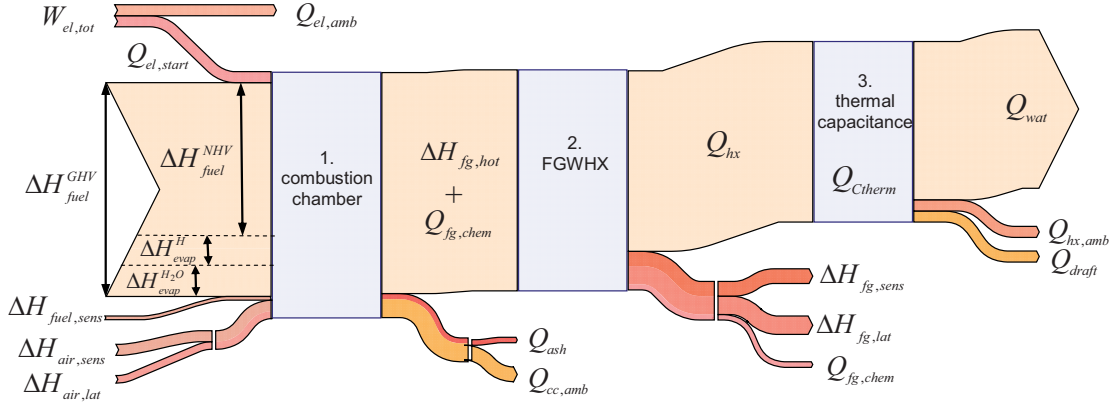
Figure 2.1: Sankey diagram of energy flows of a boiler.

Detailed calculations of the single terms based on measurements are presented in Part II, Paper IV.

2.3   Efficiency Definitions

The basic energy balance equation of a space heating boiler unit, according to the sankey diagram of energy flows shown in Figure 2.1 and Eq. 2.2 - Eq. 2.6, may be written as:

Eq. 2.7
$$Q_{fuel}^{GHV} + Q_{el,start}$$
$$= Q_{ash} + Q_{cc,amb} + Q_{fg,sens} + Q_{fg,lat} + Q_{fg,chem} + Q_{hx,amb} + Q_{draft} + Q_{Ctherm} + Q_{wat}$$

No standard definition for the term *combustion efficiency* was found in literature. Therefore, the definition used here may differ from definitions found in other sources. In the work presented here, the combustion efficiency shown in Eq. 2.8 is based on the gross heating value (GHV) of the fuel (Q_{fuel}^{GHV}) and flue gas losses, which are calculated from measurements performed on the fuel and air input as well as the flue gas output of the boiler (see also Eq. 2.4 - Eq. 2.6):

Eq. 2.8 $\quad \eta_C^{GHV} = 1 - \dfrac{Q_{fg}}{Q_{fuel}^{GHV}} = 1 - \dfrac{Q_{fg,sens} + Q_{fg,lat} + Q_{fg,chem}}{Q_{fuel}^{GHV}}$

Thus, for steady state conditions, combustion efficiency equals the fraction of the fuel energy that is transferred to the thermal capacitance of the boiler or lost by the combustion chamber's heat and ash losses:

$$Eq.\ 2.9 \qquad \eta_C^{GHV} = \frac{Q_{hx} + Q_{cc,amb} + Q_{ash}}{Q_{fuel}^{GHV}} = \frac{Q_{wat} + Q_{hx,amb} + Q_{cc,amb} + Q_{ash}}{Q_{fuel}^{GHV}}$$

For current European state of the art oil and gas boilers, losses due to incomplete combustion (Q_{ash} and $Q_{fg,chem}$) and heat losses of the combustion chamber ($Q_{cc,amb}$) are usually so small that they can be neglected for steady state operation. Thus, simplified combustion efficiency definitions can be found in literature.

The boiler efficiency ($\eta_{B,ON}^{GHV}$) during burner operation is assumed to be always lower than the combustion efficiency due to thermal heat losses through the boiler envelope. These radiation and convection heat losses from hot envelope surfaces to the ambient are a result of the high temperatures in the combustion chamber ($Q_{cc,amb}$) and in the "flue gas to water heat exchanger" (FGWHX) ($Q_{hx,amb}$). Small amounts of chemical heat losses caused by unburned residues in the ashes (Q_{ash}) may be considered, e.g. for solid fuel boilers. Sensible heat losses with ashes are not separately accounted for in the analysis presented here.

$$Eq.\ 2.10 \qquad \eta_{B,ON}^{GHV} = \eta_C^{GHV} - \frac{Q_{hx,amb} + Q_{cc,amb} + Q_{ash}}{Q_{fuel}^{GHV}}$$

The boiler efficiency η_B^{GHV} may be determined indirectly by measuring the combustion efficiency and subtracting estimated heat and ash losses from this value as shown in Eq. 2.10, or it may be determined directly by the enthalpy gain of the water flow through the boiler (Q_{wat}) divided by the fuel energy input (Q_{fuel}^{GHV}):

$$Eq.\ 2.11 \qquad \eta_B^{GHV} = \frac{Q_{wat}}{Q_{fuel}^{GHV}}$$

If a boiler is operating below its minimum power of continuous burner operation (minimum turndown ratio), it will burn fuel intermittently (ON/OFF) and additional losses may occur during OFF times due to unwanted natural draught airflow through the combustion chamber and the FGWHX. Therefore, average boiler efficiency in cycling operation includes an additional loss term accounting for natural draught losses (Q_{draft}):

$$Eq.\ 2.12 \qquad \eta_{B,cycling}^{GHV} = \frac{Q_{wat}}{Q_{fuel}^{GHV}} = 1 - \frac{Q_{fg} + Q_{hx,amb} + Q_{cc,amb} + Q_{ash} + Q_{draft}}{Q_{fuel}^{GHV}}$$

Due to electric fuel heating devices for preheating or ignition during burner start phases, also electric energy input may become relevant for the boiler's thermal energy balance and increase the useful heat output (Q_{wat}). Therefore, for a fair comparison of the energy consumption of different boilers Graf et al. (1999) recommend to also include electric energy consumption (W_{el}) of the boiler in the calculation of the boiler efficiency $\eta_{B,el}^{GHV}$:

$$Eq.\ 2.13 \qquad \eta_{B,el}^{GHV} = \frac{Q_{wat}}{Q_{fuel}^{GHV} + W_{el}}$$

In the work presented here, W_{el} includes electric energy for fans used for combustion air or flue gas circulation, stokers used for feeding fuel into the combustion chamber, ignition or preheating of fuel, and the controller. It does not

include pumps used for water circulation or any system used to transport wood fuel from a storage room into smaller reservoirs adjacent to the boiler itself. The reason for this is that the electricity consumption of these devices does not depend predominantly on the boiler itself, but on the particularities of each installed system.

In order to do justice to the higher thermodynamic and economic value of electricity, an extended boiler efficiency $\eta_{B,3el}^{GHV}$ is defined:

$$Eq.\ 2.14 \quad \eta_{B,3el}^{GHV} = \frac{Q_{wat}}{Q_{fuel}^{GHV} + 3 \cdot W_{el}}$$

For the evaluation of influences of operating conditions on boiler efficiencies, the three boiler efficiency definitions shown in Eq. 2.11, Eq. 2.13, and Eq. 2.14 will be used in Section 2.5.3.

2.4 The new space heating boiler model

A new space heating boiler model was developed based on the literature studies and the requirements defined in 2.1, and laboratory measurement results obtained from biomass, oil, and gas boilers. The model was programmed and compiled into a FORTRAN dynamic linked library (dll) which can be used for the simulation software TRNSYS and is referred to as Type 869. Details about the model are presented in Part II, Paper III. Model parameterization, uncertainty estimation, and comparison of model outputs with results from laboratory measurements are presented in detail in Part II, Paper IV. In this Section, only a brief overview of the model is given and new model features that are not commonly found in other boiler models are discussed briefly.

An information flow scheme of the boiler model is presented in Figure 2.2. The general sub-division of the model into combustion chamber (step 1), flue gas to water heat exchanger (step 2), and heat losses to the ambient (step 3) corresponds to the recommendations given by ASHRAE (2005) for a steady state model. In contrast to the ASHRAE model, the model presented here includes a thermal capacitance in step 3, and also an additional flue gas to combustion air preheater in step 2. Additional features that are not commonly found in the boiler models shown in Table 2.1 are:

– Simulation of heat losses from the combustion chamber.

– A UA-value from the boiler water to the ambient during burner operation that differs from the one during standby (burner OFF).

– Different options for the calculation of the flue gas outlet temperature with (a) the effectiveness-NTU approach with splitting of the heat exchanger into a dry section and a wet section in the case of water vapour condensation, and (b) the empirical delta-T approach with dependency on power modulation and on the water flow rate through the boiler.

– An explicit solution for the time-dependent temperature of the thermal mass (one node) that takes into account heat input from the flue gas to water heat exchanger, heat losses to the ambient and the energy balance of the water flowing through the boiler.

parameters and inputs **model / type 869** **outputs**

optional

user defined fuel:
GHV

$\gamma_C, \gamma_H, \gamma_O, \gamma_N, \gamma_S, \gamma_{ash}, cp_{fuel}$

$FuelType$

$\gamma_{H,O}$

$fr_{cc,ash}, fr_{cc,amb}$

automatic cycling calculation:
$\dot{Q}_{max}^{GHV}, \dot{Q}_{min}^{GHV}, \dot{Q}_{start}^{GHV}$

$t_{ON}, t_{SET}, t_{OFF}, t_{MAX}$

$\tau_{start}, \tau_{ON,min}, \tau_{OFF,min}$

$Q_{el,start}, m_{CO,start}$

t_{fuel}

$\dot{m}_{fuel,wet}$

modulation dependent lambda:
$\lambda_{min}, \lambda_{max}$

λ

$t_{air}, p_{air}, RH_{air}$

emissions calculation:
$ppm_{CO,min}, ppm_{CO,max}$

ppm_{CO}

auxiliary energy consumption:
$P_{el,min}, P_{el,max}, P_{el,OFF}$

$P_{nom}^{GHV}, \dot{m}_{wat,nom}$

FGWHX model 1:
$\Delta T_{nom}, \Delta T_{hx,fg}$

OR

FGWHX model 3:
$HX_{mode}, UA_{hx,nom}, n_{hx,fg}$

1-3 Paramters

$\dot{m}_{wat,in}, t_{wat,in}$

C_{therm}

$UA_{hx,amb,ON}, UA_{hx,amb,OFF}$

t_{amb}

step 1
combustion
chamber
(steady state)

step 2
FGWHX
(steady state)

step 3
balance of thermal
capacitance

STEADY STATE CALCULATION

TRANSIENT CALCULATION

GHV / NHV

$\dot{Q}_{fuel}^{GHV}$

$\dot{Q}_{ash}, \dot{Q}_{cc,amb}, \dot{Q}_{fg,chem}$

$\dot{m}_{CO}, \dot{m}_{fg,wet}$

$P_{el}, \dot{Q}_{el,therm}$

$t_{fg,out}$

$\dot{Q}_{fg,sens}, \dot{Q}_{fg,lat}$

$\dot{Q}_{hx}$

$\dot{Q}_{wat,out}, \dot{Q}_{hx,amb}, \dot{Q}_{Ctherm}$

$t_{wat,out}$

N_{start}

Figure 2.2: Information flow scheme of the boiler model Type 869, simplified for the specific application of non-condensing biomass boiler units. A detailed description of all parameters can be found in Part II, Paper III. Parameters used for the characterization of the boiler are displayed with a grey background.

2.5 Parameterization and comparison with measurements

The parameter identification process, uncertainty calculation, and the comparison of modelling results with measurements performed on oil, gas, and biomass boilers are described in detail in Part II, Paper IV. In this section, only the results for biomass boilers are summarized. General characteristics of the biomass boilers and the measurements performed are presented in Table 2.2.

Table 2.2: Overview of tested boilers and test conditions

Boiler Reference		Pel1	Pel2	Pel3	Pel4[a]	Chp1
Laboratory		SPF	SPF	Man	IWT	Man
Specifications according to the manufacturer						
$\dot{Q}_{wat,max}$	kW	10	10	40	14	150
V_{wat}	l	59	63	158	800	295
m_{empty}	kg	312	406	846	550	1972
modulating	-	YES	YES	YES	YES	YES
condensing	-	NO	NO	NO	NO	NO
Range of steady state measurements performed						
$\dot{Q}_{wat,out,min}$	kW	4	5	13	14	110
$\dot{Q}_{wat,out,max}$	kW	10	10	38	16	182
$t_{wat,in,min}$	°C	45	50	55	50	55
$t_{wat,in,max}$	°C	55	70	65	60	65
$t_{wat,out,min}$	°C	60	60	74	65	70
$t_{wat,out,max}$	°C	70	80	84	80	81
$\dot{V}_{wat,min}$	l/h	190	420	580	750	3'500
$\dot{V}_{wat,max}$	l/h	960	870	1'780	800	10'000
pts_{cond}	-	0	0	0	0	0
pts_{tot}	-	11	6	6	3	4

Pel: pellets; Chp: wood chips; SPF: Institut für Solartechnik SPF Rapperswil, Switzerland, Man: boiler manufacturer; IWT: Institute of Thermal Engineering, Graz University of Technology, Austria; $\dot{Q}_{wat,max}$: maximum (nominal) heating power; V_{wat}: water volume; m_{empty}: empty weight; [a] pellet burner integrated into a solar heat storage tank.

2.5.1 Thermal capacitance and cooling out in standby

The thermal capacitance of each boiler was determined with a discharge test described in Part II, Paper IV. For boilers Pel4 and Chp1, heat losses during standby where determined once with an open exhaust duct (draught regulator for Chp1, draught controlled to 10 Pa for Pel4), and once with the exhaust duct blocked. Blocking the exhaust duct had no significant influence on heat losses for boiler Pel4, and it decreased heat losses by 10% for boiler Chp1, despite the fact that the envelope surface temperatures increased for this boiler with a blocked exhaust duct. This could be an effect of the missing cooling draught air flow below the envelope surfaces (Figure 2.3). Taking into account these increased

surface temperatures, up to 25% of the standby heat losses may be lost by natural draught through the exhaust duct for boiler Chp1.
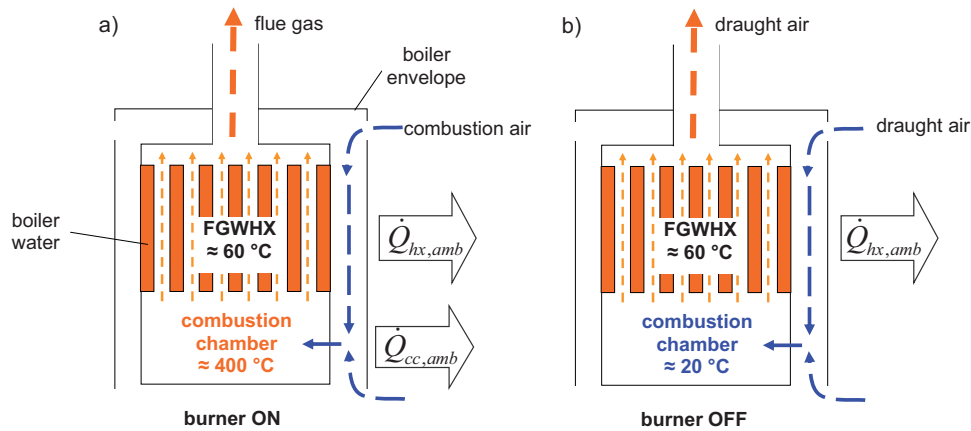
Figure 2.3: Different heat loss mechanisms of a space heating boiler with burner ON (a) and burner OFF (b).

A cooling out half-time ($\tau_{1/2}$) is defined as the time after which the temperature difference between the boiler's thermal mass and the ambient will be reduced to half of its original value due to heat losses to the ambient and to the draught air. Measured cooling out half-times in standby of the different biomass boiler units are shown in Figure 2.4. With the exception of boiler Chp1, the cooling out half-time increases more or less linearly with the effective thermal capacitance for the investigated boilers.
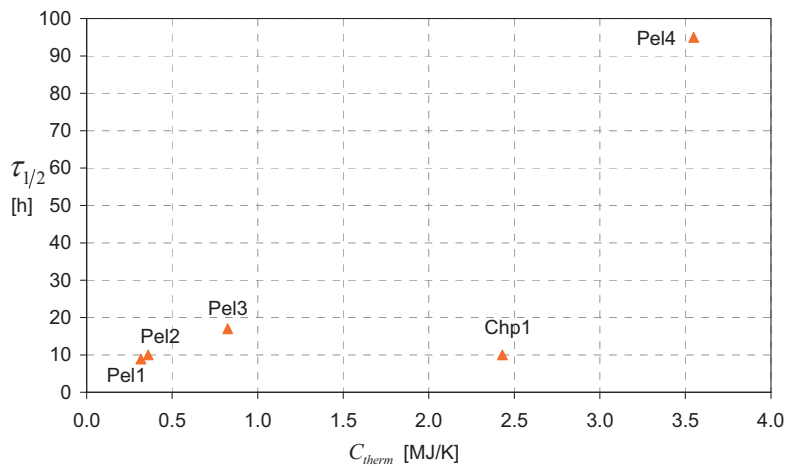
Figure 2.4: Cooling out half-times dependent on thermal capacitance for different biomass boiler units.

2.5.2 Excess air, electricity and CO emissions in steady state

Figure 2.5 shows the dependency of λ and electricity consumption of different biomass boilers on power modulation. Whereas some boilers (Pel1, Pel3) show an increase of λ up to a factor of two when decreasing combustion power to 40% of the maximum, Chp1 is able to maintain a constant excess air also at reduced combustion power. The dependency of electricity consumption on power modulation follows the linear model assumptions quite closely. The electricity demand for these boilers was in the range of 3 - 8 W per kW of fuel energy consumption for steady state operation, not including electricity for the water circulation pump or electricity for refilling the local fuel reservoir from a more distant one.
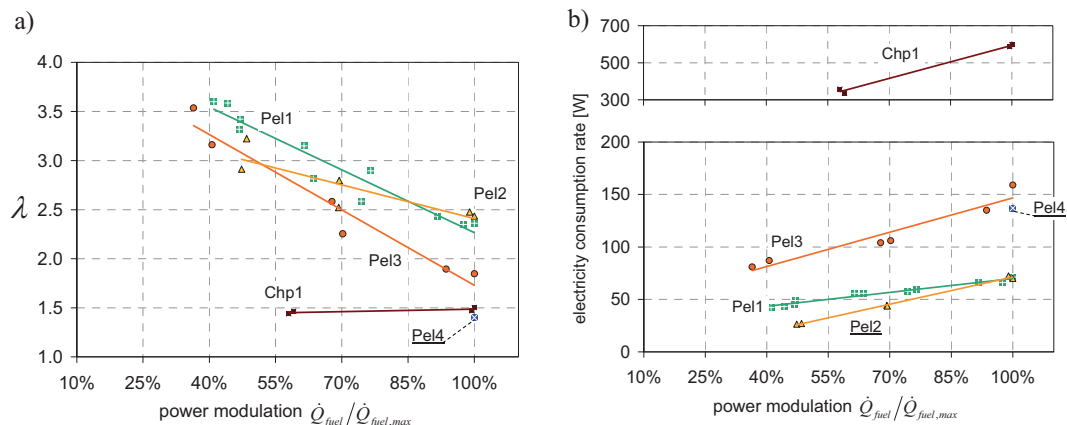
Figure 2.5: Dependency of the excess air factor (a) and the electricity consumption (b) on power modulation.
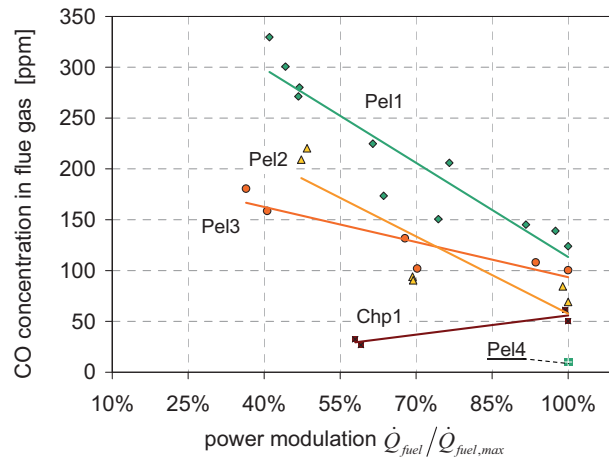
Figure 2.6: Dependency of CO emissions on power modulation.

For most of the investigated boilers, CO emissions are considerably higher at part load than at full load (Figure 2.6). Measured CO emissions of Pel1, Pel2 and Pel3 indicate that the assumption of an exponential dependency on power modulation might eventually be more appropriate than a linear dependency.

However, more measurements will be needed for the determination of parameters for an exponential curve-fit, and the scattering of the measured points is in the same range as the possible improvement by an exponential fit for boilers Pel1 and Pel3.

2.5.3 Boiler efficiencies

The comparison of measured boiler efficiencies with simulated boiler efficiencies is shown in Figure 2.7.

The boiler efficiencies of the biomass boilers sometimes – but not always – show a dependency on power modulation. In theory, combustion efficiency may increase at lower combustion power due to lower flue gas temperatures that can be achieved as the FGWHX is operating at lower power. However, the positive effect of a lower flue gas temperature at lower combustion power is often balanced by the negative effect of increasing excess air, and the increase of envelope heat losses relative to the useful heat produced. Thus, from the investigated biomass boilers, only Chp1 – which maintains a constant λ – shows increased boiler efficiency at lower loads. The effect of return temperature is not pronounced for these biomass boiler units, as they require a minimum return temperature in order to avoid condensation anyway.
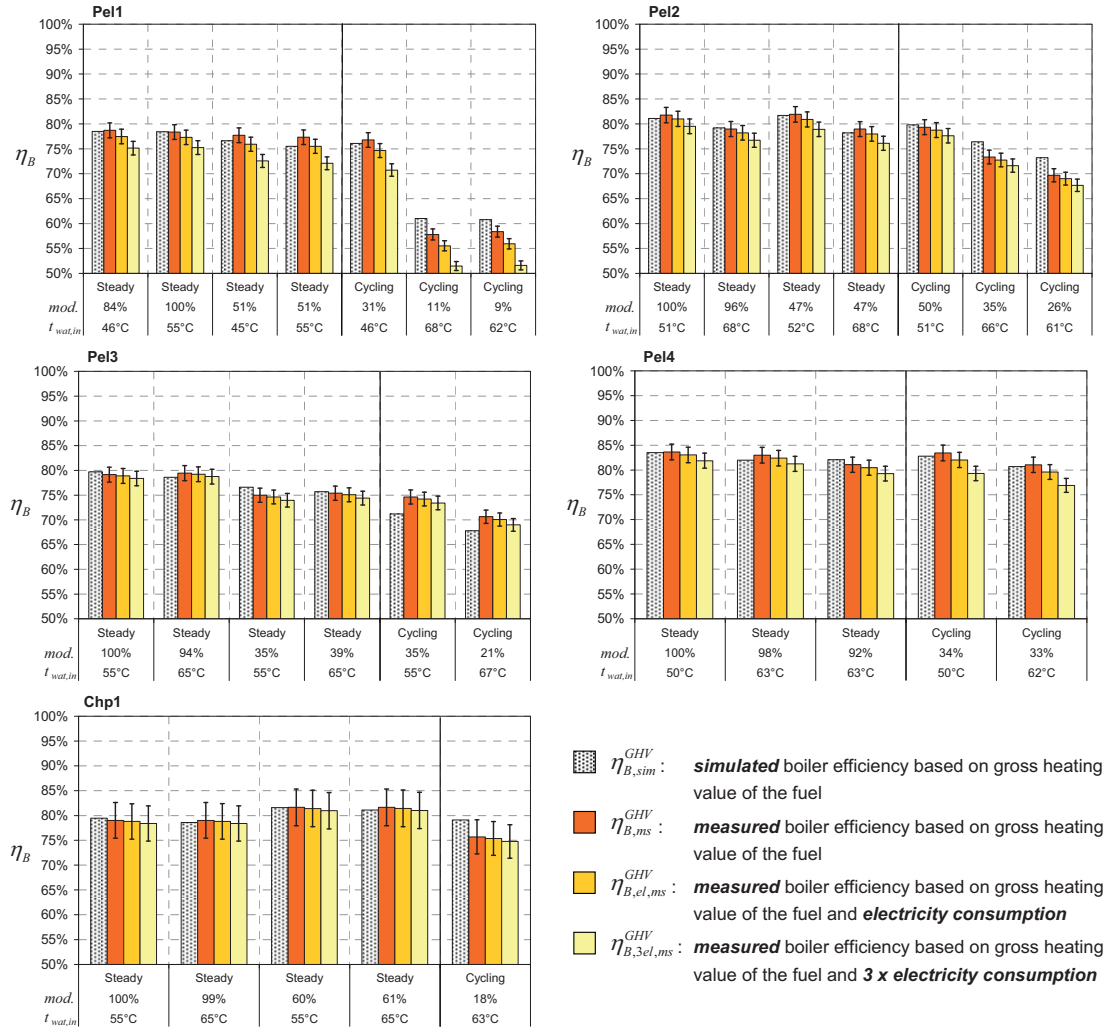
Figure 2.7: Comparison of measured and simulated boiler efficiencies. mod. = part load ratio

It can be seen in Figure 2.7 that the simulation results match the results from steady state measurements quite well, i.e. within the limits of the measurement uncertainty. Increasing differences are observed for the cycling operation modes with a slight overprediction of the efficiency for boilers Pel1, Pel2 and Chp1, and a slight underprediction for boiler Pel3.

2.5.4 Boiler cycling

A test run with an average heat load of 0.87 kW has been performed for pellet boiler Pel1. A simulation has been performed with the boiler model under boundary conditions that corresponded to the measured average heat load, and temperature hysteresis for switching the burner ON and OFF. Figure 2.8a shows that the simulated boiler cycles 25% more frequently than the real boiler if the thermal capacitance determined with the discharge test described in Part II, Paper IV, is used for the model. This deficiency of too frequent cycling can be corrected by increasing the effective thermal capacitance of the boiler by 28% (Figure 2.8b).
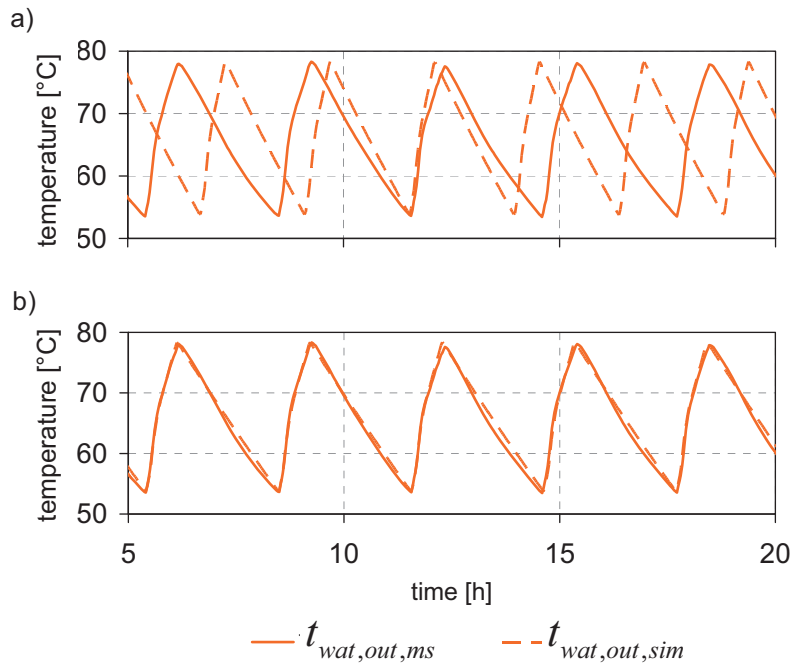
Figure 2.8: Simulated and measured cycling of pellet boiler Pel1 with boiler's thermal capacitance determined by a discharge test (a) and adapted (+28%) to observed cycling behaviour (b).

Figure 2.9 shows simulated and measured outlet temperature and heating power for the same boiler in cycling operation. Measured fuel consumption and return temperature have been used as model input data. Fuel consumption has been based on measured weight loss of the pellet storage. It can be expected that in a real pellet boiler, there is a time-delay between the fuel entering the combustion chamber and its actual reaction with the combustion air that produces heat. Therefore, especially at burner start, the measured increase of supply (outlet) temperature and heating power of the boiler is time-delayed, whereas simulated supply temperature and heating power increase is instantaneous (A) since no time lag is included in the boiler model between fuel feeding and fuel burning. It is also observed that the simulated thermal capacitance of the boiler reacts faster than the real thermal capacitance. Thus, the simulated heating power increases faster and stronger than measured (B) during the start phase and decreases faster and stronger than measured after the burner stop (C). These differences in thermal capacitance modelling can not be corrected by just assuming an increased thermal capacitance of the model. Due to the nature of the phenomenon, it is likely that more accuracy could be obtained by introducing a separate thermal capacitance for the combustion chamber that reaches higher temperatures during operation than the capacitance of the boiler water and the FGWHX. Thus, after the burning process has stopped, the heat stored in the combustion chamber material continues to be transferred to the FGWHX. Another explanation for the higher $\dot{Q}_{wat,ms}$ than $\dot{Q}_{wat,sim}$ after burner stop could also be that part of the fuel still continues burning in the combustion chamber for a while after the last pellet has been fed.
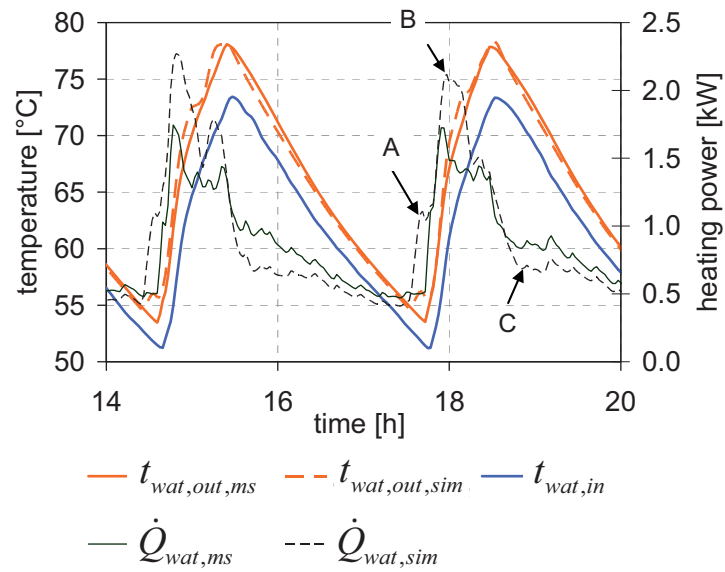
Figure 2.9: simulated and measured outlet temperature and heating power of pellet boiler Pel1.

2.5.5 Identified model parameters

The identified parameters for the simulation of the four biomass boilers are presented in Table 2.3. Details about the parameter identification process are presented in Part II, Paper IV. Due to the restrictions of the test facilities, no additional CO emissions during start and stop where quantified. These emissions may be quantified e.g. using flue gas flow rate measurements together with specialized techniques for the measurement of emissions under transient conditions (e.g. Heinz, 2007; Fiedler & Persson, 2009; Brunner et al. 2008; Nussbaumer et al. 2008).

Table 2.3: Identified boiler parameters and root mean square errors (RMSE) of fits.

Parameter	unit	Pel1	Pel2	Pel3	Pel4	Chp1
C_{therm}	kJ/K	317	360	825	3550	2430
$UA_{hx,amb,OFF}$	W/K	6.8 [a]	6.8 [a]	9.2 [b]	N/A [c]	46 [b]
$\dot{Q}^{GHV}_{fuel,min}$	kW	5.3	5.8	16.7	17.7	127.8
$\dot{Q}^{GHV}_{fuel,max}$	kW	12.8	12.8	50.0	17.7	222.2
λ_{min}	-	2.31	2.39	1.64	1.41	1.49
λ_{max}	-	3.54	3.02	3.41	1.41	1.45
$RMSE(\lambda)$	-	0.12	0.14	0.14	n.d. [d]	0.01
$ppm_{CO,min}$	ppm	120	53	89	10	29
$ppm_{CO,max}$	ppm	297	193	169	10	56
$RMSE(ppm_{CO})$	ppm	25	31	13	n.d. [d]	5
$P_{el,min}$	W	44	25	75	137	340
$P_{el,max}$	W	69	73	151	137	593
$RMSE(P_{el})$	W	2	1.2	7	n.d. [d]	10
dT_{nom}	K	67.4	77.2	139	74.5 [e]	104
$dT_{hx,fg}$	K	-0.48	-0.98	-1.0	N/A [d]	-1.47
$RMSE\left(\eta^{GHV}_C\right)$	% (abs)	0.41	0.51	0.63	N/A	0.13
fr_{ash}	%	3.3 [f]	0.0 [f]	0.1	0.2	0.2
$fr_{cc,amb}$	%			1.3	2.0	2.7
$UA_{hx,amb,ON}$	W/K	6.8 [g]	6.8 [g]	9.2 [g]	N/A [c]	4.6 [g]
$RMSE\left(\eta^{GHV}_B\right)$	% (abs)	0.83	0.46	0.87	0.82	n.d.
τ_{start}	h	0.15	0.05	0.05	0.25	1.1
$\dot{Q}^{GHV}_{fuel,start}$	kW	n.d.	n.d.	31	n.d.	67
$W_{el,start}$	Wh	111	5	33.6	36.5	56.5

N/A = not applicable; n.d. = not determined; [a] controlled exhaust duct draught of 10 Pa; [b] exhaust duct open to ambient with draught regulator, but no active draught control; [c] burner is integrated into solar thermal storage tank with different heat losses at different heights; [d] not modulating; [e] average of 3 measurements (not fitted); [f] $fr_{ash} + fr_{cc,amb}$; [g] value taken from cooling out test.

2.6 Simulation of draught losses

Chimney draught during burner OFF-times can cause considerable heat losses if air from the surroundings or the ambient is drawn into the combustion chamber and through the flue gas to water heat exchanger. In this case heat transfer takes place from the hot thermal mass of the boiler and the water in the boiler to the colder air drawn through the boiler (compare Figure 2.3). These losses depend highly on boiler- and system-design and have been reported to be in the range of 0.4 to 2.5 % of primary energy input for pellet furnace and boiler systems according to measurements and annual simulations performed by Persson et al. (2006) and Fiedler et al. (2007). For the boilers Pel4 and Chp1, the cooling out rate with a pressure in the flue gas duct that is 10 Pa below ambient pressure was compared with the cooling out rate measured with a blocked exhaust duct. It was concluded that natural draught losses had no significant effect on boiler Pel4, but might increase standby losses of Chp1 by 10-25% (compare Section 2.5.1).

Fan induced draught

Boilers may be equipped with a fan blowing combustion air into the combustion chamber and / or drawing flue gas out of the FGWHX and blowing it into the chimney. In this case, draught is maintained by the operation of the fan whenever the fan is on. This may be the case for a specified time before the burner starts (pre-purge) and after fuel supply into the combustion chamber has stopped (after-vent). These types of boilers are usually more or less airtight, i.e. no significant amount of air is leaking into the boiler during times without fan operation.

At times without combustion (burner OFF), mass flow, specific heat, and temperature of the flue gas are replaced by the corresponding values of the draught air.

Natural draught

Natural draught is wanted in all boilers without fan-assistance to maintain the flue gas flow and expulsion through the chimney, as well as to maintain the flow of combustion air into the combustion chamber. Unfortunately, natural draught may also cool out the thermal mass of the boiler during OFF-times. The rate of cooling out is difficult to predict since it does not only depend on the construction of the boiler and the temperature difference between the air in the boiler and the ambient, but also on the chimney height and the temperature of the gas in the chimney (ASHRAE 2004). Therefore, a model for a boiler alone is not able to predict natural draught for a given installation.

2.6.1 Existing approaches

If heat transfer coefficients (e.g. Nusselt-relationships or UA-values as functions of flow conditions) are used to calculate the heat transfer from the flue gas to the

thermal mass of the boiler, the same heat transfer coefficients may be used to calculate the heat transfer back to the draught air during burner OFF times with natural draught. Nordlander (2003) presented an empirical model for the mass flow rate of draught air ($\dot{m}_{da}$) based on a reference measurement of draught air flow ($\dot{m}_{da,50K}$) at 50 K temperature difference between the draught air (da) at the outlet of the boiler ($t_{da,out}$) and the ambient (t_{amb}):

$$Eq.\ 2.15 \quad \dot{m}_{da} = \dot{m}_{da,50K} \cdot \sqrt{(t_{da,out} - t_{amb})/50K}$$

Claus & Stephan (1985) present an analytical formula based on Bernoulli's principle:

$$Eq.\ 2.16 \qquad \dot{m}_{da} = A_{ch} \cdot \rho_{da} \cdot \sqrt{\frac{2 \cdot \Delta p_{ch}}{\zeta_{tot} \cdot \rho_{da}}}$$

Where A_{ch} is the cross sectional area of the chimney, ρ_{da} is the density of the draught air, and Δp_{ch} is the pressure drop in the chimney that equals the draught. The draught is calculated based on the density difference of air in the chimney and air outside the chimney. The total dimensionless flow resistance ($\zeta_{tot} = \zeta_{ch} + \zeta_B$) is composed of the single resistances of the chimney (ch) and of the boiler (B). Claus & Stephan present detailed calculation of Δp_{ch}, ζ_{ch} and ρ. A set of coefficients has to be determined additionally for the average temperature of the draught air in the chimney, dependent on mass flow, boiler temperature, heat transfer through the chimney walls and time.

2.6.2   Analytical approach

Eq. 2.17 shows the theoretically induced draught (Δp_{draft}) according to Bernoulli's principle, dependent on the ambient conditions as well as the chimney height (Γ_{ch}) and the temperature of the draught air in the chimney (T_{da}), under the assumption that the fluid inside the chimney is air. According to the ASHRAE Handbook of HVAC Systems and Equipment (ASHRAE 2004), pressure loss in a chimney (including the boiler) is calculated with Eq. 2.18, which is derived from the extended Bernoulli-equation.

$$Eq.\ 2.17 \quad \Delta p_{draft} = g \cdot \Gamma_{ch} \frac{\rho_0 \cdot T_0 \cdot p_{amb}}{p_0} \left(\frac{1}{T_{amb}} - \frac{1}{T_{da}} \right)$$

$$Eq.\ 2.18 \quad \Delta p_{ch,turb} = \frac{\zeta_{tot}}{2} \left(\frac{T_{da} \cdot p_0}{\rho_0 \cdot T_0 \cdot p_{amb}} \right) \left(\frac{4 \cdot \dot{m}_{da}}{\pi \cdot (d_{ch})^2} \right)^2$$

Assuming a steady state condition of the flow, induced draught must be equal to the pressure drop in the chimney ($\Delta p_{draft} = \Delta p_{ch}$). Thus, from Eq. 2.17 and Eq. 2.18 we get:

$$Eq.\ 2.19 \quad \dot{m}_{da} = \frac{\pi \cdot \sqrt{2 \cdot g}}{4} \frac{\rho_0 \cdot T_0}{p_0} \cdot \sqrt{\frac{\Gamma_{ch}}{\zeta_{tot}}} (d_{ch})^2 \cdot p_{amb} \sqrt{\frac{1}{T_{amb} \cdot T_{da}} - \frac{1}{(T_{da})^2}}$$

The first term on the right-hand side of Eq. 2.19 is a physical constant; the second term includes the chimney height, the resistance factor and the chimney diameter and is therefore constant for a given boiler and chimney installation. The last term includes ambient pressure and temperature as well as the temperature of the draught air and may therefore vary with time for a given installation.

If a reference measurement of the draught induced mass flow rate ($\dot{m}_{da,ref}$) is available for a given boiler and chimney, the draught induced mass flow rate can be calculated for any other condition with Eq. 2.20.

$$Eq.\ 2.20 \quad \dot{m}_{da} = \dot{m}_{da,ref,turb} \frac{p_{amb}}{p_{amb,ref}} \sqrt{\frac{\dfrac{1}{T_{amb} \cdot T_{da}} - \dfrac{1}{\left(T_{da}\right)^2}}{\dfrac{1}{T_{amb,ref} \cdot T_{da,ref}} - \dfrac{1}{\left(T_{da,ref}\right)^2}}}$$

During boiler operation, the flue gas flow can be assumed to be turbulent, which is reflected by the increase of pressure drop with the square of the mass flow on the right hand side of equation Eq. 2.18. However, during boiler stand-by the flue gas flow in the chimney is unwanted and often restrained on purpose. Thus, the flow may become laminar and in this case Eq. 2.18 is replaced by the law of Hagen-Poiseuille:

$$Eq.\ 2.21 \quad \Delta p_{ch,lam} = \frac{8 \cdot l_{ch} \cdot \mu_{da} \cdot \dot{m}_{da}}{\rho_{da} \cdot \pi \cdot \left(d_{ch}\right)^4}$$

Combining Eq. 2.21 with Eq. 2.17 leads to:

$$Eq.\ 2.22 \quad \dot{m}_{da,lam} = \frac{\pi \cdot g}{8 \cdot \mu_{da}} \left(\frac{\rho_0 \cdot T_0}{p_0}\right)^2 \frac{\Gamma_{ch} \cdot \left(d_{ch}\right)^4}{l_{ch}} \left(p_{amb}\right)^2 \left(\frac{1}{T_{amb} \cdot T_{da}} - \frac{1}{\left(T_{da}\right)^2}\right)$$

Therefore, assuming that the dynamic viscosity of the draught air (μ_{da}) does not vary significantly in the range of consideration:

$$Eq.\ 2.23 \quad \dot{m}_{da,lam} = \dot{m}_{da,lam,ref} \left(\frac{p_{amb}}{p_{amb,ref}}\right)^2 \left(\frac{\dfrac{1}{T_{amb} \cdot T_{da}} - \dfrac{1}{\left(T_{da}\right)^2}}{\dfrac{1}{T_{amb,ref} \cdot T_{da,ref}} - \dfrac{1}{\left(T_{da,ref}\right)^2}}\right)$$

Where $\dot{m}_{da,lam,ref}$ is a reference value of the draught air mass flow under laminar conditions.

Results based on the different approaches for the calculation of draught airflow in the chimney are shown in Figure 2.10. The calculations are based on a hypothetical reference measurement of the draught air mass flow at a temperature difference of 50 K between the draught air and the ambient, performed at sea level. Above 100 °C, the curves obtained from the analytical solutions flatten out, whereas in the empirical approach of Nordlander, the

draught mass flow rate continues to increase with increasing temperature difference. Shifting the same installation to a higher place - 1500 m above sea level in the example – reduces the calculated draught mass flows significantly for the assumption of laminar conditions. For a boiler in standby, it can be expected that the draught air temperature drops quickly below 100 °C. For this region, the solution of Nordlander can be expected to give results in between the solutions for laminar and for turbulent conditions obtained from the analytical solution.
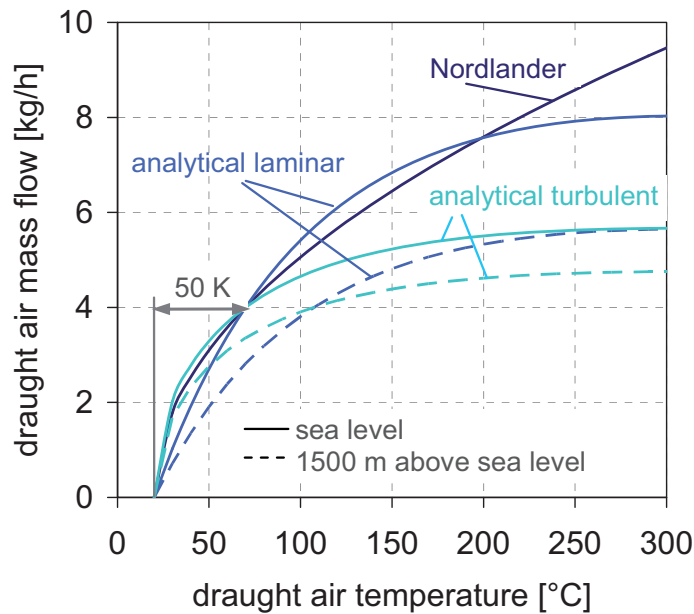
Figure 2.10: Comparison of different models for the calculation of draught airflow based on a reference measurement at a temperature difference of 50 K between draught air and ambient. Dashed curves are calculated for 1500 m. above sea level ($p_{amb} = 85kPa$).

2.6.3   Simulation of draught losses in Type 869

In the presented boiler model Type 869, draught losses are not separately accounted for. Instead, natural draught losses are included in the normal standby cooling out loss parameter $UA_{hx,amb,OFF}$. Natural draught was not the predominant loss term during standby for the investigated biomass boilers, and data collected during the measurements were not sufficient to validate a separate model for natural draught. Therefore, the model presented in this section has not been included in Type 869.

3 The thermal energy storage tank

3.1 Identification of storage tank parameters

A thermal energy storage (TES) with an integrated pellet burner was provided by a manufacturer for measurement and characterization of its performance. Basic specifications of the TES are shown in Table 3.1.

Table 3.1: TES Specifications according to the manufacturer.

Water content	800	l
Empty weight	550	kg
Height	213	cm

A schematic of the cylindrical TES is shown in Figure 3.1. Solar heat is transferred to the TES with an immersed coil heat exchanger with a means for stratification enhancement in the top that is not further specified. Domestic hot water (DHW) preparation is equally achieved with an immersed coil heat exchanger. Pipes for the direct discharging space heating loop are connected at the bottom of the TES, with immersed pipes that reach to the height of fluid intake and release of the supply line (outlet) and return line, respectively.
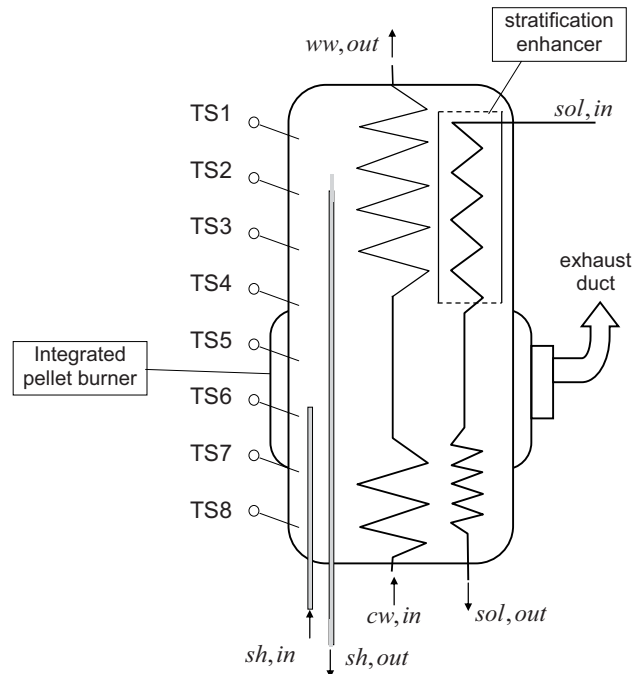
Figure 3.1: Schematic representation of the TES. TS: temperature sensor. Other abbreviations according to the list of subscripts.

Auxiliary heating is provided by a pellet burner and flue gas heat exchanger integrated directly into the TES. Further details about the dimensions and the materials inside the TES have not been given by the manufacturer or will not be displayed here due to reasons of anonymity.

3.1.1 Method

The test methods used followed partially prEN12977-3:2006, with adaptations and additional tests where appropriate. All six fluid connections (supply and return lines of space heating, DHW, and solar charging, respectively), were equipped with immersed 4-wire Pt100 class A (DIN EN 60751:2008) sensors of 3 mm diameter, and all pipe connections were insulated and equipped with heat traps of at least 10 cm height. Ambient temperature was also measured with a 4-w Pt100 class A sensor. All Pt100 temperature sensors were calibrated simultaneously against another 4-w Pt100 class A sensor in a thermostat bath in the range of 10 °C – 90 °C. Temperatures of the TES where measured with 8 thermocouples of type K that were equidistantly attached to the TES surface under its insulation. Volume flows were measured with a magnetic-inductive flow meter Promag P50 from Endress & Hauser, that was calibrated against a balance (Mettler Multirange) and a stop-watch in the range of 100 – 900 l/h. Calculation of mass flow rates and heat transfer of each tank connection was performed each second based on temperature dependent functions of density and enthalpy of water and averages were saved at 10 or 20 seconds time steps. The estimated measurement uncertainties are listed in Table 3.2.

Table 3.2: Measurement devices and uncertainty used for the measurements.

measured property	*Device*	*uncertainty (k=1)*
volume flow rate	Endress & Hauser Promag P50	± 0.6%
temperature (flow)	4w Pt100 class A	± 0.1K
temperature difference (flow inlet and outlet)	4w Pt100 class A	± 0.03K
temperature (tank)	Type K thermocouple	± 0.5K

Where pre-conditioning was necessary in order to get to a well defined starting point for an experiment, the TES was charged or discharged directly with a constant temperature via the space heating connections. Additionally, a connection at the bottom of the TES was used as an outlet in the case of pre-charging. These pre-conditioning phases are not shown.

The measurement results were used to parameterise the multiport store model (Drück 2006) that was used for system simulations in Chapter 5. The parameters were found by a combination of manual adjustments and optimization algorithms

using GenOpt[5] (Wetter 2004). If the experiment did not start with a uniform temperature in the TES, a pre-conditioning phase was also simulated in order to reach similar TES temperatures than measured for the start of the time period of interest. These pre-conditioning simulations are not shown. The evaluation procedure described in prEN12977-3 is a black box approach, i.e. it is not assumed that temperatures inside the TES are known during the experiment. In the work shown here, such temperatures are available and have therefore also been included into the fit-objective functions. Different fit-objective functions have been used for different tests. These are not shown in detail. Instead, the following Sections show measurement results together with simulation results obtained by simulating the same TES process with the multiport store model with the parameters found in the identification procedure.

The multiport store model uses a one-dimensional multi-node model for the representation of the TES that is coupled with other one-dimensional multi-node models for the representation of internal heat exchangers. The nodes are counted from bottom to top with the index $i=1$ to N_{store}. The general energy balance equation simplifies to[6]:

$$C_{store,i} \cdot \frac{\partial t_{store,i}}{\partial \tau} = \sum_{p=1}^{N_{dp}} \dot{m}_{dp,p} \cdot cp_{store} \cdot \left[\delta_{p,up} \cdot \left(t_{store,i-1} - t_{store,i} \right) + \delta_{p,down} \cdot \left(t_{store,i} - t_{store,i+1} \right) \right]$$

Eq. 3.1
$$+ \sum_{q=1}^{N_{hx}} UA_{hx,q,i} \cdot \left(t_{hx,q,i} - t_{store,i} \right)$$

$$+ k_{eff} \cdot \frac{V_{store}}{\Gamma_{store}} \cdot \frac{N_{store}}{\Gamma_{store}} \cdot \left[\left(t_{store,i-1} - t_{store,i} \right) + \left(t_{store,i+1} - t_{store,i} \right) \right]$$

$$- UA_{store,i,amb} \cdot \left(t_{store,i} - t_{amb} \right)$$

Where the left hand side of the first line is the change rate of stored energy in node i of the TES according to its temperature change rate ($\partial t / \partial \tau$) and its thermal capacitance ($C_{store,i}$). The right hand side of the first line corresponds to the energy flow associated with the mass flow that is induced by charging or discharging through the double ports. The second line is the sum of all heat transfer rates from internal heat exchangers, the third line calculates heat transfer rates caused by vertical diffusion and conduction based on the effective thermal diffusivity (k_{eff}), and the fourth line calculates the heat loss rate to the ambient. The logical switches $\delta_{p,up}$ and $\delta_{p,down}$ are 1 if the flow is upwards or downwards, respectively, and 0 if the flow is in the opposite direction or if there is no flow. Likewise, the energy balance for each node i of each internal heat exchanger is:

---

[5] The algorithms used where *Simplex (Nelder and Mead and O'Neill)* and *GPSHookeJeeves.*

[6] A slightly different notation is used by Drück (2006), but the mathematical result is the same.

$$C_{hx,i} \cdot \frac{\partial t_{hx,i}}{\partial \tau} = \dot{m}_{hx} \cdot cp_{hx} \cdot \left[\delta_{hx,up} \cdot \left(t_{hx,i-1} - t_{hx,i} \right) + \delta_{hx,down} \cdot \left(t_{hx,i} - t_{hx,i+1} \right) \right]$$

Eq. 3.2
$$+ UA_{hx,i} \cdot \left(t_{store,i} - t_{hx,i} \right)$$
$$- UA_{hx,i,amb} \cdot \left(t_{hx,i} - t_{amb} \right)$$

3.1.2   Active thermal capacitance and burner integration

Results of measurements performed for the determination of the active thermal capacitance of the TES and the characterization of the pellet burner and flue gas heat exchanger that are integrated in the TES are shown in Section 2.5 (Pel4).

3.1.3   Heat losses and effective thermal conductivity

Heat losses and effective vertical heat conductivity have been fitted based on two tests. The first test was a cooling out test that started with a hot TES, i.e. a TES that has been pre-conditioned to 50 – 60 °C for all TES sensors. The second test was a standby-destratification test that started with a hot temperature in the top 50% of the TES (45 – 55 °C) and a cold temperature at the bottom (20 – 30 °C). Figure 3.2 shows the temperature development within the TES during the two tests, both measured and simulated. The simulation parameters that have been obtained from these tests include five heat loss terms and the effective thermal conductivity. These have been found by iteratively adapting the corresponding values until the average of the absolute deviations of measured and simulated TES temperatures of both test sequences were minimal. The identified TES parameters are listed in Table 3.3. These parameters have been applied for the simulations for the determination of other parameters.
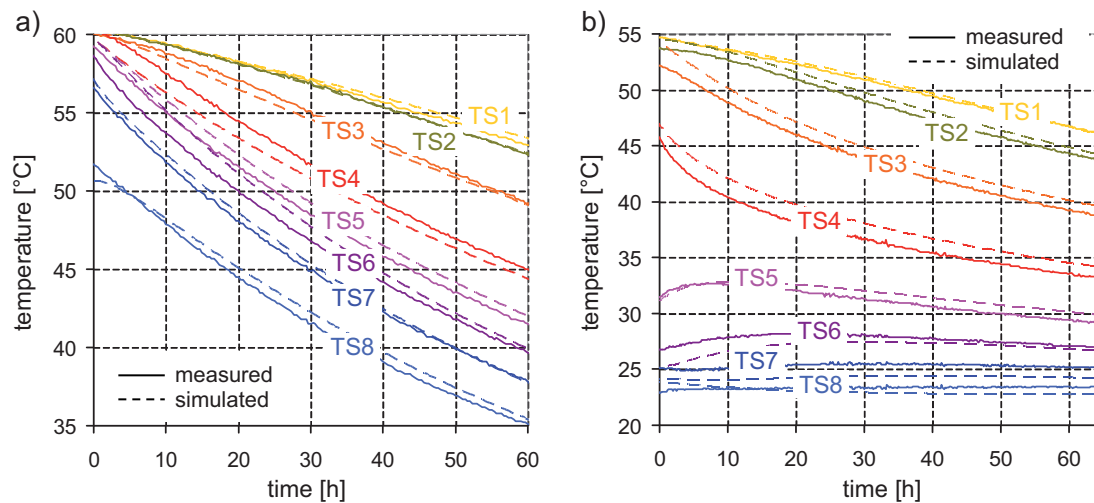
Figure 3.2: Measured and simulated temperatures during heat loss (a) and standby destratification tests (b).

3.1.4 Immersed coil solar heat exchanger

Two tests were performed on the immersed coil solar heat exchanger. For both tests, water was used in the solar collector loop. The first test started with a cold TES (≈20 °C). In this test, the TES was charged via the immersed coil solar heat exchanger with a constant inlet temperature of 60 °C and mass flow rates of 150, 300, and 600 kg/h. Each mass flow rate was kept for one hour before the next mass flow rate was applied, and after the highest mass flow rate the lowest mass flow rate was applied again (Figure 3.3a). The second test started with a hot upper section of the TES (> 50 °C), and a cold lower section of the TES (<40 °C). The same series of mass flow rates was applied, but this time the inlet temperature was 45 °C, i.e. in between the temperature of the upper section and the lower section. Thus, the stratification capability of the immersed heat exchanger was tested.

The immersed coil solar heat exchanger was modelled with one solar heat exchanger in the top section of the TES and a second heat exchanger in the bottom, connected in series. Simulation of the upper heat exchanger was difficult since measurements showed some stratification, but not as much as would result from a simulation with the option of "stratified" chosen in the model. Optimization procedures such as GenOpt have been used in order to find optimal parameters for both, stratified and unstratified simulation. Using the unstratified charging option of the model, a set of parameters was found that fits the first test well (Figure 3.3a). For this set of parameters the relative deviation of the simulated solar energy input into the TES compared to the measured energy input is -0.5%, and the average of the absolute values of the relative deviation of simulated power to measured power of all timesteps (excluding transients at times of changes of mass flow rate) is 3.6%.
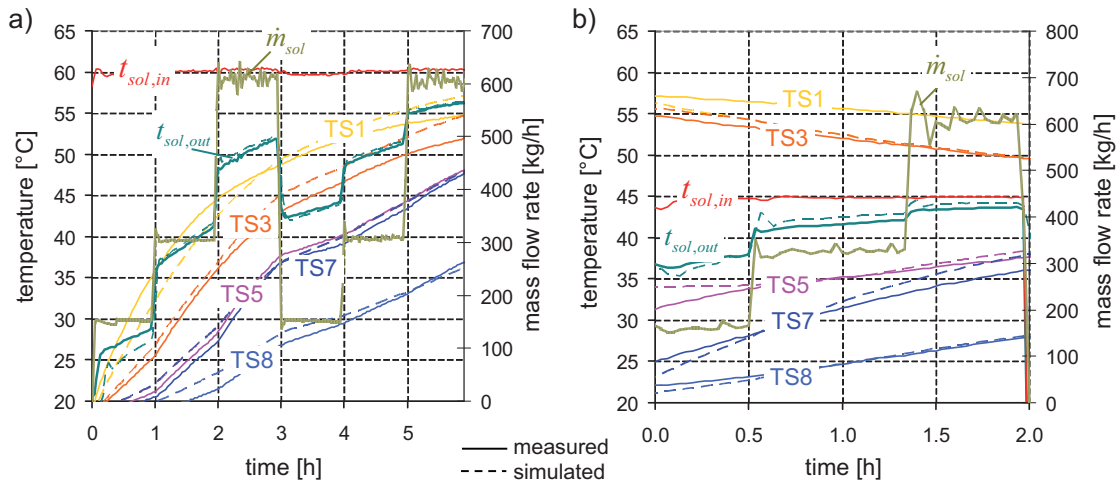
Figure 3.3: Measured and simulated temperatures during solar charging with an inlet temperature higher (a) and lower (b) than the upper TES temperatures.

Figure 3.3b shows the results of an additional test that is not included in prEN12977-3 and that was carried out in order to detect the stratification capabilities of the upper part of the immersed solar heat exchanger that cannot be bypassed. The results show that the stratification device was not able to prevent a temperature decrease of the upper part of the TES if the inlet temperature of the heat exchanger is lower than the temperatures in this part of the TES. Unfortunately, it was not possible to find a parameter set for the TES model that was capable of simulating both test cases shown in Figure 3.3 accurately. For this second test, the energy balance deviation was -14%, and the average of the absolute values of the relative power deviation was 28%, using the same parameter set as for the first test shown in Table 3.3. Simulating the upper part of the immersed solar heat exchanger with the stratifying option did not lead to a parameter set that is applicable for both cases either. For the base case simulation of Section 5.3.3, the unstratified option corresponding to the simulations shown in Figure 3.3 has been used, knowing that with these parameters the stratification capabilities of the TES are somewhat underestimated for some operating conditions.

3.1.5   Immersed coil domestic hot water heat exchanger

The immersed coil DHW heat exchanger was tested starting with a hot TES (top: 60 °C, whole TES > 45 °C). The inlet temperature was kept at $15 - 17$ °C, and the mass flow rates 900, 600, 300, and 150 kg/h were applied twice for about 15 min each.

The dependency of the UA-value (heat transfer coefficient area product) of the DHW heat exchanger on mass flow and temperature difference that is implemented in the TES model is shown in Eq. 3.3[7].

$$Eq.\ 3.3 \qquad UA_{hx,i} = \frac{UA_{base}}{N_{hx,nodes}} \cdot \left(\frac{\dot{m}_{ww}}{[kg/s]} \right)^m \cdot \left(\frac{\Delta T_i}{[K]} \right)^n$$

Where m and n stand for the dependency of the UA-value on the mass flow rate of the water inside the coil $\dot{m}_{ww}$ and on the temperature difference ΔT from the heat exchanger inlet to the water in node i of the TES, respectively as described in Drück (2006). The parameters have been found by optimization with GenOpt with a fit objective function that takes into account the differences between measured and simulated TES temperatures as well as the hot water outlet temperature.

---

[7] Dependencies on time and on average temperature are also implemented in the model, but they are not used in the work presented here.
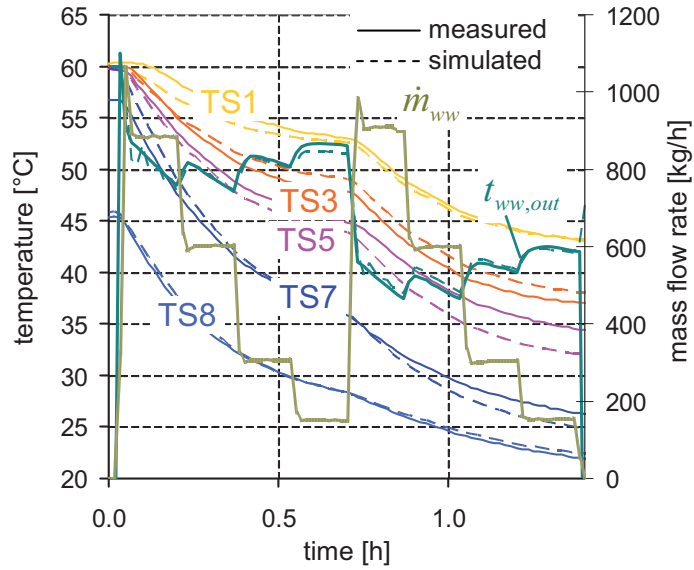
Figure 3.4: Measured and simulated values for the DHW heat exchanger characterization experiment.

Figure 3.4 shows the measured and simulated temperatures within the TES during the experiment with different mass flow rates. The resulting energy output difference is 0.3%, and the average of the absolute values of the relative power deviation is 1.5%. Although these deviations are acceptable according to prEN12977-3, Figure 3.4 shows that the simulated TES has a lower heat transfer capacity in the top (TS3) and a higher heat transfer capacity in the middle section (TS5) of the TES than could be expected from the measured temperature curves. An attempt of finding a better parameter set by splitting this heat exchanger into a top and a bottom part with no heat transfer capacity in the middle section of the TES was not successful, i.e. did not give better results. The chosen values for the parameters UA_{base}, m and n are shown Table 3.3. For mass flows of $150 - 1000$ kg/h and a temperature difference of 10 K, the resulting UA-value is in the range of $1100 - 1700$ W/K.

3.1.6   Direct space heat discharging

The stratifying capabilities of the inlet of the space heating return line has been tested starting from a TES that is hot at the top (> 50 °C), but cold at the bottom (<25 °C). The inlet (return) temperature of the space heating loop was kept between these two temperatures ($t_{sh,in} \approx 38 - 48$ °C), and the mass flow rate was 420 kg/h. Figure 3.5 shows that the temperatures in the lower part of the TES increase considerably during this discharging process, whereas temperatures in the upper part drop below the inlet temperature of the space heating return line. A probable explanation for this could be that heat is transferred from the immersed space heating inlet pipe to the TES fluid surrounding it (compare Figure 3.1), or that considerable mixing is taking place at the space heating inlet. Due to limits of the store model, it was not possible to simulate this heat transfer with additional internal heat exchangers. Instead, immersed charging and

discharging pipes have been simulated externally with heat losses towards a temperature that is set equal to the average of the fluid temperatures inside the TES at the corresponding heights. The resulting heat losses have been added as gains to the lower part of the TES using a direct charging double port with $z_{in} = 0.325$, $z_{out} = 0.1$, and a constant mass flow of $\dot{m} = 40 kg/h$ at times of space heating loop operation. Figure 3.5a shows that if this effect is not taken into account by the simulation, the simulated lower TES temperatures remain significantly colder (TS5sim ≈ TS6sim ≈ TS7sim ≈ TS8sim ≈ 22°C) than the measured values (TS5 ≈ 36°C, TS6 ≈34°C, TS7 ≈30°C). At the same time, simulated upper TES temperatures (TS1sim, TS2sim, TS3sim, hour 1 to 2) remain far higher than their corresponding measured values. Figure 3.5b shows, that simulating heat transfer from the space heating inlet and outlet pipes to the lower part of the TES reproduces the development of the temperatures in the TES significantly better (TS6 to TS8) ≈ (TS6sim to TS8sim). The space heating loop in- and outlet and all parameters for heat transfer to the bottom section have been determined using GenOpt with a fit objective function that takes into account the measured and simulated temperatures in the TES.
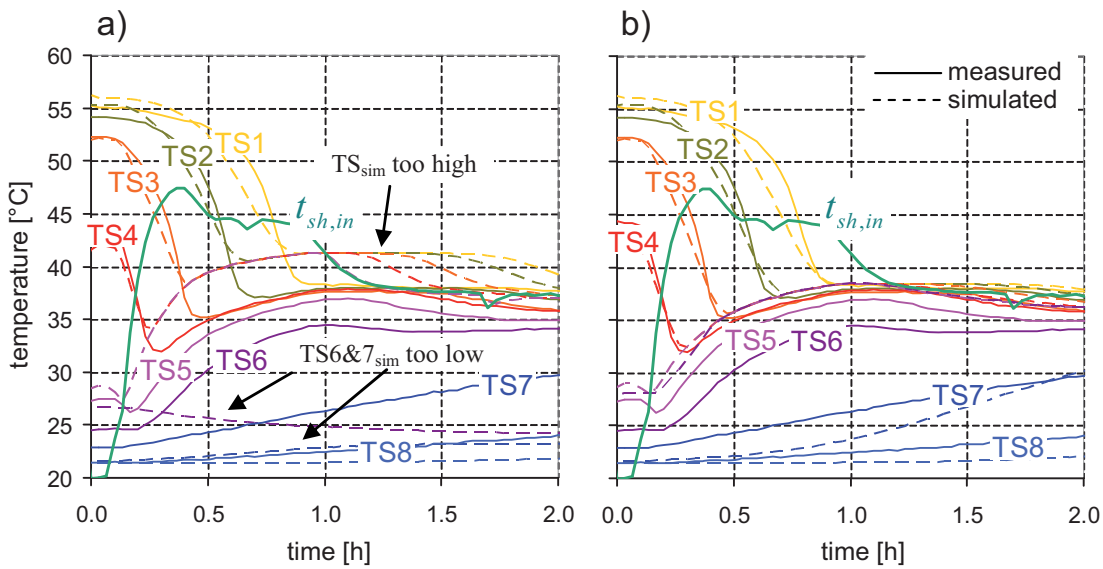
Figure 3.5: Space heating discharging with a return temperature higher than the temperatures in the lower parte of the TES and a mass flow rate of 420 kg/h. Simulation results without simulation of heat transfer to the lower part of the TES (a) and with heat transfer to the lower part of the TES (b).

3.1.7 Overview of identified TES parameters

Table 3.3 gives an overview of the parameters identified for the simulation of the tested TES.

Table 3.3: Parameters chosen for the TES model.

Symbol	Value	Unit	Description
General TES parameters			
V_{store}	848	l	Water volume (cp = 4.19 kJ/kgK, ρ = 998 kg/m³)
Γ_{store}	1.733	m	Height
N_{store}	80	-	Number of nodes for simulation
k_{eff}	1.9	W/mK	Effective vertical heat conductivity
UA_{top}	0.14	W/K	Top heat losses
UA_{bot}	1.25	W/K	Bottom heat losses
UA_{z1}	2.89	W/K	Heat loss UA-value of bottom third section
UA_{z2}	3.17	W/K	Heat loss UA-value of middle third section
UA_{z3}	0.63	W/K	Heat loss UA-value of upper third section
Immersed coil solar heat exchanger			
$z_{sol1,in}$	0.99	-	Relative inlet height of upper heat exchanger
$z_{sol1,out}$	0.55	-	Relative outlet height of upper heat exchanger
$UA_{hx,sol1}$ [a]	222	W/K	UA-value of the upper heat exchanger
$z_{sol2,in}$	0.39	-	Relative inlet height of lower heat exchanger
$z_{sol2,out}$	0.12	-	Relative outlet height of lower heat exchanger
$UA_{hx,sol2}$ [a]	167	W/K	UA-value of the lower heat exchanger
Immersed coil DHW heat exchanger			
$z_{dhw,in}$	0.05	-	Relative outlet height of heat exchanger
$z_{dhw,out}$	0.95	-	Relative inlet height of heat exchanger
$UA_{hx,dhw,base}$	1893	W/K	Base UA-value
m	0.24	-	Mass flow dependency n
n	0.1	-	Temperature difference dependency m
Direct charging space heating double port			
$z_{sh,in}$	0.45	-	Relative inlet height of double port
$z_{sh,out}$	0.97	-	Relative outlet height of double port
$UA_{sh,su,int}$	17	W/K	Fictitious heat loss coefficient of supply (outlet) line inside tank
$UA_{sh,rt,int}$	39	W/K	Fictitious heat loss coefficient of return (inlet) line inside tank

[a] *No dependency of the UA-value on mass flow rate or temperature difference.*

3.2 Method for the determination of stratification efficiency

This Section 3.2 is a summary of results that have been presented in conferences and journals (Haller et al. 2009c; Haller et al. 2009d; Haller et al. 2010a).

A key parameter for high solar gains in solar thermal heating systems is the stratification efficiency of the thermal energy storage (TES) (Lavan & Thompson 1977; Hollands & Lightstone 1989; Andersen & Furbo 2007). Stratification leads to lower collector inlet temperatures and avoids "unnecessary" auxiliary heating by reaching set temperatures for comfort faster and maintaining them longer. Both effects lead to increased savings of conventional fuels such as oil, natural gas, biomass, or electricity that are typically used to maintain the required temperature level in the upper parts of the TES.

For the development and testing of TES, and in particular of components that enhance stratification, it is desirable to have an "index" or "measure" to determine the ability of a TES to promote stratification during charging and discharging as well as to maintain stratification during "standby". Several indices have been proposed and used in the past for this purpose, but despite the extensive research in the field of TES stratification, a widely accepted parameter that can be used to quantify the stratification efficiency of a thermal storage has not emerged yet (Zurigat & Ghajar 2001; Panthalookaran et al. 2007). Existing methods to determine stratification efficiency are analyzed from a theoretical point of view in Part II, Paper I. A new method that combines advantages of the existing approaches is presented in Part II, Paper II. The new method, if applied to any storage process, determines its stratification efficiency alone, eliminating the bias of storage heat losses that some of the previous approaches showed.

3.2.1 Indicators for stratification efficiency

Stratification in TES is a natural phenomenon encountered in liquid storage systems such as water tanks above a temperature of 4 °C. Due to buoyancy forces, hot water tends to accumulate at the top of a TES, whereas colder water will always be forced to move downwards. Therefore, a TES based on water will always show a certain amount of stratification. However, different factors tend to destroy the stratification in a TES (Hollands & Lightstone 1989):

– Plume entrainment occurs when a plume of water develops caused e.g. by buoyancy of hotter fluid that is surrounded by colder fluid (e.g. if the fluid inlet is hotter than the temperature at the position of the inlet or if a TES is charged with an immersed heat exchanger). In this case, a hot plume can be observed that entrains colder surrounding water and mixes with it.

– Inlet jet mixing is caused by the kinetic energy of the water entering the TES.

– Thermal conduction and diffusion occurs within the fluid itself, within the TES wall and the components immersed in the fluid of the TES.

A completely unstratified TES can always be seen as a fully mixed TES. The ability to promote stratification during charging and discharging is not only dependent on the construction of a TES and its stratification enhancing devices, but also on the inlet mass flows and temperatures (Lavan & Thompson 1977; Carlsson 1993; Andersen et al. 2007). Therefore, the boundary conditions of the charging and discharging processes play a crucial role for the determination of any stratification efficiency.

Methods proposed in literature for the evaluation and comparison of stratification efficiencies can be classified as shown in Figure 3.6 as:

– Graphical presentations of temperature curves (not further discussed here).

– Methods based on the thermocline gradient or the thickness of the thermocline region after a particular experiment.

– Methods based on the first law of thermodynamics (considering e.g. the "useful" energy that can be discharged after a TES has been charged).

– Methods based on second law of thermodynamics (exergy or entropy balances or comparison of the exergy or entropy content of the TES after a particular experiment).

– Other methods, e.g. MIX-number proposed by Davidson et al. (1994).
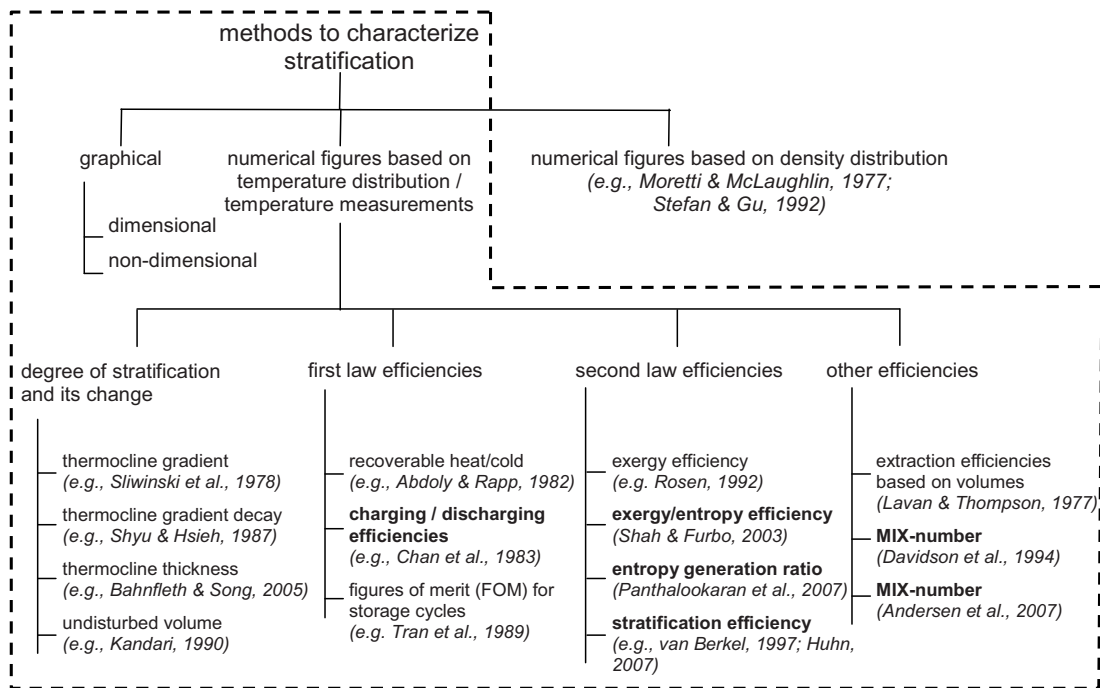
Figure 3.6: Different methods proposed to characterize thermal stratification in water storage. The area within the dashed lines contains the methods that are reviewed in Part II, Paper I.

3.2.2 Gradient or thickness of thermocline and first law efficiencies

Methods based on the thermocline gradient at its centre region have been successfully used e.g. by Sliwinski et al. (1978) and Shyu & Hsieh (1987). Also the fraction of the height of the TES occupied by the thermocline region, or its opposite, has been used for the evaluation of stratification efficiencies (Kandari 1990; Bahnfleth & Song 2005). For the calculation of these numbers, only a snapshot of the temperature distribution within the TES at the end of an experiment is needed. However, it has to be kept in mind that these methods pose certain requirements on the experiment conducted before the snapshot is taken, these are in general:

– A uniform initial temperature.

– A constant inlet temperature during the charging / discharging process.

– A time of charging / discharging that is small enough that the thermocline does not start to leave the TES.

A significant change in inlet temperature during charging might lead to more than one thermocline in the TES. Thus, a variable temperature of charging as it usually occurs in a solar heating circuit cannot be used for the determination of stratification efficiency with these methods.

Other authors have used first law efficiencies for the definition of a stratification efficiency (e.g. Abdoly & Rapp 1982; Chan et al. 1983; Tran et al. 1989). Generally spoken, these methods determine a fraction of useful heat (or cold) that can be recovered after charging and / or discharging. An arbitrary temperature limit determines whether the recovered heat (or cold) is considered to be useful or not. Thus, the recoverable fraction decreases as mixing or destratification increases. These methods generally also pose the requirements of uniform initial temperature and constant inlet temperature on the experiment conducted. Thus, they are also restricted in their application and not well suited for the evaluation of an experiment with variable inlet temperatures.

Another shortcoming of the thermocline gradient and first law methods is that they do not consider the entire temperature profile at the end of the experiment, but only certain key points of the temperature profile, such as the section of highest temperature gradient, or the position of the temperature curve where a certain limiting temperature is reached. Outside of these key points, differences in the temperature curve will not result in a different value for the determined stratification efficiency.

3.2.3 MIX numbers and second law efficiencies

The MIX number (Davidson et al. 1994) and second law efficiencies (Rosen 1992; van Berkel 1997; Shah & Furbo 2003; Panthalookaran et al. 2007; Huhn 2007) have been defined in order to consider the whole temperature curve and to overcome the shortcomings of the above mentioned methods that use thermocline gradient, thermocline thickness or first law approaches.

The mix number (MIX) has been used by Davidson et al. (1994) for the investigation of TES charging processes in solar heating applications. In this method, a "momentum of energy" (M_E) has been defined that is basically the height-weighted average TES energy content (Q). Height (y) being the vertical distance of each water volume from the bottom of the tank:

$$Eq.\ 3.4 \qquad M_E = \sum_{i=1}^{N} y_i \cdot Q_i$$

Values ranging from 0% for a fully stratified TES to 100% for a fully mixed TES can be obtained by comparing the MIX number of an experimental TES (exp) with the MIX numbers of a fully mixed reference TES (mix) and a perfectly stratified reference TES (str):

$$Eq.\ 3.5 \qquad MIX = \frac{M_E^{str} - M_E^{exp}}{M_E^{str} - M_E^{mix}}$$

It has to be noted however that the use of the MIX number defined by Davidson et al. (1994) is based on the assumption that $M_E^{str} \geq M_E^{exp} \geq M_E^{mix}$. This assumption seems to be true for the processes of charging and storing heat in a TES, but it may be violated in the case of discharging heat from a TES (see Part II, Paper I).

Second law efficiencies are based on the second law of thermodynamics and the definitions of entropy and/or exergy that are associated with this law. Looking at an adiabatic system composed of two volumes of water that are at different temperatures, mixing the two volumes will not change the overall energy content of the system, but it will increase the entropy of the system and at the same time decrease the exergy of the system. Unlike energy, entropy and exergy are not conserved in a closed system. In a TES process however, the conservation of entropy and exergy is wanted. The ideal case of any storage process (charging, storing or discharging) is thus the isentropic process.

Therefore, one way of comparing the amount of mixing that is taking place in a storage process is to show the absolute values of entropy generation or exergy losses of the TES, as has been done e.g. by Lohse et al. (2008). Although this is a useful method, the result does not tell us how far from the ideal case of perfect stratification or the worst case of full mixing the investigated process is.

For this purpose, several authors have defined stratification efficiencies η_{st} that range from 0% to 100% using values based on entropy and/or exergy. Similar to the definition of the MIX number, these methods are based on the entropy change ΔS or exergy change $\Delta \xi$ of the experimental process (exp) compared to the reference cases of the perfectly stratified process (str) and the fully mixed process (mix):

$$Eq.\ 3.6 \qquad \eta_{st,S} = \frac{\Delta S^{mix} - \Delta S^{exp}}{\Delta S^{mix} - \Delta S^{str}}$$

$$Eq.\ 3.7 \qquad \eta_{st,\xi} = \frac{\Delta \xi^{mix} - \Delta \xi^{exp}}{\Delta \xi^{mix} - \Delta \xi^{str}}$$

Unfortunately, different authors use different definitions for the perfectly stratified TES as well as for the fully mixed TES, and even different definitions for the entropy change ΔS or the exergy change $\Delta \xi$ of a storage process.

One way to obtain a fully mixed reference TES from an experimental TES is by mixing the experimental TES at any time of the experiment (Figure 3.7 left, middle to bottom). Likewise, a perfectly stratified reference TES can be obtained by rearranging the energy content of the experimental TES at any time of the experiment in a way that only two different temperatures can be found in the perfectly stratified TES (Figure 3.7 left, middle to top). The upper temperature being the highest temperature involved in the experiment (or encountered in the TES), the lower one being the lowest temperature involved in the experiment (or encountered in the TES).
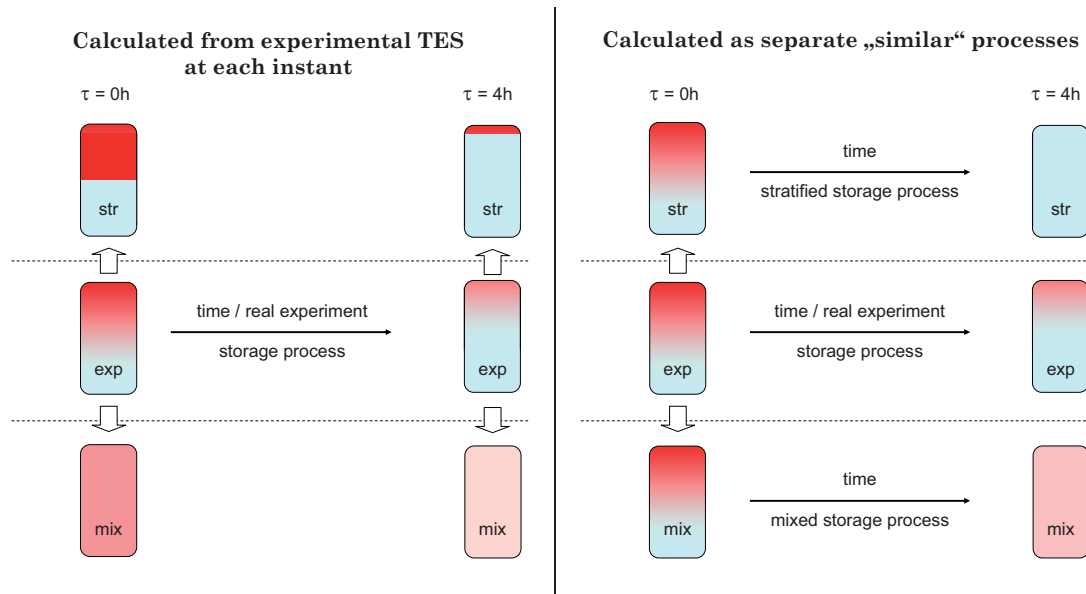
Figure 3.7: Different ways of defining a fully mixed and a perfectly stratified TES for a discharge test. From time 1 (left): Mixing or stratifying the experimental TES at any time (τ) of the experiment. From time 0 (right): Calculating the mixed and the stratified TES processes from the same starting point ($\tau = 0h$) as the experimental TES, with inlet mass flows and temperatures equal to the ones in the experiment. In the example shown, at $\tau = 4h$ the entire volume of the tank has been replaced (plug flow) for the stratified storage process.

This method has been used by Andersen et al. (2007) for the calculation of a MIX number and by Panthalookaran et al. (2007) for the calculation of an entropy generation ratio. Under certain boundary conditions, these methods may deliver useful results. However, there are some critical aspects that must be pointed out:

– In the case of variable inlet temperatures the question arises if the separation of the perfectly stratified TES into two layers of different temperature is a good representation for a perfectly stratifying TES.

– If the experimental TES has reached a uniform temperature, the method of calculation may become undefined (division by zero). Thus, this method can not distinguish (a) a well stratifying experimental TES that has a uniform temperature because it has been charged long enough with a constant inlet temperature, from (b) an experimental TES that has been charged for a short time with a higher inlet temperature, but has reached the same uniform temperature because it is fully mixed.

For experiments where a thermocline is starting to leave the TES the significance of values obtained by these methods is not clear and not in qualitative agreement with the rate of internal entropy production (see Part II, Paper I).

These problems can be avoided by defining a fully mixed or a fully stratified reference TES starting from the experimental TES at the beginning of the experiment, and then applying the same inlet mass flows and temperatures to the reference TES as are applied to the experimental TES (Figure 3.7 right). This method has been proposed by Davidson et al. (1994) for the calculation of MIX numbers, and it has been used for second law efficiencies by van Berkel (1997), Shah & Furbo (2003), and Huhn (2007). van Berkel (1997) assumed that also a fully stratified TES can not avoid thermal diffusion caused by Brownian motion of the water particles inside the TES. In this case, also the perfectly stratified TES process is anisentropic. However, other authors assumed that the perfectly stratified TES process is isentropic (Shah & Furbo 2003; Huhn 2007). This has the advantages that the fully stratified TES process does not depend on the geometry of the TES or the fluid it contains, and it simplifies computation. Davidson et al. (1994) assumed that the perfectly stratifying TES has the same heat loss coefficients as the experimental TES in order to distinguish between heat losses and mixing effects.

Yet another difference in the various methods concerns the definition of entropy change ΔS or exergy change $\Delta \xi$. Shah & Furbo (2003) as well as Panthalookaran et al. (2007) define ΔS and $\Delta \xi$ as the entropy / exergy change of the TES alone, not accounting for the entropy / exergy changes associated with mass flows in and out of the TES. On the other hand, Huhn (2007) does account for these entropy / exergy changes.

3.2.4   Combining advantages of previous approaches

From the theoretical analysis of the existing methods and based on the results presented in Part II, Paper I, the approach presented by Huhn (2007) is chosen because it is expected to have the greatest potential for the application to a wide range of experiments. There is no indication for a restriction to a very specific testing procedure (e.g. a uniform starting temperature or constant charging and discharging temperature of limited time). It has the potential to be also applicable for long term experiments of several days or for annual simulations including realistic charging and discharging profiles. However, a solution for the treatment of entropy and exergy changes that are caused by heat losses to the ambient has not been found for this method in the reviewed literature. An analytical solution for this problem has been worked out and tested on hypothetical TES processes as well as on data from laboratory experiments and is presented in detail in Part II, Paper II. This chapter gives a short summary of this work.

In the following it is assumed that the border of a TES is the boundary of the system that is to be analyzed. As shown in Figure 3.8 the entropy change of a TES may be caused by mass transfer across its boundaries ($\dot{S}_{in}$ and $\dot{S}_{out}$), by heat transfer across its boundaries ($\dot{S}_{hl,store}$) or by internal entropy generation ($\dot{S}_{irr,int}$).

$$\dot{S}_{in} \quad \dot{S}_{out}$$

$$\dot{S}_{irr,int}$$

$$\dot{S}_{hl,store}$$

TES border = system boundary
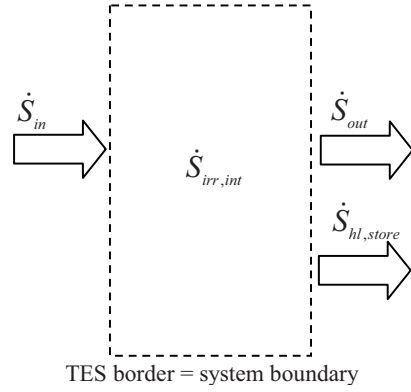
Figure 3.8: System boundary for the calculation of internal entropy generation.

The entropy change rate of a TES process, assuming heat losses and outlet mass flows to be represented by negative values of $\dot{S}_{hl,store}$ and $\dot{S}_{out}$, is:

Eq. 3.8 $\qquad \dot{S}_{store} = \dot{S}_{in} + \dot{S}_{out} + \dot{S}_{hl,store} + \dot{S}_{irr,int}$

For a given storage process of limited time, the entropy change of the TES may be expressed as:

Eq. 3.9 $\qquad \Delta S_{store} = \Delta S_{in} + \Delta S_{out} + \Delta S_{hl,store} + \Delta S_{irr,int}$

And the internal entropy generation of the process is

Eq. 3.10 $\qquad \Delta S_{irr,int} = \Delta S_{store} - \Delta S_{flow} - \Delta S_{hl,store} \geq 0$

With

Eq. 3.11 $\qquad \Delta S_{flow} = \Delta S_{in} + \Delta S_{out}$

The internal entropy generation may be calculated for an experimental TES ($\Delta S_{irr,int}^{exp}$), and for a fully mixed reference TES ($\Delta S_{irr,int}^{mix,hl}$). The fully mixed reference TES is assumed to be equal to the experimental TES at the beginning of the experiment, and fully mixed from this point on to the end of the experiment. Further, the fully mixed reference TES has the same heat loss coefficients as the experimental TES (superscript *hl*), and is subjected to the same inlet mass flows and temperatures. If the experiment does not start with a uniform temperature of the experimental TES, the internal entropy generation of the fully mixed reference TES includes also the entropy generation obtained from mixing the whole TES at the beginning of the experiment. Based on these assumptions, the stratification efficiency ($\eta_{st,S}$) is calculated based on the internal entropy generation of the experimental TES relative to the internal entropy generation of the fully mixed reference TES as shown in Eq. 3.12. This value will be 0 if the storage tank was always fully mixed during the experiment and 1 for a perfectly stratified, isentropic storage process.

Eq. 3.12 $\qquad \eta_{st,S} = 1 - \dfrac{\Delta S_{irr,int}^{exp}}{\Delta S_{irr,int}^{mix,hl}}$

Another route for the calculation of this stratification efficiency is based on the internal exergy loss of the experimental TES ($\Delta \xi_{irr,int}^{exp}$) relative to the internal exergy loss of a fully mixed reference TES ($\Delta \xi_{irr,int}^{mix,hl}$), i.e.

$$Eq.\ 3.13 \quad \eta_{st,\xi} = 1 - \frac{\Delta \xi_{irr,int}^{exp}}{\Delta \xi_{irr,int}^{mix,hl}}$$

With $\Delta \xi_{hl,store}$ being a negative value in the case of net heat losses, and $\Delta \xi_{irr,int}$ defined as:

$$Eq.\ 3.14 \quad \Delta \xi_{irr,int} = \Delta \xi_{store} - \Delta \xi_{flow} - \Delta \xi_{hl,store} \leq 0$$

In this case, the exergy changes are calculated based on the enthalpy changes (ΔH), the entropy changes (ΔS), and the thermodynamic dead state temperature (T_0).

$$Eq.\ 3.15 \quad \Delta \xi = \Delta H - T_0 \cdot \Delta S$$

Because internal mixing does not change the enthalpy content of the TES ($\Delta H_{int} = 0$), the internal exergy loss of a TES is directly proportional to the internal entropy generation (Eq. 3.16). Thus, the stratification efficiency based on the relative internal exergy loss equals the stratification efficiency based on relative internal entropy generation (Eq. 3.17).

$$Eq.\ 3.16 \quad T_0 \cdot \Delta S_{irr,int} = -\Delta \xi_{irr,int}$$

$$Eq.\ 3.17 \quad \eta_{st,\xi} = \eta_{st,S}$$

This identity has already been pointed out by Huhn (2007).

The enthalpy and entropy change of the TES caused by the charging and discharging processes, assuming that the inlet mass flow equals the outlet mass flow, evaluated at the time τ_1, are:

$$Eq.\ 3.18 \quad \Delta H_{flow}(\tau_1) = \int_{\tau_0}^{\tau_1} \dot{m}(\tau) \cdot \left[h\{T_{in}(\tau)\} - h\{T_{out}(\tau)\} \right] \cdot d\tau$$

$$Eq.\ 3.19 \quad \Delta S_{flow}(\tau_1) = \int_{\tau_0}^{\tau_1} \dot{m}(\tau) \cdot \left[s\{T_{in}(\tau)\} - s\{T_{out}(\tau)\} \right] \cdot d\tau$$

The enthalpy and entropy change of the TES, from the beginning of the experiment until the time τ_1 are:

$$Eq.\ 3.20 \quad \Delta H_{store}(\tau_1) = \int_{0}^{m_{store}} \left[h\{T_{store}(\tau_1,m)\} - h\{T_{store}(\tau_0,m)\} \right] dm$$

$$Eq.\ 3.21 \quad \Delta S_{store}(\tau_1) = \int_{0}^{m_{store}} \left[s\{T_{store}(\tau_1,m)\} - s\{T_{store}(\tau_0,m)\} \right] dm$$

The enthalpy change due to heat losses is calculated based on the heat transfer coefficient area products $UA(m)$ between each mass element and the ambient:

$$Eq.\ 3.22 \quad \Delta H_{hl,store}(\tau_1) = \int_{\tau_0}^{\tau_1} \int_{0}^{m_{store}} \frac{-UA(m) \cdot \{T_{store}(\tau,m) - T_{amb}(\tau)\}}{m_{store}} dm \cdot d\tau$$

With $\dot{S} = \dot{Q}/T$ given for the entropy change rate associated with heat transfer, the entropy change of the TES caused by heat losses is:

$$Eq.\ 3.23 \quad \Delta S_{hl,store}\left(\tau_1\right) = \int_{\tau_0}^{\tau_1} \int_0^{m_{store}} \frac{-UA(m)\cdot\left\{T_{store}\left(\tau,m\right) - T_{amb}\left(\tau\right)\right\}}{m_{store}\cdot T_{store}\left(\tau,m\right)} dm\cdot d\tau$$

For the calculation of the fully mixed reference store, the time dependent inlet temperatures and mass flows and the ambient temperatures are identical to the ones that are measured (or simulated) for the experimental TES. The TES temperature of the fully mixed reference TES is at the same time its outlet temperature. For time periods with constant charging or discharging mass flow and inlet temperature, the temperature of the fully mixed reference TES at time τ_B is calculated from the temperature at the beginning of this period ($T_{store}^{mix,hl}\left(\tau_A\right)$), the temperature T_{inf} that would be reached after an infinite time, and the time constant a of the process:

$$Eq.\ 3.24 \quad T_{out}^{mix,hl}\left(\tau_B\right) = T_{store}^{mix,hl}\left(\tau_B\right) = T_{inf} - \left[T_{inf} - T_{store}^{mix,hl}\left(\tau_A\right)\right]\cdot EXP\left(-a\cdot\left[\tau_B - \tau_A\right]\right)$$

With

$$Eq.\ 3.25 \quad T_{inf} = \frac{UA\cdot T_{amb} + \dot{C}_{flow}\cdot T_{in}}{UA + \dot{C}_{flow}}$$

$$Eq.\ 3.26 \quad a = \frac{UA + \dot{C}_{flow}}{C_{store}}$$

Where $\dot{C}_{flow}$ is the capacity flow rate of the charging or discharging process, and C_{store} is the thermal capacitance of the TES.

Detailed examples for the calculation of $\eta_{st,S}$ and $\eta_{st,\xi}$ based on measurements are shown in Part II, Paper II.

3.2.5 Theoretical and experimental validation

Simulations of a charging, standby and discharging experiment are described in detail in Part II, Paper II, and summarised briefly here. The simulation is based on a 10 node model with each node fully mixed. The experiment starts with a uniform TES temperature of 20 °C at the beginning, a charging phase with an inlet temperature of 50 °C where about 80% of the fluid is replaced, a standby period of 4.2 h and a discharge with an inlet temperature of 20 °C. In the model, the temperatures of all nodes were calculated in a stepwise manner according to the following sequence, without the need of iterations:

1. Fluid replacement during the charging or discharging process

2. Mixing of 3 nodes in the inlet region of the charging or discharging process for the simulation of inlet jet mixing

3. Vertical diffusion and conduction of heat based on the temperature distribution resulting from the previous calculation steps

4. Heat losses to the ambient based on the difference between the ambient temperature and the average temperature of each node at the beginning and at the end of this time step (using the results of step 3).

Stratification efficiencies based on relative entropy generation $\eta_{st,S}$ and relative exergy losses $\eta_{st,\xi}$ were calculated using Eq. 3.10 to Eq. 3.15. These numbers are compared to results based on a calculation that does not account for exergy and entropy changes due to heat losses in both, the experimental TES and the fully mixed reference TES:

$$Eq.\ 3.27 \quad \eta_{st0,S} = 1 - \frac{\Delta S_{store}^{exp} - \Delta S_{flow}^{exp}}{\Delta S_{store}^{mix} - \Delta S_{flow}^{mix}}$$

$$Eq.\ 3.28 \quad \eta_{st0,\xi} = 1 - \frac{\Delta \xi_{store}^{exp} - \Delta \xi_{flow}^{exp}}{\Delta \xi_{store}^{mix} - \Delta \xi_{flow}^{mix}}$$

For the calculation of exergy, a thermodynamic dead state temperature of $T_0 = 298.15$ K has been assumed.

Figure 3.9 shows that the resulting stratification efficiencies $\eta_{st0,S}$ and $\eta_{st0,\xi}$ that were calculated without taking into account the entropy / exergy change caused by heat losses are not equal to each other ($\eta_{st0,S} \neq \eta_{st0,\xi}$). The difference is quite large, even though a relatively small heat loss coefficient of 0.5 W/K has been assumed for the TES with a water content of 140 kg. If the entropy / exergy change due to heat losses is separately accounted for, the stratification efficiency based on internal entropy generation is, as expected, equal to the stratification efficiency based on internal exergy losses ($\eta_{st,S} = \eta_{st,\xi}$). From the comparison of Figure 3.9a and b, two main conclusions can be drawn. First, the deviation of the calculated stratification efficiencies $\eta_{st0,S}$ and $\eta_{st0,\xi}$ becomes larger with increasing heat loss coefficients of the TES. Second, no significant difference can be seen between the values of $\eta_{st,S}$ of the two example calculations with different heat loss coefficients.
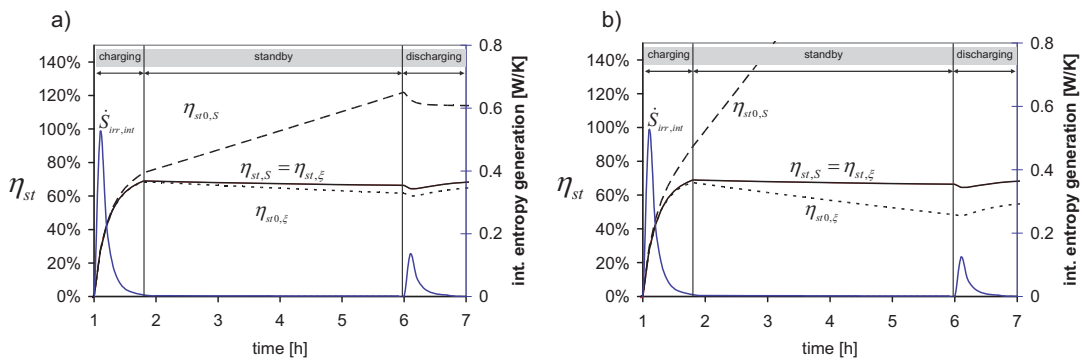
Figure 3.9: Second law stratification efficiencies for a simulated TES process with heat losses of (a) UA = 0.5 W/K and (b) UA = 2.0 W/K.

Neglecting the influence of heat losses on the exergy balance of the TES obviously results in reduced values for the stratification efficiency based on the

exergy balance. This can be explained by the fact that exergy loss associated with heat losses are unintentionally counted as internal exergy loss in the calculation procedure, thereby increasing this value and decreasing the calculated stratification efficiency. At first sight it might come as a surprise that if the stratification efficiency is calculated based on the entropy balance, neglecting the effect of heat losses has the opposite effect. This is a consequence of the entropy flow associated with heat transfer. If a TES is loosing energy to the ambient it looses at the same time entropy. Therefore, unintentionally including this entropy loss in the calculation for internal entropy generation decreases the calculated internal entropy generation.

Similar experiments have been performed on two real TES in the laboratory and the stratification efficiencies have been calculated based on measurements. Details about the experiment and the measurement procedure are presented Part II, Paper II. Figure 3.10 shows different stratification efficiencies η_{st} at the end of experiments of charging, standby and discharging performed with different mass flow rates for one TES. For two of the experiments, the heat losses have been increased from 11 W/K to 17 W/K by removing part of the insulation of the TES. It shows that $\eta_{st,\xi}$ are 7 - 10 percent-points higher than $\eta_{st0,\xi}$. At the same time, the differences between the stratification efficiencies obtained with different insulation are significantly higher for the calculations without heat loss correction $\eta_{st0,\xi}$ than for the calculations that account separately for the exergy lost to the ambient $\eta_{st,\xi}$. It is an open question if the remaining differences of 1.0 – 1.5 percent-points between the stratification efficiencies $\eta_{st,\xi}$ for experiments with different insulation is a bias caused by the uncertainty of measurement and calculation, a bias of the method itself, or a result of different amount of internal irreversibilities / mixing that occurred in reality during the performed experiments. An uncertainty of 20% for the determined heat loss coefficients e.g. leads to uncertainties of $\eta_{st,\xi}$ in the order of 1.1 – 1.7 percentage points for the experiments shown.
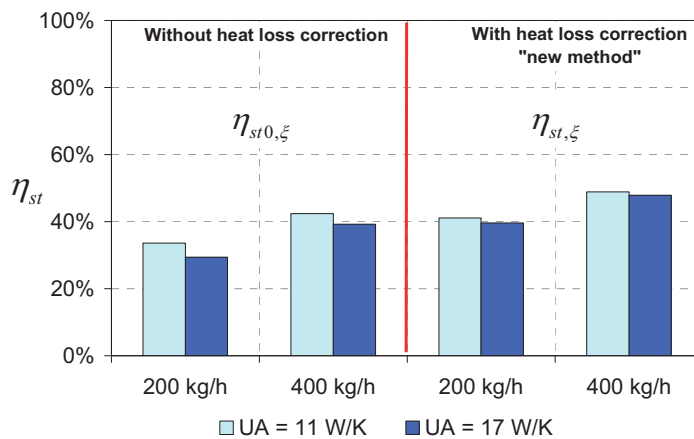
Figure 3.10: Stratification efficiencies at the end of experiments comprising charging, standby and discharging.

4 The Collector

4.1 Adaptations of the IEA-SHC Task 26 collector model

The collector model chosen for the simulations is based on the model developed within the IEA-SHC Task 26 (Perers & Bales 2002). Due to problems encountered when using this model in combination with small simulation time steps and/or a large thermal capacitance of the solar collector, the model was adapted.

In the original model, unstable outlet temperatures just after the fluid flow starts or stops were observed to cause problems for control and solver algorithms. The reason for this was found to be the different assumptions used during times without mass flow and times with mass flow. At times without mass flow, it is assumed that the whole effective thermal capacitance of the collector is at one and the same temperature. At times with mass flow, it is assumed that the temperature at the inlet is different than at the outlet, and that the stored heat can be calculated by multiplication of the thermal capacitance with the average temperature $t_m = (t_{out} + t_{in})/2$. Thus, if the mass flow starts in this timestep, but the solar heat gain within this timestep is little in comparison to the thermal capacitance, the energy stored in the thermal mass of the collector remains almost the same. This means that t_m remains about the same, and since t_{out} must be above t_m about as much as t_{in} is below t_m, the outlet temperature rises abruptly, which is not what is expected from a real collector's behaviour. Thus the possibility of splitting the collector's thermal capacitance in a number of serial segments was introduced as proposed by Antoine Dalibard (2009) to mitigate this problem. The assumptions for the segmented collector model are:

– Each segment of the collector receives the same irradiation. The outlet temperature of a segment is at the same time the inlet temperature of the next segment.

– For each segment of the collector, the heat loss rate to the ambient is the same, calculated based on the average temperature difference of the mean collector temperature $(t_m = (t_{out} + t_{in})/2)$. Thus, the steady state efficiency of the whole collector is still in agreement with the theory behind the results of collector tests according to EN 12975-2:2001.

– However, when the mass flow stops, the temperature differences between the fluids in different segments would persist if all segments would have the same heat loss rate, causing the outlet temperature of the last segment to rise higher than the expected stagnation temperature. Therefore, in the case of zero mass flow rate, the temperature difference to the ambient and the resulting heat loss rates are calculated for each segment separately, based on the temperature difference between the segment and the ambient. Thus, the temperature differences between the segments disappear with time after the fluid flow stops.

The updated model description is included in Appendix B. Figure 4.1 shows a comparison of simulation results using a small time step. More details on the

boundary conditions of the simulation shown in this figure are also listed in Appendix B.
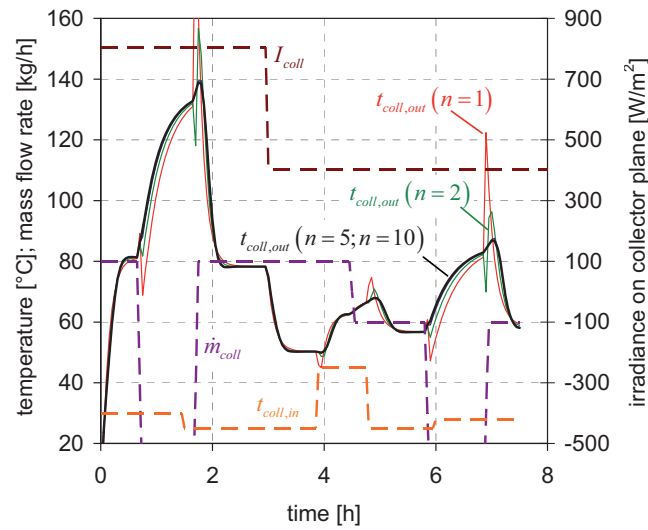
Figure 4.1: Collector model test results for n = 1,2,5 and 10 nodes simulations.

For the application used in this work, dependencies of the collector performance on wind speed and infrared radiation exchange are assumed to be negligible. Also, it has been assumed that the collector temperature is always above the ambient temperature during its operation. In this case, the model equation can be reduced to the well known steady state efficiency approximation with an additional term for the heat stored in the thermal capacitance C_{coll}:

$$Eq.\ 4.1 \quad \dot{Q}_{out}/A_{coll} = \eta_0 \cdot \left(K_b \cdot I_b + K_d \cdot I_d \right) - a_1 \cdot \left(t_m - t_{amb} \right) - a_2 \cdot \left(t_m - t_{amb} \right)^2 - \frac{C_{coll}}{A_{coll}} \cdot \frac{dt_m}{d\tau}$$

5 Combined solar and pellet heating systems

5.1 State of the art

5.1.1 Hydraulic Concepts

This overview is restricted to solar combisystems that are compact, i.e. they provide domestic hot water (DHW) and space heat from one TES (solar combistore) only. Thus, two heat sources are charging the TES: the solar thermal collectors and a pellet boiler or burner. Two heat loads are discharging the TES: DHW consumption and space heat supply. Figure 5.1 shows hydraulic concepts for the combination of these compact solar and pellets heating systems. Figure 5.1a corresponds to the TES evaluated in Section 3.1.
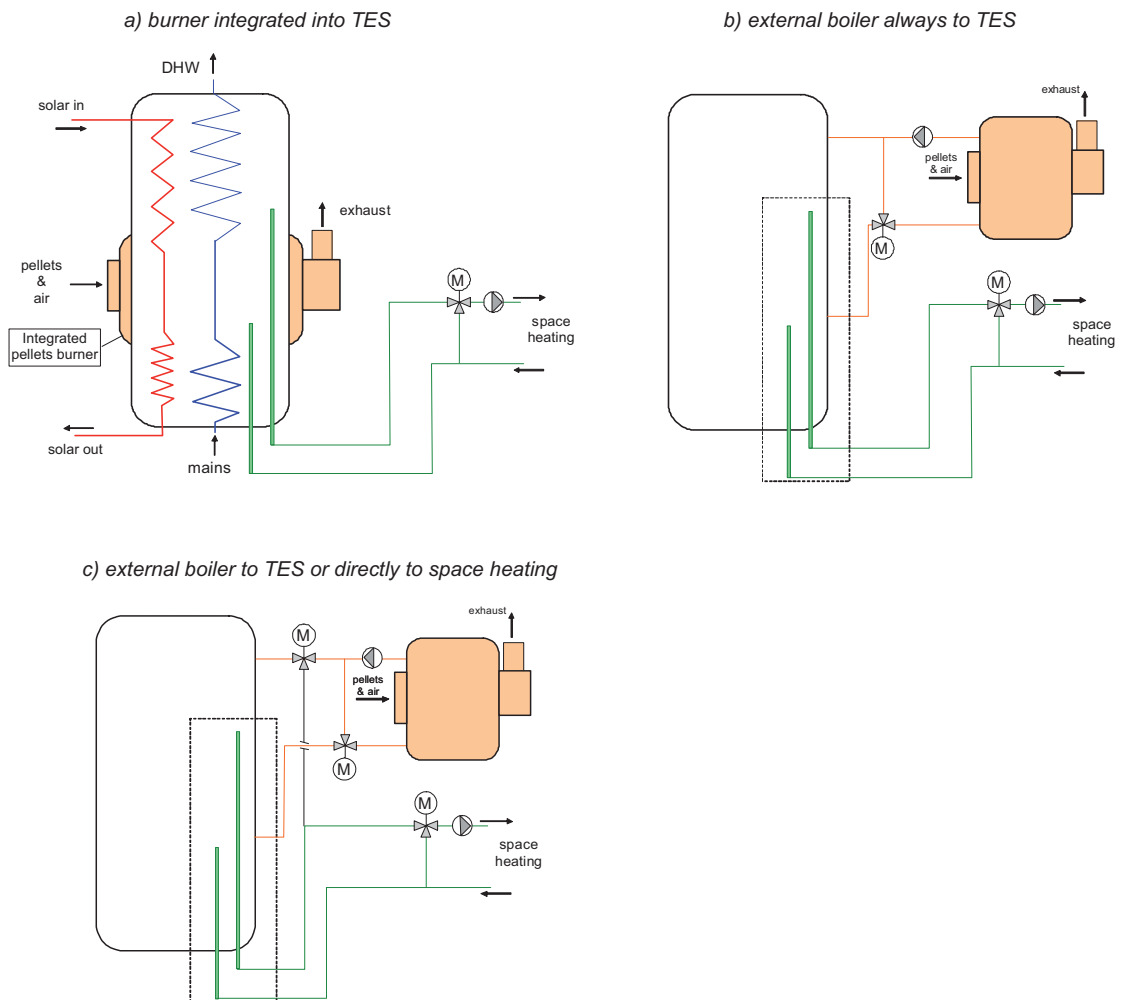
Figure 5.1: Different hydraulic concepts for the integration of the pellet burner or boiler into the system.

For the other variants shown in Figure 5.1, DHW preparation from the TES and solar heat input into the TES are not shown, and just one possible example is shown for the configuration of the space heating connections to the TES (within dashed lines). In variant b, the boiler always charges the TES. In variant c, the boiler may deliver heat directly to the space heating system, and excess heat from the boiler is charged into the TES automatically as soon as the mass flow on the secondary side (TES side) of the boiler loop is larger than the mass flow on the primary (TES side) of the space heating loop.
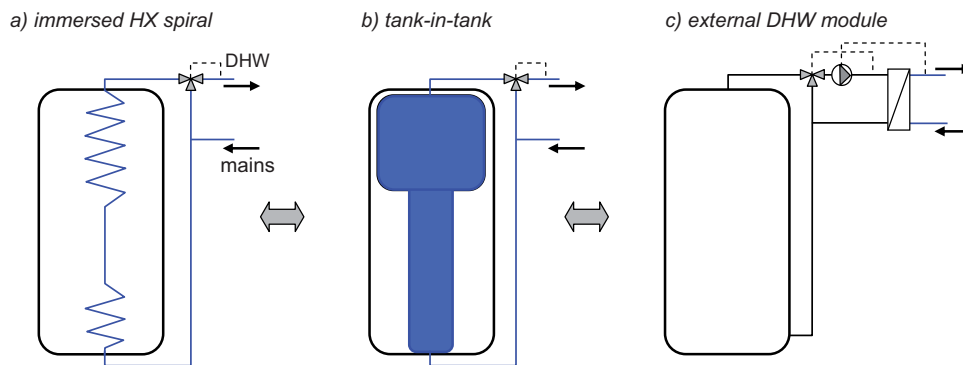
Figure 5.2: Different variants for DHW preparation from a solar combistore.

Different variants for the preparation of DHW from a solar combistore are shown in Figure 5.2, and different variants for the solar heat input in Figure 5.3. For the solar heat input it is assumed that an antifreeze solution is used in the collector loop and a heat exchanger is therefore always needed.
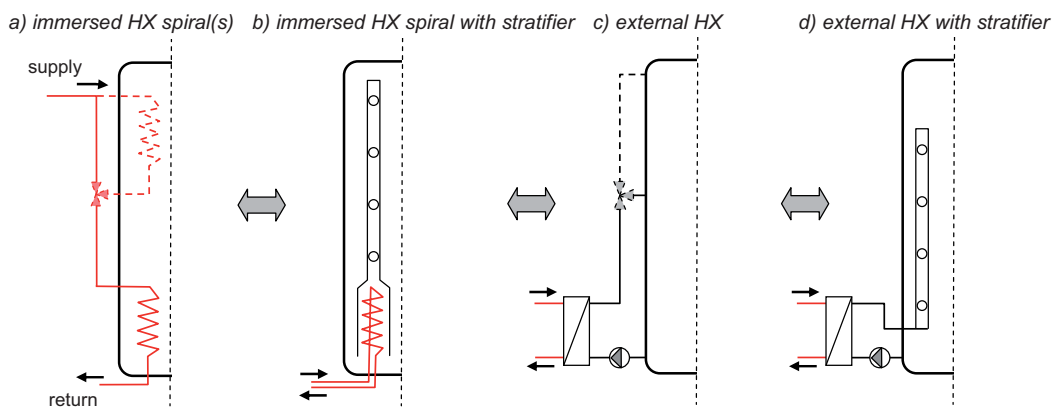
Figure 5.3: Different variants for solar heat input into a solar combistore. variants a and c are both possible with one or more inlet heights each.

The connections for the space heating discharge can be placed at the bottom, with internal pipes reaching to the levels of fluid intake and release (Figure 5.4c), or the connections can be directly to the side of the TES (Figure 5.4a). In both cases, a stratifier may be used for the return line of the space heat (Figure 5.4b & d).

a) direct connection to the side

b) direct connection to the side with inlet stratifier

c) internal pipes connected at bottom

d) internal pipes connected at bottom with inlet stratifier

supply

return
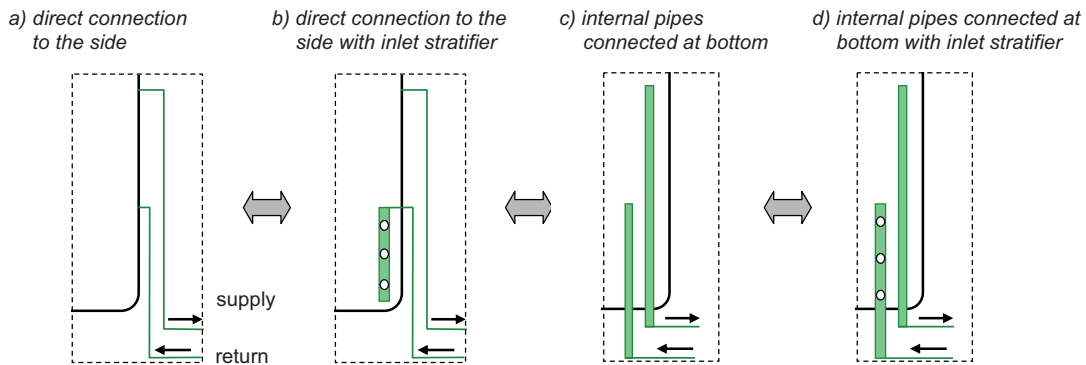
Figure 5.4: Different variants for space heating connections for a solar combistore.

5.1.2 Solar combisystems

Results from laboratory measurements and annual simulations on ten solar combisystems with oil and gas for auxiliary heating showed annual fuel energy savings[8] of up to 30% for a flat plate collector area of 15 m² and a heat load of 18.5 MWh/a (67 GJ/a) in a Central European climate (Haller & Vogelsanger 2005a; Haller & Vogelsanger 2005b). In these investigations it has also been shown that the burner integration into a TES may cause large heat losses if the difficult task of insulating the burner integration is not solved adequately. Furbo & Thür (2008) reported annual fuel energy savings in the order of 530 – 590 kWh (2.1 GJ) per m² of collector area for a house with a total heat demand for space heat and DHW of 20 MWh/a (72 GJ/a). These calculations were based on field measurements on a system with 6.75 m² of collector area and a condensing natural gas boiler. Two thirds of the savings were attributed to the solar thermal heat gain, one third to other system improvements.

An extensive theoretical study on solar combisystems has been carried out by Andersen & Furbo (2007). Solar combisystem storage tanks with different concepts for the preparation of DHW were compared based on simulations. The authors found that the tank-in-tank concept outperformed the concepts of internal heat exchanger spirals and external DHW unit if inlet stratifiers were used both in the solar collector loop and in the space heating loop. They also found that the largest increase in energy savings by using inlet stratifiers could be expected in spring and in autumn, where most of the utilizable solar yield is achieved in a solar combisystem. Andersen (2007) proposes that future research shall address the question of whether it is advantageous or not to integrate the auxiliary burner directly into the solar combistore.

Several studies have been performed on the influence of mixing or stratification on the performance on solar combisystems (e.g. Andersen 2007; Andersen & Furbo 2007; Furbo & Shah 2005). In particular, Thür & Furbo (2005) found that heat transfer through the walls of immersed PEX pipes in the tank that reach from the bottom to the place of fluid intake or release may transfer as much as

---

[8] compared to a reference heating systems without the use of solar thermal energy.

10-15% of the energy to the lower part of the TES, thereby reducing the energy savings achieved by solar heat input.

Knudsen (2002) analysed the heat transfer in a "tank-in-tank" combistore and found that the outside heat transfer coefficient of the inner tank depends very much on the flow conditions in the outer tank. Jordan & Vajen (2000) compared simulation results obtained with a realistic DHW profile on a 1-min time scale with a simplified model of 3 draw-offs per day. They found that the choice of the DHW profile may have significant impacts on the simulated performance of a solar combisystem. Furbo et al. (2005) found that the performance of solar combisystems can be increased if discharge of DHW is done from different levels of the combistore.

Lorenz et al. (2000) studied different designs of solar combisystems for the Swedish climates. A "base case" system commonly found on the Swedish market with internal heat exchanger spiral for DHW preparation was gradually improved in simulation studies. They found that fractional energy savings could be increased by over 30% from the reference combisystem, without change of system size, collector type or load size. One major improvement in performance was achieved by using an external DHW unit instead of the two internal heat exchangers in the store, which allowed for lower set temperatures in the auxiliary heated zone of the TES. Another improvement was achieved by lower return temperature from the heating circuit.

5.1.3   Combined solar and pellet heating systems

Combined solar and pellet heating systems are sold and installed in Europe today. Efficient and reliable products are available for solar thermal components as well as for pellet boilers. It is not difficult to connect both and make a combined solar and pellet heating system. However, it has been shown for solar combisystems with oil and gas as an auxiliary heat source that just connecting good components does not automatically make a good system (Haller & Vogelsanger 2005a). The reason for this is that the interaction between the two heat sources is of vital importance for the replacement of oil or gas by solar heat.

Overgaard & Ellehauge (2000) investigated 12 different types of solar & biomass heating systems for houses in Denmark, three of the systems were monitored over a year, and one of those was equipped with an automatic pellet boiler. Frequent problems encountered where a) oversized biomass boilers compared to heat demand; b) undersized storage volumes compared to boilers; c) safety problems; d) over- or undersized collector areas; e) insufficient insulation.

Detailed investigations about combined solar and pellet heating systems have been carried out by Fiedler (2006) and Persson (2006). Fiedler (2006) studied 4 solar and pellet heating systems based on laboratory measurements of system components and subsequent simulations with annual dynamic simulations, using the biomass stove and boiler model developed by Nordlander (2003). Two of the investigated systems comprised a pellet stove and two systems were solar combisystems, one with a storage integrated pellet burner, the other one with a separate pellet boiler. He found that total CO emissions can be reduced by reducing the number of start and stops, depending on the amount of emissions

increase at part load operation and on the amount of additional emissions associated with each start and stop of the burner. He concluded that the system performance (both energetic and in terms of emissions) can be significantly improved by a proper control of the pellet burner, and by sizing the pellet burner according to the size of the peak space heating demand. He also concluded that a multi node model for the thermal mass of the water in the stoves or boilers would better simulate transient behaviour than the one node approach used. Persson (2006) investigated how electrically heated single-family houses that are common for Sweden can be converted to pellet and solar heating systems, and how the annual efficiency and solar gains can be increased in such systems. He also investigated CO emissions and simulated pellet stoves and pellet boilers using the same model as Fiedler. He concluded that the reductions in pellet consumption are larger than the solar gains if the system is properly designed, and large reductions in carbon monoxide emissions are possible through the combination of a pellet boiler with a solar thermal system. The studies of Fiedler and Persson included only a few solar combisystems, and the solar thermal systems were small (5-10 m², 330-700 l) compared to solar combisystems that are common for Austria or Switzerland (10-20 m², 700 – 1000 l).

Faninger (2000) summarizes results of operational data and experiences of combined solar-biomass district heating systems in Austria. He found that small-scale biomass district heating plants cause problems when used all year. The reason for this is that the biomass boiler cannot operate efficiently outside the heating season because the heat demand is too low. Thus, the boiler is largely oversized for this period of the year which leads to frequent ON/OFF operation. Faninger claims that with solar supported district heating plants it can be achieved that heat outside of the heating period can be produced to a large extent by the solar plant. Thus, low load operation and emissions of the boiler can be reduced.

In a project funded by the European Commissions Innovation Programme, several combined solar and pellet heating systems were monitored in different countries with the purpose of elaborating guidelines for the planning of these systems (Bemmann et al. 2006). The authors concluded that the controllers of all systems they studied controlled the boiler and the solar thermal system independently of each other, and did not take into consideration knowledge about the whole system. This resulted in frequent auxiliary heating on days where there would have been enough solar energy input to cover the whole demand. An example of such a system is reported in more detail in Chasapis et al. (2008).

5.1.4 The importance of boiler cycling and power modulation

Automatic pellet boilers that are sold in Central Europe today are usually equipped with the possibility to reduce the combustion rate (power modulation) to match reduced heat demand. This capability enables the boiler to serve a wider range of heat loads without the need of stopping the burning process or reducing it to a pilot flame. Intermittent operation of the burning process (ON/OFF cycling) is unwanted because each start and stop of the combustion process (a) causes additional emissions of air pollutants (b) may reduce the lifetime of the boiler and (c) may need electric energy for fuel ignition. A

prolongation of the steady burning phase may be achieved by (a) increasing the storage capacity of the TES and the overall system, (b) increasing the temperature swing of the boiler and the system (c) controlling the combustion rate to match the load. Larger storage capacities and temperature swings usually lead to increased heat losses, since either the warm surface areas are increased (larger TES) or the temperatures in the system are increased. Therefore, the possibility to reduce the combustion rate is advantageous.

For the evaluation of the possible reduction of emissions by combustion power modulation, several aspects have to be taken into account:

1. Increased emissions of CO and hydrocarbons usually occur at the start phase and in the glowing out phase of the combustion process (Eisl 2006; Heinz 2007; Fiedler & Persson 2009), but increased emissions of particulate matter are usually only observed in the start phase (Hartmann et al. 2004; Klippel & Nussbaumer 2007a).

2. Pellet and wood chip boilers usually – but not always - emit more CO and hydrocarbons, but not more particles (in terms of mass) at part load than at full load (Hartmann et al. 2003; Hartmann et al. 2004; Hartmann et al. 2006; Fiedler & Persson 2009; Boman 2005; Good & Nussbaumer 2009).

3. Obernberger et al. (2007) found higher fraction of carbonaceous material in particles that were collected from part load operation in comparison to those that were collected in full load operation. The fraction of carbonaceous material was highest for particles that were collected during the start phase of the burning process of a tiled stove. Similar results were presented by Good & Nussbaumer (2009). This is of particular interest because Klippel & Nussbaumer (2007b) found that the toxic and carcinogenic effects of particulate matter from combustion processes increases with the fraction of carbonaceous material in the particles. In their investigations, particles that were composed mainly of inorganic salts showed similar low toxic and carcinogenic potential as the pure salt that was the main constituent.

4. For log wood stoves and boilers it has been shown that the level of emissions that occur during burner start depends significantly on the start-procedure (Vock & Jenni 2007; Nussbaumer et al. 2008). It is likely that also for automatic pellet boilers the start- and stop-procedures have a significant influence on the total additional start and stop emissions.

Fiedler et al. (2007) claim that for most systems the modulating operation mode has a positive impact on carbon monoxide emissions. Good & Nussbaumer (2009) have performed measurements on two modern automatic pellet boilers and conclude that the measured emissions are below the maximum levels set by legislation in Switzerland at continuous full load operation and in cycling ON/OFF operation with more than 80 minutes cycle-time. However, the emission levels for continuous operation set by legislation may be exceeded by a factor of 10 – 20 for CO, and by a factor of up to 5 for VOC (up to 10 for non-methane VOC), if cycling times are very short or if no steady burning phase is reached after the burner start. A large increase of CO emissions under cycling conditions was also reported by Eisl (2006) and Heinz (2007).

To which extent a reduction of boiler ON/OFF cycling by means of power modulation leads to decreased emissions of CO and particulate matter on an annual base is a question that is outside the scope of this work. From the literature cited above it can be concluded that (a) the topic is highly complex and

(b) the results might also be highly dependent on the specific boiler product under investigation. Higher emissions at part load are most likely due to cooler temperatures in the combustion zone or insufficient control or distribution of combustion air. Thus, it seems possible that technical solutions for this problem will be developed. However, it seems unlikely that additional emissions for the start- and stop of the burning process can be avoided completely. For instance, the development of oil and gas burners has been going on for decades, but still additional start and stop emissions are reported for these units (Pfeiffer et al. 1999; Heinz 2007; Eisl 2006).

Finally, the reduction of the number of start- and stop cycles is expected to decrease emissions significantly and possibly also increase the efficiency of biomass heating systems and is therefore a goal for the planning, installation and operation of such systems (compare Good et al. 2005).

5.1.5 Control of solar TES charging by external boiler units

Little literature has been found concerning the importance of the control of solar TES charging by external boiler units. Fiedler et al. (2007) investigated the influence of the availability of power modulation of the boiler as well as the influence of correct sizing of the biomass boiler by simulation studies. They found that the number of burner starts decreased from about 2000 for ON/OFF operation of an oversized boiler to about 900 for a correctly sized boiler in modulating operation with a minimum part load ratio of 40%. Konersmann et al. 2007) found a reduction from about 2900 starts per year for a severely oversized modulating boiler connected to a solar TES to about 700 starts for an optimized system. Detailed investigations on the control of TES charging including the influence of temperature set points for the boiler supply (outlet) and for the water in the TES have not been found.

Padinger (2002) developed and tested an optimized control system for a biomass boiler for direct space heating without a TES, based on a PID control of the supply temperature (outlet of the boiler) with influence of the measured return temperature from the space heating system (disturbance variable).

Bühler & Jenni (2009) and Gabathuler (2009) investigated installed small district heating networks where a pellet boiler is connected to a TES and found that most of the time a boiler that theoretically has the ability to modulate its power is not using this ability due to ineffective control strategies. They found that an average temperature measurement of the TES is the ideal process variable for the control of the combustion power of the boiler, and proposed to obtain this average temperature by averaging the temperatures measured by several sensors, or by connecting several Pt-resistance sensors in series. Thus, only one pair of sensor cables has to be connected to the electronic board of the controller.

Haberl et al. (2009) have tested three pellet and solar heating systems under realistic load profiles in a 12 days test in the laboratory and have found that in all three systems the pellet boilers did not use the ability of power modulation effectively. Thus, the number of burner starts observed was much higher than necessary for all three systems.

5.2 Field measurements

5.2.1 Method

Five combined solar and biomass heating systems have been monitored in 2008/09 within the project "PellSol Plus", financed by the Austrian Climate and Energy Fund as part of the "Energy of Tomorrow" programme. The heating systems are all located in the Austrian State of Styria, are equipped with the same type of solar collectors and TES, and have different automatic pellet and wood chip boilers. An overview of the specifications for the five systems is given in Table 5.1. Labels A to E are used to refer to the systems for reasons of anonymity. In all systems, a two line local heat network serves the space heating and DHW demand of one or several houses. The general hydraulic schematic is shown in Figure 5.5.

Table 5.1: Specification of the monitored solar and pellet heating systems.

Parameter	Unit	A	B	C	D	E
Nominal boiler heating power	kW	40	150	60	100	20
TES volume	l	2 x 1500	2 x 1500	2 x 1500	2 x 1500	1 x 800
Flat plate collector area	m^2	24	24	42	21	10.5
collector orientation (-90 = east)	°	-15	10	0	0	55
collector slope	°	45	65	45	64	80
Energy meter in solar collector loop	-	YES	YES	YES	YES	YES
Energy meter in boiler loop	-	YES	YES	NO	NO	NO
Energy meter in heat distribution	-	YES	YES	YES	NO	NO
Measured values						
Maximum load measured in Jan. 09[9]	kW	21	72	20	--	--
Average outdoor temperature during max. load	°C	-4.9	-0.1	-4.7	--	--
Supply temperature of grid	°C	58-66	57-64	47-73	--	--
Return temperature of grid	°C	35-42	42-56	30-50	--	--
Evaluated measurement period	-	11/2008 to 10/2009	11/2008 to 10/2009	11/2008 to 10/2009	--	--

---

[9] Daily average.
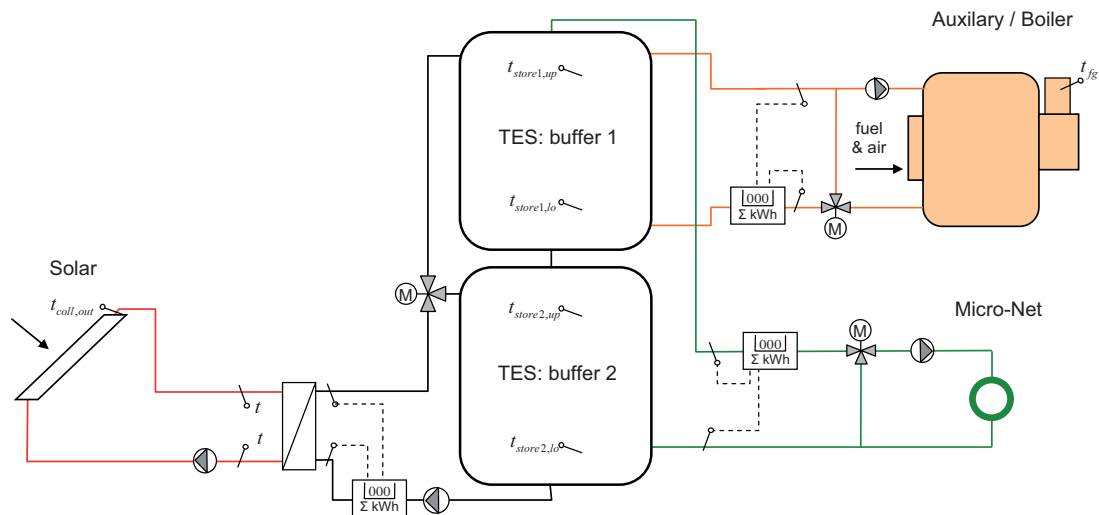
Figure 5.5: General hydraulic and monitoring schematic of the monitored systems.

Differences in the hydraulic schematic of the five systems are:

–   The boilers of systems B and D are equipped with a draught fan in the chimney because of limited flue gas chimney height.

–   System E has only one TES, and the hydraulic connection of the boiler to the system is directly to the heating supply distribution as well as to the TES.

–   For systems A, C, and D, the boiler is only charging TES 1. For system B, 75% of TES 2 is also used for charging by the boiler (Figure 5.5).

Heat meters were installed in all solar collector loops on the secondary side (TES side) of the solar heat exchanger. For three systems, heat meters were also installed on the heat load side, and only for two systems heat meters were also installed in the boiler circuit. All heat meters were of the types Kamstrup Multical or ISTA, class 3. The standard uncertainty (u) for the heat meter readings were calculated based on the standard deviation of an assumed rectangular error distribution with:

Eq. 5.1 $u = \dfrac{3\%}{\sqrt{3}} = 1.7\%$

5.2.2   Observations during the first measurement periods

Collector temperature sensor

Systems A and D were equipped with a wrong collector temperature sensor. The rigid head/tip of the sensor was too long for the curvature of the tube that it was inserted in, with the result that it got stuck in the curve and measured a

temperature that was up to 20 K lower than the collector supply (outlet) temperature during operation. These sensors had to be replaced. By the time of replacement, both systems already showed damages due to the collector loop pumps running at temperatures way above their specification. The pump of system D had to be replaced.

Solar pump control

The primary collector pump was controlled ON/OFF. The controller tried to control the secondary collector loop flow by an electronic modification of the alternating voltage potential given to the single phase pump in a way that a temperature difference of 5 K is maintained between the supply temperatures (hot side of the heat exchanger) of the primary and the secondary loop. This control strategy is highly questionable given the fact that by reducing the flow of the secondary pump only, the exergetic performance of the heat exchanger will decrease, the collector return temperature will rise, and the collector efficiency will drop. However, the maximum flow rate reduction achieved by this kind of control was only 10-12% (Nöhrer 2009), and the flow rate control was therefore not effective in these systems.

Collector yield

Figure 5.6 shows the energy input into the TES by the solar collector loop and by the pellet boiler for System A. Whereas in summer, the system is not far away from reaching full solar coverage, the solar contribution to the total energy demand is rather marginal in winter.
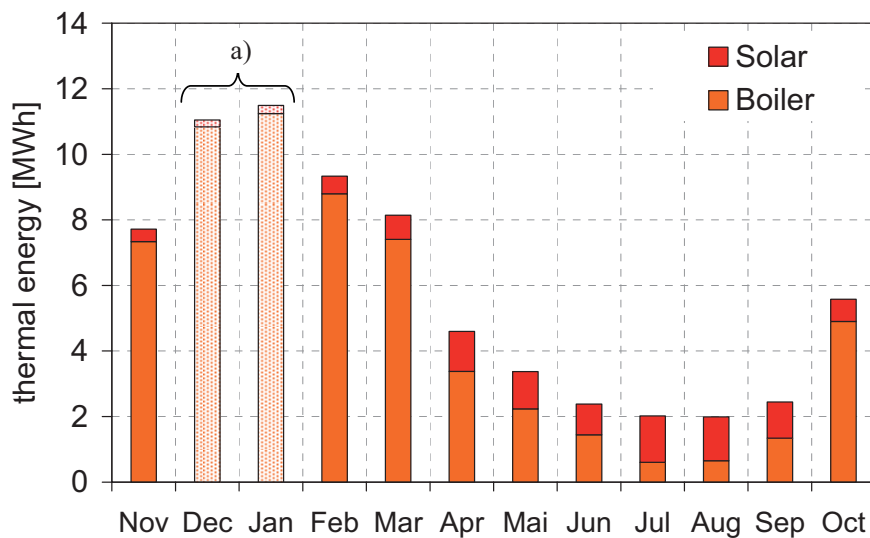
Figure 5.6: Energy input into the TES for the monitored System A from November 2008 to October 2009; a) due to interruptions in data logging, values for Jan. 1st were calculated based on an extrapolation from data from Jan. 9th.

Figure 5.7 shows the specific collector yield for those systems where a full year of data recordings was available by November 2009[10]. Systems A and C achieved a specific collector yield[11] of about 400 kWh/m²a (1.44 GJ/m²a). The specific yield of System B was only half of this value. This can be attributed a) to the fact that the collector loop of System B was turned off manually by the owner between February and March because of suspected night-circulation through the collector loop (not confirmed by analysis of measured data), and b) to the wrong collector sensor used until June.
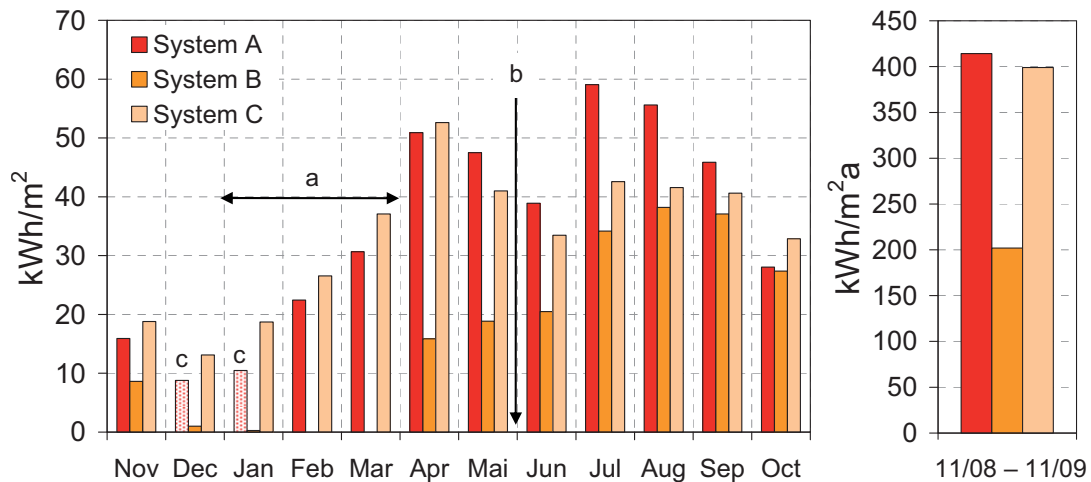
Figure 5.7: Specific collector yield per m² for Systems A, B, and C from November 2008 to October 2009. a) collector pump of System B turned off manually; b) collector temperature sensor of system B replaced; c) see Figure 5.6.

Storage losses

Only two systems (A and B) were equipped with heat meters in all circuits that are connected to the TES. Therefore, only for these systems heat losses of the storage can be calculated. Due to the limited accuracy of the heat meters and the small energetic losses of the TES in comparison with the energy turnover of the TES, heat loss calculations based on heat meter readings have large uncertainties. Figure 5.8 shows average heat loss calculations for each month of the year for Systems A and B. It can be seen that as a result of the Gaussian error propagation, the uncertainty is much lower for summer months where less energy is turned over by the TES. Based on the data from June to September, heat loss rates are about 300 – 550 W (or about 9 – 14 W/K) for the two TES of System A together, and about 400 – 800 W (about 10 – 20 W/K) for the two TES of System B together. In both cases, the estimated yearly heat losses are below 5% of the heat load.

---

[10] Data recordings of Systems D and E started later und thus no full year of data recordings was available.

[11] Measured by heat meters on the TES side of the solar heat exchanger.
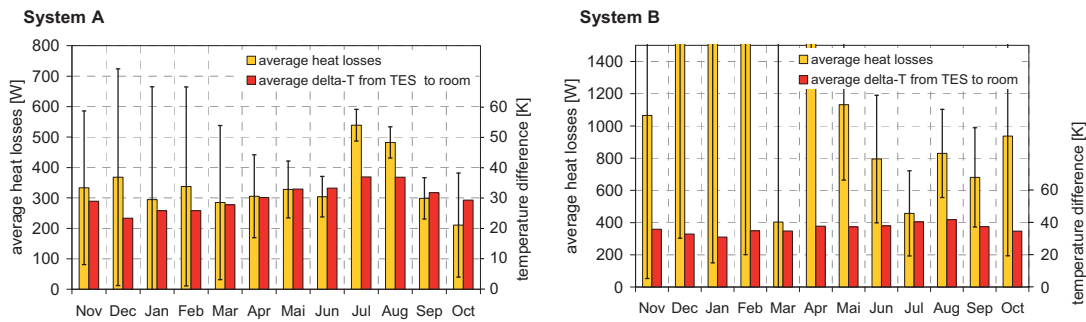
Figure 5.8: Heat losses and average TES temperature difference to utility room for Systems A and B.

Boiler modulation

Figure 5.9 shows boiler operation in system A on two days in winter where the average heat load of the micro-net ($\dot{Q}_{net}$) was 50% of the nominal boiler power (40 kW). Although this boiler theoretically has the capability of continuous part load operation down to 30% of its nominal power, it is running on a steady power and not modulating. In the laboratory, the same boiler showed a decrease in flue gas temperature (t_{fg}) of 1 K for each percent of combustion rate reduction, but no significant decrease in flue gas temperature is visible in Figure 5.9 before the burning process is stopped. Similar patterns of boiler operation could be observed for the monitored systems A – D. None of the boilers in these systems shows significant power modulation. In some cases, the reason for this might also be that the boiler is so much oversized with respect to the heat load that it is always running at minimum part load, and therefore has no capability to further reduce the combustion rate. However, this is not the case for the example shown in Figure 5.9.
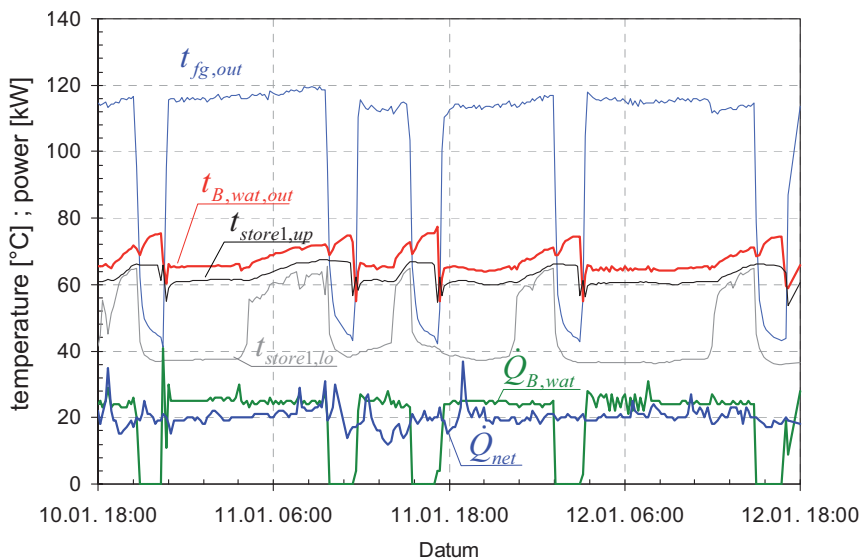
Figure 5.9: Boiler operation on two days in winter with an average heat load of 50% of nominal power for system A.

The incapability of the boiler to reduce combustion power in time before it reaches the OFF temperature can be explained by the fact that the boiler is decoupled from the heat load by the TES. Figure 5.10 shows schematically the stratifying TES at different points in time during the charging process. Excess heat produced by the boiler will lead to a downward flow inside the TES, since the charging mass flow from the boiler will be higher than the discharging mass flow of the load (a→b). Water returning from the TES to the boiler will have the same constant low temperature until the TES is charged all the way down to the outlet towards the boiler loop (c). Up to this point, the boiler has no feedback about the charging process that is happening and therefore no information about whether a reduction of heat output is desirable or not. Additionally, if the boiler requires a minimum return temperature that is maintained by mixing hot water from its supply to the return line, the temperature rise in the return from the TES will not be noticed at the boiler inlet until it rises above this minimum return temperature.
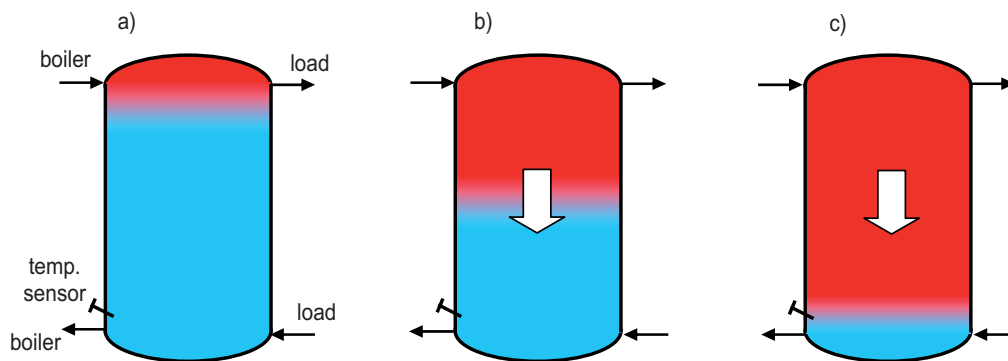
Figure 5.10: Hot plug of water moving down inside the TES when the boiler is providing excess heat.

These findings are in agreement with the field observations on small biomass heating networks made by Bühler & Jenni (2009) and Gabathuler (2009) and the results from testing of solar and pellet systems reported by Haberl et al. (2009, p.3) (compare Section 5.1.5).

The monitored system E shows good power modulation of the boiler. In this system, the TES shows an almost fully mixed behaviour because the charging mass flow rate from the boiler loop is roughly four times the volume of the TES per hour. Although this enables the boiler to get an instant feedback about the status of TES charging, it is not considered a solution that can be recommended for a solar thermal heating system where a part of the TES should never be heated by the auxiliary heating device in order to be available for solar heat input.

5.3 System simulations

In this Chapter, kWh will be used consistently as energy unit instead of the SI-Unit Joule. Conversion factors are given in the Section "Nomenclature, Abbreviations and Symbols" before Chapter 1.

5.3.1 Performance indicators

Three indicators were defined within the Tasks 26 & 32 of the International Energy Agency Solar Heating and Cooling Programme (IEA-SHC) to compare the performance of different solar thermal heating systems under equal boundary conditions and load situations (Streicher et al. 2002; Jordan et al. 2003; Heimrath & Haller 2007).

The ***fractional thermal energy savings*** $f_{sav,therm}$ correspond to the percentage of the conventional heat source – in our case wood pellets – that can be saved by the solar thermal system. Not included in this indicator is the electricity use for the operation of the facility[12]. The reduction of fuel consumption is always based on a comparison with a reference heating system (ref) that uses the same fuel, but no solar thermal heat.

$$Eq.\ 5.2 \qquad f_{sav,therm} = 1 - \frac{Q_{fuel}^{NHV}}{\dfrac{Q_{B,wat,ref}}{\eta_{B,ref}^{NHV}}}$$

The ***extended fractional energy savings*** $f_{sav,ext}$ include also electricity use for the operation of the system for both the solar and pellet heating system as well as the reference heating system. As in Task 32, it is not distinguished between electricity from renewable and from non renewable sources. The efficiency of electricity production is set to $\eta_{el} = 0.4$. This value is chosen to reflect more or less the efficiency of electricity production and distribution within the European grid, as well as the fact that electricity has a higher thermodynamic value (exergy) than heat energy, and also a higher price on the market. This is independent from the question whether the electricity has been produced from renewable energy sources or not.

$$Eq.\ 5.3 \qquad f_{sav,ext} = 1 - \frac{Q_{fuel}^{NHV} + \dfrac{W_{par}}{\eta_{el}}}{\dfrac{Q_{B,wat,ref}}{\eta_{B,ref}^{NHV}} + \dfrac{W_{par,ref}}{\eta_{el}}}$$

---

[12] Electrity use for direct heating or for the compressor of a heat pump however would be included. In our case, these two options are not considered, and therefore the equation for the fractional thermal energy savings is simplified accordingly.

In simulations it is possible to achieve a higher fuel saving by reducing the temperatures in the boiler, the TES, etc. However, there is a limit after which the temperature reduction leads to reduced comfort of the system, e.g. because the temperatures of DHW are not considered sufficient anymore by the user. For this reason, the fractional solar savings indicator f_{si} has been defined. This value includes a penalty (pen) for the reduction of comfort. The criteria for comfort are:

- DHW temperature always above 45 °C.
- Room temperature always above 19.5 °C.

A detailed explanation of the calculation of these penalties can be found e.g. in Heimrath & Haller (2007).

$$Eq.\ 5.4 \qquad f_{si} = 1 - \frac{Q_{fuel}^{NHV} + \dfrac{W_{par}}{\eta_{el}} + Q_{pen} - Q_{pen,ref}}{\dfrac{Q_{B,wat,ref}}{\eta_{B,ref}^{NHV}} + \dfrac{W_{par,ref}}{\eta_{el}}}$$

For the calculation of these performance indicators, it is necessary to define a reference heating system without solar thermal heat use. This was done within the IEA-SHC Task 32 for systems that are based on oil and gas as heat sources, but not for systems based on wood pellets. Therefore, the assumptions made for the reference pellet heating system that is used within this work are shown in Table 5.2. Differences between this reference system and the ones presented in the IEA-SHC Task 32 concern the boiler efficiency and the electricity demand of the boiler heating loop. These figures are estimated based on laboratory measurements and model calculations that have been presented in Konersmann et al. (2007).

Table 5.2: Assumptions for the reference pellet heating system without solar.

Unchanged from IEA-SHC Task 32	Value	Unit
Heat losses of DHW storage	644	kWh/a
Electric power demand of space heating pump	93	W
Adapted for a pellet heating system		
$\eta_B^{NHV} / \eta_B^{GHV}$, annual boiler efficiency relative to the NHV / GHV	76.0 / 70.6	%
Electricity demand of the pellet boiler[13] in % of useful heat delivered, including boiler loop pump	2.34	%
$N_{burn,start}$, number of burner starts per year	2000	a^{-1}

Fractional thermal energy savings ($f_{sav,therm}$) and extended fractional energy savings ($f_{sav,ext}$) are shown for the evaluation of the impact of parameter

---

[13] Without electricity used to transfer pellets from a larger reservoir to the short-term storage device attached to the boiler.

variations or of different system hydraulics. The fractional savings indicator (f_{si}) will not be shown unless its value is significantly lower than $f_{sav,ext}$. If the f_{si} is not shown, the condition $f_{sav,ext} - f_{si} \leq 0.4\%$ is fulfilled. Additional performance indicators used in this work are the specific collector yield ($Q_{coll,spec}$), the number of burner-starts ($N_{burn,start}$), and the total hours of collector field stagnation ($\tau_{coll,stag}$). Collector stagnation time is defined as the time the solar pump is not in operation despite collector temperatures that are high enough for the ON-criteria. This is the case if the temperature in the collector or in the upper part of the TES is too high ($t_{coll} > 110°C$ or $t_{store} > 90°C$).

5.3.2 Simulation environment

TRNSYS 16 (SEL et al. 2006) was used for all simulations. The load profile, climate data, building simulation and space heating loop were taken from the reference heating system of the IEA-SHC Task 32 that is described in detail in Heimrath & Haller (2007). The simulations were based on the climate of Zurich, Switzerland, and the building SFH60 with a space heating demand of 60 kWh/m²a and a heated floor area of 140 m². Key parameters of this system are shown in Table 5.3. All simulations that use a different heat load are labelled accordingly.

Type 340 (Drück 2006) was used for the simulation of the TES; Type 869 Version 5.02 (Appendix B and Part II Paper III) was used for the simulation of the pellet boiler. For the control of the space heating circuit and the charging of the upper TES volume by the pellet burner, Type 888 (Appendix B) was used. In this Type, the set temperature for the space heating loop supply is calculated based on the 24 hours average of the ambient temperature and the space heating system parameters shown in Table 5.3. The total heat load of this system, combined with the reference pellet heating efficiency from Table 5.2, leads to a pellet use of about 3000 kg/a (wet base).

Table 5.3: Key parameters of the reference heating system SFH60 for the climate of Zurich.

Parameter	Value	Unit
Space heating load	8.48	MWh
DHW demand	3.04	MWh
Design heat load at ambient temperature of -10 °C	4.6	kW
Design supply temperature for space heating at ambient temperature of -10 °C	40	°C
Design return temperature for space heating at ambient temperature of -10 °C	35	°C
Radiator exponent	1.3	-

5.3.3 System with a TES integrated pellet burner

For the simulation of a system with a TES integrated pellet burner, Type 869 was used for the simulation of the combustion chamber and the heat transfer from the flue gas to water, and Type 340 was used for the simulation of the TES,

including its effective thermal capacitance and heat losses. Parameterisation of Type 869 was according to the identified parameters for Pel4 (Section 2.5.5), and parameterisation of Type 340 was according to the identified parameters shown in Section 3.1.7. This means that the storage capacitance corresponds to 848 l of water and the burner's combustion power is 17.7 kW based on the upper heating value. Details about the connection of the two Types for the simulation of a TES integrated burner are explained in Appendix A. Figure 5.11 shows the hydraulic schematic of the system.
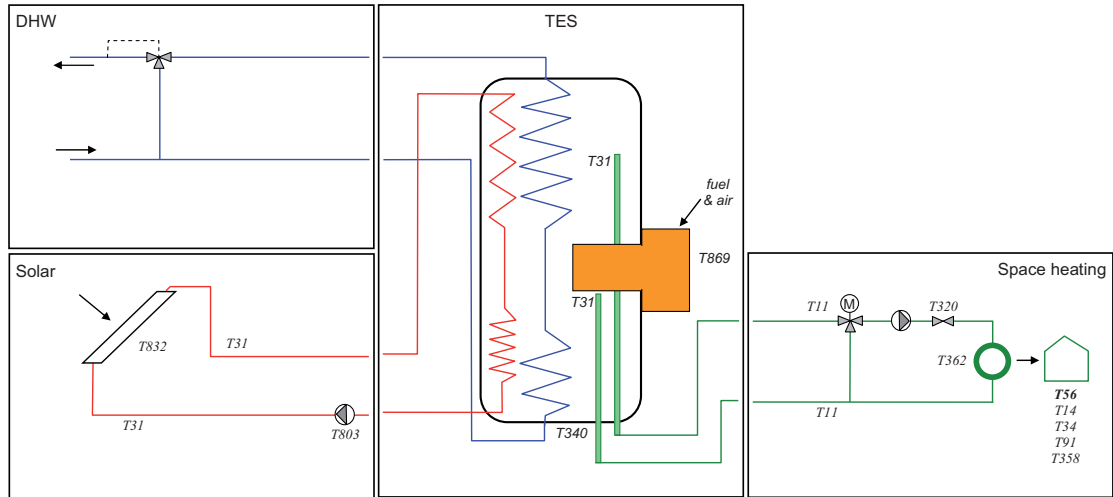
Figure 5.11: Hydraulic schematic for the simulation of the system with a pellet burner integrated into the TES, divided into different modules. T869: TRNSYS Type Nr. 869.

The collector performance data was based on a certified test report for a selective flat plate CPC collector that was provided by a manufacturer. The relevant parameters for the collector and the collector loop are listed in Table 5.4 and Table 5.5.

Table 5.4: Collector parameters.

Parameter	Value	Unit
A_{coll} , Collector field aperture area	10	m^2
β_{coll} , collector slope	45	°
α_{coll} , collector orientation (-90 ° = east)	0	°
η_0 , optical efficiency or "zero heat loss efficiency" (based on aperture area)	0.741	-
a_1 , linear heat loss coefficient (based on aperture area)	3.311	W/m^{2}K
a_2 , quadratic heat loss coefficient (based on aperture area)	0.012	W/m^{2}K^2

Incident angle modifiers									
Incident angle:	0	10	20	30	40	50	60	70	80	90
longitudinal:	1.000	1.000	0.998	0.984	0.958	0.936	0.908	0.820	0.672	0.0
transversal:	1.000	0.960	1.000	1.010	1.000	1.000	0.992	0.870	0.572	0.0

Table 5.5: Collector supply and return line parameters for the case of 10 m² collector area and 35 kg/hm² maximum flow.

Parameter	Value	Unit
$l_{pi,sol}$, length of collector supply and return line (each)	15	m
$d_{pi,sol}$, inside diameter of collector supply and return line	0.015	m
$UA_{pi,sol}$, UA-value of collector supply and return lines (each)	2.9	W/K

It was assumed that 30% of the collector supply and return lines are installed outside (heat losses to ambient), and 70% in areas with temperatures corresponding to the temperature of the utility room (constant 15 °C for the IEA-SHC Task 32 reference system). The temperature sensor for collector loop control was placed at 34% relative height of the TES (Table 5.6). This assumption is based on simulations and has not been derived from system measurements or from manufacturer data. The position of the collector loop control sensor is relatively high. The reason for this is that the upper part of the immersed solar heat exchanger in the TES can not be bypassed in this system, and the stratifying capabilities of this part are not perfect. Thus, if the collector supply (outlet) temperature is below the temperatures in the upper part of the TES, heat may be transferred from the upper part of the TES to the lower part of the TES by the immersed solar heat exchanger, and it may even occur that the heat input becomes negative[14].

Table 5.6: Collector loop control.

Parameter	Value	Unit
Rel. height of temperature sensor in TES	0.34	-
Delta-T ON	7	K
Delta-T OFF	4	K
Maximum specific mass flow rate (matched flow)	35	kg/hm²

The matched mass flow rate of the collector loop was controlled according to the control strategy described by the manufacturer (not shown here). For the calculation of the electricity demand of the collector loop pump, 50 Watt was assumed, which corresponds to the product Wilo Star-ST 25/6 running at stage II (out of III)[15]. When the pump is operated for matched flow, it was assumed that the mass flow rate can be reduced to 40% of its maximum, and that a reduction of electricity input of 10% leads to a reduction of the mass flow rate of 20%.

---

[14] Results from simulations that are not shown here. This has not been verified with measurements.

[15] According to the data of the manufacturer, this pump operated at stage II has a pressure head of 5.1 m at a flow rate of 350 kg/h.

For the calculation of a constant low-flow operation of the pump, it was assumed that the same pump is set to stage I, with an electricity demand of 40 W.

Base case

The control settings for the base case are shown in Table 5.7. The relatively high temperature settings for auxiliary heating were necessary, because with lower temperature settings the comfort criteria for DHW defined by the IEA-SHC Tasks 26 & 32 (compare Section 5.3.1) were not met.

Table 5.7: Control settings for auxiliary heating and simulation results for the base case.

Parameter	Value	Unit
Rel. height of temperature sensor in TES	0.43	-
t_{ON}, TES sensor temperature at which burners starts	58	°C
t_{OFF}, TES sensor temperature at which burners stops	68	°C
Simulation results	**Value**	**Unit**
$f_{sav,therm}$, fractional thermal savings	20.9%	-
$f_{sav,ext}$, extended energy savings	18.6%	
$Q_{coll,spec}$, specific collector yield	290	kWh/m²a

The simulation of this system with 10 m² CPC-collector area resulted in fractional thermal savings ($f_{sav,therm}$) of 20.9% compared to the reference system without solar thermal. The extended energy savings ($f_{sav,ext}$) are a bit lower, because the electricity use of the system did not decrease as well. Figure 5.12 shows annual energy flows of the reference system, a system with the TES integrated burner and no solar thermal heat input, and the system with the TES integrated burner and 10 m² of collector area.
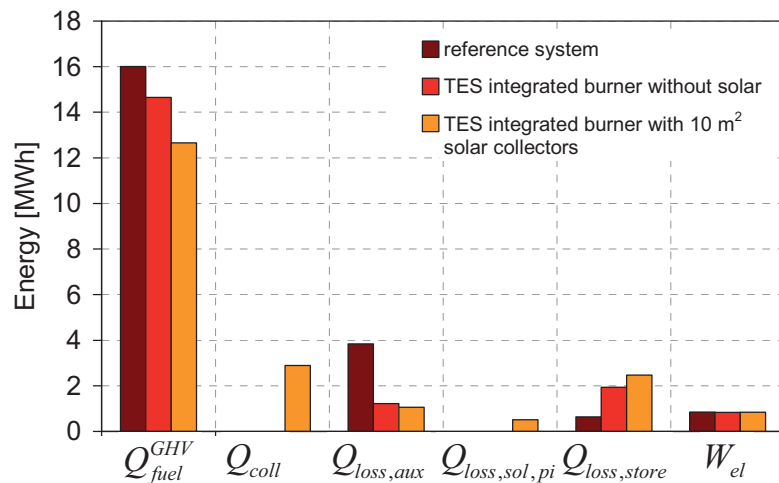
Figure 5.12: Thermal energy balance of the reference system and the systems with TES integrated burner without solar and with 10 m² flat plate collectors.

Losses from the (auxiliary) pellet boiler ($Q_{loss,aux}$) include all flue gas losses (latent, sensible, chemical) as well as losses from the combustion chamber and losses from the boiler and the pipes connecting it with the TES or heat load if present. The large differences between the energetic losses of the different systems concerning the boiler $Q_{loss,aux}$ and the TES $Q_{loss,store}$ are due to the fact that (a) for the integrated burner the heat losses from the water body are not included in $Q_{loss,aux}$ but in $Q_{loss,store}$ [16] and (b) the reference system has only a small DHW TES with low heat losses in comparison to the larger solar TES. The fuel consumption Q_{fuel}^{GHV} shows that about one third of the thermal savings are due to a better efficiency of the TES integrated burner in comparison to the reference system with the boiler and the TES as two separate units. Only the remaining two third of the savings are due to the solar heat gains.

The number of burner starts for the TES integrated burner without the use of solar heat is 3400/a and thus 70% higher than for the reference system. Even with the solar thermal heat input, $N_{burn,start}$ is about 40% higher (2800/a) than for the reference system. Explanations for this are the fact that the nominal heating power of the TES integrated system is more over-dimensioned (15 kW in comparison to 10 kW of the reference), and that the integrated burner is not modulating. The total stagnation time of the collector field is 38 h/a.

Figure 5.13 shows the thermal energy balance of the whole system (a) and the energy balances of the single sub-systems TES (b), solar collector loop (c), and burner (d). TES losses ($Q_{loss,store}$) and flue gas losses ($Q_{loss,fg}$, here including the enthalpy of condensation of water vapour) are the dominant losses of this system.

---

[16] Because of the burner integration, heat losses from the boiler water are identical to the heat losses of the TES.
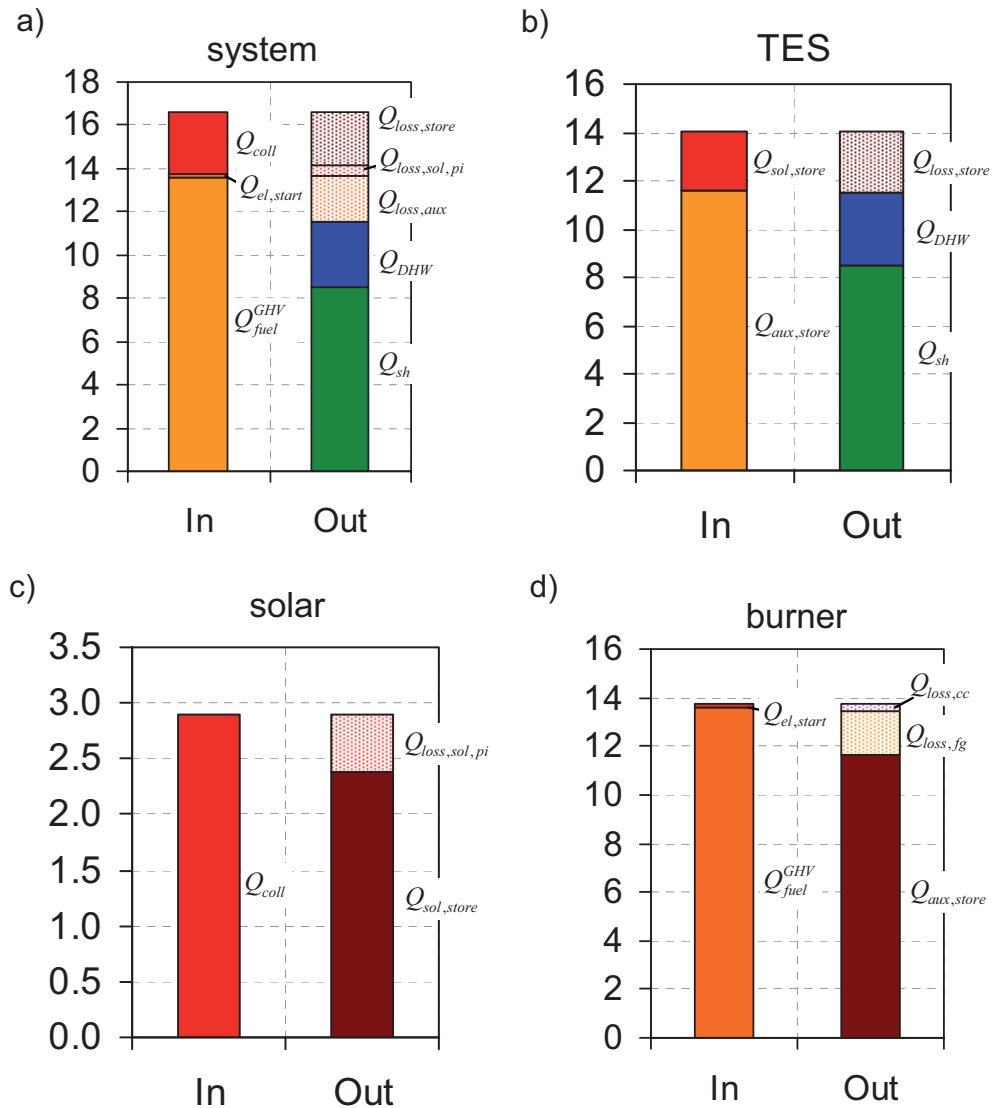
Figure 5.13: Energy flows in MWh/a of the system (a) and the sub-systems TES (b), solar (c), and burner (d).

Influence of TES heat losses

The overall heat losses of the TES are 288 W at 40 K temperature difference to the ambient. In comparison with other solar TES of comparable size, this value is quite high (see e.g. Stiftung Warentest 2009). An explanation for this is that the integration of the burner into the TES poses problems for the insulation. Increased surface temperatures in the region of the burner integration have been confirmed by thermographic pictures (not shown). Figure 5.14 shows that a reduction of the TES heat loss coefficients by 45% in the lower 66% of the TES height (corresponding to UA_{z1} and UA_{z2} in Table 3.3) results in more than 20% relative increase of thermal savings (>4% absolute).
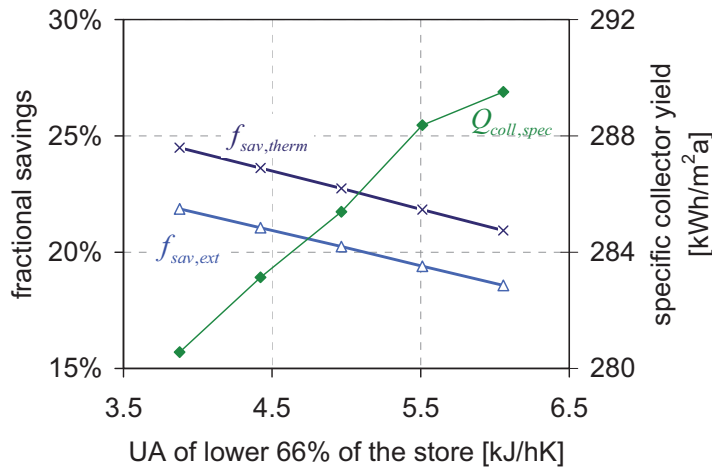
Figure 5.14: Simulated improvements by better insulation in lower 2/3 of the TES height.

Influence of the UA-value of the DHW heat exchanger

To fulfil the comfort requirements for DHW of the IEA-SHC Tasks 26 & 32, the ON/OFF temperatures of the burner had to be set at least to 58/68 °C (auxiliary heating). Lower values for the ON-temperature lead to tap water temperatures below 45 °C, and consequently to a significant difference between the indicators f_{si} and $f_{sav,ext}$. Figure 5.15 shows that the ON-temperature can be 10 K lower (48 °C) if the UA-value of the internal DHW heat exchanger is 50% higher ($UA = 1.5 \cdot UA_{ms}$). The resulting lower temperatures in the upper part of the TES reduce heat losses and at the same time increase solar gains. The resulting $f_{sav,therm}$ is 26.5%. Thermal savings do further increase if the UA-value is increased twofold and at the same time the set temperatures for auxiliary heating are further reduced.
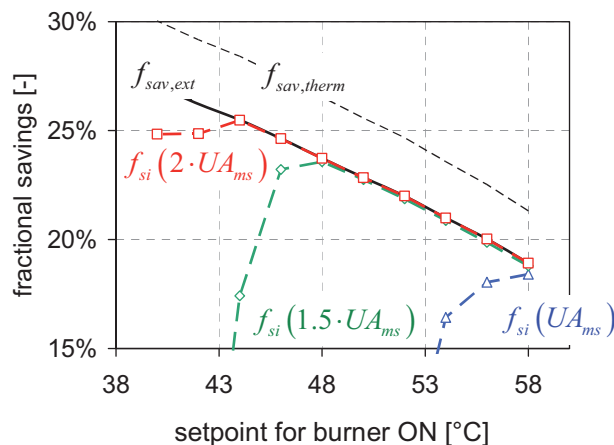
Figure 5.15: Dependency of $f_{sav,therm}$, $f_{sav,ext}$, and f_{si} on the ON-temperature of the burner ($t_{OFF} = t_{ON} + 10K$) for different UA-values of the DHW heat exchanger.

82

Influence of the collector field size

Increasing the collector field size from 10 m² to 15 m² increases $f_{sav,therm}$ from 20.9% to 23.6% (Figure 5.16a). At the same time, the specific collector yield decreases from 290 to 232 kWh/m²a. Additional energy savings of the last collector (from 12.5 m² to 15 m²) are only 98 kWh/a per added m² of collector area. At the same time, the hours of collector stagnation increase significantly (Figure 5.16b).
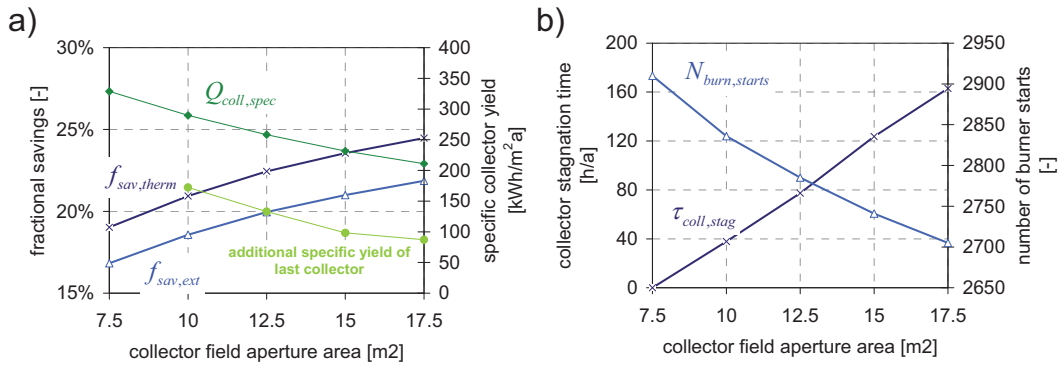
Figure 5.16: Influence of the collector area on (a) fractional savings and specific collector yield, and (b) collector stagnation time and number of burner starts.

Comparison of different options for improvement

Table 5.8 shows that higher thermal savings can be expected by a better thermal insulation of the TES or an increased UA-value of the immersed DHW heat exchanger than for adding 3 collectors (+7.5 m²) to the collector field. At the same time, the first two measures show less negative effects on the hours of collector stagnation, and are likely to be less cost intensive.

Table 5.8: Influence of different measures on thermal savings, specific collector yield, and number of burner starts.

Simulation	$f_{sav,therm}$	$f_{sav,ext}$	$Q_{coll,spec}$ kWh/m²a	$\tau_{coll,stag}$ h	$N_{burn,starts}$ -
Base case	20.9%	18.6%	290	38	2836
45% less heat losses in lower 2/3 of TES	25.3%	22.6%	277	51	2730
UA-value of DHW heat exchanger +50%, and burner ON at 48 °C	26.5%	23.7%	331	11	2582
Collector field + 7.5 m²	24.5%	21.9%	211	163	2705

Influence of immersed solar heat exchanger options

If the upper part of the immersed solar heat exchanger in the TES was simulated with the "stratifying" option of the TES model, $f_{sav,therm}$ increased from 20.9% to 22.6%, whereas moving the whole heat transfer capacity of the immersed solar heat exchanger to the lower part of the TES (without stratification) increased

$f_{sav,therm}$ to 23.0%. At the same time, this measure decreased the collector stagnation time to zero hours. Increasing the UA-value of the immersed solar heat exchanger by 50% had only little effect for the base case ($f_{sav,therm}$ = 21.6%), and no observable effect for the case of all heat transfer capacity located in the lower part of the TES.

Influence of the height of the space heating return line inlet

A lower position for the space heating return inlet does not increase the fractional savings for the base case. If the TES is simulated without heat transfer from the space heating return pipes to the bottom section (compare Section 3.1.6) the set temperature for the upper part of the TES has to be increased in order to still fulfil the DHW comfort criteria. This is likely to be an effect of generally lower temperatures in the bottom section and therefore less preheating of the DHW inside the heat exchanger spirals located in this section. In the simulations without heat transfer to the bottom section the fractional savings are not significantly higher than for the base case. Even if the space heating return is simulated as "perfectly stratified" $f_{sav,therm}$ only increases little in comparison to the base case.

Influence of combustion power modulation

In order to study the effect of burner modulation on the number of burner starts, additional assumptions had to be made for the simulation of the part load behaviour of the burner and the heat transfer to the TES water. These are shown in Table 5.9.

Table 5.9: Boiler parameters for the operation at lower combustion power

Parameter	Value	Unit
Minimum combustion power (exemplary)	30	%
dT_{fg}, change in flue gas temperature per % of combustion power reduction	-0.31	K/%
λ_{max}, excess air ratio at minimum combustion power of 30%	1.75	-
$ppm_{CO,max}$, CO emissions at minimum combustion power of 30%, in % of the measured ppm-value at full load.	200	%
$P_{el,min}$, el. energy consumption rate at minimum combustion power of 30%	69	W

Some of the simulations with power modulation, especially those with reduced nominal power of the burner, did not meet the comfort requirements for DHW when the same burner ON and burner OFF criteria were used as in the base case. Therefore, for all simulation results shown in Figure 5.17, burner ON/OFF set temperatures were increased from 68/58 °C of the base case to 71/61 °C. For simulations with combustion power modulation, 66 °C were used for the set temperature (t_{set}) for the controller that controls power modulation after the start

phase of the burner. The process variable for the control algorithm is the temperature measured at the sensor position defined in Table 5.7.

Figure 5.17 shows the reduction of the number of burner starts that can be achieved by combustion power modulation between 60-100%, and between 30-100% (minimum turndown ratio 60% and 30%, respectively), for different design heat loads and different maximum burner powers. The base case design heat load of 4.6 kW corresponds to Figure 5.17b. Figure 5.17a shows results for a design heat load of 6.5 kW[17]. The burner with a nominal combustion power of $\dot{Q}_{fuel,max}^{GHV}$ = 17.5 kW and power modulation from 60-100% does not significantly decrease the number of burner starts in this case, because 60% is still well above the design heat load. Only when the minimum part load heating power overlaps the heat load curve, i.e. it is below the design heat load, a significant reduction of the number of burner starts can be achieved. This is the case for the 30-100% power modulation with the same maximum combustion power. Figure 5.17a also shows that in the case of $\dot{Q}_{fuel,max}^{GHV}$ = 10.5 kW and 30% minimum part load, the number of burner starts can be reduced from 3000/a to about 500/a. Figure 5.17c shows that if the boiler is over-dimensioned by more than a factor of three, even power modulation between 30% and 100% has little or no effect on the number of burner starts. In this case, the TES will always be charged a lot faster than discharged, and thus the key factor that influences the number of burner starts is the ratio of TES capacitance to discharging power, with little or no influence of the charging power. Also the general decrease of the maximum of burner starts from the design heat load of 6.5 kW (Figure 5.17a) to the design heat load of 3.1 kW (Figure 5.17c) is likely to be a result of the decreasing ratio of heat load to storage capacity.
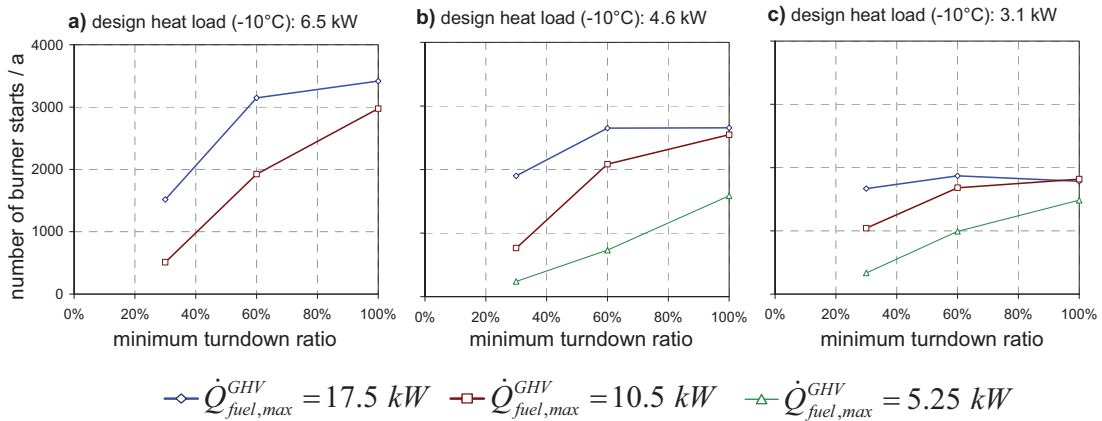
Figure 5.17: Influence of nominal power and minimum part load ratio of the boiler on the number of burner starts for different design heat loads assuming the same TES volume and configuration for all cases.

For the assumptions made for power modulation, fractional savings have the tendency to increase slightly (-1 to +4 % relative) if power modulation is enabled and the set temperatures for auxiliary heating are kept constant. However,

---

[17] SFH 100 of the IEA-SHC Task 32

systems with a nominal combustion power of 5.25 kW and power modulation of 30-100% had problems to provide the required DHW comfort ($f_{si} < f_{sav,ext} - 0.4\%$) in these simulation.

5.3.4 Improved system with a TES integrated pellet burner

Based on the results of the previous section, simulation results for two improved systems with TES integrated burners are presented in this section. Improved system A is a low cost improvement that is not expected to increase the overall system cost significantly, and improved system B is a system with increased size or heat transfer capacity of the immersed DHW heat exchanger, and thus likely to be a slightly more expensive solution. The storage volume and the collector field size are kept constant. Heat transfer from the internal pipes to the lower part of the TES is assumed to be effectively prevented in systems A and B. The differences between the base case and the improved systems A and B, respectively, are listed in Table 5.10.

Table 5.10: System improvements compared to the base case.

Parameter	Unit	base case	System A	System B
UA_{z1}, TES heat loss coefficient of zone 1	W/K	2.89	1.39	1.39
UA_{z2}, TES heat loss coefficient of zone 2	W/K	3.17	1.94	1.94
Heat transfer from immersed space heating return and supply pipes	--	simulated	zero	zero
$z_{sh,in}$, rel. height of space heating return line into TES	%	45%	25%	25%
$UA_{hx,sol,1}$, UA-value of upper solar HX	W/K	222	0	0
$UA_{hx,sol,2}$, UA-value of lower solar HX	W/K	167	389	389
Rel. height collector loop control sensor	%	34%	26%	26%
$UA_{hx,dhw,base}$, base UA-value of DHW HX	W/K	1893	1893	2839
$t_{burn,ON}$, set temperature for burner ON	°C	58	60	48.5
Simulation results	**Unit**	**base case**	**system A**	**system B**
$f_{sav,therm}$, thermal energy savings	%	**20.9**	**28.0**	**32.0**
$Q_{coll,spec}$, spec. collector yield	kWh/m²a	290	315	342
$N_{burn,start}$, number of burner starts	-	2836	2515	2480

Table 5.10 and Figure 5.18 show that system A increases the fractional savings by 34% (relative) and system B by 53% compared to the base case. At the same time the collector yield increases and the number of burner starts decreases.

Annual energy flows of the reference system, the base case, and the two improved systems are shown in Figure 5.19. This shows that system B profits both from less energy losses of the storage tank and the burner as well as from a higher collector yield than the other two systems.
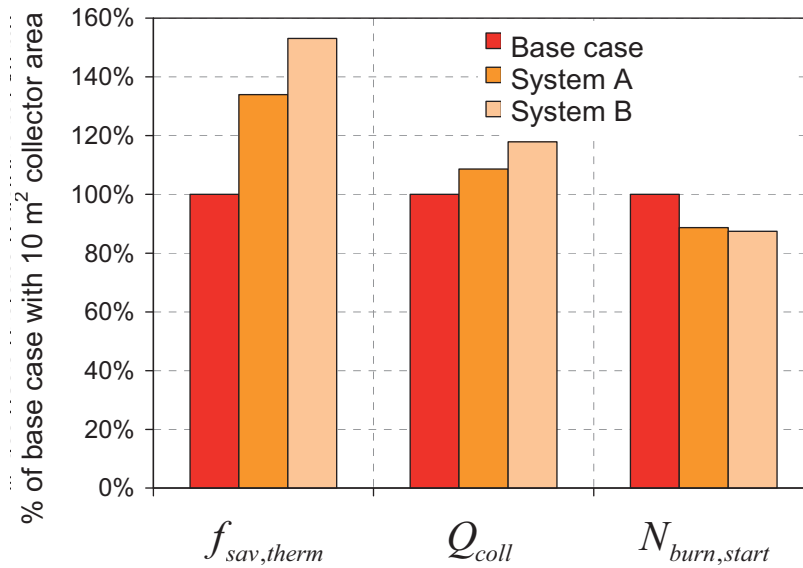
Figure 5.18: Comparison of energy savings, collector yield and number of burner starts for the base case with integrated burner, an optimised solution with only low-cost changes (System A) and an optimised solution with additionally increased UA-value of the DHW heat exchanger (System B).
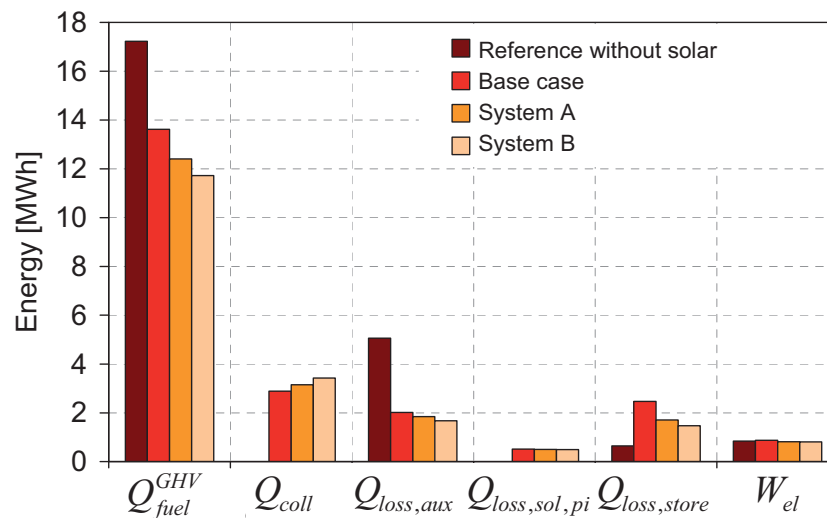
Figure 5.19: Energy flows of the reference without solar, the base case with integrated burner, an optimised system with only low-cost changes (System A) and an optimised system with additionally increased UA-value of the DHW heat exchanger (System B).

Influence of the collector type on the improved system

Figure 5.20 shows the effect of switching from the selective flat plate collector to the simulation of a vacuum tube collector that has been defined as a reference in the IEA-SHC Task 32. An additional 5.0% of fuel energy can be saved additionally, but the total stagnation time of the collector field also increases from almost zero to more than 400 h/a. The parameters used for the simulation of

the two collectors are given in Table 5.11. Details about the effective capacity and the incident angle modifiers of the vacuum tube collector are shown in Heimrath & Haller (2007).

Table 5.11: Efficiency parameters for two different collectors, based on aperture area. Calculated for System B.

Collector type	η_0	a_1	a_2
	-	W/m²K	W/m²K²
flat plate collector	0.741	3.311	0.012
IEA-SHC Task32 vacuum tube collector	0.773	1.09	0.0094
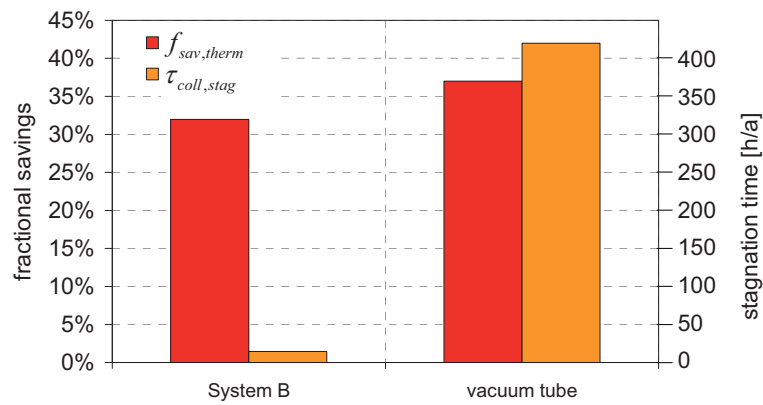
Figure 5.20: Changes in fractional savings and collector stagnation time by change of the collector type in System B.

5.3.5 System with an external pellet boiler

In this section a solar and pellet heating system is defined with an external pellet boiler that is connected to a solar TES as shown in Figure 5.21.
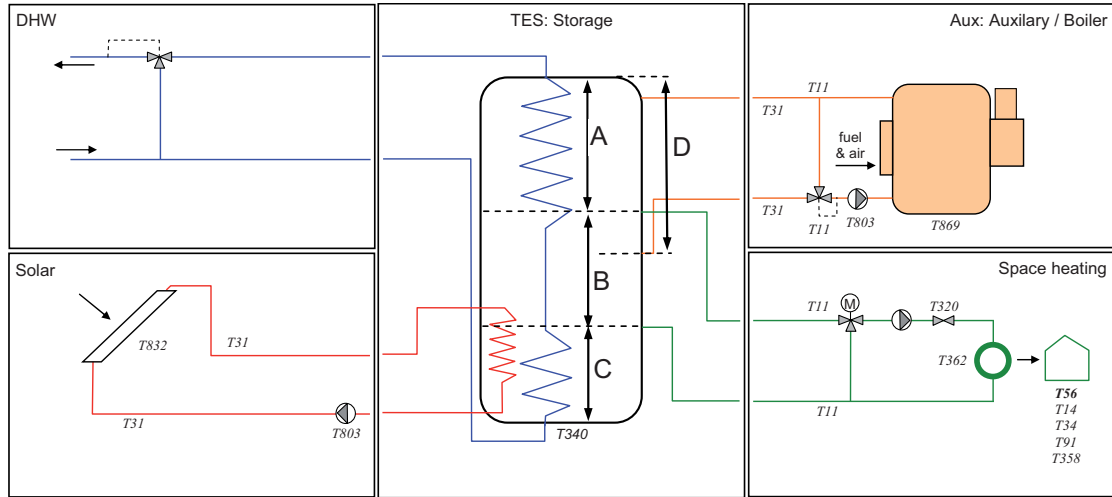
Figure 5.21: Hydraulic schematic for the simulation of a system with an external pellet boiler connected to the TES. T869: TRNSYS Type Nr. 869. A) DHW zone; B) space heat zone; C) DHW preheating zone; D) Auxiliary heated zone. Zone heights shown are not representative.

The simulation parameters for the TES are the same as for system B presented in Section 5.3.4, with the exception of the values shown in Table 5.12. Lower heat losses have been assumed because this TES does not have an integrated burner that complicates the insulation. According to measurements performed on 13 different solar combisystems and published by the German Consumer Magazine Stiftung Warentest (2009), heat losses of 131 W at a delta-T to the ambient of 40 K is a realistic assumption for a well insulated solar combistore with a volume of 800 litres.

Table 5.12: TES parameters that differ from the assumptions made for the TES with integrated pellet burner.

Parameter	Value	Unit
UA_{z1}, side heat loss coefficient of lowest 1/3 of TES height	0.63	W/K
UA_{z2}, side heat loss coefficient of middle 1/3 of TES height	0.63	W/K
$z_{sh,in}$, rel. height of space heating return connection, no internal pipe	25%	-
$z_{sh,out}$, rel. height of space heating supply connection, no internal pipe	50%	-
$z_{aux,in}$, rel. height of boiler loop inlet, i.e. supply from boiler, connection	93%	-
$z_{aux,out}$, rel. height of boiler loop outlet, i.e. return to boiler, connection	40%	-

The parameters for the external pellet boiler are mostly based on average values of Pel1 and Pel2 (Table 5.13, compare Section 2.5.5). Parameters for the simulation of the connection of the external pellet boiler with the TES are shown in Table 5.14.

Table 5.13: Parameters used for the simulation of an external pellet boiler.

Parameter	Value	Unit
$\dot{Q}^{GHV}_{fuel,max}$, nominal (=maximum) combustion power based on GHV	12.8	kW
$\dot{Q}^{GHV}_{fuel,min}$, minimum combustion power based on GHV	5.3	kW
C_{therm}, effective thermal capacitance	340	kJ/K
UA_{hx-amb}, heat loss coefficient to ambient	6.8	W/K
$fr_{cc,amb} + fr_{ash}$, fraction of GHV lost by the combustion chamber by convection, radiation, and unburnt residues in the ash.	1.8	%
λ_{min}, minimum lambda value (excess air ratio)	2.35	-
λ_{max}, maximum lambda value (excess air ratio)	3.25	-
dT_{nom}, temperature difference between flue gas and water return temperature at nominal power	72	K
$dT_{hx,fg}$, change of delta-T flue gas to water return per % of combustion power reduction	-0.73	K/%
$ppm_{CO,min}$, CO in flue gas at nominal power	153	ppm
$ppm_{CO,max}$, CO in flue gas at minimum combustion power	245	ppm
$P_{el,min}$, electricity consumption at minimum combustion power	35	W
$P_{el,max}$, electricity consumption at maximum combustion power	71	W
$W_{el,start}$, electricity use for each burner start (ignition)	58	Wh
$P_{el,OFF}$, electricity consumption in standby	11	W
τ_{start}, duration of start phase	0.15	h
$\dot{Q}^{GHV}_{fuel,start}$, average fuel consumption during start phase	6.4	kW

Table 5.14: Parameters for the simulation of the connection between the pellet boiler (auxiliary heater) and the TES.

Parameter	Value	Unit
$t_{rt,min}$, minimum return temperature	50	°C
$l_{aux,pi}$, length of the connecting pipes (once each for supply and return line)	4	m
$d_{aux,pi}$, inside diameter of the pipes	0.02	m
$U_{aux,pi}$, heat loss coefficient of the pipes, based on inside diameter	2.5	W/m2K
El. power consumption of boiler circuit pump	40	W
$\dot{m}_{aux,max}$, Mass flow rate in boiler circuit when pump is in operation	800	kg/h
Delayed pump stop (follow-up time after burner stop)	20	min

Control strategies for TES charging by the external pellet boiler

Different control strategies may be used to control the charging of the TES by the pellet boiler. Some of them are discussed here and tested within simulations C1 – C7.

The decision to switch the boiler ON and charge the TES is based on at least one temperature measurement within the stratified TES. For a solar combisystem, the upper part (DHW zone, see Figure 5.21) of the TES has to be kept at a certain minimum temperature, e.g. 62°C, to fulfil the criteria for comfort and hygiene for DHW. At the same time, the middle part (space heat zone) of the TES should be kept at a temperature that is above the required space heating supply temperature, which is well below the required DHW temperature for state of the art heating systems for houses. Whenever the measured temperature(s) within the TES drop(s) below the required level(s) (t_{ON}), the boiler starts burning fuel and the circulation pump is switched on. As soon as the temperature(s) within the TES have risen above a certain level (t_{OFF}), the boiler stops feeding fuel and the circulation pump is switched off with a certain time-delay. The most difficult part of the procedure is between the ON- and the OFF-signal, where a modulating boiler should find the fuel combustion rate that matches the heat load and thus keeps running for a longer time. It has been shown in several field and laboratory studies that pellet boilers that theoretically have the possibility to automatically adjust their combustion rates between 30% and 100% often run on a constant 100% combustion rate when the heat load is decoupled from the boiler by a stratifying TES (compare Sections 5.1.5 and 5.2.2). Assuming that the boiler controls its combustion rate to maintain a constant set temperature ($t_{B,set}$) of the boiler water outlet ($t_{B,wat,out}$), decreasing the heat output can be achieved by:

– reducing the flow rate of the water circulating through the boiler, or

– increasing the return temperature to the boiler

Water flow rate reduction by means of a speed controlled pump has the disadvantage of larger investment costs, but at the same time the advantage of possible electricity savings because of lower pump speeds. The speed of the pump must be controlled actively, e.g. based on temperature measurement(s) within the TES. On the other hand, the return temperature can be increased actively by changing the return temperature set point or passively as a result of automatically rising temperatures from the TES to the boiler. The latter is the most trivial solution, as it needs no control algorithms in addition to the one usually already implemented to control the outlet temperature of the boiler.

For all simulations in this section, the minimum return temperature set point is 50 °C. The set temperature of the boiler outlet is 62 °C unless specified differently. In order to be able to use the full modulation range of the boiler, the maximum and minimum mass flow rates are determined as:

Eq. 5.5 $\dot{m}_{B,max} \approx \dfrac{\dot{Q}_{B,wat,out,max}}{cp_{wat} \cdot \left(t_{B,set} - t_{B,rt,set,min} \right)}$

$$Eq.\ 5.6 \qquad \dot{m}_{B,min} \approx \frac{\dot{Q}_{B,wat,out,max}}{\dot{Q}_{B,wat,out,min}} \cdot \dot{m}_{B,max}$$

In the case of active power modulation by return temperature set point change, the relationship between the minimum and maximum return temperature set points is similar:

$$Eq.\ 5.7 \qquad t_{B,set} - t_{B,rt,set,max} \approx \frac{\dot{Q}_{B,wat,out,min}}{\dot{Q}_{B,wat,out,max}} \cdot \left(t_{B,set} - t_{B,rt,set,min} \right)$$

With these criteria applied for the external boiler system, the resulting values used for power modulation control are shown in Table 5.15.

Table 5.15: Parameters for the simulation of combustion power control of the pellet boiler (base case).

Parameter	Value	Unit
$\dot{Q}_{wat,max}$, maximum heat output of the boiler	12	kW
$\dot{Q}_{wat,min}$, minimum heat output of the boiler	4.8	kW
$t_{rt,set,min}$, minimum return temperature	50	°C
$t_{B,set}$, boiler outlet set temperature	62	°C
$\dot{m}_{aux,max}$, maximum mass flow rate through the boiler	860	kg/h
$\dot{m}_{aux,min}$, minimum mass flow rate through the boiler if mass flow is controlled	300	kg/h
$t_{B,rt,set,max}$, maximum return temperature set point if return temperature is controlled	58	°C

C1: passive increase of return temperature with one TES temperature sensor

If only one temperature sensor within the TES shall be used for the control of the pellet boiler, this sensor has to be placed low enough to detect when the space heat zone gets discharged, but the temperature criteria for auxiliary heating ($t_{store,ON}$ and $t_{store,OFF}$) have to be based on the temperature requirements for DHW. Thus, the space heat zone of the TES is kept at a higher temperature than actually needed. It is important that the boiler does not turn OFF immediately when its supply temperature ($t_{B,wat,out}$) surpasses its set-temperature ($t_{B,set}$), but only if the TES temperature reading (t_{store}) surpasses the OFF-criteria ($t_{store,OFF}$). In control strategy C1, combustion power is the only manipulated variable, i.e. the return temperature set point and the pump speed are not controlled and thus remain unchanged. The set point for the control algorithm is the outlet temperature $t_{B,set}$. Letters a to c are used for C1 to C7 to distinguish different strategies for the OFF-criteria of the boiler ($t_{store,OFF}$) and the set temperature of the boiler ($t_{B,set}$):

a: $t_{B,set} = 62°C$; $t_{store,ON} = 52°C$; $t_{store,OFF} = 63°C$;

b: $t_{B,set} = 62°C$; $t_{store,ON} = 52°C$; $t_{store,OFF} = 61°C$;

c: $t_{B,set} = 90°C$; $t_{store,ON} = 52°C$; $t_{store,OFF} = 61°C$.

The consequences of these different control strategies are shown in Figure 5.22 for an exemplary charging process of a TES that was at 45 °C at the beginning of the simulation. For all three control strategies (a to c) the burner starts with a reduced combustion power (1, start phase), followed by a phase with maximum combustion power (2) where the outlet temperature of the boiler ($t_{B,out}$) has not reached its set temperature ($t_{B,set}$) yet. The short drop in storage temperature ($t_{S,out}$ and $t_{S,sensor}$) during this phase is due to the simultatneous discharging by the space heating loop (not shown), and the boiler inlet temperature ($t_{B,in}$) is maintained at about 50 °C by the return temperature controlled mixing valve. For the control strategies a and b, this phase is followed by a phase where the return temperature from the TES ($t_{S,out}$) increases above the minimum return temperature of 50 °C and the controller adapts the combustion power in order to keep the outlet temperature at 62 °C (3). This is followed by a phase with minimum combustion power (4) where $t_{B,out}$ is already higher than $t_{B,set}$, but the temperature in the TES ($t_{S,sensor}$) has not reached the OFF-criteria ($t_{store,OFF}$) yet. For control strategy b $t_{store,OFF}$ is 1 K lower than $t_{B,set}$ and thus this point is reached quite sooner than for control strategy a where $t_{store,OFF}$ is 1 K higher than $t_{B,set}$.
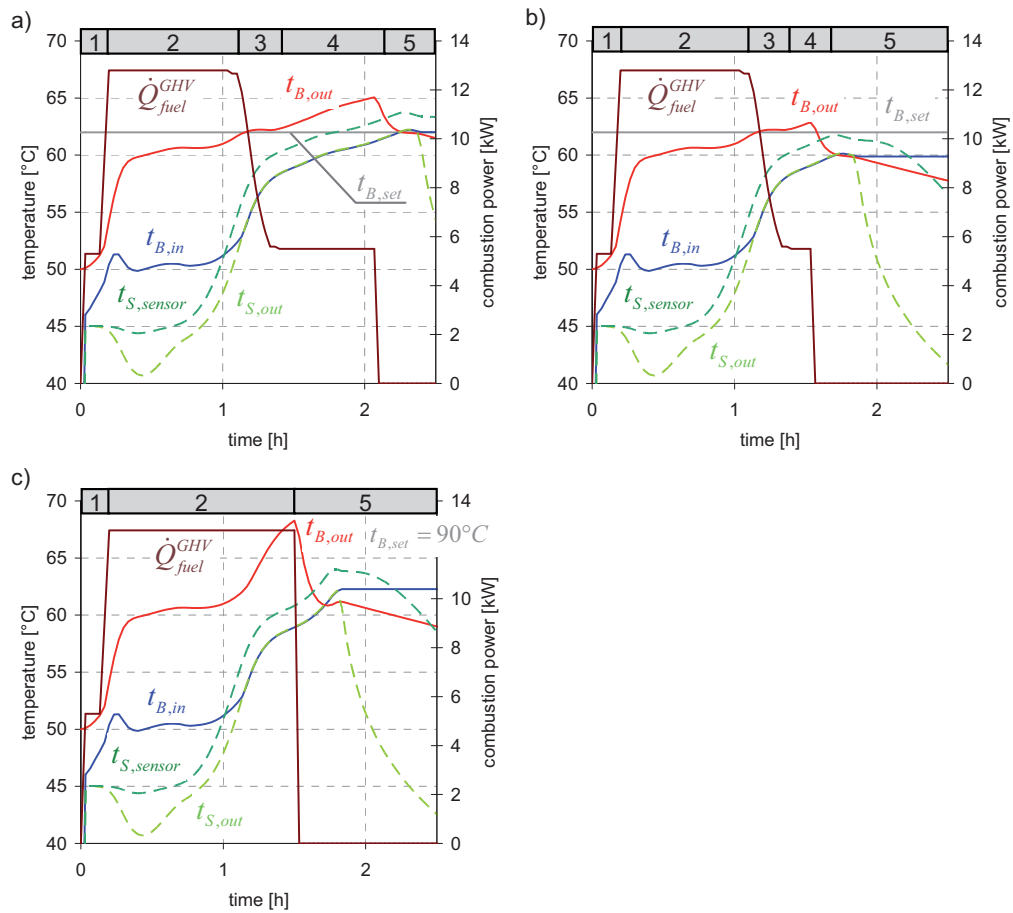
Figure 5.22: Temperatures and combustion power during TES charging for the three different control strategies a, b, and c.

C2: passive increase of return temperature with one average TES temperature measurement

Average temperature measurement has been proposed for the control of power modulation in small biomass heating networks with a stratifying TES (compare 5.1.5). The effectiveness of one average TES temperature measurement in the overlap of zones B and D for switching the burner on and off is investigated by simulation C2. It has to be noted that the idea of the average temperature measurement, the active control of power modulation based on the temperature measurement, is not reflected with simulations C2a-C2c, but with the simulations C3 and C4.

C3r and C3p: active increase of return temperature (r) or active control of pump speed (p) with one TES temperature sensor

The burner is switched ON and OFF based on one temperature sensor measurement at relative height of 45%, i.e. in the overlap of the space heat zone and the auxiliary heated zone. The ON and OFF criteria are the same as in C1. Based on the temperature measurement in the store (process variable) and the set point for the temperature in the store that equals the ON-criteria ($t_{store,set} = t_{store,ON}$) one of the following control strategies is implemented:

r: the **r**eturn temperature set point is manipulated between 50 °C and 58°C;

p: the **p**ump speed is controlled in order to achieve a mass flow rate between 300 kg/h and 860 kg/h through the boiler.

The set point for the boiler outlet ($t_{B,set}$) is kept constant at 62 °C, and thus increasing the return temperature while keeping the mass flow rate throught the boiler constant causes the boiler controller to subsequently decrease also combustion power. The same effect can be expected from decreasing the pump speed while keeping the return temperatur constant.

It has to be mentioned that an actively controlled mass flow rate of the boiler loop pump may be difficult to handle from a control perspective, because a) the mass flow rate is usually not measured, and b) the three controlled variables combustion rate, return temperature (mixing valve) and pump speed influence each others process variables.

C4r and C4p: active increase of return temperature or active control of pump speed with one average TES temperature measurement

These control strategies are similar to C3r and C3p, with the difference that an average temperature of the overlap of the auxiliary heated zone and the space heat zone is used as the process variable to control the ON and OFF signal for the burner as well as the combustion power modulation.

C5: Two temperature sensors: one for ON, one for OFF, passive increase of return temperature

If two temperature sensors placed at different heights are used to control the charging of the TES, the upper one can be used for the ON-signal, and the lower one for the OFF-signal. However, for a TES with a relatively small section of overlap between the boiler charging zone D and the space heat zone B of the TES as shown in Figure 5.21, there can not be a large difference in height between the two sensors, since both should be placed within this overlap of zones B and D.

C6r and C6p: Two temperature sensors: one for DHW, one for space heat, active control of return temperature (r) or pump speed (p)

To do justice to the different temperature requirements for DHW and space heating, one sensor is preferably placed within each zone, and used for ON and OFF signals for the corresponding zone. For space heating, a boiler outlet set temperature that is lower than the one required for DHW could be used theoretically. However, conventional pellet boilers that must avoid the condensation of water vapour in the flue gas usually require a minimum set temperature for the boiler outlet that is close to the temperature needed for the DHW charging anyway. In this case, the inlet position of the boiler charging can be kept at the top of the TES, and $t_{B,set}$ can be kept at the temperature required for DHW. In this case the only advantage of one sensor for each zone is that the ON and OFF signals as well as the combustion power of the modulating boiler can be controlled for each zone separately. Warm water preference is given whenever the temperature in the warm water zone has dropped below the ON-temperature for this zone.

C7: Two average temperature measurements: one for the DHW zone, one for space heat zone, active control of return temperature (r) or pump speed (p)

This control strategy is similar to C6, with the difference that now average temperatures of each zone are used for the control of charging of each zone.

Overview of simulations C1-C7

An overview of different settings used for the simulation of the different control strategies C1 to C7 is given in Table 5.16 to Table 5.18.

Table 5.16: Parameters used for the simulation of the external pellet boiler with one TES sensor and passive modulation control.

Parameter	Unit	C1			C2		
Control strategy		**a**	**b**	**c**	**a**	**b**	**c**
$t_{B,set}$, boiler set temperature	°C	62	62	**90**	62	62	**90**
Rel. height of sensor 1	-	0.45	0.45	0.45	**0.4-0.5**	0.4-0.5	0.4-0.5
t_{ON} sensor 1	°C	52	52	52	52	52	52
t_{set} sensor 1	°C	-	-	-	-	-	-
t_{OFF} sensor 1	°C	**63**	**61**	**61**	**63**	**61**	**61**
$\dot{m}_{aux,max}$, max. mass flow rate	kg/h	860	860	860	860	860	860
$t_{B,rt,set}$, return temp. set point of boiler	°C	50	50	50	50	50	50

Table 5.17: Parameters used for the simulation of the external pellet boiler with one TES sensor and active modulation control.

Parameter	Unit	C3r		C3p		C4r		C4p	
Control strategy		**a**	**b**	**a**	**b**	**a**	**b**	**a**	**b**
$t_{B,set}$	°C	62	62	62	62	62	62	62	62
Rel. height of sensor 1	-	0.45	0.45	0.45	0.45	**0.4-0.5**	0.4-0.5	0.4-0.5	0.4-0.5
t_{ON} sensor 1	°C	52	52	52	52	52	52	52	52
t_{set} sensor 1	°C	52	52	52	52	52	52	52	52
t_{OFF} sensor 1	°C	**63**	**61**	**63**	**61**	**63**	**61**	**63**	**61**
$\dot{m}_B$, mass flow rate	kg/h	860	860	300 – 860	300 – 860	860	860	300 – 860	300 – 860
$t_{B,rt,set}$	°C	**50 - 58**	**50 - 58**	50	50	**50 - 58**	**50 - 58**	50	50

Table 5.18: Parameters used for the simulation of the external pellet boiler with two TES sensors.

Parameter	Unit	C5			C6		C7	
Control strategy		**a**	**b**	**c**	**r**	**p**	**r**	**p**
$t_{B,set}$	°C	62	62	**90**	62	62	62	62
Rel. height of sensor 1	-	**0.5**	0.5	0.5	**0.55**	0.55	**0.5-1.0**	0.5-1.0
t_{ON} sensor 1	°C	52	52	52	55	55	56	56
t_{set} sensor 1	°C	-	-	-	55	55	56	56
t_{OFF} sensor 1	°C	-	-	-	62	62	63	63
Rel. height of sensor 2	-	**0.4**	0.4	0.4	**0.45**	0.45	**0.4-0.5**	0.4-0.5
t_{ON} sensor 2	°C	-	-	-	**+0**[a]	+0[a]	+0[a]	+0[a]
t_{set} sensor 2	°C	-	-	-	**+0**[a]	+0[a]	+0[a]	+0[a]
t_{OFF} sensor 2	°C	**63**	**61**	**61**	+20[a]	+20[a]	+20[a]	+20[a]
$\dot{m}_B$	kg/h	860	860	860	860	**300 - 860**	860	**300 - 860**
$t_{B,rt,set}$	°C	50	50	50	**50-58**	50	**50-58**	50

[a] *temperature difference to the supply temperature set point of the space heating system.*

Simulation results

Figure 5.23 shows the number of burner starts and the fractional energy savings for different control strategies of TES charging obtained from annual simulations. The figure shows that a boiler temperature set point that is below the OFF criteria of the TES temperature measurement (labelled "a") always leads to a lower number of burner starts (Figure 5.23a), but also to a lower efficiency (Figure 5.23b), than a temperature set point that is above the OFF criteria of the TES temperature measurement (labelled "b"). This is in agreement with Figure 5.22, where control strategy a leads to a longer running-time of the boiler and also to higher temperatures of the boiler and the TES. Naturally, the largest number of burner starts is obtained for systems where the set point of the boiler is high enough to keep running on maximum combustion until the OFF-criteria of the TES-sensor is met (labelled "c"). ON/OFF control with two sensors (C5 to C7) significantly reduces the number of burner starts compared to control with only one sensor (C1 to C4). Even the control with two sensors but no active combustion modulation control based on the TES temperature measurement (C5) resulted in a lower number of burner starts than the simulation of a system with one TES temperature measurement and active control by pump speed or return temperature adaption (C3 & C4). However, the lowest number of burner starts has been reached by the systems with two sensors and active control of combustion power based on the TES temperature measurements (C6 & C7). The best performing system according to these results is the system with one average TES temperature sensor in the DHW zone and another one in the space heat zone and active pump speed control (C7p). This system not only reaches a low number of burner starts, but it also reaches higher thermal energy savings. Thus,

it appears that this system is not only profiting from an optimal control of the combustion power modulation, but also from less losses and electricity savings due to pump speed control. The number of burner starts is reduced by a factor of 3.5 from simulation C2c to simulation C7p.
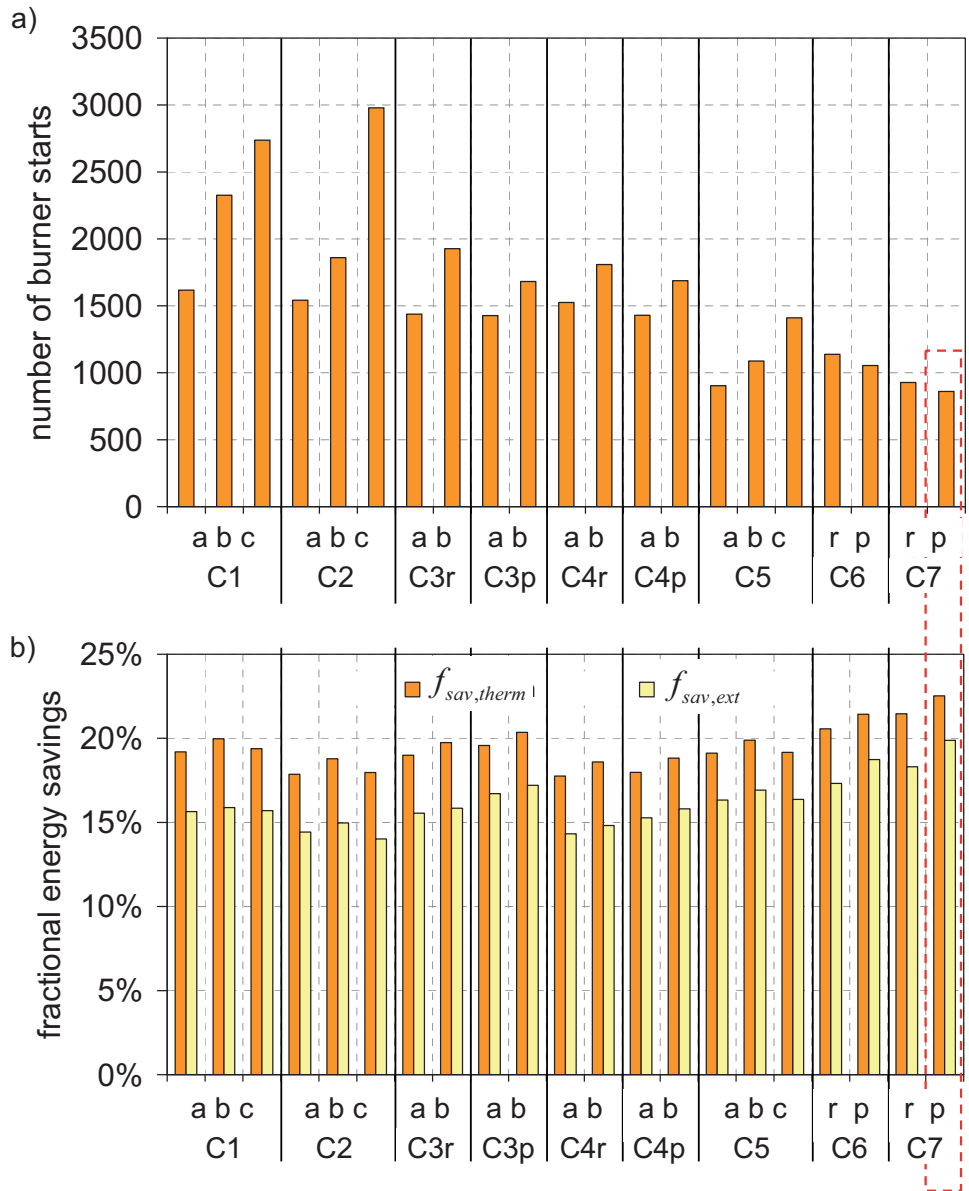
Figure 5.23: Number of burner starts (a) and fractional savings (b) for different control strategies of TES charging by the pellet boiler obtained from annual system simulations.

Inertia effects

In the simulation results C1-C7, the time delay between the TES temperature measurement or the controller decision and the actual combustion rate change was lower than 3 minutes. It can be argued that this idealised assumption does not accurately reflect the time-constants involved in the actual closed loop control of the combustion rate of a pellet boiler. Therefore, in simulation C6p*, and C7p*, an additional time-delay of 10 minutes between controller decision and actual combustion rate adaption has been introduced. The changes in the simulation results with respect to simulations C6p and C7p are presented in Table 5.19. The results indicate a less optimal power control with slightly lower savings and about 10% more burner starts. Additionally, problems to maintain the DHW comfort occurred for simulation C7p*. The latter could possibly be solved by higher set temperatures for the ON- and OFF-criteria.

Table 5.19: Change in simulation results by introduction of an additional time delay for combustion power adaption based on controller decision. Percentages are absolute differences.

	$\Delta f_{sav,therm}$	$\Delta f_{sav,ext}$	ΔN_{start}
C6p*	-0.17%	-0.14%	+123
C7p*	-0.20%[a]	-0.16%[a]	+114

[a] this simulation did not meet the warm water comfort requirements.

5.3.6   Improved system with an external pellet boiler

Apart from improving the TES and the control of TES charging by the external pellet boiler, also the external pellet boiler itself can be improved by the following measures:

– Increasing the achieved range of power modulation from the measured 43%-100% to 30%-100%.

– Reducing the heat loss coefficient from the combustion chamber and the heat exchanger by 50%, which is still not as well insulated as a state of the art solar TES with the same surface area.

– Decreasing the excess air for combustion from 2.35 - 3.25 to 1.8, independent from combustion power modulation.

A side effect of the increased power modulation range is that a new control strategy had to be found to replace the control strategy of priority for DHW preparation. In the simulations shown in the previous Section, whenever the criteria for DHW preparation was met, the control strategy was to keep the DHW temperature set point (t_{set}) in the TES, until this temperature set point was surpassed running on the lowest continuous combustion power that the boiler was capable of. This DHW preparation priority was kept independently from the temperature in the space heat section. The fundamental error of this strategy

becomes apparent when the power modulation range of the boiler includes on the lower limit power levels that are not sufficient for space heating anymore for longer time periods, and the boiler keeps running on this low power level in the DHW preparation mode. Therefore, a new combustion power control strategy was developed and applied to all simulations with power modulation range 30% - 100% and two average TES temperatures for its control. This control strategy is based on the process variable $dT_{store,ctr}$ as shown in Eq. 5.8 - Eq. 5.10.

$$Eq.\ 5.8 \qquad dT_{store,DHW} = t_{store,ms,DHW} - t_{store,set,DHW}$$

$$Eq.\ 5.9 \qquad dT_{store,SH} = t_{store,ms,SH} - t_{store,set,SH}$$

$$Eq.\ 5.10 \qquad dT_{store,ctr} = MIN\left[dT_{store,DHW} ; dT_{store,SH} \right]$$

The process variable $dT_{store,ctr}$ is positive when both temperatures measured are above the corresponding set points, but negative when one of them drops below its set point. The set point for $dT_{store,ctr}$ is zero, with decreasing action on boiler pump speed. This means that the boiler pump speed is reduced when the value of $dT_{store,ctr}$ gets larger. Apart from the changes made to improve the system, the TES-temperature of sensor 1 (t_{ON}) for switching the burner on for DHW preparation had to be increased by 1 K in order to avoid penalties for not meeting the comfort criteria.

Table 5.20 shows the changes made in the simulation parameters and the achieved simulation results for systems D to G compared to system C7p from Section 5.3.5.

Table 5.20: Parameters and results for simulations with an improved external pellet boiler.

Parameters	Unit	System C7p	System D	System E	System F	System G
$\dot{Q}_{fuel,max}^{GHV}$, maximum combustion power	kW	12.8	12.8	12.8	12.8	12.8
$\dot{Q}_{fuel,min}^{GHV}$, minimum combustion power	kW	5.3	3.8	3.8	3.8	3.8
UA_{hx-amb}, heat loss coefficient to the ambient	W/K	6.8	6.8	**3.4**	6.8	**3.4**
fr_{cc-amb}, fraction of GHV lost by the combustion chamber	-	1.8%	1.8%	**0.9%**	1.8%	**0.9%**
λ_{min}, minimum lambda	-	2.35	2.35	2.35	**1.8**	**1.8**
λ_{max}, maximum lambda	-	3.25	3.25	3.25	**1.8**	**1.8**
t_{ON} sensor 1	-	56	**57**	**57**	**57**	**57**
Simulation results						
$f_{sav,therm}$, thermal energy savings		**22.5%**	**22.5%**	**27.9%**	**24.7%**	**30.0%**
$Q_{coll,spec}$, spec. collector yield	kWh/m²a	320	319	319	319	319
$N_{burn,start}$, number of burner starts	-	861	431	484	458	519

Table 5.20 shows that the extension of power modulation from 41%-100% (system C7p) to 30%-100% (system D) reduces the number of burner starts by a factor of 2 for this system with a nominal boiler capacity that is about twice the design heat load for space heating. The results also show that improvement of the boiler insulation (system E) may save more than 5% energy over the whole year, and a reduction of the excess air for combustion (system F) more than 2%. With all measures for the improvement of the boiler together (system G), the system saves 7.5% more energy and has 40% less burner starts than the system with only improvements made on the TES and on the boiler power modulation control.

5.3.7 Tank-in-tank system with an external pellet boiler

An alternative to the DHW preparation with an immersed heat exchanger spiral is to use an immersed DHW tank in the buffer tank, a so called tank-in-tank TES, as shown in Figure 5.24.
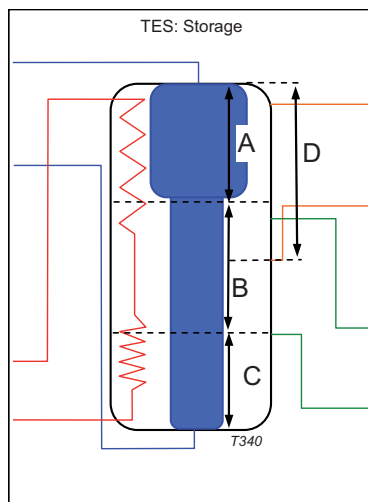
Figure 5.24: Hydraulic schematic for the tank-in-tank TES. T340: TRNSYS Type Nr. 340. A) DHW zone; B) space heat zone; C) DHW preheating zone; D) auxiliary heated zone.

For the parameterization of the TES model, a coefficient for heat transfer from the outer tank to the inner tank is needed. This heat transfer coefficient may be assumed similar to the heat transfer from a mantle tank heat exchanger to the TES if in both cases the predominant heat transfer mechanisms are the same. Nusselt-Rayleigh relationships for mantle tank systems with gap widths of 10 to 34 mm and low flow conditions have been given by a number of authors (Shah & Furbo 1998; Shah 2000; Knudsen 2004). Shah et al. (1999) investigated the flow structure in vertical mantle heat exchangers of 33 mm gap-size using a full-scale tank with Particle Image Velocimetry (PIV). Based on the data for heat transfer rates (100 – 1100 W/m²) and temperature differences (0.2 to 3.8 K) presented, the coefficient for heat transfer from the mantle fluid to the outer surface of the inner tank wall was in the range of 300 – 400 W/m²K. Knudsen (2002) determined heat transfer coefficients from the outer tank to the wall of the inner tank of a tank-in-tank combistore by means of CFD calculation. He found that these heat transfer coefficients were in the order of 190 - 280 W/m²K when there was bulk fluid motion in the outer tank from operation of space heating and/or the auxiliary charging loop, but only 20 – 30 W/m²K when there was no bulk fluid motion.

In the studies presented here, a constant heat transfer coefficient from the outer tank fluid to the inner tank fluid of 120 W/m²K is used. This corresponds to about twice the resistance of heat transfer from the outer fluid to the tank wall of the inner tank presented in the above studies for the situation of bulk fluid motion.

Table 5.21: Parameters for the simulation of a tank-in-tank TES.

Parameter	Value	Unit
V_{store}, TES volume	0.848	m³
Γ_{store}, TES height	1.733	m
d_{store}, inside diameter of the outer tank	0.79	m
V_{DHW2}/V_{DHW1}, volume of the upper / lower part of the inner tank	0.150 / 0.100	m³
d_{DHW2}/d_{DHW1}, diameter or the upper / lower part of the inner tank	0.62 / 0.32	m
$\Gamma_{DHW2}/\Gamma_{DHW1}$, height of the upper / lower part of the inner tank	0.500 / 1.233	m
A_{DHW2}/A_{DHW1}, surface of the upper / lower part of the inner tank	0.97 / 1.24	m²
UA_{DHW2}/UA_{DHW1}, heat transfer coefficient of the upper / lower part of the inner tank	116 / 149	W/K
$z_{sh,in}$, rel. height of inlet from space heating loop (return)	0.25	-
$z_{sh,out}$, rel. height of outlet to space heating loop (supply)	0.7	-
$z_{aux,in}$, rel. height of inlet from auxiliary boiler loop (supply)	0.93	-
$z_{aux,out}$, rel. height of outlet to auxiliary boiler loop (return)	0.55	-

Table 5.22: Parameters and results for two tank-in-tank systems compared to similar systems with immersed heat exchanger spirals for DHW preparation.

Parameter	Unit	System C7p	System TiTA	System G	System TiTB
$\dot{Q}_{max}^{GHV}$, maximum combustion power	kW	12.8	12.8	12.8	12.8
$\dot{Q}_{min}^{GHV}$, minimum combustion power	kW	5.3	5.3	**3.8**	**3.8**
UA_{hx-amb}, heat loss coefficient to the ambient	W/K	6.8	6.8	**3.4**	**3.4**
UA_{cc-amb}, fraction of GHV lost by the combustion chamber	-	1.8%	1.8%	**0.9%**	**0.9%**
λ_{min}, minimum lambda	-	2.35	2.35	**1.8**	**1.8**
λ_{max}, maximum lambda	-	3.25	3.25	**1.8**	**1.8**
t_{ON} sensor 1	-	56	56	**57**	**57**
Simulation results					
$f_{sav,therm}$, thermal energy savings		**22.5%**	**23.6%**	**30.0%**	**31.2%**
$Q_{coll,spec}$, spec. collector yield	kWh/ m²a	320	334	319	332
$N_{burn,start}$, number of burner starts	-	861	897	519	547

Table 5.21 shows the parameters used for the simulation of the tank-in-tank systems. The system tank-in-tank A (TiTA) was defined similar to System C7p, i.e. with exception of the parameters shown in Table 5.21, the same parameters were used as for Sytem C7p (see Table 5.18). Likewise, system tank-in-tank B (TitB) was defined similar to system G (see Table 5.20).

According to the results shown in Table 5.22, the tank-in-tank systems have slightly higher thermal energy savings and number of burner starts than the corresponding systems with immersed DHW heat exchanger.

5.3.8 Comparison of the different hydraulic approaches

Figure 5.25 and Figure 5.28 show the results of simulations that are based on measured parameters for the TES and for the boiler or burner. It has to be kept in mind that heat losses of the boiler water and connecting pipes are included in $Q_{loss,aux}$ for the system with the external boiler, whereas heat losses from the boiler or TES water to the ambient are included in $Q_{loss,store}$ for the system with the integrated burner. Although the TES losses of the integrated burner solution are more than double the TES losses of the system with an external boiler, the combined losses of the TES and the boiler to the ambient are significantly larger for the external boiler system than the TES losses of the integrated burner system. In addition, also the sensible flue gas losses of the integrated burner are lower due to a lower excess air factor for combustion. Finally, the integrated burner solution saves about 10% more energy than the simulated external boiler solution. The electricity consumption is only slightly higher for the external boiler solution than for the integrated burner.

Figure 5.26 and Figure 5.29 show the results of simulations that have been performed with the improved TES parameters of System B (Table 5.10) for the TES with the integrated burner. The external boiler solutions correspond to System C7p (Table 5.18) and System TiTA (Table 5.22). The integrated burner solution profits more from improvements of the TES because lower heat losses than for the base case have been assumed, whereas the heat loss coefficients of the other two systems had already been assumed low for the base case and therefore remained unchanged. The improvements of the external boiler solution C7p compared with its base case derive from lower temperature set points within the TES and consequently lower heat losses of the boiler and the TES as well as higher solar yield (see Figure 5.29).
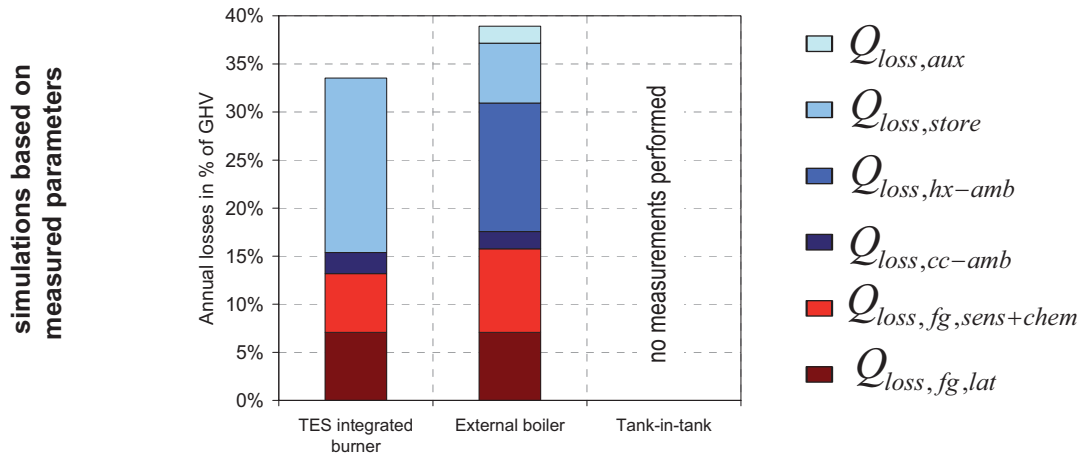
Figure 5.25: *Simulated annual losses of two different hydraulic solutions. Simulation parameters **based on measured results for burner/boilers and TES.***
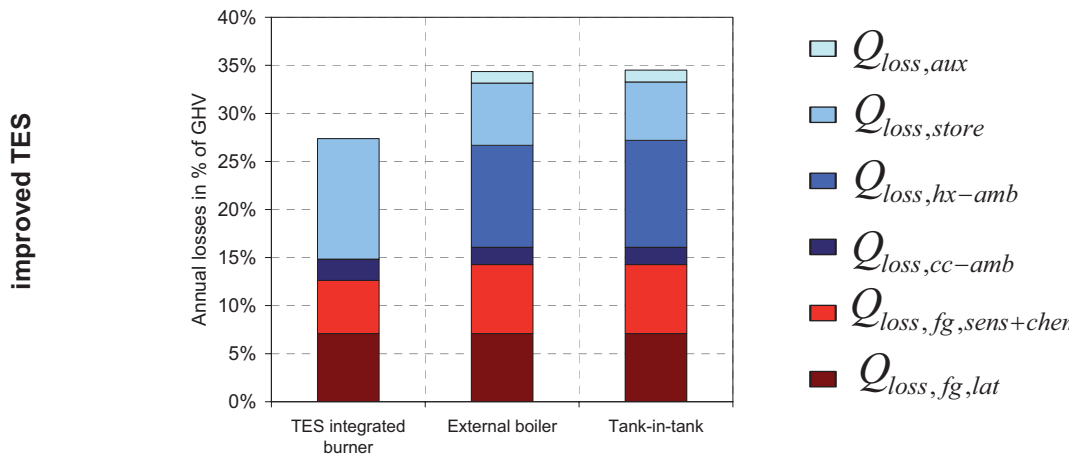
Figure 5.26: *Simulated annual losses of the three different hydraulic solutions, based on an **improved TES and TES charging control** and on measured results for the burner/boilers.*
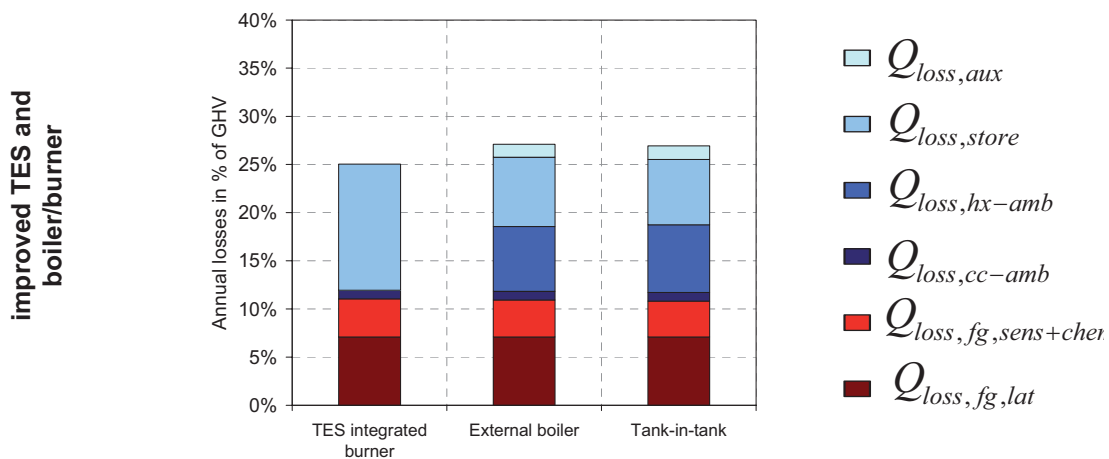
Figure 5.27: *Simulated annual losses of the three different hydraulic solutions, based on an **improved TES and TES charging control and on an improved burner/boiler.***

104
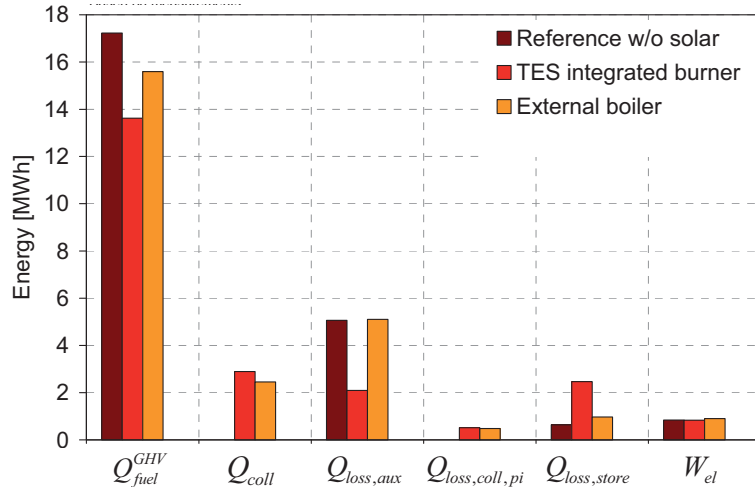
Figure 5.28: Simulated annual energy flows of different hydraulic solutions. Simulation parameters **based on measured results for burner/boilers and TES.**
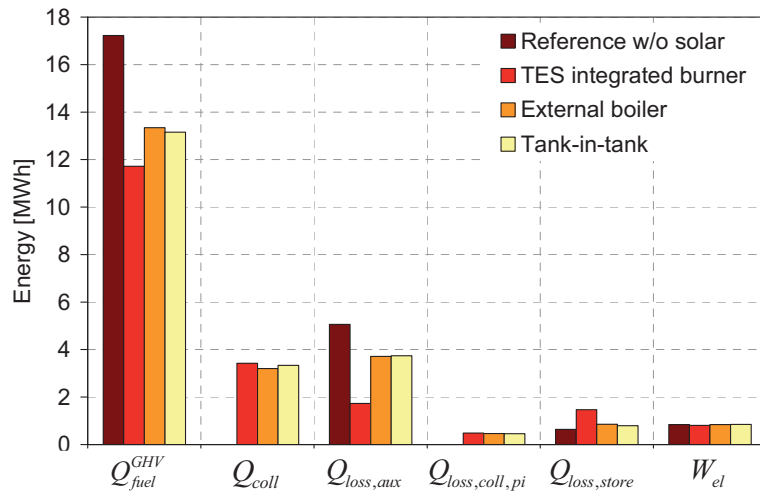
Figure 5.29: Simulated annual energy flows of different hydraulic solutions, based on an **improved TES and TES charging control** and on measured results for the burner/boilers.
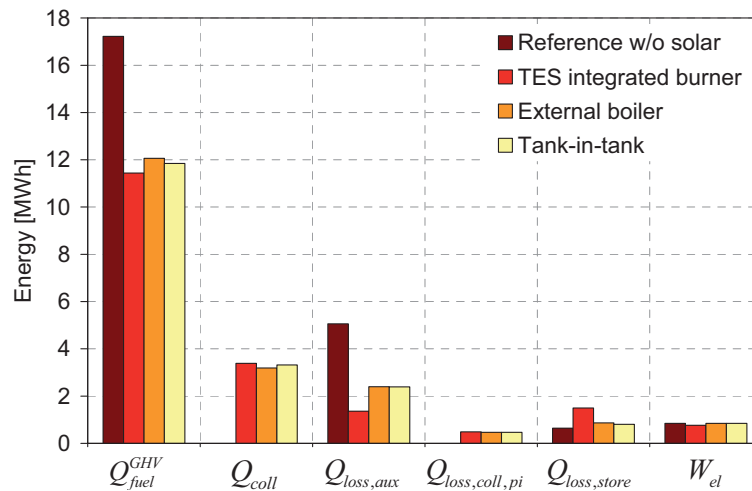
Figure 5.30: Simulated annual energy flows of different hydraulic solutions, based on an **improved TES and TES charging control and on an improved burner/boiler.**

Figure 5.27 and Figure 5.30 show results of simulations performed with improved TES parameters and improved boiler/burner parameters. These systems correspond to Systems G and TiTB (Table 5.18 and Table 5.22) for the systems with external boilers. The results for the system with the integrated burner are based on a simulation that used the values from System B (Table 5.10) with the exception of heat losses from the combustion chamber and lambda that have been set equal to the values of the systems G and TiTB. The integrated burner solution only improves its heat losses from the combustion chamber to the ambient. For this system, the heat losses from the heat exchanger to the ambient have already been reduced with the TES losses. However, the other two systems are able to reduce heat losses to the ambient as well as sensible heat losses of the flue gas of the boiler (lower excess air factor) significantly. Thus, the differences in the performance of the three systems get smaller. Still the integrated burner solution achieves the highest thermal energy savings, followed by the external boiler with tank-in-tank system that performs slightly better than the external boiler with the immersed DHW heat exchanger spiral.

In reality, the result of such a comparison will depend largely on the question how well the different manufacturers were able to achieve:

– low heat losses to the ambient of both, the TES and the boiler;

– low set temperatures for the auxiliary heated zone of the TES;

– and a low excess air factor (and flue gas exhaust temperatures) for the combustion without increasing emissions above the levels of tolerance.

It is worth noting that in all annual simulation results heat losses from the boiler (or burner TES combination) to the ambient were much more predominant than sensible flue gas losses, although the sensible flue gas losses are usually more predominant in full and part load efficiency testing.

Concerning the number of burner starts, the system with an external pellet burner with a good power modulation control between 30 and 100% achieved about 500 burner starts per year, which is about six times less than the values simulated with no possibility of power modulation or with an ineffective control of power modulation.

6 Conclusion and outlook

6.1 Conclusion

6.1.1 The boiler

A semi-physical (or semi-empirical) boiler model has been developed for the simulation of oil, gas and biomass space heating boilers. The model includes features that have already been described by previous authors, as well as new features that have been developed based on own measurements. The most important features are the ability to reflect the influence of space heating return temperature, power modulation and condensation gains on the flue gas losses of the boiler, the simulation of a thermal capacitance including its heat losses during standby and operation, and the ability to calculate carbon monoxide emissions and electricity use dependent on power modulation and number of burner starts.

New features of the presented boiler model are the unification of models for oil, gas and biomass boilers into one model, and the possibility to use the model for any fuel defined by the user by its elementary composition and the gross heating value. Further novelties include the combination of steady state calculation for the flue gas to water heat transfer with an explicit solution for the time dependent temperature change of the boiler's thermal capacitance. Thus, it is possible to simulate the boiler's thermal capacitance with shorter calculation time than e.g. for multi-node models that depend on iterative calculations for convergence. Other features that have not been found explicitly in the presented literature study are the distinction between losses from the boiler water (thermal capacitance) and the combustion chamber, the assumption of different heat loss coefficients from the boiler water to the ambient during burner operation and during burner standby, and the possibility of water vapour undersaturation of the leaving flue gas under condensing conditions (compare Part II, Paper III).

In combination with a stratified storage tank model, the presented boiler model may also be used for the simulation of a burner integrated into a solar storage tank, a combi-boiler that provides domestic hot water (DHW) and hot water for space heating within one unit, or boilers with a high degree of stratification (compare Appendix A.

The simulation results of the presented boiler model are in good agreement, i.e. usually within the range of measurement uncertainties, with results observed in steady state and cycling tests performed on the different boiler units.

Improvements of the presented model's capability to simulate biomass boilers might be possible by addition of a second thermal capacitance node for the combustion chamber. Improvements of efficiency prediction under cycling operation might be achieved by introducing additional start losses.

Concerning the simulation of draught losses, further investigations are necessary for the validation of a draught loss model.

For accurate simulation of boiler cycling, data is needed that may currently not be derived from standard test procedures and has to be estimated based on

manufacturer's data or additional tests. Cycling operation is very commonly found in small space heating boiler installations and may have a large influence on boiler efficiency, electricity consumption and emissions. Therefore, standard testing procedures for start and stop phase measurements should be developed.

6.1.2   The thermal energy storage tank

In Chapter 3.1 results are presented from measurements that were performed on a TES for the characterization of a TES model for the simulation of annual energy balances. Parameters were identified for heat losses, vertical heat transfer within the TES, localization and heat transfer characteristics of the solar and DHW heat exchangers, as well as localization of the direct discharging space heating double ports. It was difficult to obtain a good correlation between measured and simulated solar heat exchanger outlet temperature and power for all experimental conditions, because the upper part of the solar heat exchanger showed some stratification, but not quite as much as the model simulations show when the heat exchanger is simulated with stratification. Similar observations for the simulation of imperfect stratifying devices have been reported previously (Bales 2000). For further simulation studies, it has been chosen to simulate the upper part of the solar heat exchanger without the stratifying option. Furthermore, the space heating double port inlet and outlet positions were difficult to localize, since heat transfer is happening not only to or from one height of the TES. Explanations for this could be that heat is transferred across the walls of the internal pipes of the flow and return line to the lower sections of the TES volume.

In Chapter 3.2, a theoretical analysis of methods for the comparison of stratification efficiencies of TES processes was presented. This revealed that most methods found in literature are not suited for an application to experiments that include variable inlet temperatures of charging and discharging as they occur in solar heating applications. The one method that showed potential for the use with realistic temperature profiles of charging and discharging inlets however may be biased by heat losses of the storage tank. This may not be a problem if only e.g. different inlet geometries are compared within the same TES. It may be a problem however, if different TES are compared with each other, since the obtained efficiency value may be an indicator for the storage heat losses rather than for the goodness of stratification. The new method introduced in this work combines the advantages of previous methods. It is expected to be also applicable to experiments with variable inlet temperatures and mass flows. The simulated case of charging, storing and discharging of two TES with different heat loss coefficients showed that the method has the potential of eliminating the bias of heat losses effectively. This has been confirmed by application of the method to measurements on TES processes.

6.1.3   The collector

An existing model for the simulation of solar thermal collectors including the thermal capacitance of the collector was analyzed and changed in order to avoid temperature jumps that could be observed when simulating with a small time

step and / or a large thermal capacitance of the collector. The solution found is a segmentation of the collector into a number of serial segments. The results from the changed model are in agreement with the steady state efficiency of collector test results as well as with the theoretical stagnation temperature calculated based on the thermal efficiency parameters of the collector.

6.1.4 Combined solar and pellet heating systems

Combined solar and pellet heating systems for space heating and DHW preparation may contribute significantly to the goal of reducing CO_2 emissions from non-renewable fuels in this sector. In order to use wood fuel effectively the thermal energy saving of a solar and pellet heating system in comparison with a reference heating system without the use of solar energy should be as large as possible. From the presented literature study it can be concluded that the possibility of combustion power modulation of the burner or boiler should be used effectively in order to reduce the number of burner starts and thus also emissions associated with the start and stop phases of the burning process.

Field monitoring was performed on five micro heating networks with solar and biomass heating systems in the range of 20 to 150 kW maximum heating power. The field studies showed that a collector yield of 400 kWh/m²a is possible in these systems for the climate of Graz / Austria. The identified heat losses of the TES were below 5% of total energy use. At the same time it was observed that in most of these systems power modulation of the boiler was not used effectively. The same observation was made for biomass boilers that charge a thermal energy store with the use of solar thermal energy (Haberl et al. 2009) and without the use of solar thermal energy (Gabathuler 2009; Bühler & Jenni 2009).

Simulations of solar and pellet heating systems were performed with the simulation software TRNSYS, based on the measurements performed on several pellet boiler units (presented in Section 2.5) and on the 800 litre TES with integrated pellet burner (presented in Section 3.1). The simulated space heating load was 8.5 MWh and the DHW load 3.0 MWh[18]. Thermal energy savings were defined based on a comparison of the fuel energy consumption of these systems with the fuel energy consumption of a reference pellet heating system without the use of solar thermal energy.

Annual simulation results with a boiler model that was parameterized based on measurements showed that despite the fact that sensible flue gas losses are usually the main losses in steady state boiler operation, heat losses to the ambient may be far more predominant on an annual basis under realistic load conditions.

The annual simulation results for the measured system with an integrated pellet burner were compared with a system where an external pellet boiler is connected to a similar TES without pellet burner integration and therefore also better insulation. The results showed that the integrated burner solution saves considerably more fuel energy than the external pellet boiler connected to the better insulated TES. Parametric studies revealed large potential for improvements for both systems in terms of energy savings as well as in terms of

---

[18] IEA-SHC Task 32 reference heating system SFH60 for the climate of Zurich.

effective use of combustion power modulation of the burner. The most significant influencing factor for energy savings were:

– a better insulation of the TES for the integrated burner solution, and better insulation of the boiler for the external boiler solution;

– a higher heat transfer capacity for the immersed DHW heat exchanger spiral that allows for lower set temperatures for the upper part of the TES;

– a lower excess air factor for the combustion in the external boilers;

– a better insulation of the combustion chamber for both systems;

– more heat transfer capacity from the solar heat exchanger located in the lower part of the TES instead of the upper part of the TES.

Simulations were performed in order to detect the potential for improvements in energy savings and number of burner starts without changing the size of the TES or of the collector field. Simulations performed with improved TES parameters[19] lead to 11-13% more savings for both systems, the TES with the integrated burner and the system with the external pellet boiler. Simulations performed with additionally improved boiler or burner characteristics[20] and improved use of combustion power modulation revealed an additional 8% of energy savings potential for the external pellet boiler systems. The additional energy savings of the integrated pellet boiler system was in this case only 2%, because the heat losses in this system have already been reduced with the improvements of the TES heat losses. Additional simulations with a hypothetical tank-in-tank TES with external pellet boiler showed slightly more thermal energy savings for this solution compared to the TES with immersed heat exchange spiral for DHW preparation. Comparing only the systems with improved TES and improved burner or boiler, the thermal energy savings compared to the reference system without solar were in the range of 30-34%, which is considerably more energy than supplied by the collector field.

The improvement of the control of combustion power modulation was studied based on annual system simulations. In the case of the integrated pellet burner, the control strategy is relatively simple as the section of the TES above the pellet burner is quite mixed. In the simulation study, one temperature sensor was used to control the combustion power of the burner in this system effectively. Although this control strategy was simple and effective, the number of burner starts could only be lowered from 2800/a to 1700/a. The reason for this is the fact that the integrated burner has about three times the capacity of the design heat load of the heating system. For a burner with a capacity of 5.25 kW that is only slightly above the design heat load of the heating system (4.6 kW) the number of starts could be reduced from 1600/a without combustion power modulation to 240/a with combustion power modulation of 30-100%. For extremely low heat loads the number of burner starts in the investigated system does not depend significantly on the possibility of combustion power modulation. The reason for this is that the heating power of the burner has to be chosen large enough for the DHW preparation and is thus several times oversized for the heat load anyway. In this case, charging the space heating section of the TES by the burner is always

---

[19] Heat losses, DHW heat transfer capacity, lower temperature set points, etc.

[20] Combustion chamber losses for the integrated pellet burner and additionally heat losses from the water body and lambda for the external pellet boiler.

several times faster than discharging it by the heat load. Thus, the ratio of discharge rate, i.e. heat load, to storage volume determines the number of burner starts, with little or no influence of the maximum burner power or ability to modulate this power, unless the minimum part load ratio is low enough to match the heat load again.

For the external pellet boiler the control strategy for TES charging is more difficult because of the TES stratification. Out of 21 control strategies that have been simulated, the best results, both in terms of reduction of the number of burner starts as well as in terms of energy savings, were achieved with two temperature sensors that are capable of measuring the average temperature in the DHW zone and in the space heat zone of the TES, respectively. In this case, the process variable is chosen as the temperature difference between the measurement and the set point of each zone, with priority to the zone where the measured temperature is further below the set point. With this strategy it was possible to reduce the number of burner starts from 3000/a to below 1000/a even for an external boiler with twice the capacity of the design heat load and a modulation range of 43 – 100%.

6.2 Future research

6.2.1 Component simulation models

The boiler model that was developed in this work is based on a one-node thermal capacitance model. Deviations were observed between the thermal response measured and the thermal response simulated with this approach. Further investigations are needed to determine if these deviations can be reduced by addition of a second thermal capacitance, i.e. a capacitance for the combustion chamber, in addition to the one for the combined capacitance of the heat exchanger and the water body. However, this could mean that the relatively simple delta-T approach used for the flue gas outlet temperature has to be abandoned and replaced by a more complicated and more computation time consuming effectiveness-NTU approach. Furthermore, an additional heat capacitance and two additional heat transfer coefficients that connect this capacitance with the flue gas and the thermal mass of the heat exchanger and boiler water will have to be determined by boiler measurements. These additional efforts have to be balanced against the improvements in boiler simulation accuracy that can be achieved.

The investigated TES showed some stratification, but not enough stratification to justify a simulation with the option "stratifying" selected in the TES simulation model used. More work is needed to further develop this TES model, or to develop a new TES model with more freedom for the simulation of stratification efficiency of a TES dependent on the boundary conditions such as mass flow rate of the inlet and temperature differences between the inlet and the surrounding fluid.

6.2.2 Component development

Pellet boiler manufacturers are advised to effectively reduce heat losses to the ambient by convection and radiation from hot parts of the boiler. This work shows that for the investigated pellet boilers these are likely to be the

predominant losses on an annual basis, surpassing by far the sensible and chemical flue gas losses. The same applies for the TES integrated pellet burner.

In order not to compensate emission reductions by less burner starts with higher emissions at part load operation, part load operation of the pellet boilers should be improved. With the exception of the 150 kW wood chip unit, all investigated (pellet) boilers showed increased excess air and carbon monoxide emissions at part load, and none of them was able to reduce the combustion rate automatically to the often claimed 30% of full load.

The control of combustion power modulation of the investigated pellet boilers must be improved, in particular when the boilers are used to charge a TES. For this purpose control algorithms have to be developed and tested in the laboratory. Temperature sensors for the measurement of average temperatures of TES sections are currently not readily available. Prototypes of such sensors could easily be developed based on a resistive temperature device (RTD) with a linear response in the temperature range considered. Similar sensors are available for ventilation systems, but their cost is currently too high (about 200 € per sensor) to be considered for a small solar combistore.

6.2.3   Methods

For a fair comparison of different boilers, standard methods for boiler testing procedures should be developed, including burner start and stop phases as well as the measurement of electricity consumption and emissions during all phases. An extended boiler-efficiency definition should in this case also include electricity consumption. Further, testing of the ability to automatically adapt combustion power to the required load should be included into standard testing procedures.

The measurement of heat losses from the boiler to the ambient during burner operation is a problem that is still not solved satisfactorily. This work shows that heat losses from the boiler to the ambient are likely be the predominant losses of small pellet boiler units on an annual basis. Therefore, further investigations should be made to develop a method for a more accurate determination of these heat losses.

Testing procedures for the determination of a meaningful stratification efficiency based on the definition used in this work should be developed in order to be able to compare the stratification efficiency of different solar TES on a fair base.

6.2.4   Laboratory and field testing

Further studies on start and stop emissions of boilers shall reveal the importance of these emissions on an annual basis and at the same time lead to better start and stop procedures with reduced emissions.

Side-by-side comparison of tank-in-tank systems with external DHW unit systems and internal heat exchanger spiral systems are recommended in order to test the advantages of each system.

Laboratory tests of different power modulation control strategies for the charging of solar TES by pellet boilers should be made in order to confirm the results presented in this work that were obtained from simulation studies. Average

temperature sensor control and point temperature sensor control should be compared in these tests.

More laboratory work is needed in order to determine the stratification efficiency of different solar combistores and the influence of this stratification efficiency on the annual system efficiency.

7 Bibliography

Abdoly, M.A. & Rapp, D., 1982. *Theoretical and Experimental Studies of Stratified Thermocline Storage of Hot Water*. *Energy Conversion and Management*, 22(3), 275–285.

Andersen, E., 2007. *Solar Combi Systems*. PhD Thesis, Department of Civil Engineering, Technical University of Denmark.

Andersen, E. & Furbo, S., 2007. *Theoretical Comparison of Solar Water/Space-Heating Combi Systems and Stratification Design Options*. *Journal of Solar Energy Engineering*, 129(4), 438-448.

Andersen, E., Furbo, S. & Fan, J., 2007. *Multilayer Fabric Stratification Pipes for Solar Tanks*. *Solar Energy*, 81(10), 1219-1226.

ASHRAE, 2004. *ASHRAE Handbook of HVAC Systems and Equipment, SI Edition*. American Society of Heating, Refrigeration and Air Conditioning Engineers.

ASHRAE, 2005. *Chapter 32 - Energy Estimating and Modeling Methods*. In: *ASHRAE Handbook of Fundamentals*. American Society of Heating, Refrigeration and Air Conditioning Engineers.

Bahnfleth, W.P. & Song, J., 2005. *Constant Flow Rate Charging Characteristics of a Full-Scale Stratified Chilled Water Storage Tank with Double-Ring Slotted Pipe Diffusers*. *Applied Thermal Engineering*, 25(17-18), 3067-3082.

Bales, C., 2000. *Evaluation of the Thermal Performance of Solar Combistores - Comparison of Three Test Methods*. In: *Proc. of the EuroSun 2000 Conference*, Copenhagen.

Beausoleil-Morrison, I. & Haddad, K., 2003. *Simulating Fuel-Fired Combination Space and Domestic Water Heating Systems*. In: *Proc. of the Eight International IBPSA Conference*, Eindhoven, 93-100.

Bemmann, U., Bendieck, A., Heck, P., Caspary, C., Baran, M. & Hallfell, Y., 2006. *Guideline for Combined Solar Thermal and Wood Pellet Heating Systems*. Project Sollet - European Network Strategy for Combined Solar and Wood Pellet Heating Systems for Decentralised Applications .

van Berkel, J., 1997. *Thermocline Entrainment in Stratified Energy Stores*. PhD Thesis, Technical University Eindhoven.

BFE, 2005. *Schweizerische Gesamtenergiestatistik 2005*. Bundesamt für Energie BFE, Bern.

BMLFUW, 2006. *Nationaler Biomasseaktionsplan für Österreich - Begutachtungsentwurf*. Bundesministerium für Land- und Forstwirtschaft, Umwelt und Wasserwirtschaft, Wien.

Boman, C., 2005. *Particulate and Gaseous Emissions from Residential Biomass Combustion*. PhD Thesis, Univ. Umea.

Bourdouxhe, J.P., Grodent, M., Lebrun, J. & Saavedra, C., 1994. *A Toolkit for Primary HVAC System Energy Calculation - Part 1: Boiler Model*. In: *ASHRAE Trans.*, 100(2), 759-773.

Bühler, R. & Jenni, A., 2009. *Betriebsverhalten von automatischen Holzfeuerungen - Anforderungen und praktische Beispiele. Presentation held at: Workshop „Effizienzsteigerung und Emissionsminderung von Biomassekleinanlagen". Graz, 15. 0kt. 2009.*

Carlsson, P.F., 1993. *Heat Storage for Large Low Flow Solar Heating Systems.* In: <u>Proc. of the ISES Solar World Congress</u>, Budapest, 5, 441-445.

Chan, A.M.C., Smereka, P.S. & Giusti, D., 1983. *A Numerical Study of Transient Mixed Convection Flows in a Thermal Storage Tank.* <u>Journal of Solar Energy Engineering</u>, 105, 246-253.

Chasapis, D., Drosou, V., Papamechael, I., Aidonis, A. & Blanchard, R., 2008. *Monitoring and Operational Results of a Hybrid Solar-Biomass Heating System.* <u>Renewable Energy</u>, 33(8), 1759-1767.

Claus, G. & Stephan, W., 1985. *A General Computer Simulation Model for Furnaces and Boilers.* In: <u>ASHRAE Trans.</u>, 91(1), 47–59.

Dachelet, M., 1987. *Subroutine Type 211 - Static Boiler (FORTRAN Code).* Available at: http://sel.me.wisc.edu/trnsys/trnlib/trnlib16/annex17/type211.for [Accessed January 12, 2009].

Dalibard, A., 2009. *Personal Communication.*

Davidson, J.H., Adams, D.A. & Miller, J.A., 1994. *A Coefficient to Characterize Mixing in Solar Water Storage Tanks.* <u>Journal of Solar Energy Engineering</u>, 116(2), 94-99.

DIN 1942:1994 (E) Acceptance Testing of Steam Generators (VDI Code of Practice).

DIN EN 60751:2008 Industrielle Platin-Widerstandsthermometer und Platin-Temperatursensoren.

Drück, H., 2006. *Multiport Store Model for TRNSYS - Type 340 - V1.99F.*

Drück, H., Heidemann, W. & Müller-Steinhagen, H., 2004. *Comparison Test of Thermal Solar Systems for Domestic Hot Water Preparation and Space Heating.* In: <u>Proc. of the EuroSun 2004 Conference</u>, Freiburg.

Eisl, G., 2006. *Messtechnische Ermittlung der Betriebs- und Emissionsparameter von zwei Heizkesseln unterschiedlicher Bauart - Analyse der relevanten Parameter unter Berücksichtigung des realen Betriebsverhaltens im intermittierenden und stationären Betrieb des Kessels.* Diploma Thesis, Institut für Wärmetechnik IWT, TU Graz.

EN 12975-2:2001 Thermal Solar Systems and Components - Solar Collectors - Part 2: Test Methods.

EN 15316-4-1:2008 (D) Heizungsanlagen in Gebäuden - Verfahren zur Berechnung der Energieanforderungen und Nutzungsgrade der Anlagen - Teil 4-1: Wärmeerzeugung für die Raumheizung, Verbrennungssysteme (Heizungskessel).

prEN 12977-3:2006, Entwurf ÖNORM EN 12977-3 Thermische Solaranlagen und ihre Bestandteile - Kundenspezifisch gefertigte Anlagen Teil 3: Leistungsprüfung von Warmwasserspeichern für Solaranlagen.

EVA, 2002. *Energiefluss Österreich 2000.* Energieverwertungsagentur - The Austrian Energy Agency.

Faninger, G., 2000. *Combined Solar-Biomass District Heating in Austria. Solar Energy*, 69(6), 425-435.

Faninger, G., 2007. *Der Solarmarkt in Österreich 2006*. Bundesministerium für Verkehr, Innovation und Technologie BMVIT, Wien.

Fiedler, F., 2006. *Combined Solar and Pellet Heating Systems: Study of Energy Use and CO-Emissions*. PhD Thesis, Mälardalen University, Department of Public Technology.

Fiedler, F., Bales, C., Persson, T. & Nordlander, S., 2007. *Comparison of Carbon Monoxide Emissions and Electricity Consumption of Modulating and Non-Modulating Pellet and Solar Heating Systems. International Journal of Energy Research*, 31(10), 915-930.

Fiedler, F., Nordlander, S., Persson, T. & Bales, C., 2006. *Thermal Performance of Combined Solar and Pellet Heating Systems. Renewable Energy*, 31(1), 73-88.

Fiedler, F. & Persson, T., 2009. *Carbon Monoxide Emissions of Combined Pellet and Solar Heating Systems. Applied Energy*, 86(2), 135-143.

Furbo, F., Shah, L.J., Holm Christiansen, C. & Vinkler Frederiksen, K., 2004. *Kedeleffektiviteter for oliefyr og naturgaskedler i enfamiliehuse*. Danmarks Tekniske Universitet.

Furbo, S. & Thür, A., 2008. *Energy Savings for a Solar Combisystem*. In: *Proc. of the EuroSun 2008 Conference*, Lisbon.

Furbo, S., Andersen, E., Thür, A., Shah, L.J. & Dyhr Andersen, K., 2005. *Performance Improvement by Discharge from Different Levels in Solar Storage Tanks. Solar Energy*, 79(5), 431-439.

Furbo, S. & Shah, L.J., 2005. *How Mixing During Hot Water Draw Off Influences the Thermal Performance of Small Domestic Hot Water Systems*. In: *Proc. of the Solar World Congress 2005*, Orlando, Florida.

Gabathuler, H., 2009. *Regelungstechnische Lösungsansätze für Anlagen mit Speicher. Presentation held at: Workshop „Effizienzsteigerung und Emissionsminderung von Biomassekleinanlagen". Graz, 15. Okt. 2009.*

Good, J. & Nussbaumer, T., 2009. *Emissionsfaktoren moderner Pelletkessel unter typischen Heizbedingungen*. Bundesamt für Energie BFE, Bern.

Good, J., Nussbaumer, T., Jenni, A. & Bühler, R., 2005. *Systemoptimierung automatischer Holzheizungen*. Bundesamt für Energie BFE, Bundesamt für Umwelt BAfU, UVEK, Bern.

Graf, P., Nipkow, J. & Messmer, R., 1999. *Hilfsenergieverbrauch von Öl- und Gasfeuerungen*. Bundesamt für Energie BFE, Bern.

Haberl, R., Konersmann, L. & Frank, E., 2009. *PelletSolar-2 - Systemoptimierung von Pelletfeuerungen in Kombination mit thermischen Solaranlagen basierend auf dynamischen Simulationen und Messungen im Prüfstand*. Bundesamt für Energie BFE, Bern.

Haller, M., Haberl, R., Dröscher, A., Konersmann, L. & Frank, E., 2009a. *Vergleich verschiedener Ansätze zur Simulation von Öl-, Gas- und Pellets-Kesseln*. In: *19. OTTI Symposium Thermische Solarenergie*, Bad Staffelstein.

Haller, M., Konersmann, L. & Dröscher, A., 2008. *Simulation von Öl-, Gas- und Pellet-Kessel in Kombination mit Solaranlagen*. In: <u>*18. OTTI Symposium Thermische Solarenergie*</u>, Bad Staffelstein, 428 – 433.

Haller, M., Konersmann, L., Haberl, R., Dröscher, A. & Frank, E., 2009b. *Comparison of Different Approaches for the Simulation of Boilers Using Oil, Gas, Pellets or Wood Chips*. In: <u>*Proceedings of the 11th IBPSA Conference on Building Simulation*</u>, Glasgow, 732-739.

Haller, M. & Vogelsanger, P., 2005a. *Combisystem Performance Investigation*. In: J. C. Hadorn, Ed. <u>*Thermal Energy Storage for Solar and Low Energy Buildings - State of the Art by the IEA Solar Heating and Cooling Task 32*</u>. IEA-SHC, pp. 41-45.

Haller, M. & Vogelsanger, P., 2005b. *Kombi-Kompakt+ Schlussbericht, korrigierte Version von 2005*. Bundesamt für Energie BFE, Bern.

Haller, M.Y., Cruickshank, C., Streicher, W., Harrison, S.J., Andersen, E. & Furbo, S., 2009c. *Methods to Determine Stratification Efficiency of Thermal Energy Storage Processes – Review and Theoretical Comparison*. <u>*Solar Energy*</u>, 83(10), 1847-1860.

Haller, M.Y., Streicher, W., Andersen, E. & Furbo, S., 2009d. *Comparative Analysis of Thermal Energy Storage Stratification Efficiency - a New Method Combines Advantages of Previous Approaches*. In: <u>*EffStock 2009 - The 11th Intl Conference on Thermal Energy Storage for Efficiency*</u>, Stockholm.

Haller, M.Y., Yazdanshenas, E., Andersen, E., Bales, C., Streicher, W. & Furbo, S., 2010a. *A Method to Determine Stratification Efficiency of Thermal Energy Storage Processes Independently from Storage Heat Losses*. <u>*Solar Energy,*</u> 84(6), 997-1007.

Haller, M.Y., Paavilainen, J., Konersmann, L., Haberl, R., Dröscher, A., Frank, E., Bales, C. & Streicher, W., 2010b. *A Unified Model for the Simulation of Oil, Gas, and Biomass Space Heating Boilers for Energy Estimating Purposes - Part I: Model Development*. <u>*Accepted for publication in the IBPSA Journal of Building Performance Simulation, February 2010*</u>.

Haller, M.Y., Paavilainen, J., Konersmann, L., Haberl, R., Dröscher, A., Frank, E., Bales, C. & Streicher, W., 2010c. *A Unified Model for the Simulation of Oil, Gas, and Biomass Space Heating Boilers for Energy Estimating Purposes - Part II: Parameterization and Comparison with Measurements*. <u>*Accepted for publication in the IBPSA Journal of Building Performance Simulation, January 2010*</u>.

Hartmann, H., Reisinger, K., Thuneke, K., Höldrich, A. & Rossmann, P., 2003. *Handbuch Bioenergie-Kleinanlagen*. Fachagentur Nachwachsende Rohstoffe, Gülzow.

Hartmann, H., Rossmann, P., Turowski, P., Link, H. & Marks, A., 2006. *Staubemissionen aus Holzfeuerungen - Einflussfaktoren und Bestimmungsmethoden*. Technologie- und Förderzentrum - im Kompetenzzentrum für Nachwachsende Rohstoffe, Straubing.

Hartmann, H., Schmid, V. & Link, H., 2004. *Untersuchungen zum Feinstaubausstoss von Holzzentralheizungsanlagen kleiner Leistung*.

Technologie- und Förderzentrum - im Kompetenzzentrum für Nachwachsende Rohstoffe, Straubing.

Heimrath, R. & Haller, M., 2007. *Project Report A2 of Subtask A: The Reference Heating System, the Template Solar System - A Report of IEA SHC Task 32: Advanced Storage Concepts for Solar and Low Energy Buildings* .

Heinz, A., 2007. *Application of Thermal Energy Storage with Phase Change Materials in Heating Systems*. PhD Thesis, Institute of Thermal Engineering, Graz University of Technology.

Hensen, J.L.M., 1991. *On the Thermal Interaction of Building Structure and Heating and Ventilating System*. PhD Thesis, Technische Universiteit Eindhoven.

Hirsch, R.L., Bezdek, R. & Wendling, R., 2005. *Peaking of World Oil Production: Impacts, Mitigation & Risk Management*.

Hollands, K.G.T. & Lightstone, M.F., 1989. *A Review of Low-Flow, Stratified-Tank Solar Water Heating Systems*. <u>Solar Energy</u>, 43(2), 97-105.

Huhn, R., 2007. *Beitrag zur thermodynamischen Analyse und Bewertung von Wasserwärmespeichern in Energieumwandlungsketten*. PhD Thesis, Fakultät für Maschinenwesen der Technischen Universität Dresden.

IEA, 2007. *Key World Energy Statistics*. OECD/IEA.

IPCC, 2007. *Climate Change 2007: Synthesis Report - Summary for Policymakers*.

Jauch, F., 2007. *Markterhebung Sonnenenergie 2006 - Teilstatistik der Schweizerischen Statistik der Erneuerbaren Energien*. Bundesamt für Energie BFE, Bern.

Jochem, E., Favrat, D., Hungerbühler, K., von Rohr, P., Spreng, D., Wokaun, A. & Zimmermann, M., 2002. *Steps Towards a 2000 Watt Society*. PSI, EPFL, ETHZ, EMPA, Zürich, Villingen, Lausanne, Dübendorf.

Jordan, U. & Vajen, K., 2000. *Influence of the DHW Load Profile on the Fractional Energy Savings: A Case Study of a Solar Combi-System with TRNSYS Simulations*. <u>Solar Energy</u>, 69(1-6), 197-208.

Jordan, U., Vajen, K., Streicher, W. & Letz, T., 2003. *Performance of Solar Combisystems*. In: W. Weiss, Ed. <u>Solar Heating Systems for Houses - A Design Handbook for Solar Combisystems</u>. James & James, London, pp. 125-162.

Kaltschmitt, M. & Streicher, W. eds., 2009. *Regenerative Energien in Österreich, Grundlagen, Systemtechnik, Umweltaspekte, Kostenanalysen, Potenziale, Nutzung*. Viehweg+Teubner / GWV Fachverlage, Wiesbaden.

Kandari, A.M., 1990. *Thermal Stratification in Hot Storage-Tanks*. <u>Applied Energy</u>, 35(4), 299-315.

Kemna, R., van Elburg, M., Li, W. & van Holsteijn, R., 2007. *Preparatory Study on Eco-design of CH Boilers - Task 4 Report (FINAL) Technical Analysis (incl. System Model)*. European Commision, DG TREN, Unit D3, Delft.

Klippel, N. & Nussbaumer, T., 2007a. *Einfluss der Betriebsweise auf die Partikelemissionen von Holzöfen - Projektzusatz 1 + 2 zum Projekt Wirkung von Verbrennungspartikeln*. Bundesamt für Energie BFE, Bundesamt für Umwelt BAfU, Bern.

Klippel, N. & Nussbaumer, T., 2007b. *Health Relevance of Particles from Wood Combustion in Comparison to Diesel Soot*. In: <u>15th European Biomass Conference</u>, Berlin, 7–11.

Knudsen, S., 2002. *Heat Transfer in a "tank-in-tank" Combi Store*. Report BYG-DTU R-025 2002, Danmarks Tekniske Universitet.

Knudsen, S., 2004. *Investigation and Optimisation of Heat Storage Tanks for Low-Flow SDHW Systems*. Ph.D. Thesis, Danmarks Tekniske Universitet.

Konersmann, L., Haller, M. & Vogelsanger, P., 2007. *PelletSolar - Leistungsanalyse und Optimierung eines Pellet-Solarkombinierten Systems für Heizung und Warmwasser*. Bundesamt für Energie BFE, Bern.

Könighofer, K., Spitzer, J., Padinger, R., Suschek-Berger, J., Streicher, W. & Mach, T., 2001. *Anforderungsprofile für Biomassefeuerungen zur Wärmeversorgung von Objekten mit niedrigem Energiebedarf*. Bundesministerium für Verkehr, Innovation und Technologie BMVIT, Wien.

Koschak, A., Fiedler, T., Knirsch, A. & Beurer, C., 1998. *TRNSYS-TYPE 370 Erweiterung des bisherigen Gaskesselmoduls um eine Holzkesselfeuerung mit der Möglichkeit zur Brennwertnutzung - Ergänzung um einen Simulationsmodus zur realitätsnahen Simulation des Betriebsverhaltens von Gaskesseln mit Takten*.

Laret, L., 1989. *Accurate Boiler Models for Large Scale Simulation*. In: <u>Proc. of the IBPSA Building Simulation Conference</u>, Vancouver, 375-380.

Lavan, Z. & Thompson, J., 1977. *Experimental Study of Thermally Stratified Hot Water Storage Tanks*. <u>Solar Energy</u>, 19(5), 519-524.

Lebrun, J., Saavedra, C., Hore, F., Grodent, M.M. & Nusgens, P., 1993. *Testing and Modeling of Fuel Oil Space-Heating Boilers - Synthesis of Available Results*. In: <u>ASHRAE Trans.</u>, 99(2), 455-464.

Lohse, R., Urbaneck, T., Göppert, S., Schirmer, U., Rauh, H. & Platzer, B., 2008. *Gestaltungsrichtlinien für Schichtenbeladungssyteme*. In: <u>18. OTTI Symposium Thermische Solarenergie</u>, Bad Staffelstein.

Lorenz, K., Bales, C. & Persson, T., 2000. *Evaluation of Solar Thermal Combisystems for the Swedish Climate*. In: <u>Proc. of the EuroSun 2000 Conference</u>, Copenhagen.

Moretti, P.M. & McLaughlin, D.K., 1977. *Hydraulic Modeling of Mixing in Stratified Lakes*. <u>Journal of the Hydraulics Division-Asce</u>, 103(4), 367-380.

Nöhrer, D., 2009. *Auswertung der Feldmessdaten von Pellet-Solar-Systemen für Raumheizung und Warmwasser im Rahmen des Projektes PellSol Plus im Zeitraum September 2008 bis Juni 2009*. Bakkalaureat Thesis, FH Burgenland, Pinkafeld.

Nordlander, S., 2003. *TRNSYS Model for Type 210 - Pellet Stove with Liquid Heat Exchanger - Documentation of Model and Parameter Identification*. Report ISRN DU-SERC--79--SE, Högskolan Dalarna, Solar Energy Research Center SERC, Borlänge.

Nussbaumer, T., Doberer, A., Klippel, N., Bühler, R. & Vock, W., 2008. *Influence of Ignition and Operation Type on Particle Emissions from Residential*

Wood Combustion. In: <u>*Proc. of the 16th European Biomass Conference & Exhibition*</u>, Valencia.

Obernberger, I., Brunner, T. & Bärnthaler, G., 2007. *Fine Particulate Emissions from Modern Austrian Small-Scale Biomass Combustion Plants*. In: <u>*Proc. of the 15th European Biomass Conference & Exhibition*</u>, Berlin.

Overgaard, L. & Ellehauge, K., 2000. *Solar Combisystems in Denmark – Solar & Biomass Systems*. In: <u>*Proc. of the EuroSun 2000 Conference*</u>, Copenhagen.

Padinger, R., 2002. *Regelungstechnik für die Haustechnik der Zukunft - Untersuchungen zur Regelung von Biomassefeuerungen zur emissions- und effizienzoptimierten Beheizung von Wohn- und Bürobauten*. Bundesministerium für Verkehr, Innovation und Technologie BMVIT, Wien.

Panthalookaran, V., Heidemann, W. & Müller-Steinhagen, H., 2007. *A New Method of Characterization for Stratified Thermal Energy Stores*. <u>*Solar Energy*</u>, 81(8), 1043-1054.

Paulsen, O., 1999. *Technical Report Work Package I: Modelling of Part Load Efficiency - Second Revised Edition - SAVE Project: Annual Efficiency Calculation Method for Domestic Boilers - Contract No. XVII/4.1031/93-008 - Funded by the European Union, SAVE Programme - Directorate-General for Energy*.

Perers, B. & Bales, C., 2002. *A Solar Collector Model for TRNSYS Simulation and System Testing - A Technical Report of Subtask B of the IEA-SHC - Task 26*.

Persson, T., 2006. *Combined Solar and Pellet Heating Systems for Single-Family Houses: How to Achieve Decreased Electricity Usage, Increased System Efficiency and Increased Solar Gains*. PhD Thesis, KTH, Energy Technology, Stockholm.

Persson, T., Fiedler, F., Rönnelid, M. & Bales, C., 2006. *Increasing Efficiency and Decreasing CO-Emissions for a Combined Solar and Wood Pellet Heating System for Single-Family Houses*. In: <u>*Proc. on USB of Pellets*</u>, Jönköping, 87-91.

Pfeiffer, F., Struschka, M., von Lepel, F. & Baumbach, G., 1999. *Start- und Stopp-Emissionen von Öl- und Gasfeuerungen*. <u>*Wärmetechnik, Versorgungstechnik*</u>, 5(1999), 34-41.

Remund, S., 1999. *Berechnung des Nutzungsgrades von Oel- und Gasheizkesseln*. Bundesamt für Energie BFE, Bern.

Rosen, M.A., 1992. *Appropriate Thermodynamic Performance Measures for Closed Systems for Thermal Energy Storage*. <u>*Journal of Solar Energy Engineering*</u>, 114(2), 100-105.

SEL, CSTB, TRANSSOLAR & TESS, 2006. *TRNSYS 16 - A TRansient SYstem Simulation program*.

Shah, L.J., Morrison, G.L. & Behnia, M., 1999. *Characteristics of Vertical Mantle Heat Exchangers for Solar Water Heaters*. <u>*Solar Energy*</u>, 67(1-3), 79-91.

Shah, L.J., 2000. *Heat Transfer Correlations for Vertical Mantle Heat Exchangers*. <u>*Solar Energy*</u>, 69(Supplement 6), 157-171.

Shah, L.J. & Furbo, S., 1998. *Correlation of Experimental and Theoretical Heat Transfer in Mantle Tanks Used in Low Flow SDHW Systems. Solar Energy*, 64(4-6), 245-256.

Shah, L.J. & Furbo, S., 2003. *Entrance Effects in Solar Storage Tanks. Solar Energy*, 75(4), 337-348.

Shyu, R.J. & Hsieh, C.K., 1987. *Unsteady Natural-Convection in Enclosures with Stratified Medium. Journal of Solar Energy Engineering*, 109(2), 127-133.

Sliwinski, B.J., Mech, A.R. & Shih, T.S., 1978. *Stratification in Thermal Storage During Charging*. In: *6th International Heat Transfer Conference*, Toronto, 4, 149-154.

Statistik Austria, 2009. *Gesamteinsatz der Haushalte - Gesamteinsatz aller Energieträger 2007/2008*. Available at: http://www.statistik.at/web_de/ statistiken/energie_und_umwelt/energie/energieeinsatz_der_haushalte/in dex.html [Accessed November 2, 2009].

Stefan, H.G. & Gu, R., 1992. *Efficiency of Jet-Mixing of Temperature-Stratified Water. Journal of Environmental Engineering*, 118(3), 363-379.

Stiftung Warentest, 2009. *Sonne statt Öl und Gas.* , 2009(3), 59-65.

Streicher, W., Bales, C. et al., 2002. *Vergleich von Kombisystemen, der Ansatz des IEA-SHC Task 26 „Solar Combisystems"*. In: *12. OTTI Symposium Thermische Solarenergie*, Bad Staffelstein, 90-94.

TESS, *TESS Component Library General Descriptions*. Available at: http://www.transsolar.com/__software/download/en/tesslibary_shortinfo_e n.pdf [Accessed November 3, 2009].

Thür, A. & Furbo, S., 2005. *Investigations on Design of Heat Storage Pipe Connections for Solar Combisystems*. In: *NorthSun 2005 - 10th International Conference on Solar Energy at High Latitudes*, Vilnius.

Tran, N., Kreider, J.F. & Brothers, P., 1989. *Field Measurement of Chilled Water Storage Thermal Performance*. In: *ASHRAE Trans.*, 95, 1106-1112.

University of Illinois & University of California, 2007. *EnergyPlus Engineering Reference - The Reference to EnergyPlus Calculations.*

Vock, W. & Jenni, A., 2007. *Bericht zur 1. und 2. Mess-Serie: Emissionsarme Anfeuermethoden für Stückholzfeuerungen - Entwicklung von emissionsarmen Anfeuermethoden für Stückholzfeuerungen inkl. messtechnischer Erfolgsnachweis im praktischen Betrieb*. Schweizerische Kantone, BFE und BAFU.

Wetter, M., 2004. *GenOpt, Generic Optimization Program, User Manual*. Report LBNL-54199, Lawrence Berkeley National Laboratory, Berkeley.

World Energy Council, 2007. *2007 Survey of World Energy Resources*. London.

Zurigat, Y.H. & Ghajar, A.J., 2001. *Heat Transfer and Stratification in Sensible Heat Storage Systems*. In: I. Dincer & M. A. Rosen, Eds. *Thermal Energy Storage Systems and Applications*. John Wiley & Sons, West Sussex, pp. 259–301.

Appendix

Appendix A: Simulation of a TES integrated pellet burner

For the simulation of a TES integrated pellet burner, the boiler model Type 869 was used together with the multiport store model Type 340. The boiler model was parameterized according to the parameters shown in Table 2.3 (Section 2.5.5) with the following exceptions:

–   The effective thermal capacitance C_{therm} was set to 200 kJ/K in order to simulate only the additional capacitance that can be expected from the combustion chamber material. The thermal capacitance of the water volume and heat exchanger part identified by the discharge test (848 litres of water) is simulated by the thermal capacitance of Type 340.

–   The heat losses to the ambient $UA_{hx,amb,ON}$ and $UA_{hx,amb,OFF}$ have been set to zero because these are simulated with the store model Type 340 for the TES as shown in Table 3.3 (Section 3.1.7).

The mass flow rate through the boiler was set to a fictive value of 600 kg/h whenever the temperature at the outlet of the boiler was higher than the temperature at the inlet. At other times, the mass flow was zero.

The inlet temperature of the boiler was connected to the temperature at relative height $z = 0.45$ of the TES model, corresponding to the position of the pellet burner and flue gas heat exchanger in the TES.

The outlet temperature of the boiler remained unconnected. Instead, the useful heat provided by the boiler ($\dot{Q}_{B,wat}$) was transferred into the TES by a double port (dp) with a fictive inlet temperature ($t_{dp,in}$) of 89 °C and the fictive connection heights and mass flow rate set as follows:

$$z_{dp,in} = 0.42$$

$$z_{dp,out} = 0.40$$

$$\dot{m}_{dp} = \frac{\dot{Q}_{B,wat}}{cp_{wat} \cdot \left[t_{dp,in} - t\left(z_{dp,out} \right) \right]}$$

ON/OFF operation

For ON/OFF operation without combustion power modulation, fuel consumption mode 1 of Type 869 was used (Appendix B, Type 869, parameter 22). The input signal γ (input 3) has been used to switch the boiler on and off according to the TES temperature sensor reading and the control criteria for auxiliary heating. The ON-temperature given to Type 869 (input 4) was low enough, and the temperatures given to the inputs 5-7 were high enough to enable boiler operation until the OFF-criteria in the TES was reached.

Combustion power modulation

For combustion power modulation of an integrated burner, Type 869 was used in fuel consumption mode 2. Thus, the mass flow rate of fuel burning was calculated external of the boiler using the time-delay Type 817 for fuel mass flow rate at burner start and Type 889 to control the mass flow rate thereafter to meet the temperature set point in the TES. In fuel consumption mode 2, start values for additional electricity use are not added automatically by Type 869 and have therefore been added by additional equations in the TRNSYS deck, i.e. externally of Type 869.

Appendix B: Documentation of TRNSYS Types

This Appendix B contains documentation of non-standard TRNSYS Types that have been developed for the simulation studies presented in this work, as well as the updated documentation of the collector Type 832 that has originally been developed by Bengt Perers and Chris Bales and has been changed in cooperation with Antoine Dalibard and Janne Paavilainen in order to be able to use it for small timesteps.

The following Type documentation are included in this Appendix:

Type 816 Transient value averaging over time

Type 817 Timer or time delay

Type 832 Collector model

Type 869 Boiler model

Type 888 Space heating system controller

Type 889 Adapted P(I)D controller

TRNSYS Type 816 „Transient Value Averaging over Time"

Version 2.0, Michel Haller, 21.02.2010

1   Summary

Type 816 delivers the average of a time-dependent value. A maximum of 20 inputs can be averaged with individual averaging times for each one of them. Until the simulation reaches the time of averaging, the average will be taken of all available values (without time 0). As soon as the time of averaging is reached, only the values from current time minus time of averaging will be considered.

2   Parameter-List

Nr.	short	explanation	unit	range
1	NrV	number of values to be averaged	--	[0;20]
2,3,...	tav1, ...	time of averaging for value 1, value 2, etc.	[h]	[0;+inf]

3   Input-List

Nr.	short	explanation	unit	range
1	Va1	value 1	any	[-inf;+inf]
2,3,...	Va2,Va3,...	value 2, value 3, ...	any	[-inf;+inf]

4   Output-List

Nr.	short	explanation	unit	range
1	V1av	average of value 1 over time	any	[-inf;+inf]
2,3,...	V2av, V3av,...	average of value 2,3, etc. over time	any	[-inf;+inf]

5 Calculations

In order to calculate the average, this Type must store all values back to the current time minus the time of averaging. Type 816 does not simply add all values together each timestep and divide the result by the number of timesteps in the averaging period, but performs the calculations shown below. These calculations are a lot faster when dealing with long averaging periods over many timesteps.

$$X = \frac{dtAverage}{dtSim}$$

$$SUM_N = SUM_{N-1} + Value_N - Value_{N-X}$$

$$Average_N = \frac{SUM_N}{X}$$

X [-]	number of timesteps to be averaged
$dtAverage$ [h]	time of averaging
$dtSim$ [h]	simulation timestep
SUM_N [any]	sum of all values within the last X timesteps
$Value_N$ [any]	instant value of the variable at timestep N
$Average_N$ [any]	average of the variable calculated for timestep N

TRNSYS Type 817 „Timer or Time Delay"

Version 1.0, Michel Haller, 21.02.2010

1 Summary

This Type uses a trigger signal to set an output value for a specified time after the trigger signal has first appeared or after the trigger signal has last appeared.

2 Parameter-List

Nr.	short	explanation	unit	range
1	MoT1	Mode for timer 1: 1 = count from first trigger signal on; 2 count from last trigger signal on	--	[1;2]
2	dtT1	time for timer 1	[h]	[0;inf]
3-10	MoT2, dtT2 – MoT5, dtT5	same for timers 2-5		

3 Input-List

Nr.	short	explanation	unit	range
1	triSig	trigger signal; on when > 0	any	[0;+inf]
2-5	triSig2 - 5	trigger signals 2 to 5	any	[0;+inf]

4 Output-List

Nr.	short	explanation	unit	range
1-5	Bot1 ... Bot5	timer on (1) or off (0) for timers 1 to 5	any	[0,1]
6-10	tTimer1 – tTimer5	time elapsed for timers 1 to 5	h	[0;+inf]

TRNSYS Type 832 v3.07 „Dynamic Collector Model by Bengt Perers"
Updated Input-Output Reference

Michel Haller, Janne Paavilainen, Antoine Dalibard, Bengt Perers, 2 May, 2010

Contents

1 Introduction

The Type132 collector model has originally been programmed by Bengt Perers. Additional features have been added since by B. Hellström, Chris Bales and Stefan Fischer. The latest changes have been introduced by Michel Haller based on suggestions from Antoine Dalibard and Janne Paavilainen. Component model history:

Type132 – TRNSYS15 and older

Type232 – TRNSYS15

Type232 – TRNSYS16 legacy mode

Type832 – TRNSYS16 drop-in dll

Since the code has changed quite a bit during the years, and in particular new inputs and parameters have been introduced, a new documentation of the parameters, inputs and outputs is given here.

2 Summary

The number of Parameters is now 21 for optical modes Omode <= 5 and 109 for Omodes > 5, where detailed data for incidence angle modifiers are included in the parameters. The main differences to earlier versions of this TRNSYS type are:

1. Possibility to split the collector into several segments for the calculation of the thermal mass temperature to avoid unexpected temperature jumps that had disturbed controllers and convergence in previous versions. These jumps were only significant when a collector with a relatively high thermal capacitance was simulated or when relatively small time steps were chosen for the simulation.

2. Possibility to calculate the transversal and longitudinal incidence angles from data readily available from the radiation processor of TRNSYS.

3. Several bugfixes were made addressing erroneous calculations and wrongly read IAM data files in previous versions when several instances of this Type were used in the same deck.

4. The quadratic heat loss term has been adapted in order not to calculate losses when the collector temperature is below ambient temperature. This does NOT mean that the collector model should be used for below ambient temperature operation.

In the current proforma the 2-axis IAM (Incidence Angle Modifier) data can only be given as a table in a text file as this is the most convenient input for the average user. For other types of input one has to modify the TRNSYS deck file (.dck) directly with a text editor.

3 Parameter-List

Nr.	short	explanation	unit	range
1	A	Collector field aperture area	[m]	[0;inf]
2	η_0; $F'(\tau\alpha)$	Collector optical efficiency (at zero temp. difference and nominal conditions) for CMode = 1: Eta0 = Zero loss efficiency at normal incidence (-) for CMode = 2: tau-alpha = effective transmission absoptance product (-) for CMode = 3,4: = not used	[-]	[0;1]
3	K_d	IAM for diffuse radiation	[-]	[0;1]
4	a_1	Linear heat loss coefficient	[W/m^{2}K]	[0;inf]
5	a_2	Quadratic heat loss coefficient	[W/m^{2}K^2]	[0;inf]
6	$c_{w,hl}$	Wind speed dependency of heat losses	[J/m^{3}K]	[-inf;inf]
7	c_{IR}	Infrared radiation dependency of collector	?	[-inf;inf]
8	C_{eff}	Specific effective thermal capacitance of the collector, including fluid Effective area specific heat capacity of the collector, for CMode = 1: including the fluid for CMode = 2: excluding the fluid	[J/m2K]	[1;100000]
9	$c_{w,F'}$	Wind speed dependency of the zero heat loss efficiency	[s/m]	[0;inf]
10	cp	Specific heat capacity of the collector fluid	[kJ/kgK]	[0;inf]
11	β	Collector slope (tilt angle)	[°]	[-360;360]
12	CMode	Collector mode for CMode = 1: CEN 1-node model (absorber, collector and fluid = 1 thermal node) for CMode = 2: 2-node model (absorber, collector and fluid are two seperate thermal nodes) for CMode = 3: CEN 1-node model with conversion area for CMode = 4: 2-node model with conversion area	[-]	[1;4]
13	wf	Wind speed factor if wind data is not measured in collector plane	[-]	
14	rf	Sky radiation factor ($rf = \left[1 + \cos(\beta)\right]/2$) for a standard climate file)	[-]	
15	OMode	Optical mode for OMode = 1: b0 equation for OMode = 2: b0 equation according to MFC for OMode = 3: Symmetrical Kb(theta) for OMode = 4: Asymmetric 2-axis Kb(theta) in external text file for OMode = 5: Asymmetric 2-axis Kb(theta) as parameters (See source code for details) for OMode = 6-10: see source code for details	[-]	[1;9]
16	Cfl	for CMode = 2 or 4: Effective heat capacity of the fluid content (J/m2K)	[J/m^{2}K]	[0;inf]

		for CMode = 1 or 3: unused		
17	UAbsfl	for CMode 2 or 4: UAabsfl, Heat transfer rate between absorber and fluid for CMode 1 or 3: unused	[W/K]	[0;inf]
18	b0	Angle dependence of the transmittance absorptance product (tau-alpha) for OMode = 1-3: b0, IAM as b0 (first order) and b1 (second order) function of (1/cos(θ/180)-1) for OMode = 4: unused for Omode > 4: check FORTRAN code	[-]	[-inf;inf]
19	b1	Angle dependence of the transmittance absorptance product (tau-alpha) for Omode = 3: b1, IAM as b0 (first order) and b1 (second order) function of (1/cos(θ/180)-1)	[-]	[-inf;inf]
20	Nseg	Number of collector segments in flow direction for heat capacitance calculation (for simulation with small timesteps and/or high collector heat capacitance)	[-]	[1;10]
21	γ	collector azimuth angle: (negative is east, positive is west) used for calculation of θ_L and θ_T; specify as 999 if θ_L and θ_T are inputs	degree	[-inf;+inf]
22	LUI	Logical Unit for input file. 2-axis IAM table file. (Assigned automatically by Simulation Studio)	[-]	[30;+999]

Additional parameters, only IF Omode >5:

30-109		IAM tables for collector test data fitting (not available in proforma, see FORTRAN code for details)	[-]	

4 Input-List

Nr.	short	explanation	unit	range
1	ϑ_{in}	inlet temperature	C	[-inf;+inf]
2	$\dot{m}$	inlet mass flow rate	kg/h	[0;+inf]
3	ϑ_{amb}	ambient temperature	C	[-inf;+inf]
4	I_t	global radiation on collector plane	kJ/hm2	[0;+inf]
5	I_d	incidence diffuse radiation on collector plane	kJ/hm2	[0;+inf]
6	θ	incidence angle of beam radiation	deg	[0;+inf]
7	$u_{w,0}$	wind speed	m/s	[0;+inf]
8	$I_{IR,0}$	long wavelength radiation downwards from sky	kJ/hm2	[0;+inf]
9	θ_T; θ_Z	if collector azimuth angle γ = 999: incidence angle in transversal direction; if γ < 999: solar zenith angle, for calculation of θ_T; and θ_L	degrees	[0;+inf]
10	θ_L; γ_S	if γ =999: incidence angle in longitudinal direction γ < 999: solar azimuth angle for calculation of θ_T; and θ_L	degrees	[0;+inf]

5   Output-List

Nr.	short	explanation	unit	range
1	ϑ_{out}	collector outlet temperature	C	[-inf;+inf]
2	$\dot{m}$	collector outlet mass flow rate	kg/h	[0;+inf]
3	$\dot{Q}_{out}$	thermal energy gain	kJ/h	[-inf;+inf]
4	ϑ_{abs}	mean absorber temperature (only in CMode 2 and 4)	C	[-inf;+inf]
5	$\dot{q}_{rad}$	radiative energy gain per m2	W/m2	[-inf;+inf]
6	K_b	incidence angle modifier for beam radiation	-	[-inf;+inf]
7	θ_T	incidence angle in transversal direction	degree	[-inf;+inf]
8	θ_L	incidence angle in longitudinal direction	degree	[-inf;+inf]
9-10		Not used (reserved for future needs)		
11-20	$\vartheta_{out}(x)$	outlet temperature of segments x = 1-10 during this timestep	°C	[-inf;+inf]

6   Basic Equations (Cmode = 1 or 3)

Although for in-depth knowledge about the theoretical background of this model we refer to the original literature of Perers (2002), and ISO 9806-3, the basic equations are summarized here again for the quick reader:

$$\dot{q}_{out} = F'(\tau\alpha) \cdot K_b \cdot I_b + F'(\tau\alpha) \cdot K_d \cdot I_d - c_{w,F'} \cdot u_w \cdot (I_b + I_d) - c_{IR} \cdot \left(I_{IR} - \sigma \cdot T_{amb}^{\,4}\right)$$
$$-a_1 \cdot \Delta T_{amb} - a_2 \cdot (\Delta T_{amb})^3 / |\Delta T_{amb}| - c_{w,hl} \cdot u_w \cdot (\Delta T_{amb}) \qquad (1)$$
$$-C_{eff} \cdot d\vartheta_m / dt$$

with; $\Delta T_{amb} = \vartheta_m - \vartheta_{amb}$; $u_w = wf \cdot u_{w,0}$; and $I_{IR} = rf \cdot I_{IR,0}$

$\dot{q}_{out}$ heat output of the collector per area [Wm^{-2}]

$F'(\tau\alpha)$ zero loss efficiency of the collector, sometimes referred to as η_0 [-]

K_b incidence angle modifier for beam radiation [-]

I_b Beam radiation incident on collector plane [Wm^{-2}]

K_d incidence angle modifier for beam radiation [-]

I_d Diffuse radiation incident on collector plane [Wm^{-2}]

$c_{w,F'}$ Factor for a wind dependency correction of F' (and thus the zero loss coefficient $F'(\tau\alpha)$, used for unglazed collectors [sm^{-1}]

u_w wind speed parallel to the collector plane [ms^{-1}]

a_1 first order heat loss coefficient [WK^{-1}m^{-2}]

a_2 second order heat loss coefficient [WK^{-2}m^{-2}]

ϑ_m arithmetic mean of the collector temperature [°C]

ϑ_{amb} ambient temperature at location of collector field [°C]

T_{amb} absolute ambient temperature at location of collector field [K]

$c_{w,hl}$ wind speed dependency of heat losses [$Jm^{-3}K^{-1}$]

c_{IR} long wave irradiation dependency of heat losses (or gains) [-]

I_{IR} long wave irradiation on collector plane [Wm^{-2}]

σ Stefan Boltzmann constant [$Wm^{-2}K^{-4}$]

t time [s]

C_{eff} effective thermal capacitance of the collector (including fluid) [$Jm^{-2}K^{-1}$]

In the case of steady state ($d\vartheta_m/dt$), normal incidence ($K_b = K_d = 1$), no dependencies on wind speed ($c_{w,F'} = 0$, $c_{w,hl} = 0$) or infrared radiation ($c_{IR} = 0$), and collector temperatures above ambient temperatures ($\Delta T_{amb} > 0$), equation (1) can be reduced to the well known steady state efficiency approximation:

$$\dot{q}_{out} = \eta_0 \cdot (I_b + I_d) - a_1 \cdot (\vartheta_m - \vartheta_{amb}) - a_2 \cdot (\vartheta_m - \vartheta_{amb})^2 \tag{2}$$

with

$$\eta_0 = F'(\tau\alpha) \tag{3}$$

The first line of equation (1) can be seen as a term describing the radiative balance of the collector. With the approximations chosen for the long wave heat exchange in this model, it does not depend on the collector temperature, and can be calculated independently from the collector temperature as:

$$\dot{q}_{rad} = F'(\tau\alpha) \cdot K_b \cdot I_b + F'(\tau\alpha) \cdot K_d \cdot I_d - c_{w,F'} \cdot u_w \cdot (I_b + I_d) - c_{IR} \cdot (I_{IR} - \sigma \cdot T_{amb}^4) \tag{4}$$

The determination of the actual heat gain and collector output is an iterative process. In a first step, the actual collector heat gain with the inclusion of the temperature dependent thermal losses of the collector are calculated:

$$\dot{q}_{gain} = \dot{q}_{rad} - a_1 \cdot (\vartheta_m - \vartheta_{amb}) - a_2 \cdot (\vartheta_m - \vartheta_{amb})^2 - c_{w,hl} \cdot u_w \cdot (\vartheta_m - \vartheta_{amb}) \tag{5}$$

In a second step, the outlet temperature of the collector ϑ_{out} of this time step is calculated from the collector gain $\dot{q}_{gain}$, the average temperature of the collector during the last timestep $\vartheta_{m,old}$, the collector parameters, and the flow parameters of this timestep:

$$\vartheta_{out} = \frac{\left(\dfrac{(\dot{m} \cdot cp \cdot \vartheta_{in})}{A} - \dfrac{C_{eff} \cdot \vartheta_{in}}{2 \cdot \Delta t} + \dot{q}_{gain} + \dfrac{C_{eff} \cdot \vartheta_{m,old}}{\Delta t} \right)}{\dfrac{\dot{m} \cdot cp}{A} + \dfrac{C_{eff}}{2 \cdot \Delta t}} \tag{6}$$

Which is a result of the energy balance:

$$\vartheta_{out} = \vartheta_{in} + \frac{\dot{q}_{gain} - \left(\dfrac{\vartheta_{in} + \vartheta_{out}}{2} - \vartheta_{m,old} \right) \cdot \dfrac{C_{eff}}{\Delta t}}{\dot{m} \cdot cp / A} \qquad (7)$$

Where the average heat transfer to the collectors thermal capacitance is subtracted from the heat gain in order to get the heat output. $\vartheta_m = \left(\vartheta_{in} + \vartheta_{out} \right)/2$ is used for the average temperature of the collectors thermal capacitance.

In the case of no mass flow, the change of the collector temperature is:

$$\vartheta_{out} = \vartheta_m = \vartheta_{m,old} + \dot{q}_{gain} \cdot \frac{\Delta t}{C_{eff}} \qquad (8)$$

The above equations can cause troubles in simulations with small timesteps and/or high thermal capacitance. In particular, unstable outlet temperatures just after the collector loop pump starts or stops can be observed and may cause problems for control and solver algorithms. Thus the possibility of splitting the collector's thermal mass in a number of serial segments was introduced. In order to make sure that the steady state efficiency would still be in agreement with the collector test norms, the same ΔT_{amb} is used for all segments in steady state operation. However, when the mass flow stops, the temperature differences between the fluid in different segments would persist if all segments would have the same heat losses, causing the outlet temperature of the last segment to rise higher than the expected stagnation temperature. Therefore, in cases of no mass flow the temperature difference to the ambient and respective heat losses are calculated for each segment separately. This also has the effect that the temperature differences between the segments disappear with time after the pump stops. A flow chart of the FORTRAN code is given in Figure 1.
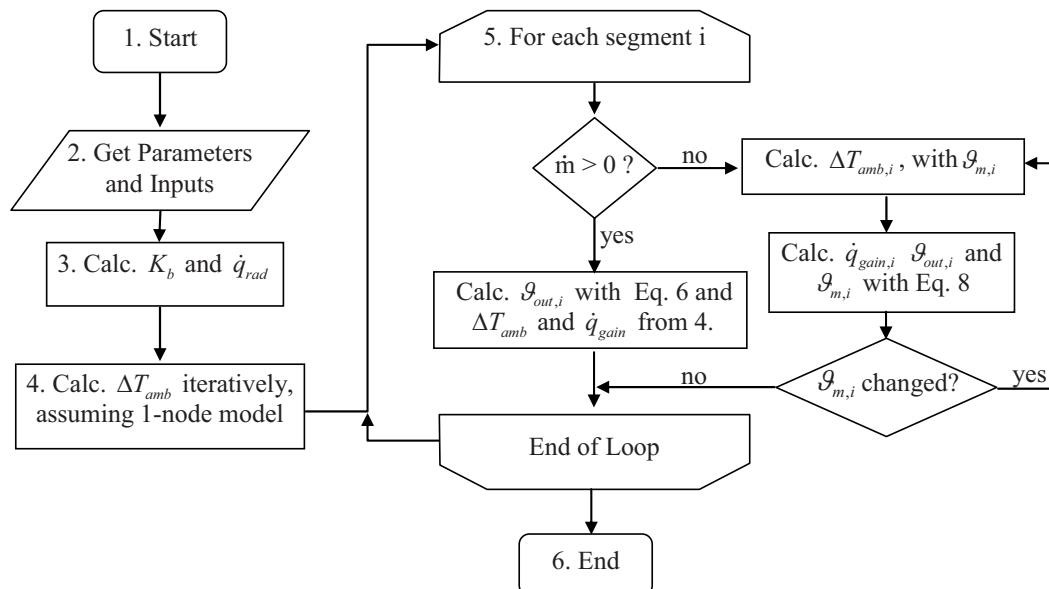
Figure 1: Flow Chart of the FORTRAN Program Code: Step 3 is only calculated once every timestep (no iteration).

7 Calculation of transversal and longitudinal incidence angles

For collectors whose incidence angle modifier in transversal direction differs from the one in longitudinal direction (e.g. vacuum tube collectors), the transversal and longitudinal components of the incidence angle have to be known separately. In this collector model these components may be given as inputs or they may be calculated internally based on data from the radiation processor of TRNSYS. The calculation of the transversal and longitudinal incidence angles is done based on equations from [Klein 1996], which had to be slightly adapted / corrected to produce the desired results in all cases, as reported in Heimrath & Haller (2007):

$$\theta_L = \left| ATAN\left(TAN\left(\theta_Z\right) \cdot COS\left(\gamma - \gamma_S\right)\right) - \beta \right|$$

$$\theta_T = ATAN\left(\frac{SIN\left(\theta_Z\right) \cdot SIN\left(\left|\gamma - \gamma_S\right|\right)}{COS\left(\theta\right)} \right)$$

θ_L Angle of incidence on collector plane in longitudinal direction

θ_T Angle of incidence on collector plane in transversal direction

θ_Z Solar zenith angle

γ Collector azimuth angle

γ_S Solar azimuth angle

θ Angle of incidence on collector plane

β Collector slope

8 Multi-segment mode

The new approach of splitting up the collector into segments addresses some problems in the original model during transients. The problems were caused by the storage term (thermal capacitance and average temperature change between time steps) in combination with a linear temperature gradient resulting in that the model in some cases extrapolated unrealistic outlet temperatures from one time step to another, specifically with small time steps. This caused further problems with e.g. controllers and convergence. By dividing the collector into segments the temperature gradient is not linear for the whole collector. To avoid differences between the energy balance of this model in steady state and parameter identification based on equation (2), thermal loss calculation of a single segment with equation (5) uses the mean **collector** temperature for ϑ_m under operating conditions. In the case of no fluid flow, the mean **segment** temperature is taken for ϑ_m in thermal loss calculation to assure agreement of the models stagnation temperature with the theory. Compared to previous versions one can expect a difference in energy balance during transients, but for steady state it should be the same as earlier. Thus, because of the difference in transient energy balance one can expect also differences for long simulations, depending on how much the system is working near steady state.

The difference in the results between one segment (n=1) and multiple segments (n=2-10) can be seen in Figure 2. General values of the simulation are listed in Table 1. The differences in heat gain between these simulations can be seen in Table 2.

Table 1: Values used for the TRNSYS test-simulation.

parameter	value	units
collector area	10	m^2
zero loss efficiency η_0 (or $F'(\tau\alpha)$)	0.8	-
linear heat loss coefficient	3.5	Wm^{-2}K^{-1}
quadratic heat loss coefficient	0.015	Wm^{-2}K^{-2}
IAM for diffuse radiation K_d	1.0	-
specific mass flow	0, 6, 8	kgh^{-1}m^{-2}
collector effective capacitance	7000	Jm^{-2}K^{-1}
timestep	0.05	h

The "unphysical" value of 1 is used for the IAM for diffuse radiation in order to simplify the validation of the changes introduced into the model. Extreme values are used for mass flow rate and capacitance for the same reason.
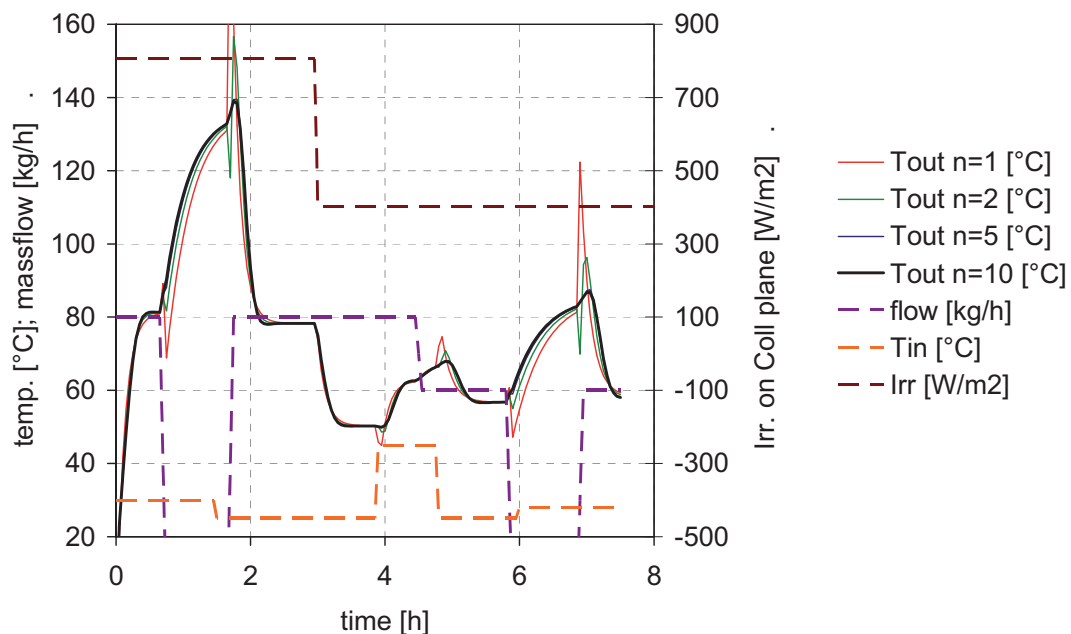
Figure 2: Simulation results for 1,2,5 and 10 nodes simulations.

Table 2: Differences in heat gains for 1, 2, 5, and 10 nodes.

Simulation	Heat Gain (kWh)	Diff.to 1 node
1 node simulation (n=1)	18.331	0%
2 nodes simulation (n=2)	18.258	-0.4%
5 nodes simulation (n=5)	18.252	-0.4%
10 nodes simulation (n=10)	18.251	-0.4%

9 License, source code, further development etc.

The Type832 component is free of charge and no license is needed. The source code is open.

10 Further development and updates

The Type832 is not actively developed by any of the authors with exception for sporadic bugfixes and improvements. Bug reports can be sent to the authors and will be looked at when time and budget allows. The user can feel free to make own bugfixes and modifications to the source code. Also, to keep the maintenance and distribution centralized, user written modifications and bugfixes are kindly received by the authors to be included into future „official" releases of the component to the general TRNSYS community.

11 Literature

Klein S.A., et al., TRNSYS 14.2 - A TRaNsient SYstem Simulation Program, Solar Energy Laboratory, Universitiy of Wisconsin-Madison, USA, 1996.

Fischer, S. & Müller-Steinhagen, H., 2007. Leistunbsprüfung von Sonnenkollektoren - Kürzere Prüfzeiten durch die Verwendung eines 2-Knoten Modelles. In 17. Symposium Thermische Solarenergie. Kloster Banz, Bad Staffelstein, Germany, (German).

Heimrath, R. & Haller, M., 2007. Project Report A2 of Subtask A: The Reference Heating System, the Template Solar System - A Report of IEA SHC Task 32: Advanced storage concepts for solar and low energy buildings.

Perers, B., 1993. Dynamic method for solar collector array testing and evaluation with standard database and simulation programs. Solar Energy, 50(6), 517-526.

Perers, B. & Bales, C., 2002. A Solar Collector Model for TRNSYS Simulation and System Testing - A technical report of Subtask B of the IEA-SHC - Task 26.

Appendix 1: Installation

The Type832 collector model is a TRNSYS16 drop-in dll component. For a complete set of files one should have:

The latest version of this manual

Type832vABC.dll – the drop-in dll file (release version)

Type832vABC.for – the FORTRAN source code

(where ABC is the version number)

Type832.tmf – the Simulation Studio proforma

Type832.bmp – the Simulation Studio proforma icon

IAM_Sample.iam – the example IAM input file
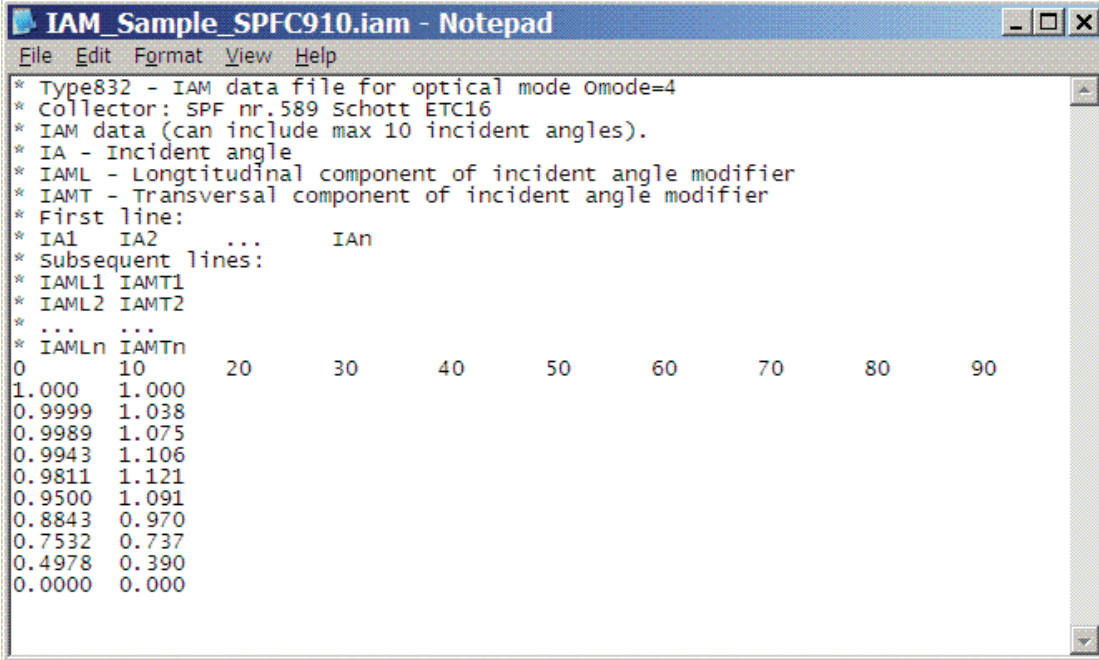
For installation:

5. Copy the .dll file to \TRNSYS16\UserLib\ReleaseDLLs\

6. Copy the .tmf and .bmp files to the \Proformas folder, e.g. C:\Trnsys16\Studio\Proformas\Nonstandard\

7. Restart simulation studio if it was running.

8. If you want to replace old components of the same Type in your project you will have to go through all instances by "Right-click→Replace" and check for possible lost connections.

The source code is for reference and further development and is not needed to run the component. An IAM input file is needed even if one does not simulate with optical mode Omode=4. This is because the simulation studio assigns a file handle automatically when it writes the deck file and thus TRNSYS will try to open the file even if it will not be used later. A dummy file can be used in this case. Note that the example IAM file is to show the format of the file and should not be treated as representative data for an average collector. For realistic IAM-data look for collector test results for the specific collector simulated.

Appendix 2: External files

The 2-axis IAM data can be given in a separate ASCII file. Multiple instances of the TYPE832 in the same project can use either the same input file or individual input files. The IAM can be given for a maximum number of 10 incidence angles. As interpolation is used the first incidence angle must be 0º and the last 90º. The file data content layout should be according to Figure 1. The number of comment lines is arbitrary.


```
* Type832 - IAM data file for optical mode Omode=4
* Collector: SPF nr.589 Schott ETC16
* IAM data (can include max 10 incident angles).
* IA - Incident angle
* IAML - Longtitudinal component of incident angle modifier
* IAMT - Transversal component of incident angle modifier
* First line:
* IA1    IA2     ...     IAn
* Subsequent lines:
* IAML1 IAMT1
* IAML2 IAMT2
* ...    ...
* IAMLn IAMTn
0       10      20      30      40      50      60      70      80      90
1.000   1.000
0.9999  1.038
0.9989  1.075
0.9943  1.106
0.9811  1.121
0.9500  1.091
0.8843  0.970
0.7532  0.737
0.4978  0.390
0.0000  0.000
```

Figure 3: Text file format for 2-axis IAM data.

Note that an IAM input file is needed even if one does not simulate with optical mode Omode=4. This is because the simulation studio assigns a file handle automatically when it writes the deck file and thus TRNSYS will try to open the file even if it will not be used later. A dummy file can be used in this case.

Type 869 Boiler Model

Version 5.02, Michel Haller, 02.05.2010

1 Overview

In contrast to previous documentation of this TRNSYS Type, this documentation includes less mathematical descriptions of the model. For the mathematical description and detailed energy flow analysis the interested reader may instead refer to Haller et al. (2009).

This boiler model programmed for TRNSYS 16.1 simulates boilers that use conventional combustion techniques for carbon-based fuels or hydrogen to heat a fluid mainly in a gas-water heat-exchanger. The user is allowed to choose from predefined fuels (oil, gas, and biomass) or to define an own fuel (by means of weight-fractions of chemical elements and the heating value). In a first step, the model calculates the flue gas products and the temperature and mass flow of the flue gas before the heat exchanger process (Figure 1). In a second step, the heat transfer across the flue gas to water heat-exchanger is calculated. For the calculation of this heat transfer, the user can choose from different simulation approaches that range from simple approaches that are easier to parametrize to more advanced approaches that need more effort for their parametrization. The third and last step determines the energy balance of the thermal mass of the boiler (a one-node approach) and calculates the temperature of the water flowing out of the boiler as well as heat losses to ambient. Burner cycling (also within one time step) is calculated and the number of times the burner switched on during a simulation is an output of the model.
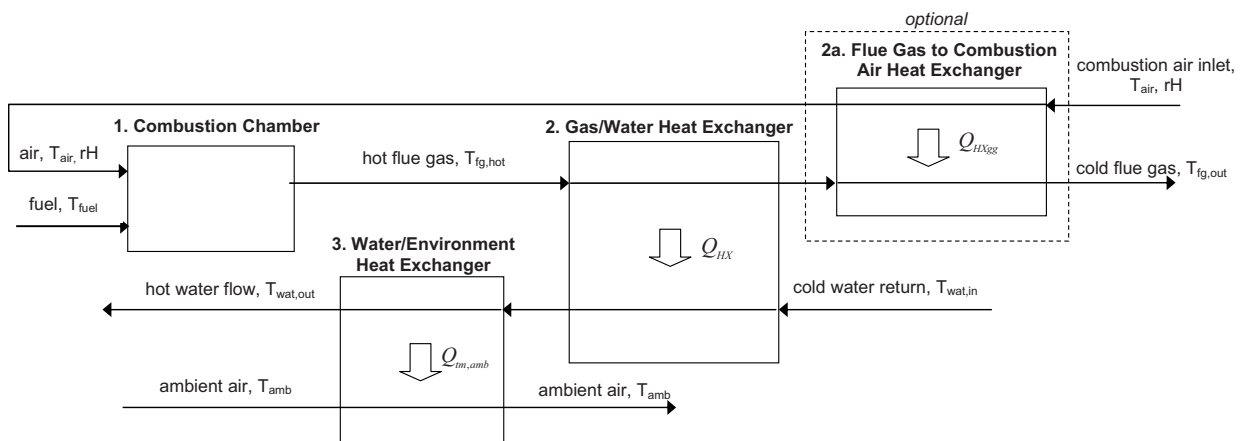
Figure 1: *model for a boiler in steady state operation, according to (ASHRAE 2005)(ASHRAE 2005)(ASHRAE 2005)* ***(ASHRAE 2005)****, adapted and extended with an optional combustion air preheating heat exchanger*

List of Model Possibilities

- Predefined fuels (natural gas H, natural gas L, oil, wood/pellets)
- Defining own fuel based on the gross heating value (GHV, Ho) and elementary composition
- Moisture content of biomass fuels adjustable
- Lambda-value (excess air) for combustion is an input or can be calculated dependent on modulation power
- Complete calculation of flue gas composition and temperature (adiabatic combustion)
- Flue gas to water heat exchange calculations by effectiveness-NTU (counterflow, cross-flow with mixed water-side, etc.) or based on empirical relationships.
- Dependence of flue gas to water heat transfer coefficient on flue gas and water mass flows
- Condensation gains with maximum relative humidity of the flue gas outlet adjustable
- Optional (flue gas mode 3) split calculation of dry part and wet part of heat exchanger for condensing boilers when condensation occurs, wet bulb temperature as driving force in the wet part (simplified Merkel theory)
- Optional (flue gas mode 3) additional flue gas to combustion air heat exchanger for combustion air preheating (simplified)
- Balance of boiler thermal mass with heat losses to ambient during operation and standby
- Modulating power or On/Off burner
- Burner can switch on several times during one time step and the number of times it switches on is reported, in this case, outlet water temperature is the average over the on/off cycles
- Separate temperatures for Ton (burner switches on) Tset (set point for modulation) and Toff (burner switches off)
- Minimum Off-Time
- Minimum On-Time (with security-temperature Tmax overriding minimum On-Time)
- Fixed Startup-Time with separate power-option (e.g. startup-power is Pmax for modulating burners)
- Modulation dependent losses due to CO in flue gas and separate value for CO-losses at startup
- Emission calculations can easily be done outside the model based on model outputs

Model Limits

- Thermal mass is not divided into several nodes (one-node approach, not suited for boilers with a high degree of stratification such as burners integrated into solar stores e.g.)
- Thermal mass of water body and heat exchanger are treated as one thermal mass
- Boiler with two power levels are not simulated (use modulating instead)
- Losses due to chimney draft during OFF-times are currently not simulated (these losses have to be included in general losses to ambient instead)

2 Getting started – simple simulation

The user that does not want to bother about detailed simulation or simply does not have the data needed to determine the parameters for a detailed boiler simulation will start with the following choices:

1. Predefined fuel definitions ($Fuel_{mode} = -1$), see sections 2.2

2. Mass flow rate of the fuel as an input to the model ($FC_{mode} = 2$)

3. Fixed lambda-value (excess air) for the combustion (Input 10 = lambda)

4. Flue gas losses based on flue gas temperature and maximum relative humidity. In flue gas mode 1($FG_{mode} = 1$) flue gas temperature is assumed to be a delta-T over water return temperature

5. No calculation of electricity consumption or energy losses due to CO in flue gas

The parameters and inputs needed for this simple simulation are described in sections 2.2 and 2.3. Please note that many options that are connected to the cycling behavior such as cycling within one time step, startup-time, special values for CO and electricity consumption at startup, etc are not available in fuel consumption mode 2 ($FC_{mode} = 2$).

Note: if you encounter severe problems using this type and cannot resolve them, please read the section "Troubleshooting"

2.1 Flue gas loss calculations in simple simulation, $FG_{mode} = 1$

In flue gas mode 1 ($FG_{mode} = 1$), the temperature of the flue gas at the exit of the boiler is assumed to be a constant delta-T (dT_{nom}) above the return water temperature of the boiler at a given modulation power and water mass flow (nominal conditions). For changes in modulation power and/or mass flow, corrections are applied to the nominal delta-T[1]:

Eq. 1 $T_{fg,out} = T_{wat,in} + dT_{fg,out}$

Eq. 2 $dT_{fg,out} = dT_{nom} + ddT_{hxFg} \cdot \left(1 - \dfrac{\dot{Q}_{fuel}^{GHV}}{P_{nom}^{GHV}}\right) \cdot 100 + ddT_{hxW} \cdot \left(1 - \dfrac{\dot{m}_{Wat}}{\dot{m}_{Wat,nom}}\right) \cdot 100$

The effect of a change in water mass flow is usually only relevant for condensing boilers. For other boilers, or if no measurement results at different water mass flow rates are available, set $ddT_{hxW} = 0$. For simple on/off boilers without modulation, set also $ddT_{hxFg} = 0$.

For condensing boilers, the maximum relative humidity of the flue gas outlet must be specified. From this maximum relative humidity and the simulated return temperature, the maximum vapor load of the flue gas outlet is determined and compared to the vapor load derived from the mass

---

[1] for general use of symbols and explanations of symbols, refer to section 13 (general) or the lists of parameters, inputs and outputs (more specific)

balance of the fuel oxidation process (including excess air). The excess vapor load in the combustion products corresponds to the amount of condensate and is used for the determination of condensation gains.

Flue gas mode 1 is a very simple approach and probably less accurate than flue gas mode 3 or (see section 6). However, it is easier to determine the parameters needed for this mode from standard test data, and its computation is faster than for the other flue gas modes.

If no corrections for flue gas or water mass flows are applied and the maximum relative humidity is set to 100%, this approach corresponds to previous simulation approaches by (Koschak et al. 1998).

2.2 Parameters (simple simulation)

	Name	Dimension	Unit	Type	Range	Default
1	$Fuel_{mode} = -1$ (must)	Dimensionless	-	real	-1	-1
2	$FuelType$ - type of fuel 1 = Natural Gas H, GHV/NHV = 51.18/46.3 MJ/kg 2 = Light Fuel Oil, GHV/NHV = 45.96/42.97 MJ/kg 3 = Wood-Pellets (abs. dry), GHV/NHV = 20.3/19.0 MJ/kg 4 = Natural Gas L, GHV/NHV = 43.13/38.9 MJ/kg For a more detailed description of the predefined fuels see section 11.	Dimensionless	-	real	1;4	1
3-7	not used, specify as 0	-	-	-	-	-
8	γ_{H_2O} - moisture content of the fuel (per kg dry fuel, used for wood fuels, typically 0.08 for pellets / 0.4 for wood chips)	Weight-frac.	kg/kg	real	0;+inf	0
9	not used; specify as 0	-	-	-	-	-
10	$BoCon$ - boolean value for condensation = 1 for burners with condensing technology = 0 for burners without condensing technology (calculated as if condensation would not exist)	Dimensionless	-	int	0;1	1
11-14	unused, specify as 0	Dimensionless	-	real	0;1	1
15	M_{therm} -thermal capacitance of empty boiler	Thermal mass	kJ/K	real	>0;+Inf	5
16	V_{boil} - volume of liquid fluid in the boiler	Volume	m³	real	>0;+Inf	0.016
17	cp_{Vol} - specific heat of liquid fluid in the boiler	Volume	kJ/kgK	real	>0;+Inf	4.18
18	δ_{Vol} - density of liquid in the boiler	Density	kg/m3	real	>0;+Inf	998
19	T_{ini} - initial temperature of the boiler	Temperature	°C	real	-Inf,+Inf	25
20	$UA_{hx,amb,0}$ - heat transfer coefficient area product for losses from boiler thermal mass / heat exchanger to ambient ($U \cdot A$) in case of burner OFF	overall heat transf coefficient times area	kJ/hK	real	0;+Inf	10

21	$UA_{hx,amb,1}$- heat transfer coefficient area product for losses from boiler thermal mass / heat exchanger to ambient ($U \cdot A$) in case of burner ON	overall heat transf coefficient times area	kJ/hK	real	0;+Inf	10
22	FC_{mode} - fuel consumption mode =2: mass flow of fuel is an Input	Dimensionless	-	real	2	2
23	FG_{mode} - flue gas calculation mode =1: Flue gas temperature is a fixed dT over return temperature with corrections for deviations of fuel and water mass flows from nominal conditions	Dimensionless	-	real	1	1
24	P_{nom}^{GHV} - nominal power at which delta-T corresponds to nominal delta-T defined by PAR(23)	Power	kJ/h	real	>0;+Inf	50000
25	$\dot{m}_{Wat,nom}$ - nominal water mass flow at which delta-T corresponds to nominal delta-T defined by PAR(23)	Mass Flow	kg/h	real	>0;+Inf	20000
26	dT_{nom} - delta-T of flue gas temperature over water return temperature at nominal conditions	Temperature Difference	K	real	-inf,+inf	10
27	ddT_{hxFg} - influence of reduced burner power (flue gas mass flow) on the delta-T of flue gas over water return temperature as defined by PAR(29), K/%: a value of -0.1 K means 0.1K is SUBTRACTED from dT_{nom} for each percent the burner power is LOWER than the nominal power defined with PAR(24)	Temperature Difference	K/%	real	-inf;+Inf	0
28	ddT_{hxW} - influence of reduced water mass flow on the delta-T of flue gas over water return temperature as defined by PAR(29), K/%: a value of 0.1 K means 0.1K is ADDED to dT_{nom} for each percent the water mass flow is LOWER than the nominal water mass flow defined with PAR(25)	Temperature Difference	K/%	real	-inf;+Inf	0
29-32	unused, specify as 0					
33	$RH_{fg,out,max}$ - maximum relative humidity of the flue gas leaving the heat exchanger (condensing boilers)	Fraction	-	real	0;1	0.8
34-37	specify as 0					
38	BmT_{mode} - boiler mean temperature mode (see 9): = 0: mean temperature of boiler is average between inlet and outlet; = 1: mean temperature equals outlet temperature (fully mixed boiler water body)	Dimensionless	-	real	0;1	1
39-51	specify as 0					

2.3 Inputs (simple simulation)

	Name	Dimension	Unit	Type	Range	Default
1	$T_{wat,in}$ - temperature of water (or other fluid) entering the boiler	Temperature	°C	real	-Inf,+Inf	25
2	$\dot{m}_{wat,in}$ - mass flow rate of water (or other fluid) entering the boiler	Flow	kg/h	real	0,+Inf	0
3	γ - signal enabling boiler operation 0 = burner off during all time step, in all modes! Overrides Input(4)! 1 = burner operation enabled	Dimensionless	-	real	0;+1	1
4	$\dot{m}_{fuel,wet}$ - fuel burning mass flow rate (wet fuel weight in case of biomass fuels / if $\gamma_{H_2O} > 0$)	mass flow rate	kg/h	real	0,+Inf	0
5-6	unused, specify as 0	Temperature	°C	real	-Inf,+Inf	0
7	T_{MAX} - a warning is printed to the log-file if boiler reaches this temperature	Temperature	°C	real	-Inf,+Inf	95
8	T_{amb} - ambient temperature in room of boiler operation, used for calculation of boiler heat losses	Temperature	°C	real	-Inf,+Inf	20
9	$fr_{ash,chem}$ - fraction of GHV lost due to unburnt residues in ashes	Energy-frac.	-	real	0;+1	0
10	λ_{input} - lambda-value, ratio of air used for the burning process relative to air used for stoichiometric reaction. specify as 0 or -1 if lambda should be calculated dependent on modulation of the boiler (see section 4)	Dimensionless	-	real	1; Inf	1.1
11	RH_{air} - relative humidity of combustion air [0,1]	Fraction	-	real	0;+1	0.5
12	p_{air} - pressure of ambient (and of the chambers where burning of the fuel and condensation of the flue gas occurs)	Pressure	bar	real	0;+Inf	1.0132
13	T_{air} - temperature of air used for burning	Temperature	°C	real	-Inf;+Inf	25
14	T_{fuel} - temperature of fuel supplied	Temperature	°C	real	-Inf;+Inf	25
15	$fr_{BC,amb}$ - fraction of fuel energy (GHV) lost to ambient by burner chamber	Fraction	-	real	-inf;+inf	0
16–18	unused					0

3 Option: Automatic fuel consumption calculation, $FC_{mode} = 1$

As an alternative to the "mass flow rate of the fuel as an input", in $FC_{mode} = 1$ the boiler can be given a maximum and a minimum burner power (parameters) as well as temperature criteria to tell the burner when to start burning, stop burning and what temperature set point the water in the boiler should reach using power modulation. In this mode, the burner will be turned on as soon as the boiler outlet temperature drops below the temperature specified with T_{ON}. Within the modulation range (P_{max}^{GHV}, P_{min}^{GHV}), the fuel consumption will be adjusted in a way that the outlet temperature will match T_{SET}. If T_{SET} is exceeded even with the lowest possible power modulation (P_{min}^{GHV}), then the burner will continue until the outlet temperature reaches T_{OFF}. In this mode, also burner on/off cycling within one time step may be calculated and special features like startup-time, minimum on-time, minimum off-time and special startup conditions like CO emissions during startup- time and electricity consumption during startup-time may be used. Special Parameters and Inputs that have to be specified for $FC_{mode} = 1$ are listed in the following sections.

Special Parameters (different from section 2.2)

11	$BoMod$ - boolean value for modulation = 1 if modulation between Pmax and Pmin is allowed = 0 if only on/off (Pmax/0)	Dimensionless	-	real	0;1	1
12	P_{max}^{GHV} - maximum burner power (based on GHV and fuel consumption rate)	Energy	kJ/h	real	>0;+Inf	0
13	P_{min}^{GHV} - minimum burner power (based on GHV and fuel consumption rate)	Energy	kJ/h	real	>0;+Inf	0
14	P_{START}^{GHV} - average burner power during startup time (based on GHV and fuel consumption rate)	Power	kJ/h	real	0;+inf	0
...						
22	FC_{mode} - fuel consumption mode =1: mass flow of fuel is determined according to Parameters 11-14 and 39-41	Dimensionless	-	real	1	1
...						
39	dt_{START} - startup time time needed for pellet-boilers to start-up and stabilize the flame, overrides T_{OFF}, but not T_{MAX}	Time	h	real	0;inf	0
40	$dt_{BURN,min}$ - minimum time burner will stay on; even if it overshoots T_{OFF}, but not if it reaches T_{MAX}	Time	h	real	0;inf	0
41	$dt_{OFF,min}$ - minimum Off-Time after Burner stopped	Time	h	real	0;inf	0

Special Inputs (different from section 2.3)

4	T_{ON} - temperature below which burner turns on	Temperature	°C	real	-Inf,+Inf	0
5	T_{SET} - set point temperature the boiler tries to reach in modulation whenever it is on	Temperature	°C	real	-Inf,+Inf	0
6	T_{OFF} - temperature at which boiler will turn off when exceeded with lowest burning power.	Temperature	°C	real	-Inf,+Inf	0
7	T_{MAX} - maximum temperature at which burner will always turn off even if minimum On-Time has not been reached yet.	Temperature	°C	real	-Inf,+Inf	0

4 Option: Modulation dependent excess-air calculation, Input(10) < 1.0

The λ-value is the ratio of air used for combustion and air that would be used for stoichiometric reaction of the fuel. Thus, $\lambda = 1 + excessair \geq 1$. The λ-value for modulating boilers is usually strongly dependent on the power modulation, especially for boilers that use wood fuels. Therefore, it is not recommended to define a fixed lambda value with Input 10. The better option is to specify Input(10) (λ_{mode}) as 0.0 or -1.0, and use parameters 35-37 to define a power dependent lambda-value as follows:

For $\lambda_{mode} = 0$, a linear dependency of λ on the fuel consumption power $\dot{Q}_{fuel}^{GHV}$ is used with $\lambda = fac_{A,\lambda}$ at the maximum fuel consumption rate $Q_{fuel}^{GHV} = P_{max}^{GHV}$, and $\lambda = fac_{B,\lambda}$ at the minimum fuel consumption rate $Q_{fuel}^{GHV} = P_{min}^{GHV}$.

For $\lambda_{mode} = -1$, λ is calculated with a 2nd order polynomial expression dependent on the fuel mass flow rate:

Eq. 3 $\lambda = fac_{A,lam} + fac_{B,lam} \cdot \dot{m}_{fuel,dry} + fac_{C,lam} \cdot \left(\dot{m}_{fuel,dry} \right)^2$

Special Parameters (different from section 2.2)

42	$fac_{A,\lambda}$ - factor for power dependent lambda calculation $\lambda_{mode} = 0.0$: minimum lambda value (at maximum burner power) $Input(10) = -1.0$: base lambda value (0 order coefficient)	Dimensionless	-	real	-inf;inf	0

43	$fac_{B,\lambda}$ - factor for power dependent lambda calculation. $\lambda_{mode} = 0.0$: maximum lambda value (at minimum burner power) $\lambda_{mode} = -1.0$: 1st order coefficient to be multiplied with fuel mass flow rate for lambda-calculation	Dimensionless	-	real	-inf;inf	0
44	$fac_{C,\lambda}$ - factor for power dependent lambda calculation. $\lambda_{mode} = 0.0$: no effect $\lambda_{mode} = -1.0$: 2nd order coefficient to be multiplied with the square of the fuel mass flow rate for lambda-calculation	Dimensionless	-	real	-inf;inf	0

Special Inputs (different from section 2.3)

10	λ_{mode} - mode of lambda simulation $\lambda_{mode} = 0.0$: linear lambda with minimum at maximum modulation and maximum at minimum modulation (parameters 35-36) $\lambda_{mode} = -1.0$: exponential lambda calculation based on fuel mass flow rate and parameters 35-37.	Dimensionless	-	real	-1;0	1.1

5 Option: Calculation of electricity consumption and energy lost due to CO in flue gas

Electricity consumption and losses due to CO in the flue gas can be calculated dependent on power modulation with a linear approach by defining a maximum and minimum electricity consumption (corresponding to maximum and minimum burner power), and maximum and minimum CO emissions (corresponding to minimum and maximum burner power). If mass flow rate of fuel is not an input ($FC_{mode} = 1$), a startup-time may be defined and special values for electricity consumption and CO emissions may be assigned to this startup time.

More detailed simulation of electricity consumption or CO emissions using non-linear relationships, or startup values that depend on the time the boiler has been off, can only be calculated outside this type. One possibility is using this type with simulation time steps that are small enough (possibly with mass flow of the fuel as an input) and determine the needed values based on a post processing of the output of this model (e.g. fuel consumption rate and number of startups are given as outputs).

Special Parameters (different from section 2.2)

45	$ppmCO_{min}$ - ppm CO (mol / mol dry flue gas) at maximum burner power (usually minimum CO value)	Fraction	-	real	0;inf	0
46	$ppmCO_{max}$ - ppm CO (mol / mol dry flue gas) at minimum burner power (usually maximum CO value)	Fraction	-	real	0;inf	0
47	gCO_{START} - g CO emissions during startup-time aditionally to the value calculated by ppmCOmin and ppmCOmax	Mass	g	real	0;inf	0
48	$P_{el,min}$ - minimum electricity consumption (at minimum burner power)	Power	W	real	0;inf	0
49	$P_{el,max}$ - maximum electricity consumption (at maximum burner power)	Power	W	real	0;inf	0
50	$P_{el,OFF}$ - electricity consumption during burner off times (controller standby)	Power	W	real	0;inf	0
51	$Q_{el,START}$ - electric heating during startup, heat added to fuel energy input – electricity counted in electricity consumption additionally to the values from $P_{el,min}$ and $P_{el,max}$.	Energy	Wh	real	0;inf	0

6 Option: Different Modes for flue gas heat exchanger simulation

6.1.1 Simple delta-T approach, $FG_{mode} = 1$

Please refer to section 2.1 for the description of flue gas mode 1.

6.1.2 Empirical effectiveness for flue gas to water heat exchange, $FG_{mode} = 2$

An empirical effectiveness of the flue gas to water heat exchanger may be given directly by parameters, instead of being based on effectiveness-NTU relationships. This simplifies calculation and allows to define also a heat exchanger effectiveness larger than 1, thereby avoiding the need for the definition of an eventual combustion air preheater[2]. No split of the heat exchanger into a dry part and a wet part is performed in this mode. Instead, the effectiveness of the heat exchanger (≠ combustion efficiency) is assumed to be composed of a base effectiveness determined at nominal conditions ε_{nom} and correction terms that account for changes in the

---

[2] Please note that the influence of the combustion air temperature before the preheater is lost in this highly simplified apprach.

mass flow rates of flue gas or boiler water, similar to the corrections applied to the delta-T approach in $FG_{mode} = 3$.

Eq. 4
$$\varepsilon_{HX} = \varepsilon_{nom} + d\varepsilon_{hxFg} \cdot \left(1 - \frac{Q_{fuel}^{GHV}}{P_{nom}^{GHV}}\right) + d\varepsilon_{hxW} \cdot \left(1 - \frac{\dot{m}_{Wat}}{\dot{m}_{Wat,nom}}\right)$$

Eq. 5
$$T_{fg,out} = T_{fg,hot} - \varepsilon_{HX} \cdot \left(T_{fg,hot} - T_{wat,in}\right)$$

Maximum relative humidity is taken into account the same way as in all flue gas modes, and therefore also condensing boilers may be simulated this way. For non-condensing boilers, $d\varepsilon_{hxW}$ is usually zero. For non modulating boilers, $d\varepsilon_{hxFg} = 0$. This calculation is certainly faster, but most likely also less accurate, than the detailed calculation in flue gas mode 1. However, it is expected to be more accurate than mode 3.

Special Parameters (different from section 2.2)

23	FG_{mode} - flue gas calculation mode =2: Efficiency of flue gas to water heat exchanger is calculated with a base efficiency and correction factors that depend on mass flow rates of flue gas and water.	Dimensionless	-	real	2;2	1
24 25	P_{nom}^{GHV} and $\dot{m}_{Wat,nom}$ as in $FG_{mode} = 3$					
26	ε_{nom} - nominal effectiveness of the flue gas to water heat exchanger (at nominal water mass flow and burner power)	Dimensionless	-	real	>0,inf	0.98
27	$d\varepsilon_{hxFg}$ - influence of reduced burner power (flue gas mass flow) on the effectiveness of the heat exchanger: a value of 1 means the effectiveness increases by 1% for each percent the burner power is LOWER than the nominal power defined with PAR(24)	Dimensionless	-	real	inf;Inf	0
28	$d\varepsilon_{hxW}$ - influence of reduced water mass flow on the effectiveness of the heat exchanger: a value of -1 means the effectiveness decreases by 1% (absolut) for each percent the water mass flow is LOWER than the nominal water mass flow defined with PAR(25)	Dimensionless	-	real	-inf;Inf	0
29-32	unused, specify as 0					
33	$RH_{fg,out,\max}$ - maximum relative humidity of the flue gas leaving the heat exchanger (condensing boilers)	Fraction	-	real	0,1	0.8

6.2 Effectiveness-NTU for flue gas to water heat exchange, $FG_{mode} = 3$

A better match of a boiler's steady state flue gas losses may be obtained using a heat exchanger effectiveness-NTU approach ($FG_{mode} = 3$). However, this mode requires more computational effort and – more important - more effort of the user to determine the appropriate

parameters. In flue gas mode 3, an additional flue gas to combustion air heat exchanger (combustion air preheater) may also be defined. This mode is described in more detail in Haller et al. (2009)

Special Parameters (different from section 2.2)

23	FG_{mode} - flue gas calculation mode =3: Effectiveness of flue gas to water heat exchanger is calculated with effectiveness-NTU; split calculation for condensing boilers if condensation occurs with wet bulb temperature difference as the driving force in the wet part	Dimensionless	-	real	3	3
24 25	P_{nom}^{GHV} and $\dot{m}_{Wat,nom}$ as in $FG_{mode}=1$					
26	HX_{mode} - heat exchanger arrangement of flue gas to water heat exchanger =1: counterflow heat exchanger (usual for condensing boilers) =2: cross flow heat exchanger, Cmax mixed, Cmin unmixed (usual for biomass boilers) =4: parallel flow heat exchanger (unusual)	Dimensionless	-	real	0;4	1
27	$UA_{HX,nom}$ - overall heat transfer coefficient area product at nominal fuel consumption and water mass flow	Heat transfer resistance including area	kJ/hK	real	>0;Inf	0
28	$frR_{HX,fg}$ - fraction of heat transfer resistance on flue gas side of heat exchanger	Dimensionless	-	real	>0;Inf	0.8
29	$frR_{HX,met}$ - fraction of heat transfer resistance in metal of heat exchanger	Dimensionless	-	real	0;Inf	0.8
30	m_{hxFg} - exponent for the dependency of the flue gas side surface heat exchanger resistance on the mass flow rate of the flue gas	Dimensionless	-	real	0;Inf	0.8
31	m_{hxW} - exponent for the dependency of the water side surface heat exchange resistance on the mass flow rate of the water	Dimensionless	-	real	0;Inf	0.
32	fac_{wet} - correction factor for heat transfer resistance of wet part of flue gas side of heat exchanger	Dimensionless	-	real	>0,inf	1.5
33	$RH_{fg,out,max}$ - maximum relative humidity of the flue gas leaving the heat exchanger (condensing boilers)	Fraction	-	real	0;1	0.8

34	$HXgg_{mode}$ - heat exchanger arrangement of flue gas to combustion air heat exchanger (combustion air preheater) =1: counterflow heat exchanger =2: cross flow heat exchanger, Cmax mixed, Cmin unmixed =4: parallel flow heat exchanger	Dimensionless	-	real	0;4	1
35	$UA_{gg,nom}$ - overall heat transfer coefficient area product for the additional flue gas to combustion air heat exchanger at nominal conditions	overall heat transf coefficient times area	kJ/hK	real	>0;Inf	0
36	m_{HXgg} - exponent for the dependency of the UA-value of the combustion air preheater on the mass flow rate of the flue gas	Dimensionless	-	real	-inf;inf	0.8
37	$RH_{fg,out,GG,\max}$ - maximum relative humidity of the flue gas leaving the heat exchanger (condensing boilers)	Fraction	-	real	0,1	0.8

6.3 Flue gas outlet conditions as inputs, $FG_{mode} = 4$

In flue gas mode 4, the flue gas outlet conditions are provided as Inputs by the user and do not have to be simulated. This mode is useful e.g. if data from steady state measurements or field measurements shall be evaluated. In this mode, parameters 23 – 30 have no effect.

Special Parameters (different from section 2.2)

23	FG_{mode} - flue gas calculation mode =4: temperature, relative humidity (or condensate mass flow rate) and ppm CO of flue gas leaving the boiler are inputs	Dimensionless	-	real	4;4	1
24-37	unused					

Special Inputs (different from section 2.3)

	Name	Dimension	Unit	Type	Range	Default
16	$T_{Fg,out,ms}$ - (measured) flue gas outlet temperature	Temperature	°C	real	-Inf;Inf	25

17	$RH_{Fg,out,ms}$ [3] - (measured) flue gas outlet relative humidity (makes sense only for condensing boilers); If $RH_{Fg,out,ms} \leq 0$; then the negative value will be taken as the measured mass flow rate of condensate $\dot{m}_{H_2O,cond,ms}$, and relative humidity will be calculated from this value, the saturation pressure at $T_{Fg,out,ms}$ and the mass balance for H_2O	Fraction	-	real	0;1	0.8
18	$ppmCO_{ms}$ - (measured) concentration of CO in flue gas (mol per mol dry flue gas)	Fraction	ppm	real	0;inf	0

7 Option: User defined fuels

A small number of researchers may want to define their own fuel based on the gross heating value (Ho) and the mass fractions of the elements in the fuel. This is possible by assigning a positive value to Parameter 1 as the upper heating value and thereafter defining the mass fraction of the elements in the fuel with Parameters 2-7.

Special Parameters (different from section 2.2)

	Name	Dimension	Unit	Type	Range	Default
1	GHV - gross (or upper) heating value (Ho) of the fuel (kJ per kg dry fuel)	Energy	kJ/kg	real	-Inf;Inf	0
2	γ_C - weight-fraction of carbon in dry fuel	Weight-frac.	kg/kg	real	0;1	0
3	γ_H - weight-fraction of hydrogen in dry fuel	Weight-frac.	kg/kg	real	0;1	0
4	γ_O - weight-fraction of oxygen in dry fuel	Weight-frac.	kg/kg	real	0;1	0
5	γ_N - weight-fraction of nitrogen in dry fuel	Weight-frac.	kg/kg	real	0;1	0
6	γ_S - weight-fraction of sulfur in dry fuel	Weight-frac.	kg/kg	real	0;1	0
7	γ_{ash} - weight-fraction of ashes (non-volatile residues of dry fuel)	Weight-frac.	kg/kg	real	0;1	0
8	γ_{H_2O} - moisture content of the fuel (per kg dry fuel, used for wood fuels, specify as 0 for oil or gas)	Weight-frac.	kg/kg	real	0;inf	0
9	cp_{fuel} - specific heat of (dry) fuel	Weight-frac.	kJ/kgK	real	0;inf	0

---

[3] Please note that if the measured relative humidity given with Input(17) exceeds the maximum possible relative humidity derived from the mass balance of hydrogen in fuel and combustion air supply, the maximum relative humidity from the mass balance will override Input(17).

8 Outputs (all modes)

Please note that depending on the modes for simulation chosen by setting Parameters and Inputs, some of the Outputs after Output 30 will not be calculated and are set to zero during all time steps.

	Name	Dimension	Unit	Type	Range	Default
1	$T_{wat,out}$ - average temperature of fluid leaving the boiler	Temperature	°C	real	-inf;inf	0
2	$\dot{m}_{wat,out}$ - mass flow rate of water leaving the boiler	Mass flow rate	kg/h	real	0;inf	0
3	$\dot{Q}_{fuel}^{GHV}$ - average energy flow rate of fuel used during this time step, calculation based on GHV = Ho	Power	kJ/h	real	0;inf	0
4	$\dot{Q}_{wat,out}$ - average heat transfer calculated form energy balance of water flowing in and out of the boiler	Power	kJ/h	real	-inf;inf	0
5	$\dot{Q}_{Mtherm}$ - average heat transfer to thermal mass / capacitance of the boiler for this time step	Power	kJ/h	real	-inf;inf	0
6	$\dot{Q}_{tm,amb}$ - average rate of energy loss to the boilers ambient by heat transfer from the boiler thermal mass	Power	kJ/h	real	-inf; inf	0
7	$\dot{Q}_{HXgw}$ - average rate of heat transfer across the heat-exchanger from flue gas to water	Power	kJ/h	real	0;inf	0
8	$\dot{Q}_{fg,sens}$ - average rate of energy loss with sensible heat of flue gas	Power	kJ/h	real	-inf;inf	0
9	$\dot{Q}_{fg,lat}$ - average rate of energy loss with latent heat of flue gas	Power	kJ/h	real	0;inf	0
10	$\dot{Q}_{fg,chem}$ - average rate of energy loss in combustion process due to CO in flue gas	Power	kJ/h	real	0;inf	0
11	$\dot{Q}_{ash,chem}$ - average rate of energy loss in combustion process due to unburnt residues in ashes	Power	kJ/h	real	0;inf	0
12	$\dot{Q}_{bc,amb}$ - average rate of energy loss from combustion chamber to ambient (radiative and convective)	Power	kJ/h	real	0;inf	0
13	$T_{fg,hot}$ - average temperature of flue gas before heat-exchanger during burner operation	Temperature	°C	real	0;inf	0
14	$T_{fg,out}$ - average temperature of flue gas after heat exchanger during operation	Temperature	°C	real	-inf;inf	0
15	$RH_{fg,out}$ - relative humidity of leaving flue gas [0-1]	Fraction	.	real	0;1	0
16	λ - current lambda of combustion	Dimensionless	-	real	1;inf	0
17	$T_{fg,dp}$ - temperature of dew point for combustion products / hot flue gas	Temperature	°C	real	0;inf	0
18	$\dot{m}_{CO}$ - flow rate of CO in flue gas, in g/h	Mass Flow	g/h	real	0;inf	0

19	$\dot{m}_{fuel,dry}$ - mass flow rate of dry fuel (average of time step)	Mass Flow	kg/h	real	0;inf	0
20	$\dot{m}_{fuel,wet}$ - mass flow rate of wet fuel (avarage of time step)	Mass Flow	kg/h	real	0;inf	0
21	$rGHVtoNHV$ - ratio of gross heating value to net heating value, both per kg dry fuel. $NHV =$ $Hu = GHV$ minus enthalpy of condensation of vapor from both, H in fuel and H_2O in fuel.	Ratio	-	real	1;inf	0
22	$\dot{m}_{fg,dry}$ - mass flow rate of dry flue gas (at last burn phase)	Mass Flow	kg/h	real	0;inf	0
23	$\dot{m}_{fg,wet}$ - mass flow rate of wet, hot flue gas (at last burn phase)	Mass Flow	kg/h	real	0;inf	0
24	$\dot{m}_{air,dry}$ - mass flow rate of dry air (at last burn phase)	Mass Flow	kg/h	real	0;inf	0
25	E_{stored} - energy stored in the thermal mass including fluid content in the boiler, with respect to initial temperature	Energy	kJ	real	-inf;+inf	0
26	fr_{ON} - fraction of time step the burner was on (start-phases included)	Dimensionless	h/h	real	0;1	0
27	N_{STARTS} - number of burner starts since beginning of simulation	Dimensionless	--	real	0; inf	0
28	$P_{BURN,END}$ - power of fuel burning at the end of this time step (based on GHV)	Power	kJ/h	real	0; inf	0
29	$ID_{Phase,End}$ - identifier for the burner phase at the end of the time step: 1 = Off, 2 = Start Phase, 3 = Steady Burn	Dimensionless	-	real	0; 3	0
30	$\dot{Q}_{Balance}$ - energy flow rate balance, should always be zero or negligible compared to Q_{fuel}	Power	kJ/h	real	-inf;inf	0
31	$fr_{HX,wet}$ - fraction of the heat exchanger that is wet (wet surface / condensing boilers) at the end of the time step	Fraction	-	real	0;1	0
32	ε_{dry} - effectiveness of the dry part of the heat exchanger at the end of the time step	Fraction	-	real	0;1	0
33	ε_{wet} - effectiveness of the wet part of the heat exchanger at the end of the time step	Fraction	-	real	0;1	0
34	ε_{HX} - overall effectiveness of the heat exchanger at the end of the time step	Fraction	-	real	0;1	0
35	$T_{wat,b}$ - temperature of the water at the dry-wet boundary at the end of the time step	Temperature	°C	real	-inf;inf	0
36	$T_{fg,b}$ - temperature of bulk flue gas at dry-wet boundary at the end of the time step	Temperature	°C	real	-inf;inf	0

37	$T_{air,out,GG}$ - outlet combustion air temperature of the flue gas to combustion air heat exchanger at the end of the time step	Temperature	°C	real	-inf;inf	0
38	$\dot{m}_{H_2O,cond}$ - condensate mass flow rate	Mass Flow	kg/h	real	0;inf	0
39	P_{el} - electricity consumption (including startup ignition energy)	Power	W	real	0;inf	0
40	$\dot{Q}_{el,therm}$ - electric heat input (startup-ignition) that is contributing to the thermal energy balance	Power	kJ/h	real	0;inf	0

9 Energy balance of the boiler thermal capacitance

To calculate the energy balance of the thermal capacitance of the boiler, the following simplifications are made:

- Thermal capacitance of the empty boiler and thermal capacitance of the water in the boiler are added and treated as one thermal node.

- Case $BmT_{mode} = 0$: the mean boiler temperature is assumed to be the average value from the inlet and outlet temperature of the boiler water.

- Case $BmT_{mode} = 1$: Corresponds to a fully mixed water body, so there is no temperature gradient and the mean temperature of the boiler equals the outlet temperature of the boiler.

The main equations for the calculation of the energy balance of the boiler thermal mass are:

Eq. 6 $\dot{Q}_{HXgw} - \dot{Q}_{tm,amb} - \dot{Q}_{wat,out} - \dot{Q}_{Mtherm} = 0$

Eq. 7 $T_{B,avg}\left(t\right) = \dfrac{T_{wat,out}\left(t\right) + T_{wat,in}}{2}$ for $BmT_{mode} = 0$

Eq. 8 $T_{B,avg}\left(t\right) = T_{wat,out}\left(t\right)$ for $BmT_{mode} = 1$

Eq. 9 $\dot{Q}_{tm,amb} = \left(T_{B,avg} - T_{amb}\right) \cdot UA_{hx,amb}$

Eq. 10 $\dot{Q}_{wat,out} = \left(T_{wat,out}\left(t\right) - T_{wat,in}\right) \cdot \dot{C}_{wat}$

Eq. 11 $\dot{Q}_{Mtherm} = M_{therm,tot} \cdot \dfrac{\left(T_{wat,in} + T_{wat,out}\left(t\right)\right)}{2}\dfrac{d}{dt}$ for $BmT_{mode} = 0$

Eq. 12 $\dot{Q}_{Mtherm} = M_{therm,tot} \cdot T_{wat,out}\left(t\right)\dfrac{d}{dt}$ for $BmT_{mode} = 1$

Where

$\dot{Q}_{HXgw}$, $\dot{Q}_{wat,out}$, $\dot{Q}_{Mtherm}$, $\dot{Q}_{amb}$, $T_{wat,in}$, $T_{wat,out}$, T_{amb} are energy transfer rates and temperatures (see sections 13 and 0)

$M_{therm,tot}$ total thermal capacitance (empty boiler + fluid inside), kJ/K

$T_{B,avg}$ average temperature of the boiler thermal capacitance / thermal mass

$UA_{hx,amb}$ overall heat transfer coefficient area product for losses from the boilers thermal mass (flue gas to water heat exchanger) to the ambient, $= UA_{hx,amb,0}$ when burner is off, $UA_{hx,amb,1}$ when burner is on, kJ/hK

$\dot{C}_{wat}$ capacity flow rate of the fluid/water, kJ/hK

t time, h

To calculate $T_{wat,out}(t)$ after a certain time and $T_{wat,out,avg}$ of a time step, the following equations are derived from the equations above:

Eq. 13
$$T_{wat,out}(t) = T_{inf} - (T_{inf} - T_{wat,out,A}) \cdot EXP(-G_1 \cdot t)$$

Eq. 14
$$T_{wat,out,avg} = T_{inf} + \frac{(T_{inf} - T_{wat,out,A}) \cdot [EXP(-G_1 \cdot t) - 1]}{G_1 \cdot t}$$

Where

$$T_{inf} = \frac{G_2}{G_1}$$

is the temperature of the water outlet of the boiler after an infinite time (in steady state), °C

With

Eq. 15
$$G_1 = \frac{UA_{hx,amb} + 2 \cdot \dot{C}_{wat}}{M_{therm,tot}} \quad \text{for } BmT_{mode} = 0$$

Eq. 16
$$G_1 = \frac{UA_{tm,amb} + \dot{C}_{wat}}{M_{therm,tot}} \quad \text{for } BmT_{mode} = 1$$

Eq. 17
$$G_2 = \frac{2 \cdot (\dot{Q}_{HXgw} - UA_{hx,amb} \cdot [T_{wat,in}/2 - T_{amb}] + T_{wat,in} \cdot \dot{C}_{wat})}{M_{therm,tot}} \quad \text{for } BmT_{mode} = 0$$

Eq. 18
$$G_2 = \frac{(\dot{Q}_{HXgw} + UA_{hx,amb} \cdot T_{amb} + T_{wat,in} \cdot \dot{C}_{wat})}{M_{therm,tot}} \quad \text{for } BmT_{mode} = 1$$

with

$T_{wat,out,A}$ water outlet temperature at the beginning of the time step $T_{wat,out,A} = T_{wat,out}(t = 0)$, °C

To calculate the time t (h) needed to bring the boiler to a certain temperature of $T_{wat,out}(t) = T_{wat,out,B}$, the following formula is used, derived from the same set of equations:

Eq. 19
$$t = \frac{LN\left(\frac{T_{inf} - T_{wat,out,A}}{T_{inf} - T_{wat,out,B}}\right)}{G_1}$$

9.1 Total energy balance (Check-Sum)

To detect problems that might occur and might lead to an improper energy balance, an energy transfer checksum $\dot{Q}_{Balance}$ is calculated as follows:

Eq. 20 $\qquad \dot{Q}_{Balance} = \dot{Q}_{fuel} + \dot{Q}_{el,therm} - \dot{Q}_{ash,chem} - \dot{Q}_{BC,amb} - \dot{Q}_{fg,chem} - \dot{Q}_{fg,sens} - \dot{Q}_{fg,lat} - \dot{Q}_{amb} - \dot{Q}_{Mtherm} - \dot{Q}_{wat,out}$

This value should always be very small with respect of the total energy turnover.

10 Flue gas enthalpy functions

For the calculation of the enthalpy of the combustion products, heat capacity values for the components of the flue gas were taken from literature (Baehr 2005). A curve fit for the specific enthalpy calculated based on these values with reference temperature 25 °C has been established for all flue gas components (Table 1).

Eq. 21 $\qquad h_X(t) = a + b \cdot t + c \cdot t^2 + d \cdot t^3 + e \cdot t^4$

The fit matches the tabular data with an accuracy of +/- 0.22% between 0 and 200 °C and +/-1% up to 2200 °C. All values are valid for gases only.

Table 1: *Curve-fit parameters for the specific enthalpy [J/mol] of flue gas components with reference 25°C, all in gaseous phase.*

	$N^*_{2(g)}$	$O_{2(g)}$	$CO_{2(g)}$	$SO_{2(g)}$	$H_2O_{(g)}$
a	-7.24751E+02	-7.33012E+02	-9.14771E+02	-9.85551E+02	-8.37435E+02
b	2.89731E+01	2.92298E+01	3.60418E+01	3.89400E+01	3.34201E+01
c	6.20236E-04	3.60882E-03	2.22271E-02	1.95227E-02	3.01727E-03
d	2.26445E-06	6.54454E-07	-1.07038E-05	-9.67682E-06	3.02713E-06
e	-7.49879E-10	-4.83700E-10	2.09076E-09	1.85472E-09	-9.51233E-10

11 Properties of Predefined Fuels

Table 2: *fuel properties for the most common fuels for residential heating, all values per kg dry base (d.b.)*

FuelType	1		2		3		4	
	Nat.Gas H		Light Fuel Oil		Wood-Pellets totally dry		Nat.Gas L	
NHV (kJ/kg, d.b.)	46300	(1)	42970	(1)	19000	(4)	38900	(1)
GHV (kJ/kg, d.b.)	51180	(1)	45960	(1)	20300	(4)	43130	(1)
γ_C (kg/kg, d.b.)	0.732	(1)	0.859	(1)	0.503	(4)	0.592	(1)
γ_H (kg/kg, d.b.)	0.222	(1)	0.137	(1)	0.057	(4)	0.194	(1)
γ_O (kg/kg, d.b.)	0.033	(1)	0.002	(1)	0.430	*	0.013	(1)
γ_N (kg/kg, d.b.)	0.012	(1)	0.000	(1)	0.002	(4)	0.201	(1)
γ_S (kg/kg, d.b.)	0.000	(1)	0.002	(1)	0.003	(4)	0.000	(1)
γ_{Ash} (kg/kg, d.b.)	0.000	(1)	0.000	(1)	0.005	(4)	0.000	(1)
cp_{fuel} (kJ/kgK)	1.97	(2)	2.07	(3)	1.27		1.90	(2)

* *calculated as* $1-\left(\gamma_C + \gamma_H + \gamma_N + \gamma_S + \gamma_{Ash}\right)$.

Sources:

(1) (Baehr 2005)*, pp. 463;*

(2) (Gaswärme-Institut Essen e.V. 1983)

(3) (Stöcker 1994)

(4) (Obernberger & Thek 2004)

12 Troubleshooting

- Boiler does not start heating:
    - Make sure that the input 3 (γ) is set to 1.
    - In fuel consumption mode 1, make sure that T_{ON} is higher than the boiler temperature
- I get an Error message oft the kind „***invalid floating point operation***" at the beginning of the simulation:
    - In TRNSYS 16.1 (or 17?) set the Overwrite Check to 1:
        - Directly in the ASCII-file (.dck-file) using the OVERWRITE_CHECK statement
        - In the Studio: „Control cards"->"9: Debug Mode" = „True"

13 General Symbolism

dT	temperature difference, K
ε	heat exchanger effectiveness, -
fr	fraction (0-1), -
fac	factor, variable units
GHV	gross heating value, upper heating value, Ho, for standard conditions of 25°C (educts and products) and all water in products is liquid, kJ/kg dry fuel
H	enthalpy, kg/kg species or kg/kg dry fuel burnt
ΔH	enthalpy difference, kJ/kg species or per kg fuel burnt
γ	mass fraction, kg/kg, - (or input signal of 0 or 1)
λ	lambda value of combustion, = 1+excess air (ratio of air used for combustion to air used for stoichiometric reaction, -
$\dot{m}$	mass flow, kg/h
m	exponent in Nusselt-relationship or parameter determining the dependency of flue gas losses on mass flows of flue gas or boiler water, -
μ	amount of flue gas species per kg dry fuel burnt, kg/kg
NHV	net heating value, lower heating value, Hu, for standard conditions of 25°C (educts and products) and all water in products is vapor, kJ/kg dry fuel
P	power (energy flow) of electricity or fuel consumption, kJ/h
p	pressure, bar
Q	energy of a heat transfer or fuel consumption, kJ
$\dot{Q}$	power (energy flow) of a heat transfer or fuel consumption, kJ/h
RH	relative humidity (0-1), -
T	temperature, °C
t	time, h
UA	overall heat transfer coefficient area product, kJ/hK

subscripts

air	combustion air
amb	ambient (at the boiler location)
avg	average
B	boiler
$chem$	chemical (losses)
$draft$	losses due to natural draft through the boiler combustion chamber and/or heat exchanger
fg	flue gas
fg,hot	flue gas at combustion chamber outlet, calculated as adiabatic reaction product of fuel and combustion air
$fuel$	fuel
gg	gas-gas (flue gas to combustion air) heat exchanger (combustion air preheater)
hx	heat exchanger
in	at inlet
inf	after an infinite time / in steady state
lat	latent (heat) of phase change
nom	under nominal conditions

out	at outlet
sens	sensible (heat)
Wat	boiler water

superscripts

GHV	calculated based on the energy content of the fuel according to its gross (upper) heating value (GHV = Ho)

14 History and Acknowledgements

This model and its implementation in TRNSYS / FORTRAN has been developed by Michel Haller until its version 2.0 (Sep. 2006) at the Institut für Solartechnik SPF / Rapperswil. The further development at the Institute of Thermal Engineering (IWT) / Graz University of Technology included the introduction of different phases for startup, burning and off-time with (minimum) times that can be set for different phases, and a complete revision of the code including new approaches for the simulation of condensing boilers and validation based on measured data. Detailed measurements on gas, oil and pellet boilers have been conducted at SPF and IWT. The measured data have been used to further develop and check the model.

Important contributions have been made by Jean Lebrun / University of Liège (condensation approaches in flue gas mode 3), Angela Dröscher / TU Graz (measurements and simulation of a condensing gas boiler), Robert Haberl and Lars Konersmann (measurements on condensing oil boilers and a wood pellet boiler as well as reviewing and testing of the code and its documentation) and Janne Paavilainen (reviewing).

15 References

ASHRAE, 2005. *Chapter 32 - Energy Estimating and Modeling Methods*. In *ASHRAE Handbook of Fundamentals*. American Society of Heating, Refrigeration and Air Conditioning Engineers.

Baehr, H.D., 2005. *Thermodynamik: Grundlagen und technische Anwendungen*, Zwölfte Auflage. Springer: Berlin Heidelberg.

Gaswärme-Institut Essen e.V., 1983. *GWI-Arbeitsblätter GAS VERBRENNUNG WÄRME III*. Vulkan-Verlag: Essen.

Haller, M., Paavilainen, J., Konersmann, L., Haberl, R., Dröscher, A., Frank, E., Bales, C. & Streicher, W., 2009. *A Unified Model for the Simulation of Oil, Gas, and Biomass Space Heating Boilers for Energy Estimating Purposes - Part I: Model Development*. *Accepted for Publication in Journal of Building Performance Simulation*.

Koschak, A., Fiedler, T., Knirsch, A. & Beurer, C., 1998. *TRNSYS-TYPE 370 Erweiterung des bisherigen Gaskesselmoduls um eine Holzkesselfeuerung mit der Möglichkeit zur Brennwertnutzung - Ergänzung um einen Simulationsmodus zur realitätsnahen Simulation des Betriebsverhaltens von Gaskesseln mit Takten*.

Obernberger, I. & Thek, G., 2004. *Physical characterisation and chemical composition of densified biomass fuels with regard to their combustion behaviour*. *Biomass and Bioenergy*, 27(6), 653-669.

Stöcker, H., 1994. *Taschenbuch der Physik, Verlag Harri Deutsch, 2*. Aufl.

TRNSYS Type 888 „Controller for Space Heating and Storage Charging by a Heat Source"

Version 1.0, Michel Haller, 03.05.2010

1   Summary

This describes TRNSYS Type 888 „Controller for Space Heating and Storage Charging by a Heat Source", programmed in FORTRAN 90. This TYPE simulates an electronic controller for heat source operation and space heat supply.

Possibilities offered include an outdoor temperature (or average outdoor temperature) controlled heating season, individual warm-water and room heating setpoints, warm water preference, room heating setpoint calculated depending on (average) outdoor temperature, minimum setpoint for the heat source during its operation, and more.

This type does not include the handling of startup time, minimum burning time, minimum off time and time needed to stop a boiler / burner. It is assumed that these tasks are done by the boiler/burner itself.

2 Parameter-List

Nr.	short	explanation	unit	range
Heating season				
1	$T_{start,HS}$	Reference outdoor temperature, below which heating season starts	°C	[-inf;+inf]
2	$T_{db,HS}$	Dead-band temperature for hysteresis. Heating season will stop when the outdoor temperature rises above Tstart+Tdb	°C	[0;+inf]
3	--	Unused		
Warm water and/or room heating preferences				
6	MoWW	Warm water Mode: 0 = room heating and Warm water heating may be done at the same time by the same heat source 1 = Warm water heating disables room heating use of heat source	--	0,1
7	MoRH	Room heating Mode: 1 = ON if Heating Season is on and not blocked by WW-Mode 2 = Additional criterion of store temperature based on absolute values 3 = additional criterion of store temperature based on values relative to the flow temperature setpoint of the heating system	--	1,2,3
8-10	--	Not used		
Heating curve				
11	MoHCcalc	Calculation mode for the heating curve: 1 = very simple 2 = simplified 3 = detailed	--	1,2,3
12	m	Radiator exponent	--	[-inf;+inf]
13	S	Slope of heating curve (for mode 1+2, not in use for mode 3)	--	[0;+inf]
14	$T_{amb,N}$	Outdoor reference temperature (for mode 2+3, not in use for mode1)	°C	[-inf;+inf]
15	$T_{Fl,N}$	Flow temperature at reference conditions (for mode 3, not in use for mode 1+2)	°C	[-inf;+inf]
16	$T_{Rt,N}$	Return temperature at reference conditions (for mode 3, not in use for mode 1+2)	°C	[-inf;+inf]
17-20	--			
Heat-Source Setpoint				
21	Tmin	Minimum setpoint temperature for heat source	°C	[-inf;+inf]
22	$T_{max,WW}$	Maximum setpoint temperature for heat source in warm water Mode	°C	[-inf;+inf]
23	$T_{max,RH}$	Maximum setpoint temperature for heat source in room heating Mode	°C	[-inf;+inf]
24	MoScOn	Mode for heat source on: Strategy to determine whether heat source shall be enabled (heating to setpoint at least) or	--	1,2,3

		off / disabled. This does not necessarily coincide with flow of water through the heat source: 1 = heat at least to minimum setpoint whenever heat-season is on or WW-Mode is on 2 = heat at least to minimum setpoint only when RH-Mode is on or WW-Mode is on 3 = always heat to minimum setpoint at least		
25	MoTww	Mode of temperature setpoint for warm water heating: 1 = absolute 2 = relative to TwwOFF 3 = relative to TwwON	--	1,2,3
26	MoTrh	Mode of temperature setpoint for room heating: 1 = absolute 2 = relative to flow temperature setpoint of the heating system 3 = relative ot TrhOFF 4 = relative to TrhON	--	1,2,3,4

3   Input-List

Nr.	short	explanation	unit	range
heating season				
1	$T_{amb,HS}$	Outdoor temperature used for the determination of the heating season	°C	[-inf;+inf]
2-5	--	Unused		
Warm water and/or room heating preferences				
6	$T_{WW,St,up}$	Upper temperature in the store that serves as a criterion to turn WW preparation by heat source on	°C	[-inf;+inf]
7	$T_{WW,St,lo}$	Lower temperature in the store that serves as a criterion to turn WW preparation by heat source off	°C	[-inf;+inf]
8	$T_{WW,ON}$	WW preparation will be turned on whenever Tww-store up drops below TwwON	°C	[-inf;+inf]
9	$T_{WW,OFF}$	WW preparation will be turned off whenever Tww-store low rises above TwwOFF	°C	[-inf;+inf]
10	$T_{RH,St,up}$	Trh-store up, Upper temperature in the store that serves as a criterion to turn heat source for room heating on	°C	[-inf;+inf]
11	$T_{RH,St,lo}$	Trh-store low, Lower temperature in the store that serves as a criterion to turn heat source for room heating off	°C	[-inf;+inf]
12	$T_{RH,ON}$	Heat source will be turned on for room heating whenever Trh-store up drops below TrhON (or TsetRH+TrhON if room heating mode MoRH = 3)	°C	[-inf;+inf]
13	$T_{RH,OFF}$	Heat source will be turned off for room heating whenever Trh-store low rises above TrhOFF (or TsetRH+TrhOFF if room heating mode MoRH = 3)	°C	[-inf;+inf]
14-15	--	Not used		
Heating Curve (mode 1)				
16	$T_{room,set}$	Room (indoorl setpoint temperature	°C	[-inf;+inf]
17	T_{amb}	(average) Outdoor Temperature	°C	[-inf;+inf]

18	dT$_N$	Value for nighttime reduction of room temperature setpoint. This negative value will be added to Ti,set to get the room temperature setpoint at night-time (connect the result of a time dependent forcing function to this input in order to use night-time reduction of setpoint)	K	[-inf;0]
19-20	--	not in use		
Heat-Source Setpoint				
21	T$_{Sc,set,ww}$	Setpoint temperature for the heat source in warm water mode. Absolute value in °C if temperature setpoint mode for warm water MoTww = 1, relative value in K if MoTww = 2 or 3	°C	[-inf;+inf]
22	T$_{Sc,set,rh}$	Setpoint temperature for the heat source in room heating mode. Absolute value in °C if temperature setpoint mode for room heating MoTrh = 1, relative value if MoTrh = 2, 3 or 4	°C	[-inf;+inf]

4 Output-List

Nr.	short	explanation	unit	range
Heating season				
1	BoHs	Boolean for heating season on	°C	[-inf;+inf]
2-5	--	Unused		
Warm water and/or room heating preferences				
6	BoWW	Boolean for Warm-Water Heating On (1) or Off (0)	--	0,1
7	BoRH	Boolean for Heat Source use for Room Heating On (1) or Off (0)	--	0,1
8-10	--	Unused		
Heating curve				
11	T$_V$	Flow setpoint temperature	°C	[-inf;inf]
12-15	--	Unused		
Heat-Source Setpoint				
16	T$_{Sc,set}$	Setpoint temperature for the heat source. If no preference for WW is set in section "warm water and/or room heating preferences" warm water mode MoWW =0, the higher value of TaWWset and TaRHset will be taken if BoWW AND BoRH are both On (both = 1).	°C	[-inf;+inf]
17	T$_{Sc,ww}$	Setpoint for source in warm water mode (independent of Par6 and Par7)	°C	[-inf;+inf]
18	T$_{Sc,rh}$	Setpoint for source in room heating mode (independent of Par6 and Par7)	°C	[-inf;+inf]
19	BoScOn	Boolean for heat source enabled / disabled according to the settings chosen by "mode for heat source on" MoScOn	--	0,1

5 Heating season

Usually the heating season is determined by the comparison of an average outdoor temperature over a certain time with a reference value. If the average outdoor temperature drops below this reference temperature, the heating season starts, if the average outdoor temperature rises above the reference temperature plus a dead-band temperature, then the heating season stops.

6 Warm-Water and/or Room Heating Preferences

If a specified reference temperature (e.g. in a warm water store) drops below a certain level, Warm-Water Mode will be turned on, if the same or another temperature measured in the store rises above a certain level, Warm-Water Mode will be turned off.

Room Heating may be turned on whenever the heating season is on, regardless of WW-Mode, or only if WW-Mode is not on (WW preference). Another restriction may be made to room heating mode by allowing it only to be on whenever the temperature in a store is below a certain level, and once it has shut off to let it start again only when the same (or another) temperature in the store has dropped below another level.

7 Flow temperature setpoint of the heating system (heating curve)

7.1 Detailed calculation (MoHCcalc=3)

In theory, there are two ways of calculating the temperature setpoint for the flow line of a heating system dependent on the radiator exponent m, the outdoor temperature t_a and the room temperature setpoint t_i. The first way uses the arithmetic mean of the flow and return temperature to calculate the average radiator temperature, the second uses the logarithmic mean. Acording to [Recknagel, Sprenger, 1997], the criterion to use the logarithmic mean is:

$$\left(\frac{t_R - t_i}{t_V - t_i} \right) < 0.7$$

However, since the formula for the calculation of the flow setpoint temperature that is based on the logarithmic mean can only be solved with iterations, and the exactness of the calculation will be overriden by heat losses and inexactness of temperature measurements and control in a real system anyway, only the arithmetic mean will be used here. The exact solution for the flow setpoint temperature tV based on the arithmetic mean temperature of the radiator is:

$$t_V = t_i + \frac{t_{V_N} - t_{R_N}}{2} \cdot \frac{t_i - t_a}{t_i - t_{a_N}} + \left(\frac{t_{V_N} + t_{R_N}}{2} - t_i \right) \cdot \left(\frac{t_i - t_a}{t_i - t_{a_N}} \right)^{\frac{1}{m}}$$

To include night-time temperature setpoint reduction, a formula corresponding to a previous TRNSYS type by Sulzer and Wetter [Sulzer, Wetter, 1996] will be used:

$$t_V = t_i + dT_N + \frac{t_{V_N} - t_{R_N}}{2} \cdot \frac{t_i + dT_N - t_a}{t_i - t_{a_N}} + \left(\frac{t_{V_N} + t_{R_N}}{2} - t_i \right) \cdot \left(\frac{t_i + dT_N - t_a}{t_i - t_{a_N}} \right)^{\frac{1}{m}}$$

The expected return temperature is:

$$t_R = t_i + dT_N - \frac{t_{V_N} - t_{R_N}}{2} \cdot \frac{t_i + dT_N - t_a}{t_i - t_{a_N}} + \left(\frac{t_{V_N} + t_{R_N}}{2} - t_i \right) \cdot \left(\frac{t_i + dT_N - t_a}{t_i - t_{a_N}} \right)^{\frac{1}{m}}$$

Where:

t_V = Temp. of flow (calculated), °C

t_R = Temp. of return (calculated), °C

t_i = setpoint indoor temperature (daytime), °C

dT_N = nighttime-reduction (a negative value), °C

t_{V_N} = Temp. of flow at norm conditions, °C

t_{R_N} = Temp. of return at norm conditions, °C

t_a = Current (or average) outdoor temperature, °C

t_{a_N} = Outdoor Temp. at norm-conditions, °C

7.2   *Simplified (MoHCcalc = 2)*

In a simplified version, t_V can be approximated by:

$$t_V = t_i + dT_N + S \cdot \left(t_i - t_{a,N} \right) \cdot \left(\frac{t_i + dT_N - t_a}{t_i - t_{a_N}} \right)^{\frac{1}{m}}$$

with S = slope of the heating curve that corresponds to:

$$S = \left(\frac{t_{V_N} - t_i}{t_i - t_{a_N}} \right)$$

The slope S will be taken directly from the input S (slope), and not calculated in this mode.

7.3   *Very simple (MoHCcalc = 1)*

Or even more simplified:

$$t_V = t_i + dT_N + S \cdot 20 \left(\frac{t_i + dT_N - t_a}{20} \right)^{\frac{1}{m}}$$

This simplification is based on the assumption that reference ambient temperature is 0 °C and room heating setpoint is 20 °C.

7.4 Reduced room temperature setpoints during the night

A common way to consider a shift in room-setpoint for the night is to subtract the difference between room-setpoint of the day and room-setpoint of the night from t_V. However, we propose here to just substitute t_i, which usually is the setpoint of the day, with the setpoint for the night.

7.5 Examples and further explanation

Independent of the mode of calculation chosen, the flow setpoint temperature for the heating system will be set to $t_i + dT_N$ whenever $t_i + dT_N - t_a < 0$. Examples for heating curves for a heating system with 35/30 °C and radiator exponents of 1.0 and 1.4 are given in *Figure 1*.
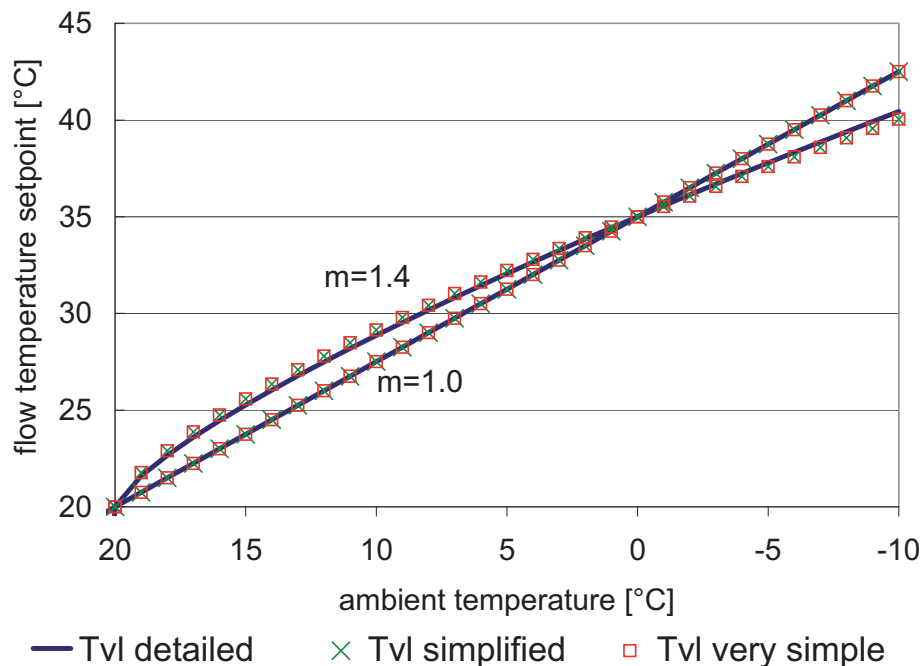
Figure 1: Example for a heating system with T_{VN}=35, T_{RN}=30, T_{aN}=0, T_i=20, dTn=0, and m=1.0 and 1.4 respectively. These values correspond to a slope of S=0.75.

8 Temperature Setpoint for the heat source

The temperature setpoint of the boiler may be different in WW-Mode and in RH-mode. In both modes, the setpoint may or may not be related to temperatures setpoints for the heat store or the flow of the heating distribution system.

At the same time, it may be necessary to narrow the range of possible setpoints with a T_{min} (e.g. boilers that have to avoid condensation in flue gas) and a T_{max} (for material reasons or to avoid steam).

9 References

Sulzer M., Wetter M.; TRNSYS Type "Aussentemperatureabhängiger Vor-
/Rücklauftemperatursollwert" Modellbeschreibung und Implementation in
TRNSYS, 7. Oktober 1996, Zentralschweizerisches Technikum Luzern,
Ingenieurschule HTL, Technikumstrasse, 6048 Horw

Recknagel, Sprenger, Schramek; Taschenbuch für Heizung und Klimatechnik –
einschliesslich Warmwasser- und Kältetechnik 97/98, 68. Auflage, 1997, R.
Oldenbourg Verlag

TRNSYS Type 889 „Adapted P(I)D Controller"

Version 1.0, Michel Haller, 03.05.2010

1 Summary

This describes TRNSYS Type 889 „Adapted P(I)D Controller", programmed in FORTRAN 99. This TYPE simulates a microprocessor control that calculates a scalar action (e.g. boiler power, pump speed, heating power) depending on a setpoint variable and the corresponding process variable. Two adaptations are made that make this controller differ from traditional computed PID-control:

1. In a real microprocessor controlled feedback loop, the process variable is read at time t_0, the new value for the manipulated variable is calculated very quickly and sent out to act on the system. The change induced by this action will not be noticed by the microprocessor until the next reading of the process variable takes place at timestep t_1. In TRNSYS simulations however, if we take the actual value of a process variable and calculate a new value for the manipulated variable that acts on the process variable, the change will affect the process variable already in the next iterative calculation of the same timestep. First of all, this will unavoidably cause convergence problems for the TRNSYS solver algorithms. Second, this is not the way a PID-control works in real life. Therefore, the author suggests making use of the option of this Type to ***base the calculation not on the current value of the process variable, but on its value of the previous timestep***. Of course this implies that the simulation timesteps chosen for simulations that include this Type have to be sufficiently small in order to ensure a fast enough reaction of the manipulated variable that is an output of this type.

2. The theory of PID-control algorithms is very complex and the parameters a user has to define are not very intuitive. Therefore, the algorithm proposed here is a simplified version that presents the controller parameters in a way that the user can – hopefully - easier understand than the parameters of a traditional PID-controller.

2 Parameter-List

Nr.	short	explanation	unit	range
1	Mo_{TS}	Mode of timesteps: 1 = use value of previous timestep for process variable (connect actual value to Input1, previous timestep will be remembered internally by this type) 0 = use current value of process variable. Using this mode is discouraged because of convergence problems that might result	--	1,0
2	U_{min}	lowest possible output value for the manipulated variable	$U_M{}^*$	[-inf;+inf]
3	U_{max}	highest possible output value for the manipulated variable	U_M	[-inf;+inf]
4	Mo_{Ac}	Mode of action: 1 = positive acting (increasing manipulated variable causes increase in process variable) -1 = negative acting (an increasing manipulated variable causes a decrease in process variable)	--	-1,1
5	P	Proportional correction term for the manipulated variable. By how much shall the manipulated variable be changed per hour if the process variable is 1 unit off?	$U_M/(U_P*h)$	[0;+inf]
6	D	Correction term acting on the derivative of the error of the process variable. A high value for D counteracts overshoot / counteracts high rates of increase or decrease in the process variable.	$U_M/(U_P*h)$	[0;+inf]
7	dSP_{max}	Maximum rate of setpoint change per hour	U_S/h	[0;+inf]
8	dU_{max}	Maximum rate of increase of the manipulated variable (positive value)	U_M/h	[0;+inf]
9	dU_{min}	Maximum rate of decrease of the manipulated variable (negative value)	U_M/h	[-inf;0]

*U_M stands for the **U**ser chosen unit of the **M**anipulated variable, U_P stands for the **U**ser chosen unit of the **P**rocess variable. The unit of the process variable is at the same time the unit of the setpoint variable U_S.

3 Input-List

Nr.	short	explanation	unit	range
1	PV	Process Variable (e.g. Output temperature of the heat source)	$U_M{}^*$	[-inf;+inf]
2	SP_{User}	User setpoint. This may e.g. be the temperature of a heat store or boiler outlet, the flow temperature of a heating system or the mass flow of a fluid	$U_S{}^*$	[-inf;+inf]
3	Bo_{Freeze}	Set this value to 1 if the manipulated variable should be frozen at its current value (also freezes in manual mode)	--	0,1
4	Bo_{Man}	Set this value to 1 if the manipulated variable should be set to a manual value (Par5)	--	0,1
5	U_{Man}	Value of the manipulated variable if manually controlled (Inp4 = 1)	$U_M{}^*$	[-inf;+inf]

4 Output-List

Nr.	short	explanation	unit	range
1	U	Manipulated variable (boiler/heating power, pump speed / mass flow)	U_M^*	[-inf;+inf]
2	SP	Current setpoint under consideration of the maximum rate of setpoint change	U_S^*	[-inf;+inf]
3	PVerr	Error between Setpoint and Process variable as calculated according to Par1	U_P^*	[-inf;+inf]

5 Calculation

Remarks: This controller does not match the traditional PID-control algorithms. It is calculated in the following way that is thought to be easier to understand and to handle than the traditional way:

Eq. 1 $\quad dU_{calc}(t_X) = -Mo_{Ac} \cdot \left[P \cdot E(t_X) + D \cdot (E(t_X) - E(t_{X-1})) \right]$

Eq. 2 $\quad U_{calc}(t_X) = U(t_{X-1}) + MAX \left[MIN\{dU_{max}; dU_{calc}(t_X)\}; dU_{min} \right] \cdot dtsim$

Eq. 3 $\quad U(t_X) = MAX \left[MIN\{U_{max}; U_{calc}(t_X)\}; U_{min} \right]$

Where

Eq. 4 $\quad E(t_X) = PV(t_{X-Mo_{TS}}) - SP(t_X)$

Eq. 5 $\quad SP(t_X) = SP(t_{X-1}) + dSP(t_X) \cdot dtsim$

Eq. 6 $\quad dSP(t_X) = MAX \left[MIN\{dSP_{max}; (SP_{User}(t_X) - SP(t_{X-1}))/dtsim\}; dSP_{min} \right]$

$U(t_X)$ Manipulated variable

$E(t_X)$ Error of Process variable (Difference between Process variable and Setpoint)

$dtsim$ simulation timestep

$PV(t_X)$ Process Variable

Remark: Eq. 1 unintentionally introduces a dependency on the choice of the timestep into the control algorithm. In version 2.0 of this type this equation was therefore replaced with Eq. 7.

Eq. 7 $\quad dU_{calc}(t_X) = -Mo_{Ac} \cdot \left[P \cdot E(t_X) + D \cdot \dfrac{(E(t_X) - E(t_{X-1}))}{dtsim} \right]$

Part II: Articles and Papers included in this work

Paper I

Haller, M.Y., Cruickshank, C., Streicher, W., Harrison, S.J., Andersen, E. & Furbo, S., 2009. *Methods to Determine Stratification Efficiency of Thermal Energy Storage Processes – Review and Theoretical Comparison.* <u>Solar Energy</u>, 83(10), 1847-1860.

Methods to determine stratification efficiency of thermal energy storage processes – review and theoretical comparison

Michel Y. Haller[1,a], Cynthia Cruickshank[b], Wolfgang Streicher[a], Stephen J. Harrison[b], Elsa Andersen[c], Simon Furbo[c]

[a] Institute of Thermal Engineering, Graz University of Technology, Inffeldgasse 25/B, 8010 Graz, Austria
[b] Mechanical and Materials Engineering, Queen's University, Kingston, Ontario, Canada
[c] Department of Civil Engineering, Technical University of Denmark, Brovej, building 118, DK-2800, Kgs. Lyngby, Denmark

Abstract

This paper reviews different methods that have been proposed to characterize thermal stratification in energy storages from a theoretical point of view. Specifically, this paper focuses on the methods that can be used to determine the ability of a storage to promote and maintain stratification during charging, storing and discharging, and represent this ability with a single numerical value in terms of a stratification efficiency for a given experiment or under given boundary conditions. Existing methods for calculating stratification efficiencies have been applied to hypothetical storage processes of charging, discharging and storing, and compared with the rate of entropy production caused by mixing calculated for the same experiments. The results depict that only one of the applied methods is in qualitative agreement with the rate of entropy production, however, none of the applied methods is in agreement with the rate of entropy production and also able to distinguish between the entropy production caused by mixing and the entropy changes due to heat losses.

Key words: thermal stratification, thermal energy storage, solar heating systems, thermocline

---

[1] Corresponding author. Tel.: +43 316 873 7318; fax: +43 316 873 7305. E-mail address: michel.haller@tugraz.at

Nomenclature

c	specific heat capacity (J/kg K)
E	energy contained in node / volume of a thermal energy storage (TES) (J)
H	storage height (m)
M_E	moment of energy (Jm)
m	mass (kg)
$\dot{m}$	mass flow rate (kg/s)
R_{EG}	entropy generation ratio (-)
S	entropy (J/K)
ΔS^{irr}	entropy generation (J/K)
ST_{Wu}	stratification coefficient of Wu and Bannerot (1987)
T	absolute temperature (K)
t	time (s)
y	vertical coordinate inside the tank that corresponds to the distance of the center of a node (or the center of a volume element) from the bottom of the tank (m)
η	efficiency (-)
ξ	exergy contained in a node or volume of a TES (J)
$\Delta\xi^L$	exergy loss (J)

Superscripts

*	non-dimensional value
irr	specifies irreversible part of entropy change (=entropy production)

Subscripts

0	thermodynamic dead state (i.e., state with no exergy content), or start of the experiment in the case of t_0
And	referring to Andersen et al. (2007)
avg	mass weighted average of storage
Ch	referring to Chan et al. (1983)
Dav	referring to Davidson et al. (1994)
d	specifies time at which the temperature of the fluid leaving the TES reaches the limit of usefulness
del	"useful" temperature limit of delivery
exp	experimentally determined "real case" (generally includes heat losses and mixing)
flow	value attributed to the flow of fluid into and out of the TES
hl	calculated including heat losses assuming the same heat loss coefficients as for the experimental storage
Hu	referring to Huhn (2007)
i	index for the vertical position of a horizontal layer in the tank
ini	initial, e.g., at the beginning of a charging/discharging or standby experiment
inlet	fluid entering the TES
m	counter for simulation (or calculation) timestep
min	minimum

max   maximum

MIX   based on the MIX number

mix0   perfectly mixed from the beginning of the experiment by constantly mixing the inlet
        fluid with the tank fluid. The temperature of the outlet fluid is the same as the
        temperature of the mixed tank fluid, which is gradually approaching the temperature
        of the inlet fluid. Energy content is thus not the same as in the experimental storage

mix1   perfectly mixed by mixing the volume of the experimental storage at any moment of
        evaluation. Energy content is thus always the same as in the experimental storage

out   fluid leaving the TES

REG   based on the entropy generation ratio

Rg   referring to Rosengarten et al. (1999)

store   value for total storage

Sh   referring to Shah and Furbo (2003)

str0   perfectly stratified from the beginning of the experiment assuming adiabatic,
        isentropic plug flow. Energy content is not the same as in the experimental storage

str0d   perfectly stratified plug flow from the beginning of the experiment including diffusion
        and conduction within the fluid (i.e., anisentropic)

str1   perfectly stratified by rearranging the energy content of the storage at any moment of
        evaluation into two zones with uniform temperature that correspond to the maximum
        and minimum temperature of the experimental storage (str1a) or of the entire
        experiment (str1b)

VB   referring to van Berkel (1997)

ZG   referring to Zurigat and Ghajar (2002)

1 Introduction

It has been shown that temperature stratification[2] (Fig. 1) in a thermal energy storage (TES)
of a solar heating system may considerably increase system performance, especially for low
flow solar heating systems (e.g., Lavan and Thompson, 1977; Phillips and Dave, 1982;
Hollands and Lightstone, 1989; Cristofari et al., 2003).

Stratification of a water-based TES may be destroyed by different physical processes:

- Plume entrainment (Hollands and Lightstone, 1989) is caused by mixing of water due to
  natural convection inside the tank driven by an adverse temperature gradient, typically
  caused by heat supplied to the bottom of the TES or by heat loss from the top. In these
  cases, a thermal plume can be observed that entrains surrounding water.

- Inlet jet mixing is caused by the kinetic energy of water entering the storage tank.

- Thermal conduction and diffusion within the water and within other materials in the TES
  including the storage tank wall reduces temperature differences within the TES.

A TES with no stratification corresponds to a fully mixed TES.

---

[2] the existence of a temperature gradient in the storage that allows the separation of fluid at different temperatures
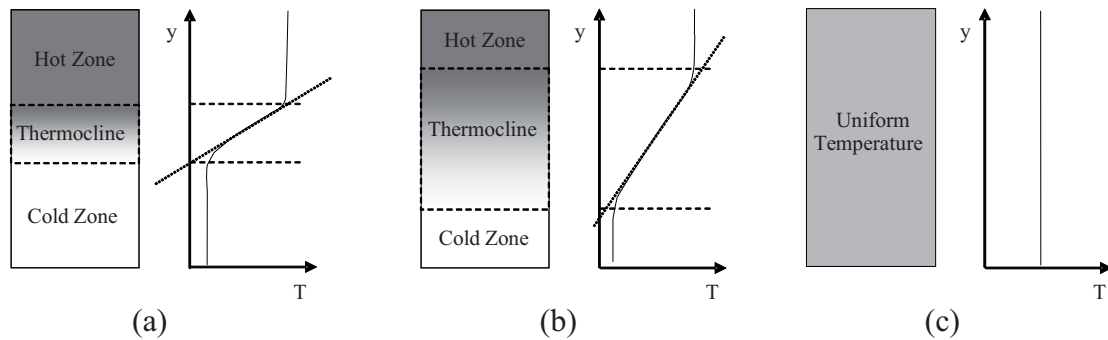
Fig. 1. Differing degrees of stratification within a storage tank with the same amount of stored heat (a) left, highly stratified, (b) center, moderately stratified and (c) right, showing fully mixed, unstratified storage.

For the development of TES components and processes (e.g., stratification enhancers and inlet mass flows), as well as for the comparison of different TES on the market, it is desirable to have an index or "measure" to determine the ability of a TES to promote and maintain stratification during charging, storing and discharging. Ideally, this measure is given in terms of a stratification efficiency that will range from 0 – 100%, with 0% corresponding to a fully mixed TES that shows no stratification and 100% corresponding to a "best case" TES with perfect stratification. Alternatively, the degree of mixing may be defined ranging from 0% for perfect stratification to 100% for fully mixed (Davidson et al., 1994).

In this paper, numerical figures that show the actual degree of stratification or mixing without putting it into the context of the history of charging/discharging and storing will be called indices for the degree of stratification. Numerical figures that are given in terms of an efficiency or ratio usually compare the experimental storage process with a hypothetical storage process and thus include information about the history of the storage process. These figures will be referred to as stratification efficiencies. To better understand how these two terms differ, consider a storage tank at a uniform temperature (i.e., a tank with the lowest possible degree of stratification according to the definition used here). Taking into account the history of the storage process, its stratification efficiency may have been very low if the uniform temperature is the result of a mixing process. At the same time, stratification efficiency may have been very high if the uniform temperature is the result of a fully stratified charging or discharging process with constant inlet temperature, after the whole storage volume has been replaced in ideal plug flow.

Furthermore, it is important to distinguish between factors that influence stratification and figures that evaluate the degree of stratification or the stratification efficiency of a specific TES after a specific process of charging, storing and discharging. The height to diameter ratio, for example, is a factor that influences stratification. However, it is not a figure that gives any information about the actual degree of stratification in a TES. Other factors that influence stratification include the location and geometry of inlets and outlets, the temperature and mass flow histories of charging and discharging, as well as dimensionless numbers of heat and mass transfer (e.g., Peclet, Richardson, Froude). Theoretically, the degree of stratification or stratification efficiency could be calculated if all influencing factors and their combined effect would be known sufficiently. Empirical correlations between factors that influence stratification and the stratification efficiency itself are usually derived from a number

of experiments where only the investigated influencing factor is changed. From these correlations, useful guidelines for TES engineering can be deduced.

Overviews of methods used to characterize stratification efficiency in a TES have been given by Zurigat and Ghajar (2002), Panthalookaran et al. (2007) or Han et al. (2009). However, a detailed analysis and discussion of their characteristics, including their advantages and disadvantages for the evaluation of the stratification efficiency for the particular storage processes of charging, discharging and storing, has not been completed to date and is the focus of this work. The discussion will be illustrated with hypothetical experiments of charging, storing and discharging upon which different methods for the determination of the stratification efficiency are applied.

2   Review of methods to characterize stratification in a TES

Numerous methods have been proposed for the characterization of thermal stratification in water storages. Figure 2 gives an overview of different approaches found in the literature. Two fundamentally different ways of looking at stratification are a density approach used by environmental scientists (e.g., Moretti and McLaughlin, 1977; Stefan and Gu, 1992), and a temperature approach used by thermal engineers (e.g., Sliwinski et al., 1978; Kandari, 1990; Davidson et al., 1994). In this paper, only approaches based on temperatures will be discussed, since energy storages and the thermodynamic quality or temperature of the energy stored are of primary interest in thermal engineering (see Fig. 2).

A subdivision into graphical presentations and numerical figures can be made, and further subdivided into values used to show the actual degree of stratification and into dimensionless numbers given in terms of an efficiency or ratio – although this separation is not always clear. As proposed by Panthalookaran et al. (2007), most efficiencies or ratios can be classified as being either based on the first law of thermodynamics (i.e., the "energy approach") or the second law of thermodynamics (i.e., the "exergy or entropy approach"). The efficiencies or ratios that do not fit clearly into either one of the previously mentioned categories are summarized under "other efficiencies" within this paper (Fig. 2).

The terminology used to characterize stratification in TES systems differs from author to author and consequently a similar term used by one author may have a different meaning for another. In this article, the terms given by the authors are used when they are cited, and the first letters of the first author's name are used as a subscript to refer to definitions introduced by these authors.

To characterize stratification efficiency in a TES, the concept of comparing a value derived from an experimentally investigated storage with a value derived from a fully mixed or perfectly stratified theoretical storage has been widely adopted (e.g., Abu-Hamdan et al., 1992; Davidson et al., 1994; van Berkel, 1997; Shah and Furbo, 2003; Andersen et al., 2007; Panthalookaran et al., 2007; Huhn, 2007). The definition of the theoretical storage is based on values derived from the experiment (i.e., process of charging, storing and discharging) under investigation and differs from author to author. The definitions and the subscripts used in this work to identify these definitions are pointed out here in order to emphasize the particular differences. To simulate a theoretical TES with perfect stratification from the beginning of the experiment, diffusion across the temperature boundaries may be included in the calculation (identified here as str0d) (van Berkel, 1997) or not included (str0) (Davidson et al., 1994;

Shah and Furbo, 2003). Another method to obtain a perfectly stratified TES is just to "rearrange" the energy content within the storage at any time of the evaluation into two zones at the maximum and minimum temperatures found in the experimental storage (str1a) (Andersen et al., 2007) or found during the entire experiment of charging and / or discharging (str1b) (Panthalookaran et al., 2007). Also a fully mixed storage may be obtained assuming complete mixing from the beginning of the experiment (mix0) (Davidson et al., 1994) or based on a mixing of the experimental storage at the instant of evaluation (mix1) (Andersen et al., 2007; Panthalookaran et al., 2007). In the case of simulating full mixing or perfect stratification from the beginning of the experiment, thermal losses based on the heat loss coefficients derived from the experimental storage may be considered in the simulation (hl) (Davidson et al., 1994) or not considered (Huhn, 2007).
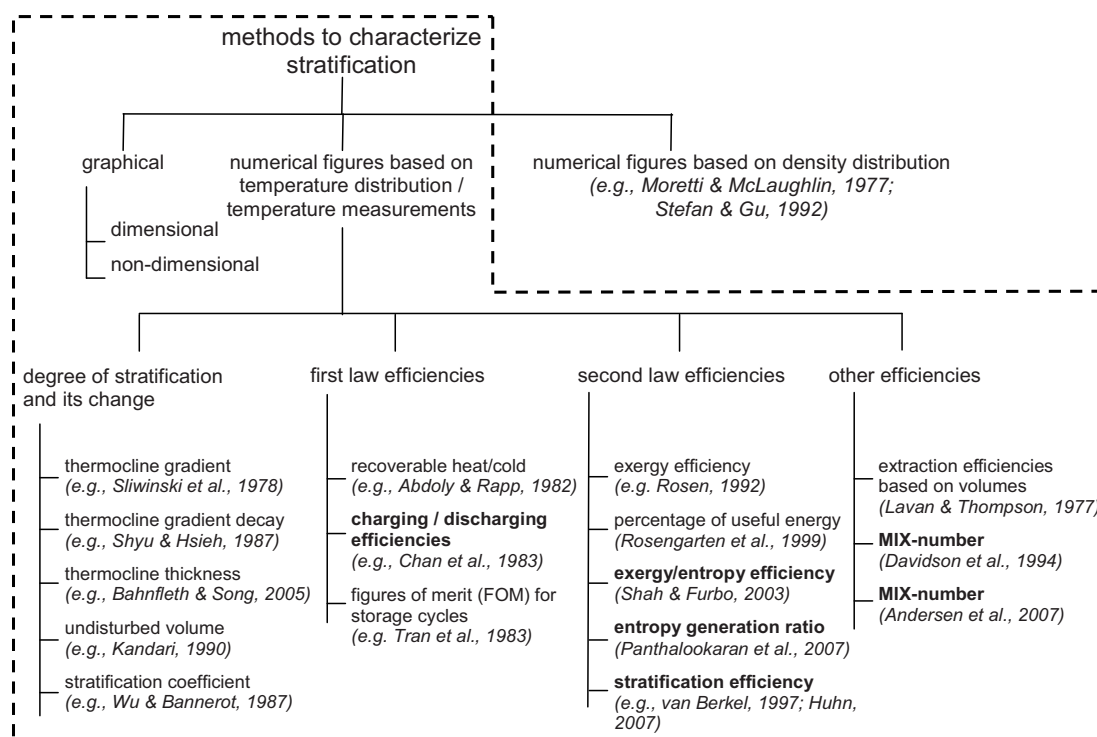

Fig. 2. Different methods proposed to characterize thermal stratification in a water storage. The area within the dashed line contains the methods that are reviewed in this paper. Methods in bold are applied to theoretical experiments within this paper.

2.1   Graphical presentations and non-dimensional temperature, height and time

A simple way of showing the degree of stratification of a TES is by 2D plots (e.g., temperature is represented on one axis and storage height on the other axis). Several curves may be plotted to represent the temperature distribution at different times of an experiment, or to represent results from different experiments (e.g., Davidson et al., 1994). Labeling of axes and data-series for these graphs can be dimensional (e.g., Abdoly and Rapp, 1982) or non-dimensional (e.g., Chan et al., 1983). Non-dimensional values are usually derived for storage height y^*, Eq. (1), temperature T^*, Eq. (2), and time t^*, Eq. (3), by dividing the dimensional value minus the lowest possible value, by the difference between the highest possible and the

lowest possible value. The highest and lowest possible values depend on the storage (i.e., height) and the temperature extremes used during the experiment. Non-dimensional time is usually calculated for charging and discharging sequences in a way that the minimum time corresponds to the start of the experiment and the maximum time corresponds to the time when a full replacement of the tank volume would have occurred under the assumption of ideal plug flow.

$$y^* = \frac{y}{H} \tag{1}$$

$$T^* = \frac{T - T_{min}}{T_{max} - T_{min}} \tag{2}$$

$$t^* = \frac{t \cdot \dot{m}}{m_{store}} \tag{3}$$

Examples of graphs using dimensionless numbers are shown in Figs. 4, 7 and 10. Using non-dimensional values has the advantage of showing the experimental results on a single graph with their magnitudes normalized to the maximum values of TES height, temperature difference and time of the experiment.

2.2 Indices for the degree of stratification

Thermocline thickness and related methods

One concept used to characterize the degree of stratification within a TES is to quantify the temperature gradient and thickness of the thermocline (intermediate region) that separates the hot and cold regions within the storage. This concept is also illustrated in Fig. 1(a-c) where three storage tanks containing equivalent energy are illustrated. In Fig. 1(a) the temperature gradient between the hot and cold regions of the storage is observed to be large and the thickness of the thermocline small. In Fig. 1(b) the temperature gradient is smaller and the thickness of the thermocline is larger than the storage shown in Fig. 1(a). In effect, the storage shown in Fig. 1(a) is more highly stratified than the storage shown in Fig. 1(b). Finally, in Fig. 1(c), the storage is at a uniform temperature and is observed to be unstratified.

Indices for the degree of stratification and the change of the degree of stratification at a particular time have been derived from the temperature gradient of the thermocline (Sliwinski et al., 1978; Huhn, 2007) and its rate of decay (Shyu and Hsieh, 1987; Shyu et al., 1989). In addition, the thermocline thickness (Bahnfleth and Song, 2005; Huhn, 2007) and the percentage ratio of undisturbed volume have also been used (Kandari, 1990). Although these methods have been applied successfully for the evaluation of results from particular experiments, problems may arise, as pointed out by Zurigat and Ghajar (2002), if the inlet temperature during an experiment is variable, and no single thermocline is formed.

Wu and Bannerot stratification coefficient

Wu and Bannerot (1987) defined an index for the degree of stratification called the stratification coefficient based on a mean square deviation of temperatures in the storage from the mean storage temperature.

$$ST_{Wu} = \frac{1}{m_{store}} \cdot \sum_i m_i \cdot \left[T_i - T_{avg} \right]^2 \qquad (4)$$

Liu et al. (2004) slightly modified the stratification coefficient of Wu and Bannerot to account for the height of tube bundles within an integrated storage collector.

This method does not put the actual temperature distribution profile into the context of the history of charging and discharging. Its intentional use is for cases where the most pronounced thermocline has to be expected for the best case of stratification. As mentioned in Section 1, this assumption may not be true for experiments that differ from the one used by the author (e.g., a full charging process).

2.3   Stratification efficiencies based on the first law of thermodynamics

Stratification efficiencies based on the first law of thermodynamics most often calculate a fraction of energy that is recovered with a certain charging and discharging procedure with fixed inlet temperature and mass flow. Between the charging and discharging, a storing period may, or may not, be included.

Abdoly and Rapp (1982) define a fraction of recoverable heat as a measure of thermocline degradation during storing. In a discharging process, for example, they only consider heat to be useful if it has not been degraded more than 20% of its original temperature value towards the ambient temperature, the latter being, at the same time, the initial temperature below the thermocline. A similar approach was also used by Nelson et al. (1999), and has been summarized by Zurigat and Ghajar (2002) and given in terms of a discharge or charge efficiency:

$$\eta_{ZG} = \frac{\int_0^{t_d} \dot{m} \cdot c \cdot \left| T_{out} - T_{inlet} \right| dt}{m_{store} \cdot c \cdot \left| T_{inlet} - T_{ini} \right|} \qquad (5)$$

where t_d represents the time at which the temperature difference has been degraded more than 20% ($\left| T_{out} - T_{inlet} \right| < 0.8 \cdot \left| T_{ini} - T_{inlet} \right|$). It has to be noted that the choice of 20% is an arbitrary percentage in this method.

Chan et al. (1983) analyzed thermal storage efficiencies of charging and discharging processes for a TES used for solar heating and cooling in buildings. During the experiments, a TES with initially uniform temperature along its vertical axis was charged or discharged with an inlet temperature different from the initial temperature of the storage. Two related charging and discharging efficiencies were defined. $\eta_{1,Ch}$ representing the actual energy change at time t divided by the maximum energy change after ideal plug flow replacement of the entire storage volume, i.e.,

$$\eta_{1,Ch}(t) = \frac{m_{store} \cdot c \cdot \left[T_{avg}(t) - T_{ini} \right]}{m_{store} \cdot c \cdot \left[T_{inlet} - T_{ini} \right]} = \frac{T_{avg}(t) - T_{ini}}{T_{inlet} - T_{ini}} \qquad (6)$$

The term $\eta_{2,Ch}$ represents the actual energy change divided by the energy change that would have occurred in the same experiment assuming an ideal plug flow.

$$\eta_{2,Ch}(t) = \frac{m_{store} \cdot c \cdot \left[T_{avg}(t) - T_{ini} \right]}{t \cdot \dot{m} \cdot c \cdot \left[T_{inlet} - T_{ini} \right]} = \frac{\eta_{1,Ch}(t)}{t^*} \tag{7}$$

Similar approaches were used by Yoo and Pak (1993), Mavros et al. (1994), Hahne and Chen (1998), Bouhdjar and Harhad (2002), and Shah et al. (2005). Further development of charging and discharging efficiencies lead to figures of merit (FOM) derived from cycles of full or partial charging and subsequent discharging (Tran et al., 1989; Wildin, 1990; van Berkel et al., 1999; Bahnfleth and Song, 2005). The efficiency definition according to Eq. 7 has been chosen for further analysis in this paper and will therefore be discussed more in detail in Section 4.

2.4   *Efficiencies based on the second law of thermodynamics*

Methods based on the second law of thermodynamics are especially, but not only, useful when the energy stored will be used to produce work. In this case, the exergy stored, and not the energy stored, is the thermodynamic limit of the work that can be produced. For the calculation of values based on exergy, a reference "dead-state" has to be defined that corresponds to the thermodynamic state of the environment (i.e., temperature, pressure, chemical equilibrium). A system in equilibrium with the dead-state contains no exergy at all (Baehr, 2005). In the case of a TES, only the dead-state temperature (T_0) is of interest, since no chemical energy or expansion work is being stored. Several authors have studied entropy generation and exergy losses in sensible heat storage units as systems intended to store useful work (Bejan, 1978; Moran and Keyhani, 1982). Detailed descriptions and general treatment of this topic has been published by Krane (1987), Rosen (1992) and Rosen et al. (1999, 2004).

As pointed out by Rosen (2004), a TES with a more pronounced temperature gradient and hence better stratification always contains more exergy than a comparative storage with equal energy content but less pronounced stratification. Therefore, figures of merit based on the second law of thermodynamics may be used to give information about the stratification efficiency. However, in a system that is not used to produce work, the choice of the "dead-state" temperature T_0 is quite arbitrary. Different authors have brought up arguments for different choices of T_0.

Rosengarten et al. (1999) cite Rosen and Hooper (1991) for the extension of the second law analysis to stratified hot water storages. Rosengarten et al. (1999) defined a non-dimensionalized exergy or exergy efficiency η_{Rg} calculated from the actual distribution of temperatures in the storage, i.e.,

$$\eta_{Rg} = \frac{\xi}{m \cdot c \cdot \left[T_{del} - T_{avg} \right]} = 1 - \frac{T_0}{T_{del} - T_{avg}} \cdot \int_0^1 \ln \left(\frac{T_{del}}{T(y^*)} \right) \cdot dy^* \tag{8}$$

Although Rosengarten et al. referred to this value as "stratification efficiency", it is an index for the degree of stratification rather than a stratification efficiency according to the definitions used in this paper. η_{Rg} corresponds to the percentage of the energy that is available energy ξ (i.e., the exergy), that could be discharged from the storage in an isentropic process until all layers of the storage reach the "useful" temperature limit of delivery T_{del}. Unlike stratification efficiencies introduced by other authors, this efficiency does not place the

experimental TES between a perfectly stratified and a mixed TES. It should also be noted that T_{del} is a value different from the dead-point temperature T_0. Therefore, the method of Rosengarten differs from methods used by other authors like Rosen (2001) who studied the exergy content of different stratified TES in detail and did not use different values for T_{del} and T_0. In contrast to this method, Rosen et al. (1999) defined the exergy efficiency of a storage cycle as the percentage of exergy input that can be recovered in the output of the storage during a storage cycle.

Van Berkel (1997) introduced a stratification efficiency based on the Gibb's free enthalpy. He defined a stratification efficiency based on the comparison of an actual experimental storage with the optimal case of a fully stratified storage and the worst case of a fully mixed storage. In the case of a TES, Gibb's free enthalpy equals exergy, and his definition of stratification efficiency may in this case be written as

$$\eta_{VB} = \frac{\Delta \xi_{mix0}^L - \Delta \xi_{exp}^L}{\Delta \xi_{mix0}^L - \Delta \xi_{str0d}^L} \tag{9}$$

where $\Delta \xi^L$ is exergy lost during any storage cycle. It is important to note that for the calculation of lost exergy, exergy changes of the storage due to exergy difference between the inflowing and outflowing fluid must be correctly accounted for. A similar approach using entropy generation instead of exergy losses has been used by Homan (2003).

Huhn (2007) later simplified this calculation by assuming that the perfectly stratified case is isentropic, hence $\Delta \xi_{str0d}^L$ is replaced by $\Delta \xi_{str0}^L = 0$ and therefore

$$\eta_{Hu} = 1 - \frac{\Delta \xi_{exp}^L}{\Delta \xi_{mix0}^L} = 1 - \frac{\Delta S_{exp}^{irr}}{\Delta S_{mix0}^{irr}} \tag{10}$$

This efficiency definition has been chosen for further analysis in this paper and will therefore be discussed in Section 4.

Inspired by Rosengarten and van Berkel, Shah and Furbo (2003) defined a different exergy efficiency that is the ratio of the exergy of an experimental storage (exp) to the exergy of an ideally stratified storage (str0). The cold water inlet temperature was proposed as the reference dead state temperature T_0 for discharging experiments of a hot water TES.

$$\eta_{\xi,Sh} = \frac{\xi_{exp}}{\xi_{str0}} \tag{11}$$

In a similar way, Shah and Furbo defined the entropy efficiency as the entropy difference between the fully stratified storage and a fully discharged storage divided by the entropy difference of the experimental storage and a fully discharged storage. The fully discharged storage was assumed to be at the cold inlet temperature for discharging experiments, which was also the dead state temperature for the exergy calculations.

$$\eta_{S,Sh} = \frac{S_0 - S_{str0}}{S_0 - S_{exp}} \tag{12}$$

Both efficiency definitions of Shah and Furbo have been chosen for further analysis in this paper and will therefore be discussed in Section 4.

Panthalookaran et al. (2007) defined an internal entropy generation ratio as the difference in entropy change of an experimental TES to the entropy change of a perfectly stratified TES,

divided by the difference of entropy change of a fully mixed TES and a perfectly stratified TES, i.e.,

$$R_{\text{EG}} = \frac{\Delta S_{\text{exp}} - \Delta S_{\text{str1b}}}{\Delta S_{\text{mix1}} - \Delta S_{\text{str1b}}}$$

(13)

It is important to note that ΔS in this method is calculated as the entropy change that a TES would undergo from a reference state with the lowest temperature encountered in the storage process to the current state (Panthalookaran 2008). Therefore, at any time of the experiment: $\Delta S_{\text{mix1}} \geq \Delta S_{\text{exp}} \geq \Delta S_{\text{str1}}$. It has been claimed that this entropy generation ratio isolates the internal entropy generation from entropy changes that are due to heat losses and fluid exchange. The entropy generation ratio has been chosen for further analysis in this paper and will therefore be discussed in Section 4.

2.5 Other stratification efficiency definitions

Volume fraction extraction efficiency

Lavan and Thompson (1977) defined an extraction efficiency as the fraction of the volume that can be discharged from a storage at initially uniform temperature with a minimum temperature difference of 90% of the difference between initial storage temperature and inlet temperature. This method is, however, limited in application, since no variable inlet temperature may be used. Also in this method the criterion of 90% temperature difference conservation appears arbitrary.

MIX-number

The dimensionless MIX-number (Davidson et al., 1994) expresses the degree of mixing that occurs during a charging process based on the so called "moment of energy" M_E. The moment of energy of a TES is an integration of the sensible energy content along its vertical axis, weighted with the height of its location along the vertical axis. In practice a summation over i storage segments along the vertical axis is used to calculate M_E, i.e.,

$$M_E = \sum_{i=1}^{N} y_i \cdot E_i$$

(14)

The MIX-number is the difference of moment of energy between a perfectly stratified storage and the experimental storage, divided by the difference of moment of energy between a perfectly stratified storage and a fully mixed storage.

$$MIX_{Dav} = \frac{M_{E,str0,hl} - M_{E,\text{exp}}}{M_{E,str0,hl} - M_{E,mix0,hl}}$$

(15)

It is important to note that both "theoretical" storage temperature profiles, stratified and fully mixed, are calculated assuming full stratification and mixing, respectively, from the beginning of the experiment, and including heat losses to the surroundings calculated with the heat loss coefficient that was determined for the experimental storage.

The "moment of energy" introduced by Davidson was later adapted and used by Andersen (Andersen et al., 2007). In contrast to the method of Davidson, the theoretical storages in this

later method are mixed or stratified at each instant and thus have the same energy content as the experimental storage at any time.

$$MIX_{And} = \frac{M_{E,str1a} - M_{E,\exp}}{M_{E,str1a} - M_{E,mix1}}$$ (16)

The advantage of this latter method is that the determination of the heat loss coefficient of the experimental storage is not necessary.

Both definitions of the MIX number have been chosen for further analysis in this paper and will therefore be discussed in Section 4.

3   Stratification efficiencies applied to example cases

In this section, stratification efficiencies based on the methods described in the previous section are applied to hypothetical experiments of charging discharging and storing. Hypothetical experiments have the advantage of not being influenced by measurement uncertainties. In addition, heat losses can be eliminated in hypothetical experiments, whereas this can not be done in a "real" experiment. For cases where several authors have proposed very similar approaches, only one method has been selected to represent the corresponding "group". The selected methods are the discharge efficiency ($\eta_{2,Ch}$) as proposed by Chan et al. (1983); the stratification efficiencies based on the change of exergy ($\eta_{\xi,Sh}$) and entropy content ($\eta_{S,Sh}$) as defined by Shah and Furbo (2003); and the stratification efficiency based on exergy losses or entropy production (η_{Hu}) as defined by Huhn (2007). In contrast to these, some ratios introduced in the previous section are expected to return a value close to 0% for perfect stratification and close to 100% for full mixing. These are the MIX numbers of Davidson et al. (1994) and Andersen et al. (2007) as well as the entropy generation ratio of Panthalookaran et al. (2007). In this case, stratification efficiency based on these methods is defined according to:

$$\eta_{MIX,Dav} = 1 - MIX_{Dav} \text{ and } \eta_{MIX,And} = 1 - MIX_{And}$$ (17)

$$\eta_{REG} = 1 - R_{EG}$$ (18)

In order to illustrate differences between these stratification efficiencies, results of their application to cases of charging, discharging and storing of a hypothetical TES are shown in the following sections.

3.1   Example cases of hypothetical charging and discharging

The general assumptions for the TES during the hypothetical charging and discharging processes are:

- The vertical tank is filled with 1000 kg of water.
- The tank is modeled as 20 homogeneous horizontal layers of 50 kg each.
- The density of water is constant for the analysis.
- The specific heat of water is constant at 4.18 kJ/kg K (i.e., temperature independent).
- The inlet is located at the top of the tank and the outlet at the bottom of the tank for the charging, and vice versa for the discharging.

- The charge / discharge mass flow rate is constant at 400 kg/h.

- The initial temperature of the TES is 20 °C for charging and 60 °C for discharging.

- The inlet temperature is constant at 60 °C for charging and 20 °C for discharging.

- For reasons of simplicity, heat losses to the ambient and thermal conduction of heat between the layers are assumed to be zero.

- As shown in Fig. 3, the highest 25% (charging) or lowest 25% (discharging) of the mass of the storage is assumed to be fully mixed due to plume entrainment of the entering water-jet (Hollands and Lightstone, 1989).
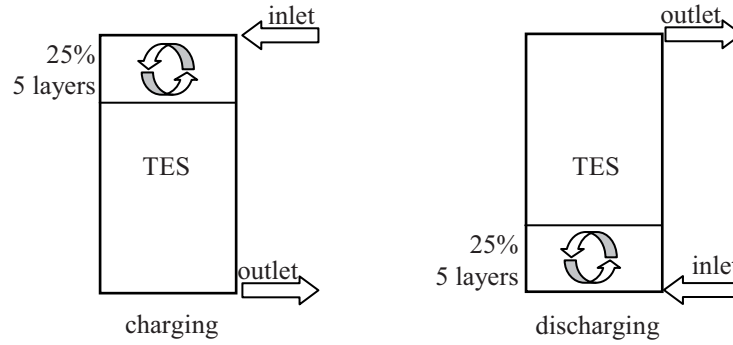

Fig. 3. Hypothetical charging and discharging experiments with full mixing at the top (charging) or at the bottom (discharging).

Temperature distributions of the hypothetical experimental TES are calculated at a timestep of 0.125 h. Thus, the fluid in any tank layer is replaced by the fluid from the adjacent layer above or below within each timestep, thereby eliminating numerical diffusion in the calculation. In order to introduce some mixing in the storage, the top (charging) or bottom (discharging) five layers are mixed after each timestep for the case of the hypothetical experimental TES (exp). The reference TES that is fully mixed from the beginning is calculated according to its analytical solution as one mixed zone, i.e.,

$$\frac{dT_{mix0}(t)}{dt} = \frac{\dot{m} \cdot c \cdot \left[T_{mix0}(t) - T_{inlet} \right]}{m_{store} \cdot c} \tag{19}$$

where T_{mix0} is calculated and used with Eq. (3) for $t_0 = 0$ and $T_{mix0}(t_0) = T_{ini}$ to give:

$$T_{mix0}(t^*) = T_{inlet} + \left[T_{ini} - T_{inlet} \right] \cdot e^{-t^*} \tag{20}$$

The temperature of the reference case that is mixed at each instant (mix1) is calculated as

$$T_{mix1}(t) = \frac{1}{20} \cdot \sum_{i=1}^{20} T_{exp}(t, y_i) \tag{21}$$

The reference TES that is assumed to be perfectly stratified from the beginning (str0) is calculated as one zone at the initial temperature and one zone at the inlet temperature, separated at dimensionless height $y^* = t^*$ for the case of discharging and $y^* = 1 - t^*$ for the case of charging. The temperature distribution of the stratified TES that is based on the experimental storage at each instant (str1) is calculated according to:

$$T_{str1}(t, y^*) = T_{exp,min}(t) \quad \text{for } y^* \leq \frac{T_{max}(t) - T_{mix1}(t)}{T_{max}(t) - T_{min}(t)}, \tag{22}$$

$$T_{str1}(t, y^*) = T_{exp,max}(t) \quad \text{for } y^* > \frac{T_{max}(t) - T_{mix1}(t)}{T_{max}(t) - T_{min}(t)}, \tag{23}$$

where T_{max} and T_{min} are the maximum and minimum temperatures, respectively, encountered in the experimental storage (str1a) or in the entire experiment (str1b).

The calculated stratification efficiency curves are compared with the internal entropy generation rate $\Delta S_m^{irr} / \Delta t$ over the time of the experiment:

$$\frac{\Delta S_m^{irr}}{\Delta t} = \frac{\Delta S_{store,m} - \Delta S_{flow,m}}{\Delta t} = \sum_{i=1}^{20} \left[\frac{m_{store}}{20} \cdot c \cdot \ln\left(\frac{T_i(t_m)}{T_i(t_{m-1})} \right) \right] \bigg/ \Delta t - \dot{m} \cdot c \cdot \ln\left(\frac{T_{inlet}(t_m)}{T_{out}(t_m)} \right) \tag{24}$$
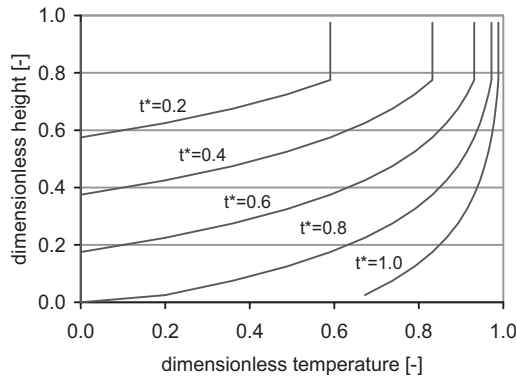

Fig. 4. Temperature profiles of the TES during the described charging experiment.

Fig. 5. Entropy generation by mixing during the described charging experiment.

Fig. 6. Stratification efficiencies based on energy or moment of energy (left) and based on the second law of thermodynamics (right) and their evolution during the described charging experiment.

The internal entropy generation rate has been used previously for the evaluation of destratification inside TES (e.g., Lohse et al., 2008). It is reasonable to assume that the internal entropy generation is a good measure for the amount of mixing taking place in a TES, since:

- Mixing two volumes of water – or heat exchange between two volumes of water – with different temperatures will always lead to entropy generation.

- Entropy generation associated with the mixing of two volumes of water increases with both the size of the volumes and the temperature difference of the volumes.

- No entropy is produced when two volumes of water that are at the same thermodynamic state (including equal temperature) are mixed. On the other hand, there is always entropy production when two volumes that are at different temperatures are mixed.

For these reasons, we expect the results of a stratification efficiency parameter to be in some qualitative agreement with the rate of entropy generation due to mixing. For example, we do not expect the stratification efficiency to drop while there is no internal entropy generation, and we do not expect it to rise if the TES, at the same instant, is fully mixing. If a stratification efficiency parameter is not always in qualitative agreement with the internal entropy generation, it shows us limits of interpretability. However, we do not deduce that the method it is based on is not a valid method in general.

The temperature distribution curves and the internal entropy production rates of the hypothetical experimental TES is shown in Figs. 4 and 5 for the described charging process, and in Figs. 7 and 8 for the described discharging process. The stratification efficiencies calculated based on the above mentioned methods are shown in Fig. 6 for the charging process and in Fig. 9 for the discharging process.

Fig. 7. *Temperature profiles of the TES during the described discharging experiment.*
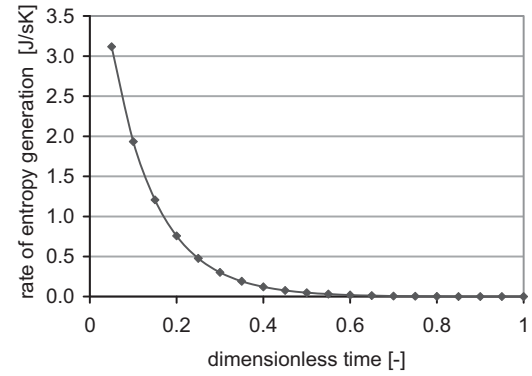
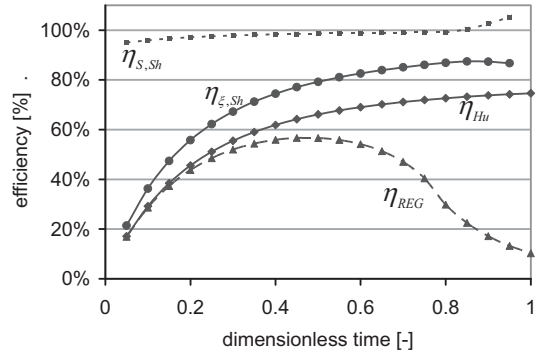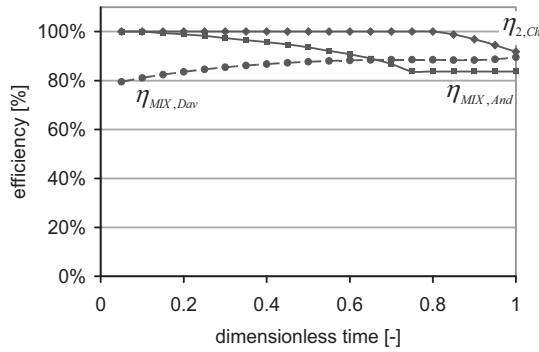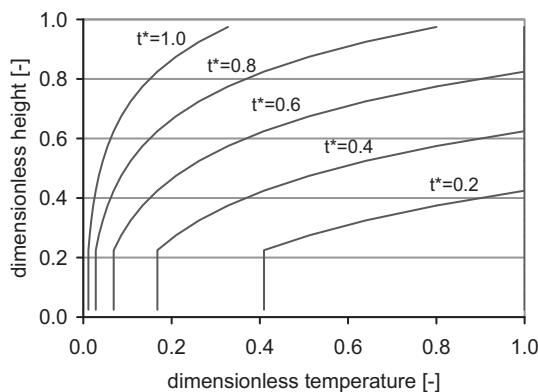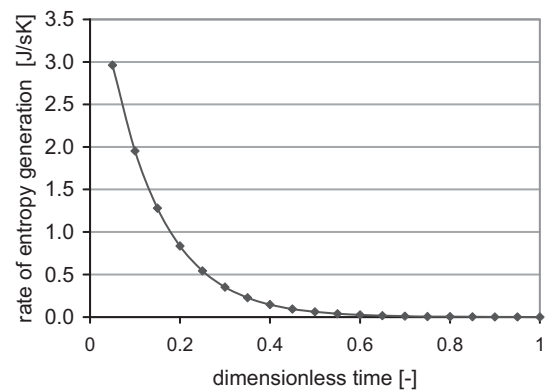Fig. 8. *Entropy generation by mixing during the described discharging experiment.*
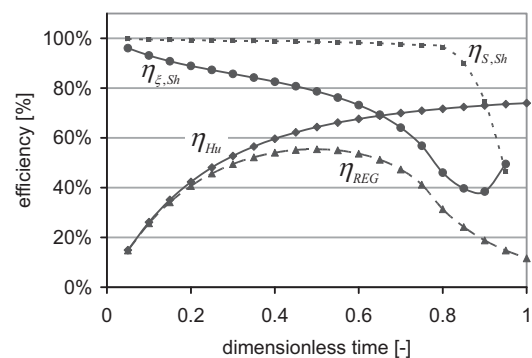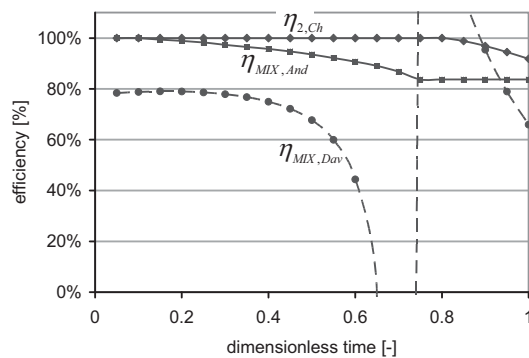

Fig. 9. *Stratification efficiencies based on energy or moment of energy (left) and based on the second law of thermodynamics (right) during the described discharging experiment.*

3.2   Example case of energy storing / standby

In the case of a TES with a pronounced thermocline, stratification efficiency can be used to evaluate thermal conduction and diffusion during a period without mass flows in and out of the tank. This period may be called a storing or standby process. Assumptions made for the hypothetical experimental TES during standby are the same as for the hypothetical charging and discharging experiments, with the following modifications:

- The initial temperatures in the TES are 20 °C for the lower half, and 60 °C for the upper half.

- There are no mass flows in and out of the TES and therefore no mixing by plume entrainment.

- After each timestep, 20% of the mass of each layer is "exchanged" with the adjacent layers to simulate thermal conduction and diffusion.

For the calculation of $\eta_{\xi,Sh}$ and $\eta_{S,Sh}$, the initial temperature in the lower half of the storage is taken as the reference or dead state temperature.

The parameter $\eta_{2,Ch}$ is not calculated for the evaluation of the standby process alone, since mass flows are necessary for its determination.

Temperature distribution curves and internal entropy production of the hypothetical experimental TES and the described storing process are shown in Fig. 10 and 11. Stratification efficiency parameters calculated for this hypothetical experiment are shown in Fig. 12.
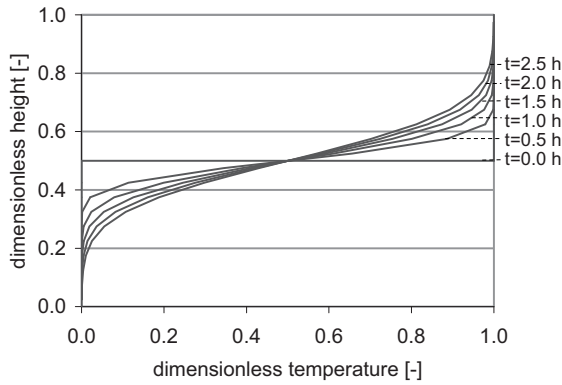

Fig. 10. Temperature profiles of the TES during the described storing / standby process.
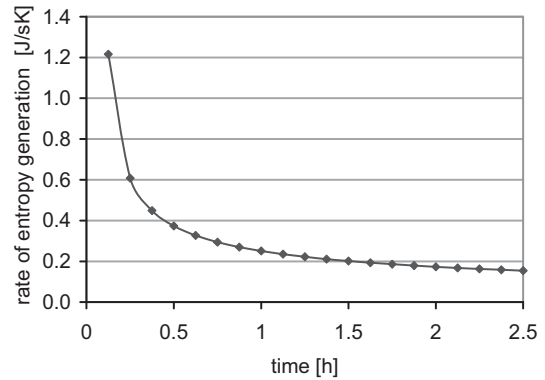
Fig. 11. Entropy generation by mixing during the described storing / standby process.
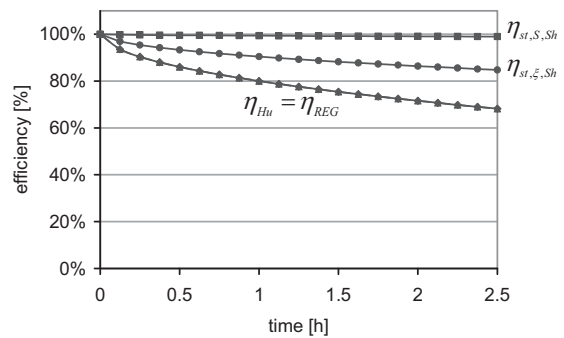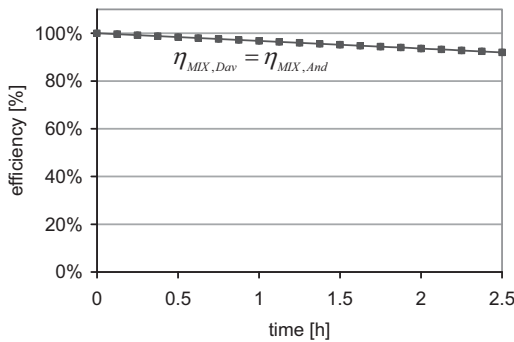

Fig. 12. Stratification efficiencies during the described storing / standby process.

4   Discussion

In the hypothetical charging and discharging experiments described, an incoming fluid of constant temperature is mixed with 25% of the water contained in the storage. The temperature difference between the incoming fluid and the water in the mixing layers of the TES decreases steadily as time proceeds. Therefore, although the amount of fluid being mixed is constant during the experiment, the effect on stratification becomes less severe as time proceeds. Finally, mixing of two fluids with equal temperature will not cause any destratification at all. This is also reflected by the rate of entropy generation due to mixing, which is largest at the beginning of the hypothetical experiments and decreases steadily thereafter (Figs. 5 and 8). During the charging experiment, only $\eta_{MIX,Dav}$, $\eta_{\xi,Sh}$ and η_{Hu} reflect this tendency (Fig. 6). In the discharging experiment, only η_{Hu} is in agreement with the rate of entropy production due to mixing (Fig. 9).

Looking at the discharging efficiency $\eta_{2,Ch}$ for example, this value may return a useful result at t* = 1, but plotting it over the time of the experiment does not give any additional information that could be used to find out at which time mixing was most severe (Figs. 6 and 9). In addition to this, all parameters that are based only on the first law of thermodynamics lost information about the quality of energy being discharged, e.g., for the discharge efficiency, it was only known how much energy could be discharged until t*=1 (Eq. 7) or until a certain limit for the temperature is reached (Eq. 5). The previous temperature levels at which the discharge occurred remain unknown and have no effect on the determined efficiency.

The MIX number $\eta_{MIX,Dav}$ has been used successfully in charging experiments but, as illustrated in Fig. 9, it is less informative for discharging experiments. The faster drop in energy content for the discharging of a perfectly stratified storage, in comparison to a mixed storage, is in disagreement with the assumption that the moment of energy of a perfectly stratified storage is always greater than the moment of energy of the experimental storage or the fully mixed storage (Fig. 13). Although the MIX-number as defined by Andersen et al. $\eta_{MIX,And}$ overcomes this deficiency, it equally does not show at what time mixing was most severe during a charging or discharging process.
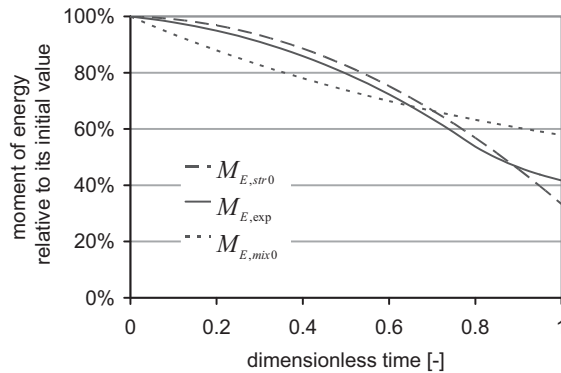

Fig. 13.   Relative moments of energy during the described discharging experiment.

The entropy and exergy parameters given by Shah and Furbo (2003) do not show entropy production or exergy loss. They are based on the exergy and entropy content of the storage alone and do not take into account the energy and exergy balance of the fluid flowing into and

out of the storage. Furthermore, it can be observed that the values of indices that do not take into account the energy and/or exergy leaving the storage may vary significantly, often abruptly, as soon as the first fluid layers that are affected by mixing start to leave the tank, (i.e., at t*>0.75). This is the case for $\eta_{MIX,And}$, $\eta_{2,Ch}$, and $\eta_{S,Sh}$. For the discharging experiment, this is also the case for $\eta_{\xi,Sh}$.

The stratification efficiency based on the entropy generation ratio by Panthalookaran et al. (2007), η_{REG}, shows a large decrease near the end of the hypothetical charging and discharging experiments, which does not correspond to an increased mixing or increased internal entropy generation at the corresponding time.

In the case of the hypothetical heat storing process without mass flow, it must be noted that not all methods that can be applied for charging and discharging processes may equally be applied to a storing process. It can further be observed that in the case of no mass flow and no heat losses, the two proposed MIX-numbers $\eta_{MIX,And}$ and $\eta_{MIX,Dav}$ equal one another. At the same time, also η_{Hu} and η_{REG} return the same results in this case.

Finally, among the parameters investigated, only the relative entropy production η_{Hu} as defined by Huhn (2007) is in agreement with the entropy production rate caused by mixing in all three hypothetical experiments. Similar methods have been proposed by van Berkel (1997) and Homan (2003), however, the latter assume that heat conduction or thermal diffusion occurs in the perfectly stratified TES. Thus, entropy production or exergy losses have to be calculated also for this TES, which requires more computational effort.

In the hypothetical example cases of charging, discharging and storing that have been investigated, heat losses to ambient have not been considered and were therefore not simulated. In any real storage process however, heat losses will occur. Some methods try to eliminate the effect of heat losses by including heat losses in the calculation for the reference storages that are perfectly stratified or fully mixed (e.g., Davidson et al., 1994) or by calculation of the reference storage based on the actual energy content encountered in the experimental TES (Andersen et al., 2007; Panthalookaran et al., 2007). The advantage of the latter methods is that heat loss coefficients of the TES do not have to be determined. The intention of the method of Huhn is to compare the actual internal entropy generation of a TES with the internal entropy generation of a fully mixed TES. However, the mathematical description that has been given does not subtract entropy generation caused by heat losses from the entropy change of the TES. It must therefore be assumed that with this method, different stratification efficiencies will be obtained for two TES with the same stratification behavior, but different heat losses. It is theoretically possible to calculate the entropy changes due to heat losses if it is known at which temperature level(s) the TES looses its heat. If this is practically feasible remains on open question and shall be addressed in further studies.

Table 1 summarizes basic characteristics for the stratification indices and the stratification efficiency methods evaluated in this paper. The table is based on the results from this paper and additional reasoning based on the method description. Of course, the applicability and usefulness of a particular method may be disputed, and different authors might come to different conclusions for a particular method or case. The entropy generation ratio of Panthalookaran et al. (2007) has not been included in the table since the method is quite recent and its limits of applicability and interpretability are still up for debate.

Finally, the purpose of the investigation also plays an important role for the choice of an appropriate stratification efficiency parameter. For a simple storage process where an initially isothermal TES is charged half way with a constant inlet temperature, graphical

representations or the MIX number may be equally appropriate, easier to calculate, and easier to communicate than values based on entropy generation. Fractions of recoverable heat and cold are particularly useful where a strict temperature limit for the usefulness of heat or cold makes sense. For solar thermal applications, which are the main concern of this investigation, we usually assume that the useful temperature is always provided. If solar heat is not enough, then some auxiliary backup is switched on. Under this understanding, it makes a difference if we "miss" the useful temperature by 1 K or by 5 K, because the amount of auxiliary backup heating will be different. Therefore, we are looking for methods that include the whole range of temperatures found in a TES. Furthermore, fractions of recoverable heat and charging / discharging efficiencies have the advantage that, depending on their definition, temperatures inside the TES do not have to be known. For a more complex process of combined sequences of charging, discharging and standby with changing inlet temperatures and mass flows, one might have to make a bigger effort to determine a meaningful value for a stratification efficiency, possibly by the use of values based on entropy production or exergy losses.

Table 1: General characteristics of selected indices for the degree of stratification and stratification efficiency definitions for TES processes.

	index for degree of stratification	stratification efficiency or ratio	applicable for charging	applicable for discharging	applicable for storing / standby	identification of the instant of destratification / mixing possible	isolates mixing from heat losses	applicable to variable temperatures and mass flows	in qualitative agreement with entropy production	internal temperature measurement needed
thermocline thickness and related methods	X	0	X	X	X	X	0	0	-	0/X
Wu & Bannerot	X	0	X	X	X	X	0	?	-	X
discharge / charge efficiencies	0	X	X	X	0	0	0	0	0	0/X
MIX$_{DAV}$	0	X	X	0	X	X	X	(X)	0	X
MIX$_{And}$	0	X	X	X	X	X	X	(X)	0	X
Shah & Furbo	0	X	X	X	X	X	0	0	0	X
Huhn / van Berkel	0	X	X	X	X	X	0	X	X	X

X = applies for this method, 0 = does not apply for this method, (X) = limited application, ? = unknown

5   Conclusions

Stratification efficiency is of vital importance for TES in solar thermal energy systems. Different parameters have been proposed to describe the actual degree of stratification in a TES as well as to evaluate its stratification efficiency during a defined charging, discharging or storing process. In general, stratification efficiency cannot be evaluated based on the actual degree of stratification alone, without knowledge of the boundary conditions that lead to the observed degree of stratification. Knowing the boundary conditions, e.g., the history of charging, standby and discharging, an efficiency value can be calculated for the particular storage process that spans from 0% in the case of a fully mixed TES to 100% in the case of a perfectly stratifying TES. This efficiency may be referred to as stratification efficiency.

In this paper, parameters that have been proposed for the evaluation of stratification efficiencies have been applied to charging, discharging and storing processes for a hypothetical experimental TES. It is concluded that not all parameters are equally applicable to all three processes of charging, discharging and storing alone. Furthermore, some parameters are capable of showing the precise time at which mixing or destratification takes place during a process, whereas others will only quantify mixing that has occurred at the end of the experiment. Parameters that are able to show the precise time of mixing during a process always require the temperature distribution inside the TES to be known, i.e., they require inside tank temperature measurements in the case of a real TES. This may be a disadvantage since inside tank temperatures may not always be available. In the case of testing commercially sold TES it might also be difficult or even impossible to place the sensors in the correct positions without damaging the insulation of the TES. Some methods for the calculation of stratification efficiencies try to clearly separate effects due to heat losses from the effects due to mixing. Methods that do not make this separation might return different values for the stratification efficiency of storage tanks that have different insulation, but identical stratification capabilities.

Many methods require experiments with constant initial temperature of the TES, as well as, constant mass flow and inlet temperatures during charging and discharging. Only few methods allow for full flexibility in the variability of temperature and mass flows applied during the process. In a real solar energy storage application, inlet temperatures and mass flows are typically not constant, and uniform starting TES conditions are considered more of an exception rather than the rule. Therefore, methods that allow the application of such complex experiments are of particular interest for testing TES used for solar thermal applications.

Most stratification efficiency parameters that have been proposed were not always in qualitative agreement with the internal rate of entropy generation for the hypothetical TES experiments shown in this paper. The reason for this may be that these methods were originally not intended to be used for this kind of experiment. The results therefore show limits of applicability or interpretability.

The method proposed by Huhn (2007), which is similar to methods proposed earlier by van Berkel (1997) and Homan (2003), was in qualitative agreement with the internal rate of entropy generation in all three hypothetical experiments studied. A drawback of this method is that – in its present form - it does not separate entropy changes due to heat losses from entropy generation due to internal mixing and heat conduction. It is therefore recommended to further study the bias from heat losses of the TES within this method, and possibly develop

the method further to separate the external entropy production caused by heat losses from the internal entropy production caused by mixing.

References

Abdoly, M.A., Rapp, D., 1982. Theoretical and experimental studies of stratified thermocline storage of hot water. Energy Conversion and Management 22, 275-285.

Abu-Hamdan, M.G., Zurigat, Y.H., Ghajar, A.J., 1992. An experimental study of a stratified thermal storage under variable inlet temperature for different inlet designs. International Journal of Heat and Mass Transfer, vol. 35, no. 8, 1927-1934.

Al-Najem, N.M., Al-Marafie, A., Ezuddin, K.Y., 1993. Analytical and experimental investigation of thermal stratification in storage tanks. International Journal of Energy Research 17, 77-88.

Andersen, E., Furbo, S., Fan, J., 2007. Multilayer fabric stratification pipes for solar tanks. Solar Energy 81, 1219-1226.

Baehr, H.D., 2005. Thermodynamik – Grundlagen und technische Anwendungen. Springer Verlag, Berlin, Heidelberg, 152-156.

Bahnfleth, W.P., Song, J., 2005. Constant flow rate charging characteristics of a full-scale stratified chilled water storage tank with double-ring slotted pipe diffusers. Applied Thermal Engineering 25, 3067–3082.

Bejan, A., 1978. Two thermodynamic optima in the design and operation of thermal energy storage systems. Journal of Heat Transfer 100, 708–712.

Bouhdjar, A., Harhad, A., 2002. Numerical analysis of transient mixed convection flow in storage tank: influence of fluid properties and aspect ratios on stratification. Renewable Energy 25, 555–567.

Chan, A.M.C., Smereka, P.S., Giusti, D., 1983. A Numerical Study of transient mixed convection flows in a thermal storage tank. Transactions of the ASME, Journal of Solar Energy Engineering 105, 246-253.

Cristofari, C., Notton, G., Poggi, P., Louche, A., 2003. Influence of the flow rate and the tank stratification degree on the performances of a solar flat-plate collector. International Journal of Thermal Sciences 42, 455-469.

Davidson, J.H., Adams, D.A., Miller, J.A., 1994. A coefficient to characterize mixing in solar water storage tanks. Transactions of the ASME, Journal of Solar Energy Engineering 116, 94-99.

Han, Y., Wang, R., Dai, Y., 2009. Thermal stratification within the water tank. Renewable and Sustainable Energy Reviews, 13(5), 1014-1026.

Hahne, E., Chen, Y., 1998. Numerical study of flow and heat transfer characteristics in hotwater stores. Solar Energy 64, 9-18.

Hollands, K.G.T., Lightstone, M.F., 1989. A review of low-flow, stratified-tank solar water heating systems. Solar Energy 43, 97-105.

Homan, K.O., 2003. Internal entropy generation limits for direct sensible thermal storage. Journal of Energy Resources Technology. Transactions of the ASME 125, 85–93.

Huhn, R., 2007. Beitrag zur thermodynamischen Analyse und Bewertung von Wasserwärmespeichern in Energieumwandlungsketten. Ph.D. Thesis, Technische Universität Dresden, Germany. pp. 21.

Kandari, A.M., 1990. Thermal stratification in hot storage-tanks. Applied Energy 35, 299-315.

Krane, R.J., 1987. A second law analysis of the optimum design and operation of thermal energy storage systems. International Journal of Heat Mass Transfer 30, 43–57.

Lavan, Z., Thompson, J., 1977. Experimental study of thermally stratified hot water storage tanks. Solar Energy, 19, 519-524.

Liu, W., Davidson, J.H., Kulacki, F.A., 2004. Thermal characterization of prototypical IKCS systems with immersed heat exchangers. Proceedings of ISEC 2004, July 11-14 2004, Portland, Oregon.

Lohse, R., Urbaneck, T., Göppert, S., Schirmer, U., Rauh, H., Platzer, B., 2008. Gestaltungsrichtlinien für Schichtenbeladungssyteme. In: 18. Symposium Thermische Solarenergie, 23. – 25. April 2008, Kloster Banz, Bad Staffelstein, Germany.

Mavros, P., Belessiotis, V., Haralambopoulos, D., 1994. Stratified energy storage vessels: Characterization of performance and modeling of mixing behavior. Solar Energy 52, 327-336.

Moran, M.J., Keyhani, V., 1982. Second law analysis of thermal energy storage systems. In: Proceedings of the Seventh International Heat Transfer Conference, Munich, vol. 6, 473–478.

Moretti, P.M., McLaughlin, D.K., 1977. Hydraulic modeling of mixing in stratified lakes. Journal of the Hydraulics Division 103, 367–380.

Tran, N., Kreider, J.F., Brothers, P., 1989. Field measurements of chilled water storage thermal performance. ASHRAE Transactions 95, 1106–1112.

Nelson, J.E.B., Balakrishnan, A.R., Murthy, S.S., 1999. Experiments on stratified chilled water tanks. International Journal of Refrigeration 22, 216-234.

Panthalookaran, V., Heidemann, W., Müller-Steinhagen, H., 2007. A new method of characterization for stratified thermal energy stores. Solar Energy 81, 1043-1054.

Panthalookaran, V., 2008. Personal communication by electronic mail of January 15th, 2008.

Phillips, W.F., Dave, R.N., 1982. Effects of stratification on the performance of liquid-based solar heating systems. Solar Energy 29, 111-120.

Rosen, M.A., 2001. The exergy of stratified thermal energy storages. Solar Energy 71, 173–185.

Rosen, M.A., Tang, R., Dincer, I., 2004. Effect of stratification on energy and exergy capacities in thermal storage systems. International Journal of Energy Research 28, 177-193.

Rosen, M.A., Pedinelli, N., Dincer, I., 1999. Energy and exergy analyses of cold thermal storage systems. International Journal of Energy Research 23, 1029 – 1038.

Rosen, M.A., 1992. Appropriate thermodynamic performance measures for closed systems for thermal energy storage. Transactions of the ASEM, Journal of Solar Energy Engineering 114, pp.100-105.

Rosengarten, G., 1999. A second law approach to characterising thermally stratified hot water storage with application to solar water heaters. Transactions of the ASME, Journal of Solar Energy Engineering 121, 194-200.

Shah, L.J., Furbo, S., 2003. Entrance effects in solar storage tanks; Solar Energy 75, 337-348.

Shyu, R.J., Lin, J.Y., Fang, L.J., 1989. Thermal analysis of stratified storage tanks. Transactions of the ASME, Journal of Solar Energy Engineering 111, 54–61.

Shyu, R.J., Hsieh, C.K., 1987. Unsteady natural convection in enclosure with stratified medium. Transactions of the ASME, Journal of Solar Energy Engineering 109, 127–133.

Sliwinski, B.J., Mech, A.R., Shih, T.S., 1978. Stratification in thermal storage during charging. In: Proceedings of the 6th International Heat Transfer Conference, Toronto, vol. 4, pp. 149-154.

Stefan, H.G., Gu, R., 1992. Efficiency of jet-mixing of temperature stratified water. Journal of Environmental Engineering, ASCE 118, 363–379.

van Berkel, J., Rindt, C.C.M., van Steenhoven, A. 1999. Modelling of two-layer stratified stores. Solar Energy 67, 65-78.

van Berkel, J., 1997. Thermocline entrainment in stratified energy stores. Ph.D. Thesis, Technische Universiteit Eindhoven, The Netherlands, p. 32.

Wildin, M.W., 1990. Diffuser design for naturally stratified thermal storage; ASHRAE Transactions 96, 1094–1102.

Wu, L., Bannerot, R.B., 1987. Experimental Study of the Effect of Water Extraction on Thermal Stratification in Storage. In: Proceedings of the 1987 ASME-JSME-JSES Solar Energy Conference, Honolulu, Vol. 1, pp. 445-451.

Yoo, H., Pak, E., 1993. Theoretical model of the charging process for stratified thermal storage tank. Solar Energy 51, 513–519.

Zurigat, Y.H., Ghajar, A.J., 2002. Chapter 6: Heat Transfer and Stratification in Sensible Heat Storage. in: Dincer, I., Rosen, M. (Eds.), Thermal energy Storage – Systems and Applications, John Wiley & Sons, New York, pp. 264-270.

Paper II

Haller, M.Y., Yazdanshenas, E., Andersen, E., Bales, C., Streicher, W. & Furbo, S., 2010. *A Method to Determine Stratification Efficiency of Thermal Energy Storage Processes Independently from Storage Heat Losses.* Solar Energy, 84(6), 997 - 1007.

A method to determine stratification efficiency of thermal energy storage processes independently from storage heat losses

Michel Y. Haller[*a], Eshagh Yazdanshenas[b], Elsa Andersen[b], Chris Bales[c], Wolfgang Streicher[a], Simon Furbo[b]

[a] Institute of Thermal Engineering, Graz University of Technology, Inffeldgasse 25/B, 8010 Graz, Austria

[b] Department of Civil Engineering, Technical University of Denmark, Brovej, building 118, DK-2800, Kgs. Lyngby, Denmark

[c] Solar Energy Research Center SERC, Högskolan Dalarna, 781 88 Borlänge, Sweden

Abstract

A new method for the calculation of a stratification efficiency of thermal energy storages based on the second law of thermodynamics is presented. The biasing influence of heat losses is studied theoretically and experimentally. Theoretically, it does not make a difference if the stratification efficiency is calculated based on entropy balances or based on exergy balances. In practice, however, exergy balances are less affected by measurement uncertainties, whereas entropy balances can not be recommended if measurement uncertainties are not corrected in a way that the energy balance of the storage process is in agreement with the first law of thermodynamics. A comparison of the stratification efficiencies obtained from experimental results of charging, standby, and discharging processes gives meaningful insights into the different mixing behaviors of a storage tank that is charged and discharged directly, and a tank in tank system whose outer tank is charged and the inner tank is discharged thereafter. The new method has a great potential for the comparison of the stratification efficiencies of thermal energy storages and storage components such as stratifying devices.

Key words: thermal stratification, thermal energy storage, solar heating systems, thermocline

---

[*] Corresponding author. Tel.: +41 55 222 4836; fax: +41 55 222 4844. E-mail address: michel.haller@solarenergy.ch

Nomenclature

a	time constant (s^{-1})
c	specific heat capacity (J/kg K)
C	thermal capacitance (J/K)
$\dot{C}$	capacity flow rate (W/K)
h	specific enthalpy (J/kg)
H	enthalpy (J)
i	index of summation for mass series (-)
j	index of summation for time series (-)
k	coverage factor (-)
m	mass (kg)
$\dot{m}$	mass flow (kg/s)
M	number of assumed homogenous mass elements of the TES, upper bound of summation for mass series (-)
N	upper bound of summation for time series (-)
Q	thermal energy (J)
$\dot{Q}$	thermal power (W)
s	specific entropy (J/kg K)
S	entropy (J/K)
$\dot{S}$	entropy flow rate (W/K)
T	absolute temperature (K)
τ	time (s)
$\Delta\tau$	time step (s)
UA	overall heat transfer coefficient area product for heat losses to ambient (W/K)
η	stratification efficiency (-)
ξ	exergy (J)

Superscripts

exp	experimentally determined "real case" (generally includes heat losses and mixing)
hl	calculated including heat losses, assuming the same heat loss coefficients as for the experimental storage
mix	perfectly mixed from the beginning of the experiment by constantly mixing the inlet fluid with the entire tank fluid; the energy content is thus not the same as in the experimental storage

Subscripts

A	at the beginning of a time period with constant inlet flow rate and temperature
B	at the end of a time period with constant inlet flow rate and temperature
0	thermodynamic dead state (= state with no exergy) in the case of T_0, or start of the experiment in case of τ_0
amb	ambient of the TES
$corr$	correction / corrected value
$flow$	attributed to the charging / discharging mass flows
hl	attributed to heat losses
inf	after an infinite time
int	caused by internal processes of mixing or heat conduction
$inlet$	fluid entering the TES

irr	irreversible part of entropy or exergy change
ms	measured
out	fluid leaving the TES
st	stratification efficiency according to the new method presented in this article
st0	stratification efficiency with exergy / entropy changes caused by heat losses erroneously attributed to internal processes
store	value attributed to the TES
S	based on entropy balance
wat	water
ξ	based on exergy balance

1   Introduction

Temperature stratification in a thermal energy storage (TES) of a solar heating system may considerably increase system performance, especially for low flow solar heating systems (e.g., Lavan and Thompson, 1977; Phillips and Dave, 1982; Hollands and Lightstone, 1989; Cristofari et al., 2003; Andersen and Furbo, 2007). For the development of TES components and processes, as well as for the comparison of different TES on the market, it is desirable to have an index or "measure" to determine the ability of a TES to promote and maintain stratification during charging, storing and discharging. Several indices and numbers have been proposed for this purpose (Davidson et al., 1994; van Berkel, 1997; Shah and Furbo, 2003; Huhn, 2007; Panthalookaran et al., 2007; Andersen et al., 2007). A summary of such numbers has been given by Zurigat and Ghajar (2002), Panthalookaran et al. (2007) and Haller et al. (2009). Destratification, or mixing of two fluids with different temperatures, always results in generation of entropy and loss of exergy (Rosen et al., 2004). The better a TES process is stratifying and maintaining stratification, the less entropy is generated. Therefore, entropy generation or exergy loss can be used as a measure for the ability of a TES to promote and maintain stratification (van Berkel et al., 1999; Shah and Furbo, 2003; Rosen et al., 2004; Panthalookaran et al., 2007; Huhn, 2007; Lohse et al., 2008). In a real TES process, exergy is not only lost by mixing or destratification, but also by heat losses. Since destratification may be viewed as a process occurring only inside of a TES, exergy losses caused by destratification have been referred to as internal exergy losses, or losses due to internal irreversibilities. Exergy losses caused by heat losses to the ambient outside the TES have been referred to as external exergy losses (Rosen et al., 1999; Rosen, 2001; Panthalookaran et al., 2007; Bakan et al., 2008).

Generally, it is of great interest how far from the ideal case of perfect stratification or the worst case of full mixing a TES process is. Therefore, stratification efficiencies or degrees of mixing that range from 0 – 100% have been defined by several authors (e.g. Davidson et al., 1994; Shah and Furbo, 2003; Panthalookaran et al., 2007; Huhn, 2007; Andersen et al., 2007). Haller et al. (2009) applied these methods to hypothetical storage processes of charging, discharging and storing. The result has been compared to the rate of entropy generation caused by internal mixing. It has been concluded that from the methods applied according to their description in literature, only the relative entropy generation as described by Huhn (2007) was always in qualitative agreement with the internal rate of entropy generation. In the hypothetical storage processes that were analyzed, heat losses have been set to zero such that all entropy generation was internal entropy generation. In a real storage process,

however, heat losses can not be eliminated. Unlike other methods (e.g. Davidson et al., 1994; Andersen et al., 2007; Panthalookaran et al., 2007) the method of Huhn does not separate internal entropy generation from entropy changes due to heat losses to the ambient. Therefore, different stratification efficiencies may be obtained for two TES with different insulation, even if the stratification capability is the same for both stores. In this article, the influence of heat losses on stratification efficiency determined by using the relative entropy generation / exergy loss methods is studied, and an attempt is made to further develop the method of Huhn in order to separate internal exergy losses from exergy losses to the ambient, or internal entropy generation from entropy changes caused by heat losses, respectively. This new method is applied to results from simulations and measurements likewise.

2   Definition of a stratification efficiency based on relative internal exergy losses

Entropy and exergy balances have been widely used in TES analysis (e.g. Rosen, 1992; Rosen et al., 1999; van Berkel et al., 1999; Shah and Furbo, 2003; Huhn, 2007; Rosen et al., 2004; Panthalookaran et al., 2007). Unlike energy, the entropy in a closed system is not constant. In a TES process entropy may be generated by mixing as well as by heat conduction and diffusion. Thus, entropy generation is an unwanted but unavoidable phenomenon. In the following it is assumed that the border of a TES is the boundary of the system that is to be analyzed. As shown in Fig. 1, the entropy change of a TES system may be caused by mass transfer across the system boundaries as indicated by $\dot{S}_{inlet}$ and $\dot{S}_{out}$ respectively, by heat transfer across the system boundary $\dot{S}_{hl,store}$ or by internal entropy generation $\dot{S}_{irr,int}$.

TES border = system boundary
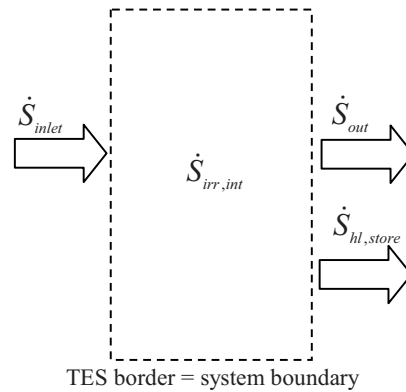
Fig. 1. System boundary for the calculation of internal entropy generation.

The entropy change rate of a TES process $dS_{store}/d\tau$, assuming heat losses and outlet mass flows to be represented by negative values of $\dot{S}_{hl,store}$ and $\dot{S}_{out}$, is

$$dS_{store}/d\tau = \dot{S}_{inlet} + \dot{S}_{out} + \dot{S}_{hl,store} + \dot{S}_{irr,int} \qquad (1)$$

For a given storage process that takes place between time 0 and time 1, the entropy change of the TES between time 0 and time 1 may be expressed as

$$\Delta S_{store} = \Delta S_{inlet} + \Delta S_{out} + \Delta S_{hl,store} + \Delta S_{irr,int} \qquad (2)$$

and the internal entropy generation of the process is

$$\Delta S_{irr,int} = \Delta S_{store} - \Delta S_{flow} - \Delta S_{hl,store} \geq 0 \qquad (3)$$

with

$$\Delta S_{flow} = \Delta S_{inlet} + \Delta S_{out} \qquad (4)$$

The internal entropy generation may be calculated for an experimental TES ($\Delta S_{irr,int}^{exp}$), and for a fully mixed reference TES ($\Delta S_{irr,int}^{mix,hl}$). The fully mixed reference TES is assumed to be equal to the experimental TES at the beginning of the experiment, and fully mixed from this point on to the end of the experiment. Further, the fully mixed reference TES has the same heat loss coefficients as the experimental TES (indicated by the superscript hl), and is subjected to the same inlet mass flows and temperatures. If the experiment does not start with a uniform temperature of the experimental TES, the internal entropy generation of the fully mixed reference TES includes also the entropy generation obtained from mixing volumes with different temperatures at the beginning of the experiment. Based on these assumptions, the stratification efficiency $\eta_{st,S}$ is calculated based on the internal entropy generation of the experimental TES relative to the internal entropy generation of the fully mixed reference TES as shown in Eq. 5. This value will be 0 if the storage tank was always fully mixed during the experiment and 1 for a perfectly stratified, isentropic storage process.

$$\eta_{st,S} = 1 - \frac{\Delta S_{irr,int}^{exp}}{\Delta S_{irr,int}^{mix,hl}} \qquad (5)$$

Another route for the calculation of this stratification efficiency is based on the internal exergy loss of the experimental TES $\Delta \xi_{irr,int}^{exp}$ relative to the internal exergy loss of a fully mixed reference TES $\Delta \xi_{irr,int}^{mix,hl}$, i.e.

$$\eta_{st,\xi} = 1 - \frac{\Delta \xi_{irr,int}^{exp}}{\Delta \xi_{irr,int}^{mix,hl}} \qquad (6)$$

With $\Delta \xi_{hl,store}$ being a negative value in the case of net heat losses, $\Delta \xi_{irr,int}$ is defined as

$$\Delta \xi_{irr,int} = \Delta \xi_{store} - \Delta \xi_{flow} - \Delta \xi_{hl,store} \leq 0 \qquad (7)$$

In this case, the exergy changes are calculated based on the enthalpy changes ΔH, the entropy changes ΔS, and the thermodynamic dead state temperature T_0.

$$\Delta \xi = \Delta H - T_0 \cdot \Delta S \qquad (8)$$

Because internal mixing does not change the enthalpy content of the TES ($\Delta H_{int} = 0$), the internal exergy loss of a TES is directly proportional to the internal entropy generation. Thus, the stratification efficiency based on the relative internal exergy loss equals the stratification efficiency based on relative internal entropy generation.

$$T_0 \cdot \Delta S_{irr,int} = -\Delta \xi_{irr,int} \qquad (9)$$

$$\eta_{st,\xi} = \eta_{st,S} \qquad (10)$$

This identity has already been pointed out by Huhn (2007).

The enthalpy and entropy change of the TES caused by charging and discharging processes, assuming that the inlet mass flow equals the outlet mass flow, evaluated at the time τ_1, are:

$$\Delta H_{flow}(\tau_1) = \int_{\tau_0}^{\tau_1} \dot{m}(\tau) \cdot \left[h\{T_{inlet}(\tau)\} - h\{T_{out}(\tau)\} \right] \cdot d\tau \tag{11}$$

$$\Delta S_{flow}(\tau_1) = \int_{\tau_0}^{\tau_1} \dot{m}(\tau) \cdot \left[s\{T_{inlet}(\tau)\} - s\{T_{out}(\tau)\} \right] \cdot d\tau \tag{12}$$

The enthalpy and entropy change of the TES, from the beginning of the experiment until the time τ_1 are:

$$\Delta H_{store}(\tau_1) = \int_{0}^{m_{store}} \left[h\{T_{store}(\tau_1,m)\} - h\{T_{store}(\tau_0,m)\} \right] dm \tag{13}$$

$$\Delta S_{store}(\tau_1) = \int_{0}^{m_{store}} \left[s\{T_{store}(\tau_1,m)\} - s\{T_{store}(\tau_0,m)\} \right] dm \tag{14}$$

The enthalpy change due to heat losses is calculated based on the heat transfer coefficient area products $UA(m)$ between each mass element and the ambient:

$$\Delta H_{hl,store}(\tau_1) = \int_{\tau_0}^{\tau_1} \int_{0}^{m_{store}} \frac{-UA(m) \cdot \{T_{store}(\tau,m) - T_{amb}(\tau)\}}{m_{store}} dm \cdot d\tau \tag{15}$$

With $\dot{S} = \dot{Q}/T$ given for the entropy change rate associated with heat transfer, the entropy change of the TES caused by heat losses is:

$$\Delta S_{hl,store}(\tau_1) = \int_{\tau_0}^{\tau_1} \int_{0}^{m_{store}} \frac{-UA(m) \cdot \{T_{store}(\tau,m) - T_{amb}(\tau)\}}{m_{store} \cdot T_{store}(\tau,m)} dm \cdot d\tau \tag{16}$$

For the calculation of the fully mixed reference store, the time dependent inlet temperatures and mass flows and the ambient temperatures are identical to the ones that are measured (or simulated) for the experimental TES. The TES temperature of the fully mixed reference TES is at the same time its outlet temperature. For time periods with constant charging or discharging mass flow and inlet temperature, the temperature of the fully mixed reference TES at time τ_B is calculated from the temperature at the beginning of this period $T_{store}^{mix,hl}(\tau_A)$, the temperature T_{inf} that would be reached after an infinite time, and the time constant a of the process:

$$T_{out}^{mix,hl}(\tau_B) = T_{store}^{mix,hl}(\tau_B) = T_{inf} + \left[T_{store}^{mix,hl}(\tau_A) - T_{inf} \right] \cdot EXP\left(-a \cdot [\tau_B - \tau_A]\right) \tag{17}$$

With

$$T_{inf} = \frac{UA \cdot T_{amb} + \dot{C}_{flow} \cdot T_{inlet}}{UA + \dot{C}_{flow}} \tag{18}$$

$$a = \frac{UA + \dot{C}_{flow}}{C_{store}} \tag{19}$$

Where $\dot{C}_{flow}$ is the capacity flow rate of the charging or discharging process, and C_{store} is the thermal capacitance of the TES.

$$\dot{C}_{flow} = \dot{m}_{flow} \frac{h(T_{out}) - h(T_{inlet})}{T_{out} - T_{inlet}} \tag{20}$$

3 Application to a simulated experiment

3.1 Description of the simulation

Simulations of the charging and discharging experiment described in Table 1 were performed with a simplified 10 nodes TES model programmed in Visual Basic. The simulation time step of 0.1 hours corresponded to the time needed to replace the fluid in one node by the fluid from the upstream node during the charging and discharging processes. This way, numerical diffusion was avoided. The only sources of internal entropy generation for the simulated experimental TES were therefore caused by the well defined processes of effective vertical thermal conductivity and mixing listed in Table 2.

In the model, the temperatures of all nodes were calculated in a stepwise manner according to the following sequence, without the need of iterations:

1. Fluid replacement during the charging or discharging process

2. Mixing of 3 nodes in the inlet region of the charging or discharging process for the simulation of inlet jet mixing

3. Vertical diffusion and conduction of heat based on the temperature distribution resulting from the previous calculation steps

4. Heat losses to the ambient based on the difference between the ambient temperature and the average temperature of each node at the beginning and at the end of this time step (using the results of step 3).

Table 1. Assumptions for the simulated charging and discharging experiments.

Mass of the TES	140 kg
Fluid / material specific heat	4.18 kJ/kgK
Initial temperature	20 °C
Mass flow for charging and discharging	140 kg/h
Inlet position for charging = outlet position for discharging	top
Inlet position for discharging = outlet position for charging	bottom
Charging time period [a]	hour 1 – 1.8
Charging temperature	50 °C
Standby time period [a]	hour 1.8 – 6
Discharging time period [a]	hour 6 - 10
Discharging temperature	20 °C
Overall heat loss coefficient of simulation 1 [b]	0.5 W/K
Overall heat loss coefficient of simulation 2 [b]	2.0 W/K

a) from the beginning of the experiment
b) distributed evenly between all mass elements

Number of nodes	10
Number of mixed nodes at top (during charging)	3
Number of mixed nodes at bottom (during discharging)	3
Height	1 m
Cross sectional area	0.14 m^2
Fluid / material density	1000 kg/m^3
Effective vertical thermal conductivity	2.5 W/mK

The calculation of the fully mixed reference TES was performed according to Eq. 17 – 20 and Table 1.

Stratification efficiencies based on relative entropy generation $\eta_{st,S}$ and relative exergy losses $\eta_{st,\xi}$ were calculated using Eq. 3 - 8. These numbers are compared to results based on a calculation that does not account for exergy and entropy changes due to heat losses in both, the experimental TES and the fully mixed reference TES, as given by Eq. 21 and 22.

$$\eta_{st0,S} = 1 - \frac{\Delta S_{store}^{exp} - \Delta S_{flow}^{exp}}{\Delta S_{store}^{mix} - \Delta S_{flow}^{mix}} \tag{21}$$

$$\eta_{st0,\xi} = 1 - \frac{\Delta \xi_{flow}^{exp} - \Delta \xi_{store}^{exp}}{\Delta \xi_{flow}^{mix} - \Delta \xi_{store}^{mix}} \tag{22}$$

For the calculation of exergy, a thermodynamic dead state temperature of T_0 = 298.15 K has been assumed.

3.2 Results and Discussion

Fig. 2a shows that the stratification efficiencies $\eta_{st0,S}$ and $\eta_{st0,\xi}$ that were calculated without taking into account the entropy / exergy change caused by heat losses are not equal to each other ($\eta_{st0,S} \neq \eta_{st0,\xi}$). The difference is quite large, even though a relatively small heat loss coefficient of 0.5 W/K has been assumed for the TES of 140 kg water. If the entropy / exergy change due to heat losses is separately accounted for, the stratification efficiency based on internal entropy generation is, as expected, equal to the stratification efficiency based on internal exergy losses ($\eta_{st,S} = \eta_{st,\xi}$). From the comparison of Fig. 2a and Fig. 2b two main conclusions can be drawn. First, the deviation of the calculated stratification efficiencies $\eta_{st0,S}$ and $\eta_{st0,\xi}$ becomes larger with increasing heat loss coefficients of the TES. Second, no notable difference can be seen between the $\eta_{st,S}$ of the two example calculations with different heat loss coefficients.

Neglecting the influence of heat losses on the exergy balance of the TES obviously results in reduced values for the stratification efficiency based on the exergy balance. This can be explained by the fact that exergy loss associated with heat losses are unintentionally added to the internal exergy loss in the calculation procedure, thereby increasing this value and decreasing the calculated stratification efficiency. At first sight it might come as a surprise that if the stratification efficiency is calculated based on the entropy balance, neglecting the effect of heat losses has the opposite effect. This is a consequence of the entropy flow associated

with heat transfer. If a TES is loosing energy to the ambient it looses at the same time entropy. Therefore, not accounting for this entropy loss separately will decrease the calculated internal entropy generation.

a)

b)
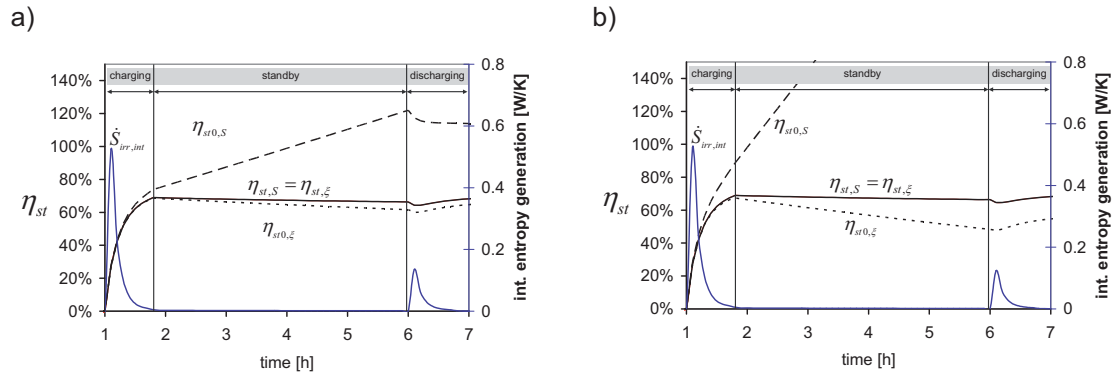
Fig. 2. Second law stratification efficiencies for a simulated TES process with heat losses of 0.5 W/K (a) and 2.0 W/K (b).

4   Application to experimental results

4.1 Measurement setup and uncertainties

Measurements were performed on two solar TES that may be used for the storage of thermal energy for domestic hot water preparation and space heating. TES1 is an 800 liter storage tank with an integrated biomass burner that has been tested in direct charging and discharging mode (Fig. 3, left). It contained internal heat exchangers for solar charging and domestic hot water production that were filled with water during the experiments.
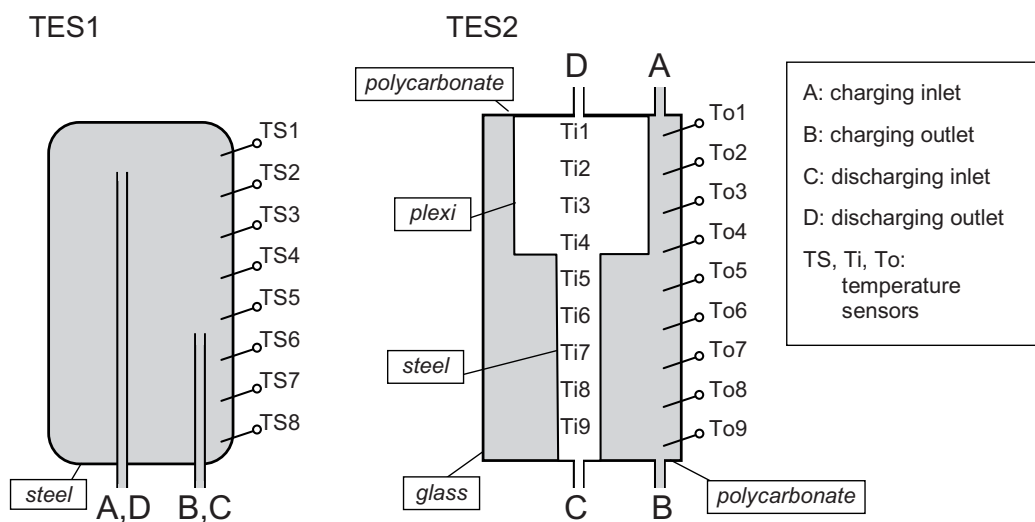
Fig. 3. Simplified schematic pictures of the two TES that have been used for experiments.

The integrated burner and the internal heat exchangers have not been used during the experiments and are therefore not shown in Fig. 3. TES2 is a tank-in-tank storage system (Fig. 3, right) with a total volume of 124.5 liter, of which 29.5 liter were contained in the inner tank.

Table 3 and 4 show the applied measurement instruments and their estimated uncertainties for TES1 and TES2, respectively. Inlet and outlet flow rates of TES1 were measured with a magnetic inductive sensor that has been calibrated with a scale and a stop-watch in the range of 100 – 900 l/h. Inlet and outlet temperatures were measured with immersed 4 wire Pt100 class A sensors that have been calibrated simultaneously against another 4 wire Pt100 class A sensor in a thermostat bath in the range of 10 – 90 °C. A total of 8 thermocouple sensors of Type K were attached to the outside of the steel tank, below its insulation, equally spaced along a vertical line. Then, they were calibrated against the average of the inlet and outlet temperatures of the flow and return line in steady state in the range of 20 – 60 °C. Measurements were taken at intervals of 1 s and averaged values were stored at intervals of 10 s.

TES2 was measured in a different laboratory, and therefore different measurement devices have been used. Inlet and outlet flow rates of TES2 were measured with vortex flow sensors (VFS) that have been calibrated with a scale and a stop-watch in the range of 120 – 840 l/h. Inlet and outlet temperatures were measured with immersed copper/constantan thermopiles whose uncertainty is estimated according to Furbo (1984). A total of 18 thermocouple sensors of Type TT were immersed into the TES, 9 of them in the outer tank and 9 of them in the inner tank, as shown in Fig. 3, all of them with known positions on a vertical line. Measurements were taken at intervals of 5 s and stored at intervals of 5 s.

Table 3. Measurement devices and uncertainty used for the measurements on TES1.

measured property	*Device*	*uncertainty (k=1)*
volume flow rate	Endress & Hauser Promag P50	± 0.6%
temperature (flow)	4w Pt100 class A	± 0.1K
temperature difference (flow inlet and outlet)	4w Pt100 class A	± 0.03K
temperature (tank)	Type K thermocouple	± 0.5K

Table 4. Measurement devices and uncertainty used for the measurements on TES2.

measured property	*Device*	*uncertainty (k=1)*
volume flow rate charging	vortex flow sensor (VFS)	± 7.6%
volume flow rate discharging	vortex flow sensor (VFS)	± 7.1%
temperature (flow)	copper/constantan thermocouple	± 0.5 K
temperature difference (flow inlet and outlet)	copper/constantan thermopiles	± 0.05 K
temperature (tank)	Type TT thermocouple	± 0.5 K

4.2 Calculation procedure

A number of discrete time steps $j = 1...N$ were used instead of a continuous integration over time for the calculation of enthalpy and entropy changes due to mass flows and heat losses. The calculation time steps were $\Delta\tau$ = 10 s for TES1, and $\Delta\tau$ = 5 s for TES2. A number of discrete mass elements (M = 8 for TES1 and M = 18 for TES2) that correspond to the number of sensors used to measure the temperatures inside the TES have been used for the calculation of enthalpy changes of the TES, together with a thermal capacitance $C_{store,i}$ associated with each sensor measurement i.e.:

$$\Delta H_{store} = \sum_{i=1}^{M} C_{store,i} \cdot \left[T_{store,i}(\tau) - T_{store,i}(\tau_0) \right] \tag{23}$$

The total thermal capacitance C_{store} of TES1 has been measured with a complete charge and discharge test, and the mass of each TES element corresponding to a different temperature sensor has been calculated with $C_{store,i} = C_{store}/M$. Because of the different volumes associated with the different temperature sensors of TES2, $C_{store,i}$ has been calculated for each sensor individually based on the geometrical data of TES2. The thermal capacitance of the outer wall, without insulation, has been attributed to the corresponding fluid mass element and temperature inside the TES. The thermal capacitance of the wall separating the inner tank from the outer tank has been attributed half to the mass element of the inner tank and half to the mass element of the outer tank. The properties of the materials used for this calculation are shown in Table 5.

Table 5. Materials and properties for the calculation of the thermal capacitance of TES2.

material	volume m^3	specific heat kJ/m^{3}K
water	0.1216	4148
glass	0.0164	1890
polycarbonate	0.0017	1404
plexiglass	0.0014	1786
steel	0.0013	3398

To calculate the entropy change of the TES, an equivalent water mass $m_{store,i} = C_{store,i}/c_{wat}$ has been calculated for each mass element with c_{wat} = 4.18 kJ/kgK. The entropy change was then calculated using the entropy function of water, i.e.:

$$\Delta S_{store} = \sum_{i=1}^{M} m_{store,i} \cdot \left[s\{T_{store,i}(\tau)\} - s\{T_{store,i}(\tau_0)\} \right] \tag{24}$$

The enthalpy change and entropy change caused by heat losses were calculated with Eq. 25 and 26:

$$\Delta H_{hl,store} = \sum_{j=1}^{N} \sum_{i=1}^{M} -UA_i \cdot \{T_{store,i}(j) - T_{amb}(j)\} \cdot \Delta\tau \tag{25}$$

$$\Delta S_{hl,store} = \sum_{j=1}^{N} \sum_{i=1}^{M} \frac{-UA_i \cdot \{T_{store,i}(j) - T_{amb}(j)\}}{T_{store,i}(j)} \cdot \Delta\tau \tag{26}$$

For the calculation of heat losses for the single mass elements, overall heat transfer coefficient area products UA_i have been obtained by simulating the cooling out behavior during a standby period, and comparing the simulation results with the measurements. For TES1, which was not evenly insulated, the TES was split into three different zones with different overall heat loss coefficients. TES2 was evenly insulated and therefore a constant heat loss coefficient has been assumed for all surface areas.

Measurement uncertainties inevitably lead to calculated results for $\Delta H_{store,ms}$, ΔH_{flow}, and $\Delta H_{hl,store}$ that are not in perfect agreement with the law of conservation of energy ($\Delta H_{store,ms} \neq \Delta H_{flow} + \Delta H_{hl,store}$). It is reasonable to assume that the first law of thermodynamics will never be violated, and thus it can be justified that the measured results are "corrected" within the limits of measurement uncertainties in order to be in agreement with the first law of thermodynamics. Inevitably, the question arises which measured values should be corrected. For the calculation of the energy balance, each TES temperature sensor has been assumed to represent the temperature of a certain section / mass element of the TES. In reality, the temperatures within these sections or mass elements are not uniform. This adds additional uncertainty to the uncertainty of the temperature measurement at the location of the sensor itself. Additionally, the temperature sensors attached to the outer surface of TES1 register temperature changes inside the TES only with a time delay, thus contributing further to the uncertainty of values calculated based on these temperatures. For this reason, the mentioned correction has been applied to the measured TES temperature measurements, i.e.:

$$T_{store,i}\left(j \right) = T_{store,i,ms}\left(j \right) + \Delta T_{store,corr}\left(j \right) \tag{27}$$

The correction term $\Delta T_{store,corr}\left(j \right)$ is chosen within the uncertainties of the energy balance, such that at each time step:

$$\Delta H_{store} = \Delta H_{flow} + \Delta H_{hl,store} \tag{28}$$

For the calculation of exergy, a thermodynamic dead state temperature of $T_0 = 298.15$ K has been assumed.

4.3 Description of the experiments

The experiments that have been performed with the two TES shown in Fig. 3 consisted of three sequential periods. The first period was a heat charging process that started from a uniform TES temperature and ended when about 75% of the TES volume had been replaced. This was followed by a standby period (i.e. a period without fluid exchange) of about 4 hours. In the third and last period, the stored energy was discharged, if possible until the initial temperature was reached again. All inlet temperatures and mass flows were kept constant during the charging and discharging processes respectively.

Four experiments with different mass flows and different insulation were performed with TES1. Nominal values of these experiments are shown in Table 6. Different flow rates were chosen in order to evaluate their influence on the stratification efficiency. Different insulation was chosen in order to determine the ability of the new method presented in section 2 to reduce the biasing influence of heat losses on the calculated stratification efficiency.

Table 6. Nominal values for the different experiments performed on TES1.

Experiment		1	2	3	4
Overall heat loss coefficient	W/K	**11**	**11**	**17**	**17**
Charging / discharging mass flow rate	kg/h	**200**	**400**	**200**	**400**
Charging time	h	**3.0**	**1.5**	**3.0**	**1.5**
Standby time	h	4.0	4.0	4.0	4.0
Discharging time	h	6.0	4.5	6.0	4.5
End of the experiment	h	13	10	13	10
Initial tank temperature [a)]	°C	20	20	20	20
Charging inlet temperature	°C	60	60	60	60

a) Initial tank temperature is at the same time discharging inlet temperature and temperature at the end of the experiment.

4.4 Results and Discussion

Fig. 4a shows the measured temperatures (TS1 – TS8) of TES1 over the time of experiment 2 listed in Table 6. The simulated temperature of the fully mixed reference store $T_{store}^{mix,hl}$ is also shown.

Figs. 4b – 4d show the calculated enthalpy changes, entropy changes, and exergy changes of the same experiment. If the total turnover of enthalpy, entropy, and exergy is defined as the maximum values of ΔH_{flow}^{exp}, ΔS_{flow}^{exp}, $\Delta \xi_{flow}^{exp}$, respectively, at the end of the charging process, then the figures show that the changes due to heat losses that are represented by ΔH_{hl}^{exp}, ΔS_{hl}^{exp}, and $\Delta \xi_{hl}^{exp}$ are only a small fraction of the respective total enthalpy, entropy and exergy turnover. The internal entropy generation $\Delta S_{irr,int}^{exp}$ shown in Fig. 4c is small compared to the total entropy turnover of the experiment. It is even smaller – in absolute values - than the entropy loss caused by heat losses ΔS_{hl}^{exp}. This underlines the importance of a proper estimation of heat losses when working with entropy balances. However, the exergy loss caused by internal irreversibilities $\Delta \xi_{irr,int}^{exp}$ shown in Fig. 4d is much larger than the exergy loss caused by heat losses $\Delta \xi_{hl}^{exp}$.
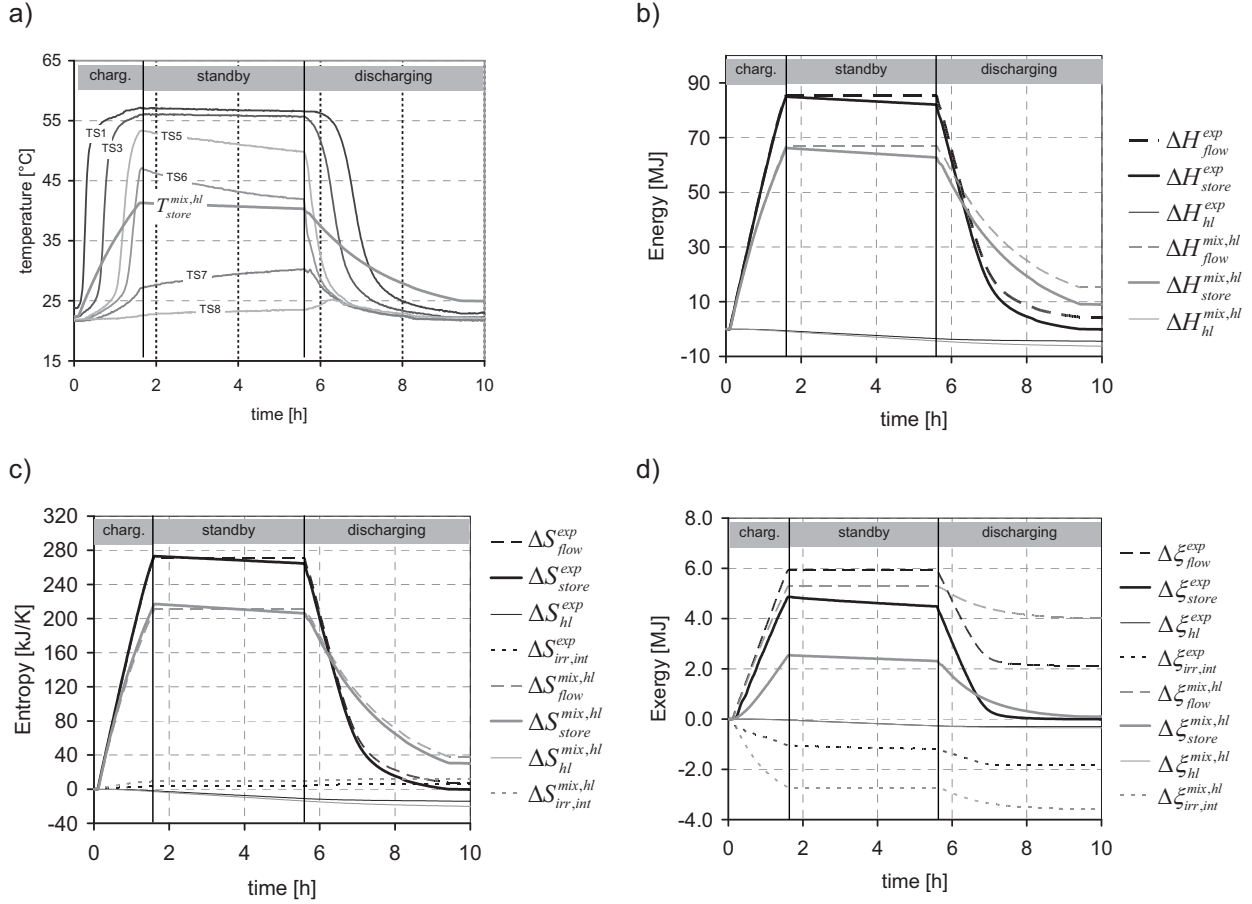
Fig. 4. Temperature profiles (a), enthalpy changes (b), entropy changes (c), and exergy changes (d) during the charging, standby, and discharging sequence of TES1.

Fig. 5a shows the calculated stratification efficiency over the time of the experiment. The stratification efficiency curve shows similar characteristics as the one in the simulated experiment shown in Fig. 2. The wavy shape of the curve during the charging process is interpreted as a bias caused by the limited number of temperature sensors of the TES. The frequency of the waves corresponds well to the time lag between the temperature response of one sensor and the next sensor in the path of the fluid moving inside the TES (see Fig. 4a). For the interpretation of the results, it has to be kept in mind that the stratification efficiency is an integrated value over the whole experiment. Thus, stratification efficiency at a certain time of the experiment is not independent from stratification efficiencies and experimental conditions of previous times within the experiment.

The decrease of η_{st} during standby can be attributed to internal heat conduction and convection. The decrease of η_{st} at the beginning of the discharging process corresponds to a time where cold fluid flowing into the TES meets hotter fluid in the TES. During the discharge, the temperature at the point of the inlet decreases, and thus also the temperature difference of the mixing fluids decreases and consequently also the internal exergy loss rate. Fig. 5b shows that if uncorrected values are taken for the TES temperatures, then the stratification efficiencies based on entropy $\eta_{st,S}$ and based on exergy $\eta_{st,\xi}$, calculated with Eq. 3 and 5,

and with Eq. 7 and 6, respectively, are not equal. In this case, the difference between $\eta_{st,S}$ and $\eta_{st,\xi}$ at the end of the experiment is 10%, although the deviation of the energy balance at the end of the experiment is only 0.5% of the total energy turnover of the experiment.
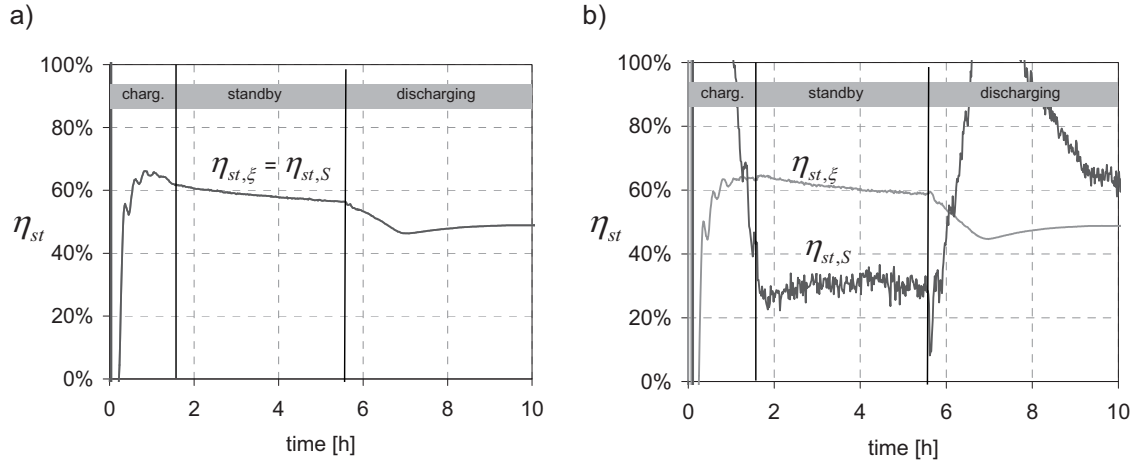
a)

b)

Fig. 5. Stratification efficiency during the charging, standby, and discharging sequence of TES1 with correction (a) and without correction (b) of TES temperatures.

Since the stratification efficiency η_{st} is based on integrated values of entropy or exergy changes, its value at the end of an experiment may be considered to be of more importance than a value at the beginning of an experiment. Furthermore, in the experimental results shown here, the temperature of the TES at the end of the experiment is uniform, and similar to its temperature at the beginning of the experiment. Thus, uncertainties associated with the determination of ΔH_{store}^{exp}, ΔS_{store}^{exp}, and $\Delta \xi_{store}^{exp}$ are lower at the end of the experiment.

Fig. 6 shows different stratification efficiencies η_{st} calculated for TES1 at the end of the experiments listed in Table 6. For two of the experiments, heat losses have been increased from 11 W/K to 17 W/K by removing parts of the insulation. Fig. 6 shows that $\eta_{st,\xi}$ are 7 - 10 percent points higher than $\eta_{st0,\xi}$ for the same reason as in the simulation results shown in Fig. 2. At the same time, the differences between the stratification efficiencies obtained with different insulation are significantly higher for the calculations without heat loss correction $\eta_{st0,\xi}$ than for the calculations that account separately for the exergy lost to the ambient $\eta_{st,\xi}$. It is an open question if the remaining differences of 1.0 – 1.5 percentage points between the stratification efficiencies $\eta_{st,\xi}$ for experiments with different insulation is a bias caused by the uncertainty of measurement and calculation, a bias of the method itself, or a result of different amounts of internal irreversibilities / mixing that occurred in reality during the performed experiments. An uncertainty of 20% for the determined heat loss coefficients e.g. leads to uncertainties of $\eta_{st,\xi}$ in the order of 1.1 – 1.7 percentage points for the experiments shown.
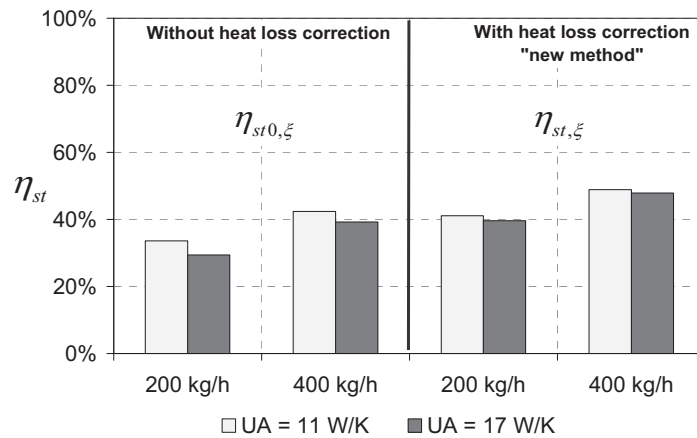
Fig. 6. Stratification efficiencies at the end of the experiments of TES1 as listed in Table 6.

At first sight it is surprising that the stratification efficiencies of the experiments performed with mass flow rates of 400 kg/h are higher than the ones performed with 200 kg/h. Due to the higher kinetic energy of the inlet stream, more inlet jet mixing is expected for an experiment with a higher mass flow. Fig. 7 shows that the temperature changes during the 400 kg/h charging process are indeed steeper, and the resulting temperatures at the top of the TES are higher for this experiment.
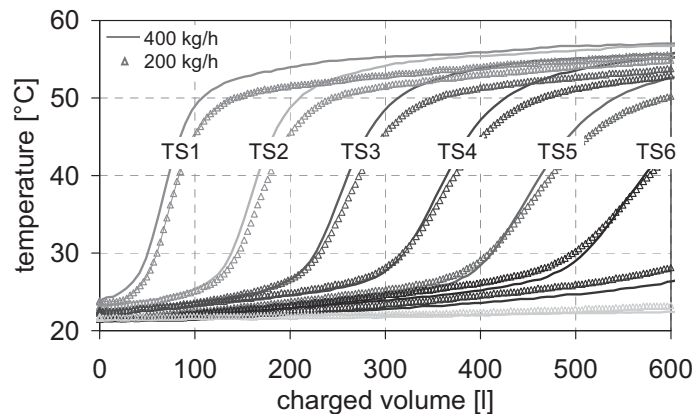
Fig. 7. Temperatures of TES1 during two charging processes with different mass flows.

This is in agreement with the higher stratification efficiency calculated for this experiment. It is possible that heat transfer from the hot inlet pipe that enters the TES at the bottom and crosses the cold tank section before it releases the fluid in the upper part of the TES is the source of more temperature degradation during the slower charging process. Since the charging time of the experiment with 200 kg/h was twice as long as the one with 400 kg/h, more heat was lost from the fluid moving up to the end of the pipe, and transferred to the

bottom section of the TES. This process has been reported as a significant source of temperature degradation for solar TES by Thür (2007).

The evolvement of the temperatures during the experiment with the tank-in-tank TES2 is shown in Fig. 8.
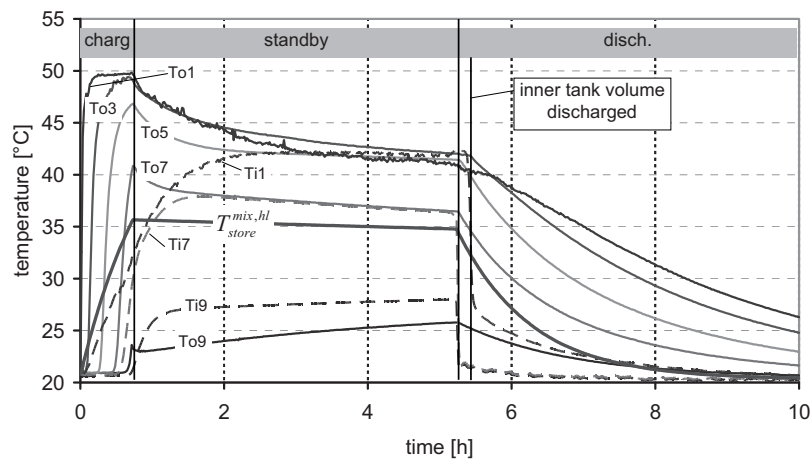
Fig. 8. Temperature profiles during the charging (charg), standby, and discharging sequence of TES2 (tank-in-tank). Ti,To = inside (i) and outside (o) tank temperatures (see Fig. 3).

In Fig. 9, a significant decrease in stratification efficiency can be seen just after the charging process for TES2. This decrease may be attributed to the process of heat transfer from the outer tank of the TES to the inner tank of the TES. As a result of the second law of thermodynamics, every heat transfer process generates entropy. During the discharging of the inner tank, it can be noted that the stratification efficiency drops to values comparable to those of TES1. Only when the inner tank is almost completely discharged, the stratification efficiency drops to very low values. This can be attributed to the limited heat transfer rate from the outer part of the tank to the inner part, which leads to exergy losses comparable to those of any under dimensioned heat exchanger. This result is interesting for the evaluation of the capability of the new method, but it cannot be used to answer the question which TES concept is better from the point of view of stratification.
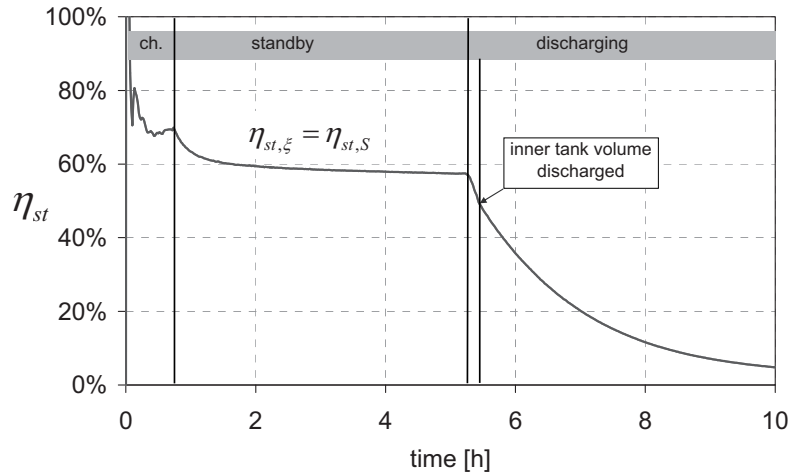
Fig. 9. Stratification efficiency during the charging (ch), standby, and discharging sequence of TES2.

The experiments used to test the two TES were chosen in order to proof the concept of the stratification efficiency calculation, but they do not correspond to charging and discharging profiles that are relevant for the operation of these TES in solar thermal systems. The question inevitably arises what a relevant test profile of charging, standby and discharging for solar TES should look like for the determination of a meaningful and representative stratification efficiency. To our knowledge, this question has not been addressed systematically yet.

5   Conclusion

A stratification efficiency based on relative exergy loss or relative entropy generation of an experimental TES has been defined. This stratification efficiency is independent from the dead-state temperature T_0 chosen for the exergy calculation. A fully mixed reference TES with equal heat loss coefficients has been used for the reference process. Theoretically, the influence of heat losses can be eliminated with this method, as has been shown with simulation results. It has also been shown by simulation and measurements that even for the case of moderate heat losses, the effect of neglecting heat losses in the calculation of stratification efficiencies based on relative exergy losses / entropy generation of the TES is significant.

The application of the new method to experimental results showed that small deviations in the energy balance that are caused by measurement uncertainties have a large effect on the entropy balance and the stratification efficiency calculated based on the entropy balance. Therefore, measured results have to be corrected within the limits of measurement uncertainties in order to be in agreement with the first law of thermodynamics. Only if this is the case, the stratification efficiency calculated based on the entropy balance is identical with the stratification efficiency based on the exergy balance. With this correction applied to experimental results, the new method was able to significantly reduce the differences between calculated stratification efficiencies of comparable TES processes performed with

higher and lower insulation of the TES. However, it is recommended that the stratification experiments are done with well insulated TES since the uncertainty of the calculated stratification efficiency increases with increased uncertainty and amount of the heat lost by the TES.

The stratification efficiency curves obtained from experimental results correspond well to the curves that had been obtained previously by simulations. The higher stratification efficiency obtained for a charging process with larger mass flow was in agreement with the better conservation of the charging temperature for the same experiment. Comparison of the stratification efficiency obtained for a storage process of a directly charged and discharged TES and a tank in tank TES whose outer tank was charged and whose inner tank was discharged thereafter gave meaningful insights into the different mixing processes taking place inside the two TES at different times of the experiments.

If temperatures inside the TES are known, a meaningful stratification efficiency may be calculated and plotted over the whole time of the experiment. Theoretically, the presented stratification efficiency calculation method is also suitable for varying inlet temperatures and mass flows. Stratification efficiency not only depends on the TES itself, but also on the test profile, i.e. the temperature and mass flow rate profile of the experiment. Test profiles should be developed depending on the intended application of a TES. For solar thermal storages, a relevant test profile is likely to include variable temperatures of charging and discharging. The development of such a profile is still a topic of future work. The presented method, together with relevant test profiles, has a great potential for the comparison of the stratification efficiencies of storage systems and storage components such as stratifying devices.

Acknowledgements

References

Andersen, E., Furbo, S., Fan, J., 2007. Multilayer fabric stratification pipes for solar tanks. Solar Energy 81, 1219-1226.

Andersen, E., Furbo, S., 2007. Theoretical comparison of solar water/space-heating combi systems and stratification design options. Journal of Solar Energy Engineering, 129, 438-448.

Bakan, K., Dincer, I., Rosen, M.A., 2008. Exergoeconomic analysis of glycol cold thermal energy storage systems. International Journal of Energy Research 32, 215-225.

Cristofari, C., Notton, G., Poggi, P., Louche, A., 2003. Influence of the flow rate and the tank stratification degree on the performances of a solar flat-plate collector. International Journal of Thermal Sciences 42, 455-469.

Davidson, J.H., Adams, D.A., Miller, J.A., 1994. A coefficient to characterize mixing in solar water storage tanks. Transactions of the ASME, Journal of Solar Energy Engineering 116, 94-99.

Furbo, S., 1984. Varmelagring til solvarmeanlæg. Ph.D. thesis. Technical University of Denmark, Thermal Insulation Laboratory, Report 162. (Danish).

Haller, M.Y., Cruickshank, C., Streicher, W., Harrison, S.J., Andersen, E., Furbo, S. , 2009. Methods to determine stratification efficiency of thermal energy storage processes– review and theoretical comparison. Solar Energy, in press, doi:10.1016/j.solener.2009.06.019.

Hollands, K.G.T., Lightstone, M.F., 1989. A review of low-flow, stratified-tank solar water heating systems. Solar Energy 43, 97-105.

Huhn, R., 2007. Beitrag zur thermodynamischen Analyse und Bewertung von Wasserwärmespeichern in Energieumwandlungsketten. Ph.D. Thesis, Technische Universität Dresden, Germany. pp. 21.

Lavan, Z., Thompson, J., 1977. Experimental study of thermally stratified hot water storage tanks. Solar Energy, 19, 519-524.

Lohse, R., Urbaneck, T., Göppert, S., Schirmer, U., Rauh, H., Platzer, B., 2008. Gestaltungsrichtlinien für Schichtenbeladungssyteme. In: 18. Symposium Thermische Solarenergie, 23. – 25. April 2008, Kloster Banz, Bad Staffelstein, Germany, 452-457, (German).

Panthalookaran, V., Heidemann, W., Müller-Steinhagen, H., 2007. A new method of characterization for stratified thermal energy stores. Solar Energy 81, 1043-1054.

Phillips, W.F., Dave, R.N., 1982. Effects of stratification on the performance of liquid-based solar heating systems. Solar Energy 29, 111-120.

Rosen, M.A., 1992. Appropriate thermodynamic performance measures for closed systems for thermal energy storage. Journal of solar energy engineering, 114, 100-105.

Rosen, M.A., Pedinelli, N., Dincer, I., 1999. Energy and exergy analyses of cold thermal storage systems. International Journal of Energy Research 23, 1029-1038.

Rosen, M.A., 2001. The exergy of stratified thermal energy storages. Solar Energy 71, 173-185.

Rosen, M.A., Tang, R., Dincer, I. 2004. Effect of stratification on energy and exergy capacities in thermal storage systems. International Journal of Energy Research 28, 177-193.

Shah, L.J., Furbo, S., 2003. Entrance effects in solar storage tanks; Solar Energy 75, 337-348.

Thür, A., 2007. Compact Solar Combisystem - High Efficiency by Minimizing Temperatures. Ph.D. Thesis, Department of Civil Engineering, Technical University of Denmark.

van Berkel, J., 1997. Thermocline entrainment in stratified energy stores. Ph.D. Thesis, Technische Universiteit Eindhoven, The Netherlands, p. 32.

van Berkel, J., Rindt, C.C.M., van Steenhoven, A. 1999. Modelling of two-layer stratified stores. Solar Energy 67, 65-78.

Zurigat, Y.H., Ghajar, A.J. 2002. Chapter 6: Heat Transfer and Stratification in Sensible Heat Storage. in: Dincer, I., Rosen, M. (Eds.), Thermal energy Storage – Systems and Applications, John Wiley & Sons, New York, pp. 264-270.

Paper III

A Unified Model for the Simulation of Oil, Gas, and Biomass Space Heating Boilers for Energy Estimating Purposes

Part I: Model Development

M.Y. Haller[1*], J. Paavilainen[2], L. Konersmann[3], R. Haberl[3], A. Dröscher[1], E. Frank[3], C. Bales[2], W. Streicher[1]

[1] Institute of Thermal Engineering, Graz University of Technology, Inffeldgasse 25/B, 8010 Graz, Austria

[2] Solar Energy Research Center SERC, Högskolan Dalarna, 781 88 Borlänge, Sweden

[3] Institut für Solartechnik SPF, Hochschule für Technik Rapperswil, 8640 Rapperswil, Switzerland

* corresponding author: michel.haller@tugraz.at, +43 316 873 7318

Full names, phone, fax, email:

Michel Yves Haller, +43 316 8737318, +43 316 8737305, michel.haller@tugraz.at

Janne Paavilainen, +46 23 778728, +46 23 778701, jip@du.se

Lars Konersmann, +41 55 2224827, +41 55 2224844, lars.konersmann@solarenergy.ch

Robert Haberl, +41 55 2224832, +41 55 2224844, Robert.Haberl@solarenergy.ch

Angela Dröscher, +43 316 8737804, +43 316 8737305, angela.droescher@tugraz.at

Elimar Frank, +41 55 2224823, +41 55 2224844, Elimar.Frank@solarenergy.ch

Chris Bales, +46 23 778707, +46 23 778701, cba@du.se

Wolfgang Streicher, +43 316 8737306, +43 316 8737305, w.streicher@tugraz.at

Abstract

A unified model for the simulation of oil, gas, pellet and wood chip space heating boilers for energy estimating purposes has been developed based on a literature review and laboratory measurements on four different boilers. The presented model is a compromise between a model that is able to reflect as accurately as possible transient energy balances, emissions and number of burner starts of all kinds of space heating boilers, and a model that is easy to parameterize and requires little computation time for the determination of seasonal results. Whereas for the parameterization of steady state behaviour standard test data for energy efficiency and emissions may be sufficient, this is not the case for the transient behaviour where the burner is operating in on and off cycles.

Keywords: Simulation and Modelling; Boiler; Biomass; Oil; Gas

Symbols

C_{therm}	effective thermal capacitance, J/K
$\dot{C}$	capacity flow rate, W/K
cp	specific heat, J/kgK
E_{el}	electric energy, J
ε	heat exchanger effectiveness, -
η	efficiency, -
fac	factor, -
fr	fraction, -
GHV	gross (or upper) heating value (reference temperature 25 °C), J/kg
γ_X	mass fraction of the elements (X = C,H,O,S,N) of ash (X = ash) and of water (X = H_2O) in the fuel per kg dry fuel, kg/kg
ΔH	enthalpy difference (reference temperature of 25 °C for sensible part and for enthalpy of reaction), J
Δh	specific enthalpy difference (reference temperature of 25 °C for sensible part and for enthalpy of reaction), J/kg
HX_{mode}	choice of heat exchanger arrangement, -
k	coverage factor for uncertainty calculation, -
λ	excess air factor for combustion ($\lambda = 1$ for stoichiometric amount), -
m	mass, kg
$\dot{m}$	mass flow rate, kg/h
N	counter, -
n	exponent for the dependency of the heat transfer resistance on the mass flow, -
NHV	net (or lower) heating value (reference temperature 25 °C), J/kg
O_{min}	stoichiometric oxygen demand per kg dry fuel, kg/kg
P	power, W
p	pressure, bar
ppm	volumetric concentration, ppm
Q	energy, J
$\dot{Q}$	thermal energy (heat) transfer rate, W

R	overall heat transfer resistance, Km^2/W
R^*	overall resistance term of the flue gas to water heat exchanger (includes heat exchanger surface area), K/W
R_{ratio}	ratio between molar mass of water and molar mass of dry flue gas or air, -
RH	relative humidity, -
ρ	density, kg/m^3
t	temperature, °C
T	thermodynamic temperature, K
dT	temperature difference, K
τ	time, s
UA	overall heat transfer coefficient area product (W/K)
$\dot{V}$	volume flow rate, m^3/h
w	water vapour load of air or flue gas per kg dry gas, kg/kg
X	coil characteristic, kgK/J

Subscripts

air	combustion air
amb	ambient / lost to the ambient
ash	ashes
avg	average
B	boiler
b	dry-wet boundary of heat exchanger surface
cc	combustion chamber
C	combustion (efficiency)
CO	carbon monoxide
chem	chemical (losses)
cond	condensate
cycling	under cycling (burner on and off) conditions
Ctherm	thermal capacitance
dp	dew point
draft	flue gas duct draught
dry	dry heat exchanger surface, dry flue gas
el	electricity
end	at the end of an experiment
empty	empty boiler
evap	evaporation (enthalpy)
fg	flue gas
fuel	fuel
gg	(flue) gas to (combustion air) gas heat exchanger
hot	hot flue gas before heat exchanger (flue gas temperature after adiabatic combustion)
hx	heat exchanger (flue gas to water if not further specified)
H_2O	water in fuel or flue gas
in	inlet (boiler return line)
inf	after an infinite time
lat	latent
max	maximum

met	metal wall of heat exchanger
min	minimum
mod	modulation
ms	based on measurements
nom	under nominal conditions (of water mass flow and combustion power)
OFF	burner is not in operation
ON	burner is in operation
out	outlet (boiler flow line or outlet of flue gas)
Rhx	heat exchanger resistance
SET	temperature set point
s	heat exchanger surface
sat	saturation (with water vapour)
sens	sensible
start	at the start of an experiment or during burner start phase
tot	total
vap	vapour
wet	wet heat exchanger surface or wet flue gas
wat	water
wb	wet bulb

Superscripts

dry	dry (biomass) fuel
d.b.	dry base; per kg of dry (biomass) fuel
wet	wet (biomass) fuel
w.b.	wet base (per kg wet fuel)
H	from (chemically bound) hydrogen in dry fuel
H_2O	from water in wet fuel
GHV	based on the gross heating value
NHV	based on the net heating value

1   Introduction

For the simulation e.g. of solar thermal energy systems for space heating and domestic hot water supply, adequate models for the main components of the energy production and storage system are needed. For the simulation software TRNSYS (SEL et al. 2006), quite sophisticated and validated models are available for the collector (Isakson & Eriksson 1994; Perers & Bales 2002) and the heat store (Drück 2006), but only rudimentary or limited models are available for the simulation of auxiliary oil, gas, and biomass boilers[1]. The seasonal efficiency of space heating boilers varies depending on the type of boiler, the load and the operating conditions within a wide range from below

---

[1] The term 'boiler' in this article is referring to the combination of a burner and a vessel or heat exchanger transferring the heat from the flue gas to the boiler water and includes the boiler water itself.

50% (Furbo et al. 2004) to about 95% with respect to the gross heating value of the fuel. Therefore it is important to simulate the overall heating system with a boiler model that reflects accurately dependencies of the boiler efficiency on load, return temperature, power modulation, and cycling operation. Without a boiler model that is able to reflect changes in boiler efficiency due to these influences, comparison of fuel consumption derived e.g. from simulations of solar assisted heating systems with different control strategies and different system designs is questionable.

Simple methods for the calculation of the seasonal efficiency of a boiler within a given heating system use e.g. a spreadsheet calculation that takes into account parameters of the heating system (e.g. average heating load and return temperatures) as yearly, monthly, daily or even hourly values. Examples are the BoilSim method developed within the European SAVE program (Paulsen 1999), as well as the three methods described in the European standard EN 15316-4-1:2008. For detailed studies on the control of the heating system and interactions between different parts of the heating system, however, transient system simulations are more adequate.

A number of boiler models with different features have been presented for spreadsheet calculations and for simulation software. An overview of documented boiler models and their features is given in Table 1.

Bourdouxhe et al. (1994) classified boiler simulation models as white box (physical), black box (empirical) or grey box (mixture of both) models according to their modelling approach. For energy estimating simulations of complex systems, only black box and grey box models are common. The advantages of these models in comparison to white box models are shorter calculation time and simpler parameterization. In addition to the models mentioned in Table 1, other black box models (DeCicco 1990; Landry et al. 1993) and grey box models (Ottin 1986; Idem et al. 1992; Hanby & Li 1995) can be found in literature. A unified simulation model that is capable of simulating the whole range of today's oil, natural gas and wood boilers and at the same time includes flue gas water vapour condensation, power modulation, and the cooling out of the thermal capacitance of the boiler has not been found in this literature review.

Table 1. Features of boiler models based on a literature review.

	black (B) or grey (G) box	fuels			influence of			thermal capacitance			start/stop, standby, and electricity			
		oil	natural gas	wood	return temp.	power mod.	cond. gains	loss separation[a]	Thermal capacitance nodes	combi-boilers[b]	pilot flame	separate draught losses	other start/stop losses[c]	electricity use
Spreadsheet methods														
BoilSim (Paulsen 1999)	B	?	√	?	√	√	√	√	0	√	√	√	O	O
EN 15316-4-1[d] (2008)	G	√	√	√	√	√	√	√	0	?	?	√	O	√
Eco-Boiler (Kemna et al. 2007)	G	√	√	O	√	√	√	√	1	?	√	O	√	√
TRNSYS														
TRNSYS standard Type 6 (SEL et al. 2006)	B	N/A[f]	N/A[f]	N/A[f]	O	O	O	√	0	N/A	O	O	O	O
TESS Type 751 (Thornton 2004)	B	N/A[g]	N/A[g]	N/A[g]	√	√	N/A	√	0	N/A	O	O	O	O
HVAC 1 Primary Toolkit (Lebrun et al. 1993; Bourdouxhe et al. 1994)	G	√	√	O	√	√	O	√	0	N/A	O	O	O	O
IEA ECBCS Annex 10 (Dachelet 1987; Laret 1989)	G	N/A[h]	N/A[h]	N/A[h]	√	√	O	√	0	N/A	O	O	O	O
TRANSSOLAR Type 370 (Koschak et al. 1998)	G	O	√	√	√	O	√	√	1[i]	N/A	O	O	O	O
SERC Type 210 (Nordlander 2003; Persson et al. 2009)	G	O	O	√	√	√	O	√	2	(√)[k]	O	√	√[m]	√
Other simulation tools														
ESP-r (Hensen 1991)	B	O	√	O	√	O	√	√	2	O	O	?	√	O
ESP-r (Beausoleil-Morrison & Haddad 2003)	B	O	√	O	O	O	O	√	1	√	O	O	O	O
EnergyPlus (University of Illinois & University of California 2007)	B	N/A[n]	N/A[n]	N/A[n]	O	√	O	O	0	N/A	O	O	O	√
EMPA NNG model (Remund 1999)	G	√	√	O	√	O	√	√	N	O	O	?	O	O
Claus & Stephan (1985)	G	√	√	O	√	√	O	√	1	O	O	√	O	O

√: included; O: not included; ?: unknown; N/A: not applicable; [a] separation of flue gas losses and thermal losses; [b] boiler used for domestic hot water and space heating fluid in one unit; [c] other than draught losses; [d] boiler cycling method, pp. 29-38; [e] two node & on/off control, pp. 5.31-5.34; [f] constant combustion efficiency; [g] performance map; [h] fuel defined by its heating value only; [i] multi-node version has also been reported; [k] possibility shown in combination with a storage tank model; [m] by means of additional CO emissions; [n] part load ratio efficiency calculation.

Based on these literature studies as well as on own measurements, the following requirements are proposed that a universal space heating boiler model should meet:

- Possibility to simulate different combustibles such as oil, natural gas, and biomass.

- Distinction between losses to flue gas and thermal losses through the boiler envelope to the ambient.

- Possibility to calculate condensation gains.

- Effect of return water temperature on flue gas losses and condensation gains.

- Effect of power modulation on flue gas losses and condensation gains.

- Transient behaviour and cooling out of the thermal capacitance of the boiler with and without water mass flow.

- Calculation of the electricity consumption.

- On-Off cycling of the burner: number of burner starts, additional electricity use, emissions, and losses during start and stop phases.

- Possibility to calculate boiler's annual emissions either within the model or based on model outputs.

For the development of a unified model, the different boiler units listed in Table 2 have been installed and tested in different laboratories. Steady state measurements have been performed covering the range of power modulation. Additional measurements have been performed in cycling operation at and below the minimum turndown ratio, and special test sequences have been used for the determination of the boiler's effective thermal capacitance and heat losses during standby. The investigated boilers were all constructed later than year 2000, and all oil and gas boilers were condensing boilers. Details about the methods used for measurements and parameter identification will be given in a second article submitted to this journal (Haller et al. 2009).

Table 2. Specifications of the investigated boilers based on manufacturers' data.

Reference	nominal heating power [kW]	water volume [l]	empty weight [kg]	modulating [-]	condensing [-]
Pel1	10	59	312	YES	NO
Pel3	40	158	846	YES	NO
Oil1	15	15	58	YES	YES
Gas1	14	N/A	39	YES	YES

Pel: pellets; Oil: fuel oil; Gas: natural gas.

2   Energy balance of boiler units

Energy balances of boiler units are described e.g. in the European standard EN 15316-4-1:2008 (hot water boilers for space heating), DIN 1942:1994 (steam boilers), and Baehr (2005). A Sankey-diagram for the energy balance of a boiler unit is shown in Figure 1. It is common practice for wood fuels to specify values for the wet fuel per kg of wet fuel (wet base, w.b.) and values given for a dry fuel per kg of dry fuel (dry base, d.b.). The conversion from gross heating value to net heating value and from wet base to dry base can be done if the hydrogen content of the fuel (γ_H) and the moisture content of the fuel (γ_{H_2O}) in kg per kg dry fuel are known:

$$NHV^{dry,d.b.} = GHV^{d.b.} - \Delta h_{evap} \cdot 9.079 \cdot \gamma_H \tag{1}$$

$$NHV^{wet,d.b.} = GHV^{d.b.} - \Delta h_{evap} \cdot \left(9.079 \cdot \gamma_H + \gamma_{H_2O}\right) \tag{2}$$

$$NHV^{wet,w.b.} = \left[GHV^{d.b.} - \Delta h_{evap} \cdot \left(9.079 \cdot \gamma_H + \gamma_{H_2O}\right)\right] \cdot \frac{1}{1+\gamma_{H2O}} \tag{3}$$

The boiler model as shown schematically in Figure 1 has been divided into the three processes combustion chamber (1), heat exchanger(s) (2), and heat storage in the thermal capacitance (3). The enthalpy of the fuel, represented by ΔH_{fuel}^{GHV}, is the main energy input into the combustion chamber. It can be divided into the energy input according to its net heating value (ΔH_{fuel}^{NHV}) and two latent parts corresponding to the enthalpy of condensation of water formed from hydrogen in the dry fuel (ΔH_{evap}^{H}) and from the moisture content of e.g. biomass fuel ($\Delta H_{evap}^{H_2O}$), respectively. Further energy inputs result from the sensible and latent parts of the enthalpy of the combustion air ($\Delta H_{air,sens}$ and $\Delta H_{air,lat}$), and the sensible heat of the fuel itself ($\Delta H_{fuel,sens}$). Also electric energy consumed by a boiler (E_{el}) may be converted into thermal energy and contribute to the energy balance of the combustion chamber, e.g. in the case of electric ignition of biomass fuels or in the case of electric fuel oil preheating during burner start ($Q_{el,start}$). Losses of the combustion chamber on the other hand may be due to unburned residues in the ashes (Q_{ash}) and heat losses from the combustion chamber to the ambient ($Q_{cc,amb}$). Hot flue gas produced in the combustion chamber is entering the flue gas to water heat exchanger (FGWHX) (2) with its enthalpy ($\Delta H_{fg,hot}$) and chemical energy contained in unburned components, ($Q_{fg,chem}$). In the heat exchanger process, heat (Q_{hx}) is transferred to water (Q_{wat}) and the thermal capacitance of the boiler (Q_{Ctherm}), whereas the chemical energy ($Q_{fg,chem}$) is lost to the ambient together with the sensible enthalpy ($\Delta H_{fg,sens}$) and the latent enthalpy ($\Delta H_{fg,lat}$) of the flue gas.

Figure 1. Sankey diagram of enthalpy and energy flows of a space heating boiler.

Sensible and latent flue gas losses ($Q_{fg,sens}$ and $Q_{fg,lat}$) are defined by the difference between the sensible and latent enthalpies associated with the mass streams entering the combustion chamber and leaving the boiler with the flue gas:

$$Q_{fg,sens} = \Delta H_{fg,sens} - \Delta H_{air,sens} - \Delta H_{fuel,sens} \qquad (4)$$

$$Q_{fg,lat} = \Delta H_{fg,lat} - \Delta H_{air,lat} \qquad (5)$$

The total flue gas losses also include the chemical losses ($Q_{fg,chem}$):

$$Q_{fg} = Q_{fg,sens} + Q_{fg,lat} + Q_{fg,chem} \qquad (6)$$

Finally, the useful heat leaving the boiler (Q_{wat}) equals the energy transferred by the FGWHX (Q_{hx}), reduced by the energy lost to the ambient ($Q_{hx,amb}$), lost to the boiler draught in standby (Q_{draft}), or stored in the thermal mass (Q_{Ctherm}).

3   The model

3.1   General model concept

A new model for the simulation of space heating boilers has been developed and programmed in FORTRAN (called Type 869) for the use within the simulation environment TRNSYS 16. Its mathematical description is presented in this section. Figure 2 shows the general information flow diagram of the model.

The three main calculation steps shown in Figure 2 are similar to the modelling schemes proposed by Lebrun et al. (1993) and ASHRAE (2005). In a first step (Figure 2, step 1) the combustion chamber energy and mass balances are calculated. In a second step (step 2) the temperature and enthalpy of the flue gas after the flue gas to water heat exchanger (FGWHX) are calculated. Depending on the type of boiler, this step may include the calculation of an additional flue gas to combustion air heat exchanger (FGAHX). Up to this point, all calculations are performed assuming steady state conditions. A time dependent, hence transient, calculation is only

performed for the heat balance of the boiler's thermal capacitance (step 3). From this third step, losses from the heat exchanger to the ambient, heat transfer to the boiler water flow, and the change of stored heat in the thermal capacitance of the boiler are obtained.

parameters and inputs   **model / type 869**   **outputs**

optional

user defined fuel:
GHV
$\gamma_C, \gamma_H, \gamma_O, \gamma_N, \gamma_S, \gamma_{ash}, cp_{fuel}$

$FuelType$

γ_{H_2O}

$fr_{cc,ash}, fr_{cc,amb}$

automatic cycling calculation:
$\dot{Q}_{max}^{GHV}, \dot{Q}_{min}^{GHV}, \dot{Q}_{start}^{GHV}$
$t_{ON}, t_{SET}, t_{OFF}, t_{MAX}$
$\tau_{start}, \tau_{ON,min}, \tau_{OFF,min}$
$Q_{el,start}, m_{CO,start}$

t_{fuel}

$\dot{m}_{fuel,wet}$

modulation dependent lambda:
$\lambda_{min}, \lambda_{max}$

λ

$t_{air}, p_{air}, RH_{air}$

emissions calculation:
$ppm_{CO,min}, ppm_{CO,max}$

ppm_{CO}

auxiliary energy consumption:
$P_{el,min}, P_{el,max}, P_{el,OFF}$

FGWHX model 1:
$dT_{nom}, dT_{hx,fg}, dT_{hx,wat}$

$P_{nom}^{GHV}, \dot{m}_{wat,nom}$

$RH_{fg,max}$

OR

FGWHX model 2:
$\varepsilon_{nom}, d\varepsilon_{hx,fg}, d\varepsilon_{hx,wat}$

1-10 Paramters

OR

FGWHX model 3:
$HX_{mode}, UA_{hx,nom}, n_{hx,fg}$
$fr_{Rhx,fg}, fr_{Rhx,met}, n_{hx,wat}, fac_{wet}$
$UA_{gg,nom}, m_{hx,gg}, RH_{fg,gg,max}$

$\dot{m}_{wat,in}, t_{wat,in}$

C_{therm}

$UA_{hx,amb,ON}, UA_{hx,amb,OFF}$

t_{amb}

step 1
combustion chamber
(steady state)

step 2
FGWHX
(steady state)

(2a option)
FGAHX

step 3
balance of thermal capacitance

S T E A D Y   S T A T E   C A L C U L A T I O N

T R A N S I E N T   C A L C U L A T I O N

GHV / NHV

$\dot{Q}_{fuel}^{GHV}$

$\dot{Q}_{ash}, \dot{Q}_{cc,amb}, \dot{Q}_{fg,chem}$

$\dot{m}_{CO}, \dot{m}_{fg,wet}$

$P_{el}, \dot{Q}_{el,start}$

$t_{fg,out}, \dot{m}_{H_2O,cond}$

$\dot{Q}_{fg,sens}, \dot{Q}_{fg,lat}$

$\dot{Q}_{hx}$

$\dot{Q}_{wat,out}, \dot{Q}_{hx,amb}, \dot{Q}_{Ctherm}$

$t_{wat,out}$

N_{start}, fr_{ON}

$\dot{Q}_{Balance}$

Figure 2. General information flow diagram of the boiler model. Grey background indicates "boiler parameters" that are used for the characterization of the boiler itself.

3.2 Combustion chamber

3.2.1 *Excess air and carbon monoxide emissions in steady state*

For modulating boilers the excess air factor (λ) for combustion and the carbon monoxide (CO) concentration in the flue gas may depend on the power modulation, hence on $\dot{Q}_{fuel}^{GHV}$. In Type 869 λ is calculated as a quadratic function or a linear function of $\dot{Q}_{fuel}^{GHV}$. The linear function is shown in Equation

(7) and Figure 3(a). The volumetric CO concentration (ppm_{CO}) is calculated as a linear function of $\dot{Q}_{fuel}^{GHV}$ with Equation (8), (Figure 3(b)).

$$\lambda = \lambda_{min} + \left(1 - fr_{mod}\right) \cdot \left(\lambda_{max} - \lambda_{min}\right) \qquad (7)$$

$$ppm_{CO} = ppm_{CO,min} + \left(1 - fr_{mod}\right) \cdot \left(ppm_{CO,max} - ppm_{CO,min}\right) \qquad (8)$$

With:

$$\dot{Q}_{fuel}^{GHV} = \dot{m}_{fuel,wet} \cdot GHV^{w.b.} \qquad (9)$$

$$fr_{mod} = \frac{\dot{Q}_{fuel}^{GHV} - \dot{Q}_{min}^{GHV}}{\dot{Q}_{max}^{GHV} - \dot{Q}_{min}^{GHV}} \qquad (10)$$
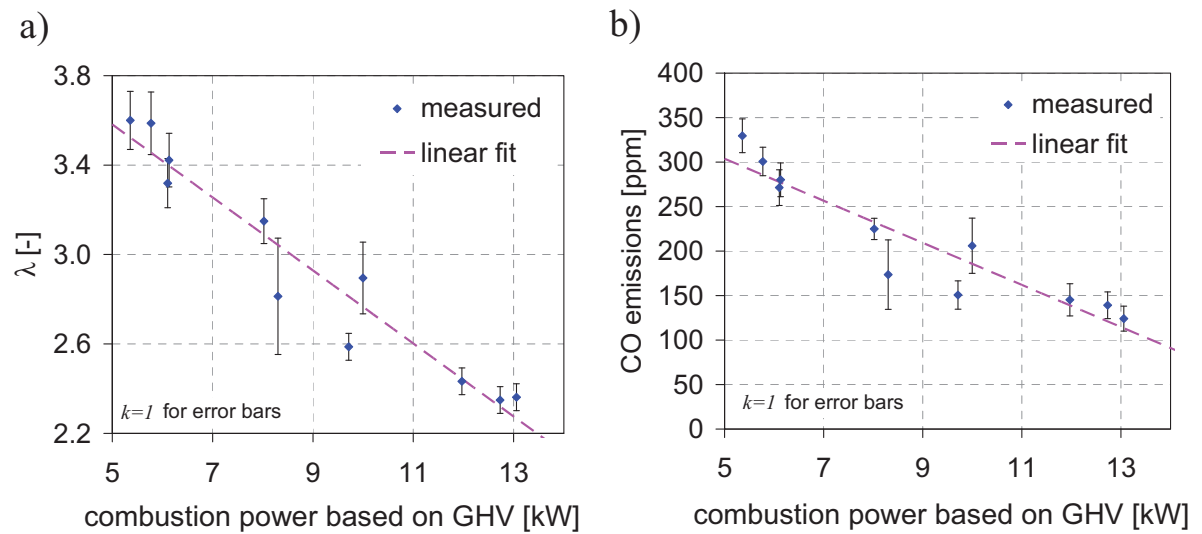
a)

b)

Figure 3. Dependency of λ (a) and CO emissions (b) on the combustion power for the boiler Pel1, with combined measurement uncertainty (type A and type B).

3.2.2 Combustion chamber losses

The main influencing factors on heat losses through the boiler envelope are the temperature difference between the boiler envelope and the ambient, and the combined surface heat transfer coefficient (convection and radiation). Most existing models assume that heat losses through the boiler envelope depend on the temperature difference between the boiler water and the ambient. Persson (2006, p 27) found that heat losses through the boiler envelope additionally depended on the combustion power for two out of three investigated pellet boilers. This dependency on the combustion power is also shown by Konersmann et al. (2007) for boiler Pel1. Thermographic pictures (Figure 4) show that the envelope surface temperatures of boiler Pel3 depend on both, the boiler water temperature and the combustion power. Additional thermographic pictures also showed that the dependency of heat losses on the combustion power is most likely a result of heat losses from the combustion chamber.

In the presented model, thermal heat losses from the combustion chamber and losses due to unburned residues in the ash are calculated as a constant fraction of the combustion power:

$$\dot{Q}_{cc,amb} = fr_{cc,amb} \cdot \dot{Q}_{fuel}^{GHV} \tag{11}$$

$$\dot{Q}_{ash} = fr_{cc,ash} \cdot \dot{Q}_{fuel}^{GHV} \tag{12}$$
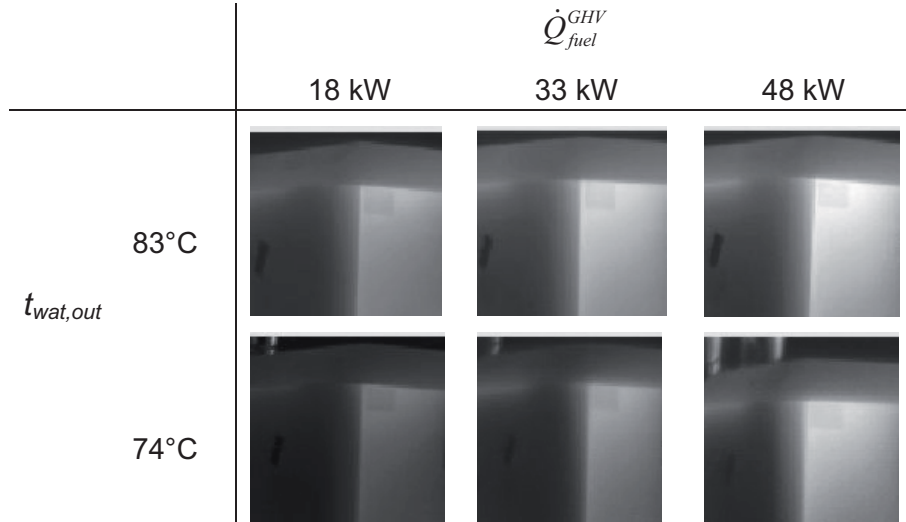
Figure 4. Thermographic pictures of a 40 kW pellet boiler (Pel3) with different flow temperature and different combustion power in steady state. Scale: 25°C (black) – 50°C (white).

3.3 Flue gas to water heat exchanger and flue gas losses

Flue gas losses are usually the predominant losses during steady state operation. Therefore, the model for the calculation of flue gas losses has to be chosen carefully. Three different approaches have been tested for the calculation of the temperature of the leaving flue gas ($t_{fg,out}$) in steady state operation. This temperature is needed later on for calculating sensible losses as well as latent gains. The general scheme of flue gas loss calculation is presented in Figure 5. In step 1, the excess air of combustion (λ) and the CO concentration in the flue gas (ppm_{CO}) are calculated as functions of the current combustion power (see section 3.2). In step 2, $t_{fg,out}$ is first calculated as a function of the operating conditions of the boiler and, depending on the model chosen, also of other previously calculated values (e.g. λ, O_{min},...).

Figure 5. General scheme for the prediction of flue gas losses (simplified).

Different models for the calculation of $t_{fg,out}$ are presented in the following section.
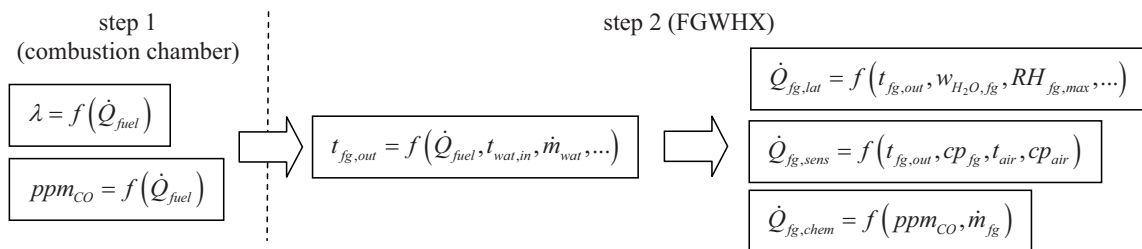
3.3.1 Different models for the flue gas to water heat exchanger

Model 1: The empirical deltaT-approach

A simple approach for the modelling of the leaving flue gas temperature ($t_{fg,out}$) has been used e.g. by Koschak et al. (1998). In this approach shown with Equation (13), it is assumed that the temperature of the leaving flue gas is a constant temperature difference $dT_{fg,out}$ above the inlet water temperature ($t_{wat,in}$). (Equation (13)) The measurement results presented in Figure 6 show that the experimentally determined $dT_{fg,out}$ may depend on power modulation ($\dot{Q}_{fuel}^{GHV}$) and on the water mass flow rate ($\dot{m}_{wat}$). Therefore, these dependencies have been introduced in the empirical delta-T approach with Equation (14).

$$t_{fg,out} = t_{wat,in} + dT_{fg,out} \qquad (13)$$

$$dT_{fg,out} = dT_{nom} + dT_{hx,fg} \cdot \left(1 - \frac{\dot{Q}_{fuel}^{GHV}}{\dot{Q}_{nom}^{GHV}}\right) \cdot 100 + dT_{hx,wat} \cdot \left(1 - \frac{\dot{m}_{wat}}{\dot{m}_{wat,nom}}\right) \cdot 100 \qquad (14)$$

Where $dT_{hx,fg}$ and $dT_{hx,wat}$ are boiler specific parameters whose values may be smaller or larger than zero.
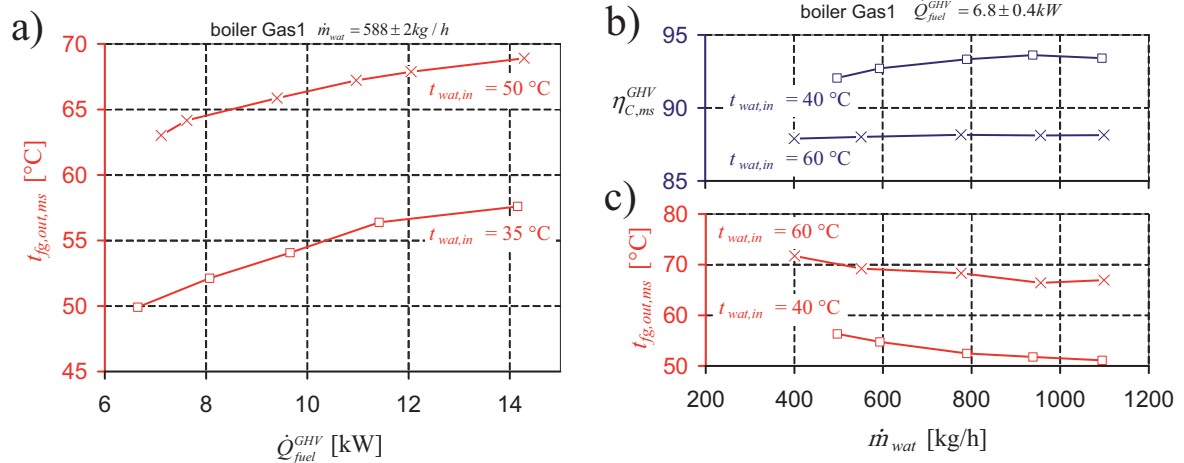

Figure 6. Dependency of the leaving flue gas temperature on the combustion power (a) and dependency of the combustion efficiency (b) and the flue gas temperature (c) on the water return temperature for boiler Gas1.

Model 2: The empirical effectiveness approach

In this approach the flue gas to water heat transfer is modelled with an empirical heat exchanger effectiveness. The effectiveness of the heat exchanger is assumed to be composed of a base effectiveness determined at nominal conditions and correction terms that account for changes in $\dot{Q}_{fuel}^{GHV}$ and $\dot{m}_{wat}$ shown in Equation (15) and (16).

$$\varepsilon_{hx} = \varepsilon_{nom} + d\varepsilon_{hx,fg} \cdot \left(1 - \frac{\dot{Q}_{fuel}^{GHV}}{\dot{Q}_{nom}^{GHV}}\right) + d\varepsilon_{hx,wat} \cdot \left(1 - \frac{\dot{m}_{wat}}{\dot{m}_{wat,nom}}\right) \tag{15}$$

$$t_{fg,out} = t_{fg,hot} - \varepsilon_{hx} \cdot \left(t_{fg,hot} - t_{wat,in}\right) \tag{16}$$

The temperature of the flue gas before the FGWHX ($t_{fg,hot}$) is calculated with the governing mass and energy balances (e.g. Baehr 2005) and the assumption of adiabatic combustion.

Model 3: The effectiveness-NTU approach

The effectiveness-NTU approach has been used by Lebrun et al. (1993) for the calculation of FGWHX of oil boilers with up to 1 MW of heating power. This method has been further developed based on suggestions by Lebrun (personal communication by email, 26 June 2007) and tests on the condensing gas boiler Gas1 (Dröscher 2008). Effectiveness-NTU relationships for counterflow, parallel flow and crossflow from Kays & London (1984) have been implemented in Type 869. The mathematical description of this model is shown in Appendix 1.

3.3.2 Calculation of sensible losses, chemical losses and latent gains

From the calculations above, λ, $t_{fg,out}$, and ppm_{CO} are known. Thus, sensible losses ($Q_{fg,sens}$) can be calculated based on mass balances and enthalpy functions of flue gas and air with Equations (14) and (17) to (19). For the enthalpy functions $\Delta h_{fg,sens}$ and $\Delta h_{air,sens}$ it is assumed that all water is in its gaseous state.

$$\Delta H_{fg,sens} = m_{fg,wet} \cdot \Delta h_{fg,sens}\left(\lambda, t_{fg,out}, w_{fg,hot}\right) \tag{17}$$

$$\Delta H_{air,sens} = m_{air} \cdot \Delta h_{air,sens}\left(t_{air}, w_{air}\right) \tag{18}$$

$$\Delta H_{fuel,sens} = cp_{fuel} \cdot \left(t_{fuel} - 25°C\right) \tag{19}$$

Latent gains are sometimes calculated assuming saturation of the flue gas with water vapour whenever its temperature at the outlet of the FGWHX is below the dew point of the hot flue gas before the FGWHX (Koschak et al. 1998; EN 15316-4-1:2008). However, literature of thermodynamics (Baehr 2005, p. 475) as well as own measurements indicate that under saturation may well occur. This can be explained by the fact that the temperature at the surface of the FGWHX on the flue gas side may be well below the dew point –

thereby causing condensation – before the bulk flue gas temperature reaches the dew point. Type 869 calculates latent gains based on the known water load of the hot flue gas ($w_{fg,hot}$) before the FGWHX, the temperature at which the flue gas leaves the boiler, and the assumption of a maximum relative humidity ($RH_{fg,max}$) that may not be surpassed. Thus, the maximum vapour load of the leaving flue gas ($w_{fg,vap,max}$), and the condensate mass (m_{cond}) are:

$$w_{fg,vap,\max} = R_{ratio} \cdot \frac{RH_{fg,\max} \cdot p_{sat,fg}}{p_{air} - RH_{fg,\max} \cdot p_{sat,fg}} \tag{20}$$

$$m_{cond} = MAX\left(w_{fg,hot} - w_{fg,vap,\max}; 0\right) \cdot m_{fg,dry} \tag{21}$$

Latent losses are calculated with Equation (5) and the remaining enthalpy of condensation of water vapour in the leaving flue gas:

$$\Delta H_{fg,lat} = \left(m_{fg,H_2O} - m_{cond}\right) \cdot \Delta h_{evap}\left(t_{fg,out}\right) \tag{22}$$

Chemical losses ($Q_{fg,chem}$) are calculated with the specific enthalpy of reaction of the oxidation of CO ($\Delta h_{CO \to CO_2} = -10'106 kJ/kg$):

$$Q_{fg,chem} = -\Delta h_{CO \to CO_2} \cdot m_{CO} \tag{23}$$

3.4 Transient behaviour of the thermal capacitance

In this model, transient behaviour is assumed to be relevant only for the boiler's thermal capacitance (Figure 2).

To calculate the energy balance of the thermal capacitance of the boiler, the following simplifications are made:

- Thermal capacitance of the empty boiler and thermal capacitance of the water in the boiler are lumped into one effective thermal capacitance and treated as one thermal node.

- The boiler's effective thermal capacitance is simulated like a fully mixed water body. Thus, the mean temperature of the boiler's thermal capacitance equals the temperature of the boiler water outlet (flow temperature).

Heat losses from the effective thermal capacitance to the ambient are calculated with an overall UA-value ($UA_{hx,amb}$) that depends on the burner operation. If no combustion is taking place, its value may be higher due to the missing cooling effect of combustion air flow between the FGWHX and the boiler envelope (Figure 7). Additionally, natural draught airflow during burner standby may have a cooling effect on the boiler envelope, and at the same time cool out the FGWHX from the inside. These effects are not modelled in detail in separately in Type 869, but lumped into $\dot{Q}_{hx,amb,OFF}$ instead.

$$\dot{Q}_{hx,amb} = UA_{hx,amb} \cdot \left(t_{B,avg} - t_{amb}\right) \tag{24}$$

With

$UA_{hx,amb} = UA_{hx,amb,OFF}$ during times without combustion

and

$UA_{hx,amb} = UA_{hx,amb,ON}$ during times with combustion.
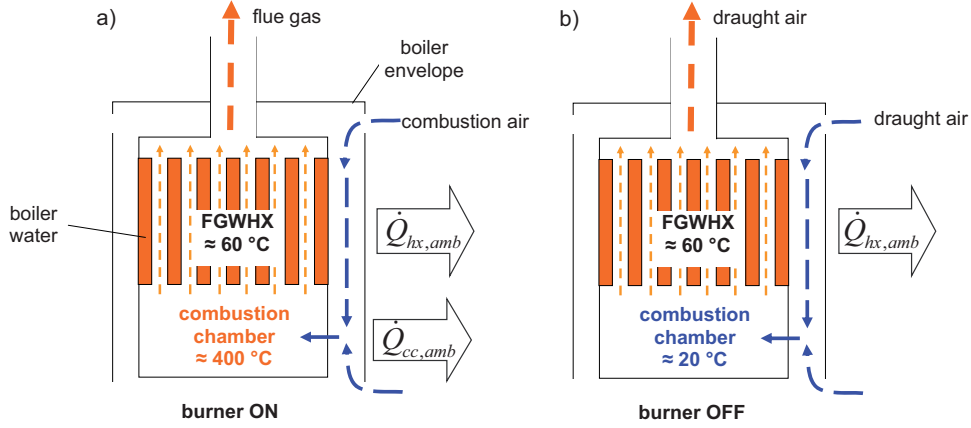
Figure 7. Different heat loss mechanisms of a space heating boiler with burner ON (a) and burner OFF (b).

Heat transferred in the FGWHX ($\dot{Q}_{hx}$) is either carried away with the water flow ($\dot{Q}_{wat,out}$), lost to the ambient ($\dot{Q}_{hx,amb}$) or stored in the thermal mass of the boiler (Q_{Ctherm}):

$$\dot{Q}_{hx} - \dot{Q}_{wat,out} - \dot{Q}_{hx,amb} - \dot{Q}_{Ctherm} = 0 \tag{25}$$

$$t_{B,avg}(\tau) = t_{wat,out}(\tau) \tag{26}$$

$$\dot{Q}_{wat,out} = \dot{C}_{wat} \cdot \left[t_{wat,out}(\tau) - t_{wat,in} \right] \tag{27}$$

$$\dot{Q}_{Ctherm} = C_{therm} \cdot t_{B,avg}(\tau) \frac{d}{d\tau} \tag{28}$$

To calculate $t_{wat,out}(\tau)$ after a certain time and the average outlet temperature of a time step ($t_{wat,out,avg}$), the following equations are derived from the equations above:

$$t_{wat,out}(\tau) = t_{inf} - \left[t_{inf} - t_{wat,out,A} \right] \cdot EXP(-G_1 \cdot \tau) \tag{29}$$

$$t_{wat,out,avg} = t_{inf} + \frac{\left[t_{inf} - t_{wat,out,A} \right] \cdot \left[EXP(-G_1 \cdot \tau) - 1 \right]}{G_1 \cdot \tau} \tag{30}$$

Where $t_{wat,out,A} = t_{wat,out}(\tau = 0)$ is the outlet temperature at the beginning of the time step, and t_{inf} is the temperature of the water outlet of the boiler after an infinite time with constant $\dot{Q}_{hx}$, t_{amb}, $\dot{C}_{wat}$, and $t_{wat,in}$.

$$t_{inf} = \frac{G_2}{G_1} \tag{31}$$

$$G_1 = \frac{UA_{hx,amb} + \dot{C}_{wat}}{C_{therm}} \qquad (32)$$

$$G_2 = \frac{\dot{Q}_{hx} + UA_{hx,amb} \cdot t_{amb} + \dot{C}_{wat} \cdot t_{wat,in}}{C_{therm}} \qquad (33)$$

The time τ needed to bring the boiler to a certain temperature of $t_{wat,out}(\tau) = t_{wat,out,B}$ is:

$$\tau = \frac{LN\left(\dfrac{t_{inf} - t_{wat,out,A}}{t_{inf} - t_{wat,out,B}}\right)}{G_1} \qquad (34)$$

3.5   Electricity use

Electricity use during burner operation is calculated as a linear function of power modulation, i.e.:

$$P_{el} = P_{el,min} + \dot{fr}_{mod} \cdot \left(P_{el,max} - P_{el,min}\right) \qquad (35)$$

While the burner is not in operation, electricity consumption is $P_{el} = P_{el,OFF}$. This electric power is considered to be lost to the ambient ($\dot{Q}_{el,amb} = P_{el}$) and does therefore not influence the thermal energy balance of the boiler. Thermally relevant electricity consumption is treated in section 3.6.

3.6   Control of burner start, power modulation and stop

Type 869 offers the possibility to provide the fuel mass flow rate into the combustion chamber ($\dot{m}_{fuel,wet}$) as a variable input which may be fed by user written controller components. Alternatively, the following control algorithm for burner start, power modulation and burner stop is implemented in Type 869: Whenever the outlet temperature of the boiler drops below the temperature t_{ON}, the burner start phase begins and lasts for the time τ_{start} with combustion power $\dot{Q}_{start}^{GHV}$. After this time, normal burner operation begins and lasts for at least $\tau_{ON,min}$. During normal burner operation, the combustion power is controlled within the limits of power modulation set by $\dot{Q}_{min}^{GHV}$ and $\dot{Q}_{max}^{GHV}$ in order to reach and maintain the outlet temperature set point (t_{SET}). If the boiler outlet temperature surpasses t_{SET} running on $\dot{Q}_{min}^{GHV}$, the burner will be switched off as soon as t_{OFF} is reached. During τ_{start} and during $\tau_{ON,min}$, the burner will not turn off when its outlet temperature reaches t_{OFF}, but only when it reaches t_{MAX}. Once the burner is off, it will remain off at least for the time $\tau_{OFF,min}$.

Additional CO emissions and electricity use for start and stop phases are lumped together in the values $m_{CO,start}$ and $Q_{el,start}$ which are added to the other CO emissions and electricity use during each τ_{start}. Unlike electricity use during normal burner operation, additional electric energy use during τ_{start} is considered to be used for fuel ignition or preheating and therefore enters the combustion chamber calculation as thermal energy.

4 Discussion

The development of the presented boiler model was motivated by the demand for a versatile unified model for the simulation of space heating boilers for energy estimating software such as TRNSYS. Starting from a detailed physical analysis of the processes in the boiler, several simplifications had to be made in order to meet the aim of simplicity, ease of parameterization and low computation time. These simplifications are discussed in this section.

The presented boiler model strictly separates the FGWHX from the combustion chamber, although in reality the latter already takes up part of the heat of the reaction and transfers it to water which may be in direct contact with the material of the combustion chamber. Furthermore, the combustion chamber itself is not considered to have a thermal capacitance on its own. In reality however, the thermal capacitance of the combustion chamber of, e.g., large biomass boilers may be significant, and the temperature of this thermal mass may be far higher than the temperature of the boiler water. This may also have a considerable effect on the inertia of the boiler's temperature response during transient operation.

In the presented model, combustion chamber and flue gas calculations are always performed assuming steady state conditions. This is a simplification, since changes of the combustion power or of the inlet temperature will also lead to transients in flue gas temperatures and condensation gains. However, assuming the new steady state efficiency too early will be compensated to some extent by assuming the next steady state efficiency too early as well. In the long run, these effects are expected to partially compensate each other.

The effectiveness-NTU relationships used for model 3 do not include heat transfer by radiation, and the assumption of an adiabatic flue gas temperature at the entrance of the heat exchanger may significantly differ from reality.

Further, so called combi-boilers that provide domestic hot water and space heating energy within one unit, boilers with considerable temperature stratification within the boiler water, and burners integrated in solar heat storages can not be simulated with this boiler model alone. For these cases, the presented model may be combined with a stratified storage tank model.

For biomass boilers, the burner start phase could be further divided into (a) feeding fuel into the combustion chamber (b) ignition of the fuel, and (c) stabilising the flame. Each of these sub-phases has its own ventilation rate, fuel burning rate, electricity use and CO emission. The duration of the ignition might thereby be dependent on the time that has passed since the last burner stop. Also a separate burner stop phase could be considered where remaining solid fuel in the combustion chamber is burned (the amount of remaining fuel at the time of the stop signal might be variable) and an induced draught fan operating until the fuel is completely burned, etc. In Type 869, all these effects are lumped into a few parameters for start phase time and associated additional electricity use, CO-emissions and fuel consumption power.

During standby, the model does not distinguish between losses caused by flue gas duct draught and heat losses from the boiler envelope to the ambient. However, draught losses are difficult to predict since they do not only depend on the boiler, but also on the flue gas duct or chimney of a particular installation and the meteorological conditions.

In addition to the electric heating energy during the start phase considered as heat input to the boiler, also a fraction of electricity use during steady burner operation might enter the thermal balance of the boiler. However, these inputs are expected to be negligible compared to the combustion power of the boiler.

Furthermore, effects such as heat exchanger fouling, a pilot flame during burner standby and pre-purge ventilation losses are not included explicitly in this model.

Other emissions than CO such as nitrous oxides or particles are not included in the model, and the linear dependency of CO on the combustion power might be too simple for some boiler units. In this case, additional emissions calculations can be done outside Type 869 based on the outputs of this model.

In all these points, the presented boiler model uses simplifying approximations in order to save work needed to determine additional boiler characteristics, computation time, or simply because the processes involved are too stochastic to be simulated accurately. Most of these effects can be lumped together and integrated into the available loss terms of the boiler, or treated with external calculations based on the outputs of the presented boiler model.

5   Conclusion

A semi-physical (or semi-empirical) boiler model has been developed for the simulation of oil, gas and biomass space heating boilers. The model includes features that have already been described by previous authors, as well as new features that have been developed based on own measurements. The most important features are the ability to reflect the influence of space heating return temperature, power modulation and condensation gains on the flue gas losses of the boiler, the simulation of a thermal capacitance including its heat losses during standby and operation, and the ability to calculate carbon monoxide emissions and electricity use dependent on power modulation and number of burner starts.

New features of the presented boiler model are the unification of models for oil, gas and biomass boilers into one model, and the possibility to use the model for any fuel defined by the user by its elementary composition and the gross heating value. Further novelties include the combination of steady state calculation for the flue gas to water heat transfer with an explicit solution for the time dependent temperature change of the boiler's thermal capacitance. Thus, it is possible to simulate the boiler's thermal capacitance with shorter calculation time than e.g. for multi-node models that depend on iterative calculations for convergence. Other features that have not been found explicitly in the presented literature study are the distinction between losses from the boiler water (thermal capacitance) and the combustion chamber, the

assumption of different heat loss coefficients from the boiler water to the ambient during burner operation and during burner standby, and the possibility of undersaturation of the leaving flue gas.

The parameterization of the model and a detailed comparison of modelling results with measured data from different boilers will be presented in a second article within this journal.

Acknowledgement

Appendix 1: Effectiveness-NTU model

When condensation occurs, the flue gas side of the FGWHX (flue gas to water heat exchanger) is split into a dry section and a wet section where condensation occurs (Figure 8). The heat exchanger effectiveness ε is calculated separately for the dry section and for the wet section. If no condensation occurs, the calculation simplifies to the dry section only. The dry-wet boundary shown in Figure 8 has to be found iteratively by application of the mass balances and the thermodynamic states of the two flow streams.
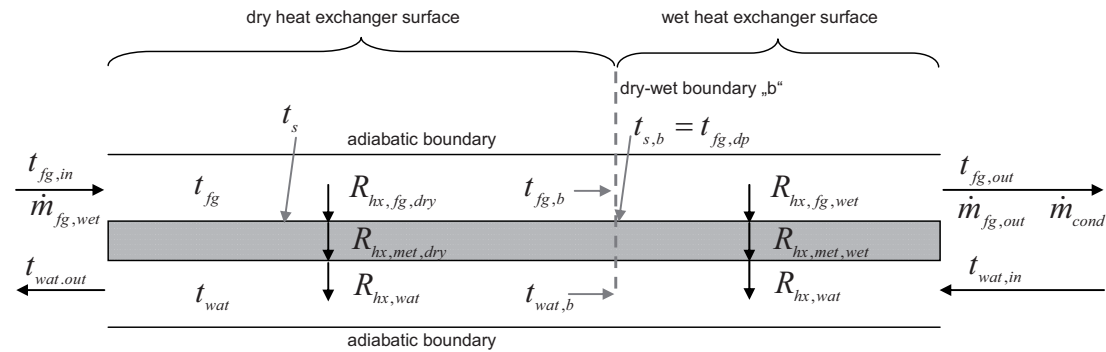
Figure 8. Flue gas to water heat exchanger split into a dry section and a wet section in the case of water vapour condensation.

The overall heat transfer coefficient area product for the dry section ($UA_{hx,dry}$) and the wet section ($UA_{hx,wet}$) is calculated with Equations (36) and (37):

$$UA_{hx,dry} = \frac{1 - fr_{hx,wet}}{R^*_{tot,dry}} \tag{36}$$

$$UA_{hx,wet} = \frac{fr_{hx,wet}}{R^*_{tot,wet}} \tag{37}$$

The overall heat transfer resistance term ($R^*_{tot,dry}$) of the completely dry heat exchanger is the sum of the heat transfer resistances on the water side ($R^*_{hx,wat}$), in the metal wall ($R^*_{hx,met,dry}$), and on the flue gas side of the heat exchanger ($R^*_{hx,fg,dry}$):

$$R^*_{tot,dry} = R^*_{hx,fg,dry} + R^*_{hx,met,dry} + R^*_{hx,wat} \tag{38}$$

$R^*_{hx,fg,dry}$ and $R^*_{hx,wat}$ may both be dependent on the mass flow rate of the fluid on the respective sides:

$$R^*_{hx,fg,dry} = R^*_{hx,fg,nom} \cdot \left(\frac{\dot{m}_{fg,wet,nom}}{\dot{m}_{fg,wet}} \right)^{n_{hx,fg}} \tag{39}$$

$$R^*_{hx,wat} = R^*_{hx,wat,nom} \cdot \left(\frac{\dot{m}_{wat,nom}}{\dot{m}_{wat}} \right)^{n_{hx,wat}} \tag{40}$$

Where $R^*_{hx,fg,nom}$ and $R^*_{hx,wat,nom}$ are the heat transfer resistance terms under nominal, non-condensing conditions. $n_{hx,fg}$ and $n_{hx,wat}$ are boiler dependent exponents that reflect the heat transfer resistance's dependency on the respective mass flow rates. The nominal resistances are calculated based on the UA-values obtained from a test under nominal conditions together with parameters that specify which fraction of the heat transfer resistance is attributed to the flue gas side ($fr_{Rhx,fg,nom}$) and to the wall ($fr_{Rhx,met,nom}$) of the heat exchanger. These additional parameters are determined with additional tests to the one at nominal conditions.

$$R^*_{hx,fg,nom} = fr_{Rhx,fg,nom} \cdot \left(UA_{hx,nom}\right)^{-1} \tag{41}$$

$$R^*_{hx,met,nom} = fr_{Rhx,met,nom} \cdot \left(UA_{hx,nom}\right)^{-1} \tag{42}$$

$$R^*_{hx,wat,nom} = \left(1 - fr_{Rhx,fg,nom} - fr_{Rhx,met,nom}\right) \cdot \left(UA_{hx,nom}\right)^{-1} \tag{43}$$

If necessary, the heat transfer resistances for the wet side can be increased with the parameter fac_{wet}. This affects the overall heat transfer resistance term ($R^*_{hx,tot,wet}$) for a completely wet heat exchanger.

$$R^*_{hx,fg,wet} = fac_{wet} \cdot R^*_{hx,fg,dry} \tag{44}$$

$$R^*_{hx,met,wet} = fac_{wet} \cdot R^*_{hx,met,dry} \tag{45}$$

$$R^*_{hx,tot,wet} = R^*_{hx,fg,wet} + R^*_{hx,met,wet} + R^*_{hx,wat} \tag{46}$$

If no condensation occurs and only the heat transfer resistance on the flue gas side is relevant, Equations (36) to (46) are reduced to:

$$UA_{hx} = UA_{hx,nom} \cdot \left(\frac{\dot{m}_{fg,wet}}{\dot{m}_{fg,wet,nom}}\right)^{n_{hx,fg}} \tag{47}$$

The capacity flow rates of the flue gas used for the calculation of $\varepsilon_{hx,dry}$ and $\varepsilon_{hx,wet}$ are calculated with:

$$\dot{C}_{fg,dry} = \dot{m}_{fg,wet} \cdot \frac{\Delta h_{fg,hot} - \Delta h_{fg,b}}{t_{fg,hot} - t_{fg,b}} \tag{48}$$

$$\dot{C}_{fg,wet} = \dot{m}_{fg,wet} \cdot \frac{\Delta h_{fg,b} - \Delta h_{fg,out}}{t_{fg,b} - t_{fg,out}} \tag{49}$$

For a given heat exchanger arrangement, the effectiveness of the heat exchanger ε_{hx} is defined by the effectiveness-NTU relationship of the form:

$$\varepsilon_{hx} = f\left(UA_{hx}, \dot{C}_{fg}, \dot{C}_{wat}\right) \tag{50}$$

This effectiveness is applied to enthalpy differences instead of temperature differences for the dry section.

$$h_{fg,out} = h_{fg,hot} - \varepsilon_{hx,dry} \cdot \left(\Delta h_{fg,hot} - \Delta h_{fg,b,min}\right) \tag{51}$$

Where $h_{fg,b,min}$ is the fictive enthalpy of a flue gas at the temperature of the water at the dry-wet boundary.

For the wet section of the FGWHX, wet bulb temperature differences are taken as the driving force for the heat transfer. This approach is derived from the Merkel theory of evaporative cooling (Merkel 1925) and is commonly used for the calculation of dehumidifying coils (VDI 2006; ASHRAE 2000). Its application for the calculation of heat exchangers of condensing boilers has also been proposed by J. Lebrun (personal communication by email, 26 June 2007).

$$t_{fg,out,wb} = t_{fg,b,wb} - \varepsilon_{hx,wet} \cdot \left(t_{fg,b,wb} - t_{wat,in} \right) \tag{52}$$

The determination of the wet fraction of the heat exchanger is done with the known surface temperature at the dry-wet boundary and the heat exchanger characteristic X (termed coil characteristic e.g. in ASHRAE 2000):

$$t_{s,b} = t_{fg,dp} \tag{53}$$

$$X = \frac{R^*_{hx,wat} + R^*_{hx,met,dry}}{R^*_{hx,fg,dry} \cdot cp_{fg}} = \frac{t_{s,b} - t_{wat,b}}{h_{fg,b} - h_{fg,dp}} \tag{54}$$

To solve the set of equations, the energy balances of both heat exchanger sections are used:

$$\left(\Delta h_{fg,b} - \Delta h_{fg,out} \right) \cdot \dot{m}_{fg,wet} = \left(t_{wat,b} - t_{wat,in} \right) \cdot \dot{C}_{wat} \tag{55}$$

$$\left(\Delta h_{fg,hot} - \Delta h_{fg,b} \right) \cdot \dot{m}_{fg,wet} = \left(t_{wat,out} - t_{wat,b} \right) \cdot \dot{C}_{wat} \tag{56}$$

Finally, the leaving flue gas temperature is obtained from the enthalpy of the leaving flue gas and the restriction of maximum relative humidity set by $RH_{fg,max}$.

An additional combustion air pre-heater has been introduced in the model because measured flue gas temperatures of boiler Oil1 were significantly lower than the return temperatures of the heated fluid. It is assumed that this is the effect of combustion air pre-heating by the leaving flue gas. Therefore, an additional heat exchanger is calculated with the effectiveness-NTU method and a simplified dependency of the UA value on the flue gas mass flow rate only as the mass flow rates on both sides of this heat exchanger are almost equal.

$$UA_{gg} = UA_{gg,nom} \cdot \left(\frac{\dot{m}_{fg,wet}}{\dot{m}_{fg,wet,nom}} \right)^{n_{hx,gg}} \tag{57}$$

No splitting into a dry and a wet section is performed for this heat exchanger.

6   Literature

ASHRAE, 2005. Chapter 32 - Energy Estimating and Modeling Methods. In: *ASHRAE Handbook of Fundamentals*. Atlanta, GA: American Society of Heating, Refrigeration and Air Conditioning Engineers.

ASHRAE, 2000. Chapter 21 - Air-Cooling and Dehumidifying Coils. In: *ASHRAE Handbook of HVAC Systems and Equipment*. Atlanta, GA: American Society of Heating, Refrigeration and Air Conditioning Engineers.

Baehr, H.D., 2005. *Thermodynamik: Grundlagen und technische Anwendungen*, 12. Auflage. Heidelberg Berlin: Springer. ISBN 3-540-23870-0. (German)

Beausoleil-Morrison, I. & Haddad, K., 2003. Simulating Fuel-Fired Combination Space Heating and Domestic Water Heating Systems. In: *Eight Internationl IBPSA Conference*. Eindhoven, Netherlands, pp. 93-100.

Bourdouxhe, J., Grodent, M., Lebrun, J., Saavedra, C., 1994. A Toolkit for Primary HVAC System Energy Calculation - Part 1: Boiler Model. In: *ASHRAE Trans.* 100(2), 759-773.

Claus, G. & Stephan, W., 1985. A general computer simulation model for furnaces and boilers. In: *ASHRAE Trans.*, 91(1), 47–59.

DIN 1942:1994 (E) *Acceptance testing of steam generators*. VDI Code of practice.

Dachelet, M., 1987. Subroutine Type 7 – static boiler [online]. Available from: http://sel.me.wisc.edu/trnsys/trnlib/trnlib16/annex17/type211.for. Accessed 12 January, 2009.

DeCicco, J., 1990. Applying a Linear Model to Diagnose Boiler Fuel Consumption. In: *ASHRAE Trans.* 96(1), 296-304.

Dröscher, A., 2008. *Flue gas to water heat transfer in residential gas boilers with modulation and vapour condensation*. Thesis (Master). Institute of Thermal Engineering, Graz University of Technology, Austria.

Drück, H., 2006. *Multiport store model for TRNSYS - Type 340 - V1.99F*.

EN 15316-4-1:2008 (D) *Heizungsanlagen in Gebäuden - Verfahren zur Berechnung der Energieanforderungen und Nutzungsgrade der Anlagen - Teil 4-1: Wärmeerzeugung für die Raumheizung, Verbrennungssysteme (Heizungskessel)*. CEN - European Committee for Standardization. (German)

Furbo, F., Shah, L.J., Holm Christiansen, C. & Vinkler Frederiksen, K., 2004. *Kedeleffektiviteter for oliefyr og naturgaskedler i enfamiliehuse*. DTU-BYG Rapport R-072 2004. ISBN 87-7877-135-8. (Danish)

Fiedler, F. & Persson, T., 2009. Carbon monoxide emissions of combined pellet and solar heating systems. *Applied Energy*, 86(2), 135 -143.

Haller, M.Y., Paavilainen, J., Konersmann, L., Haberl, R., Dröscher, A., Frank, E., Bales, C., Streicher, W., 2009. A Unified Model for the Simulation of Oil, Gas and Biomass Space Heating Boilers for Energy Estimating Purposes – Part II: Parameterization and Comparison with Measurements. Submitted to Journal of Building Performance Simulation, Nov. 2009.

Hanby, V. & Li, G., 1995. Modelling of Gas-Fired Boiler Systems for Building/HVAC Plant Simulation. In: *Proceedings of the IBPSA Building Simulation Conference and Exhibition*. Madison, Wisconsin, 42 - 47.

Hensen, J.L.M., 1991. *On the Thermal Interaction of Building Structure and Heating and Ventilating System*. Thesis (PhD). Technische Universiteit Eindhoven.

Heinz, A., 2007. *Application of Thermal Energy Storage with Phase Change Materials in Heating Systems*. Thesis (PhD). Institute of Thermal Engineering, Graz University of Technology, Austria.

Idem, S., Jacobi, A. & Maxwell, G., 1992. A Performance Model of an Instantaneous, Condensing, Gas-fired Hot Water Boiler. In: *ASHRAE Trans.* 98(2), 165-171.

Isakson, P. & Eriksson, L., 1994. MFC 1.0Beta *Matched Flow Collector Model for simulation and testing - User's manual*. Stockholm: Royal Institute of Technology.

Kemna, R., van Elburg, M., Li, W. & van Holsteijn, R., 2007. *Preparatory Study on Eco-design of CH Boilers - Task 4 Report (FINAL) Technical Analysis (incl. System Model)*. European Commision, DG TREN, Unit D3: Delft, The Netherlands.

Kays, W.M. & London, A.L., 1984. *Compact heat exchangers*, Third Edition. Malabar, Florida: Krieger Publishing Company. ISBN 1-57524-060-2.

Konersmann, L., Haller, M. & Vogelsanger, P., 2007. *PelletSolar - Leistungsanalyse und Optimierung eines Pellet-Solarkombinierten Systems für Heizung und Warmwasser*. Swiss Federal Office of Energy SFOE. (German)

Koschak, A., Fiedler, T., Knirsch, A., Beurer, C., 1998. *TRNSYS-TYPE 370 Erweiterung des bisherigen Gaskesselmoduls um eine Holzkesselfeuerung mit der Möglichkeit zur Brennwertnutzung - Ergänzung um einen Simulationsmodus zur realitätsnahen Simulation des Betriebsverhaltens von Gaskesseln mit Takten.* (German)

Landry, R., Maddox, D. & Bohac, D., 1993. Seasonal Efficiency and Off-Cycle Flue Loss Measurements of Two Boilers. In: *ASHRAE Trans.* 99(2), 440-454.

Laret, L., 1989. Accurate Boiler Models for Large Scale Simulation. In: *Proceedings of the IBPSA Building Simulation Conference and Exhibition*. Vancouver, British Coloumbia, Canada, 375-380.

Lebrun, J. Saavedra, C., Hore, F., Grodent, F., Nusgens, P., 1993. Testing and Modeling of Fuel Oil Space-Heating Boilers - Synthesis of Available Results. In: *ASHRAE Trans.* 99(2), 455-464.

Merkel, F., 1925. Verdunstungskühlung. *VDI Forschungsarbeiten*, 275, 123-128. (German)

Nordlander, S., 2003. *TRNSYS model for Type 210 - Pellet stove with liquid heat exchanger - Documentation of model and parameter identification*. Borlänge, Sweden: Högskolan Dalarna, Solar Energy Research Center SERC.

Ottin, T., 1986. *Etude et simulation du comportement dynamique de chaufferies*. Thesis (PhD). École Polytechnique Fédéral Lausanne. (French)

Paulsen, O., 1999. *Technical report Work package I: Modelling of part load efficiency - second revised edition - SAVE Project: Annual Efficiency Calculation Method for Domestic Boilers* - Contract No. XVII/4.1031/93-008 - Funded by the European Union, SAVE programme - Directorate-General for Energy.

Perers, B. & Bales, C., 2002. *A Solar Collector Model for TRNSYS Simulation and System Testing - A technical report of Subtask B of the IEA-SHC - Task 26*.

Persson, T., 2006. *Combined solar and pellet heating systems for single-family houses: how to achieve decreased electricity usage, increased system efficiency and increased solar gains*. Thesis (PhD). KTH, Energy Technology, Stockholm.

Persson, T., Fiedler, F., Nordlander, S., Bales, C., Paavilainen, J., 2009. Validation of a dynamic model for wood pellet boilers and stoves. *Applied Energy*, 86(5), 645-656.

Remund, S., 1999. *Berechnung des Nutzungsgrades von Oel- und Gasheizkesseln*. Swiss Federal Office of Energy SFOE. (German)

SEL, TRANSSOLAR, CSTB, TESS, 2006. *TRNSYS 16 - A TRansient SYstem Simulation program*. Solar Energy Research Laboaratory, University of Wisconsin-Madison.

Thornton, J.W., 2004. TRNSYS *Type 751 – Simple boiler with efficiency from data file*. Software from TESS – Thermal Energy Systems Specialists, http://www.tess-inc.com.

University of Illinois & University of California, 2007. *EnergyPlus Engineering Reference - The Reference to EnergyPlus Calculations*.

VDI, 2006. Mk: Be- und Entfeuchten von Luft. In: *VDI Wärmeatlas*. Verein Deutscher Ingenieure. Berlin Heidelberg: Springer Verlag. (German)

Paper IV

A Unified Model for the Simulation of Oil, Gas and Biomass Space Heating Boilers for Energy Estimating Purposes

Part II: Parameterization and Comparison with Measurements

M.Y. Haller[1*], J. Paavilainen[2], L. Konersmann[3], R. Haberl[3], A. Dröscher[1], E. Frank[3], C. Bales[2], W. Streicher[1]

[1] Institute of Thermal Engineering, Graz University of Technology, Inffeldgasse 25/B, 8010 Graz, Austria

[2] Solar Energy Research Center SERC, Högskolan Dalarna, 781 88 Borlänge, Sweden

[3] Institut für Solartechnik SPF, Hochschule für Technik Rapperswil, 8640 Rapperswil, Switzerland

* corresponding author: michel.haller@tugraz.at, +43 316 873 7318

Full names, phone, fax, email:

Michel Yves Haller, +43 316 8737318, +43 316 8737305, michel.haller@tugraz.at

Janne Paavilainen, +46 23 778728, +46 23 778701, jip@du.se

Lars Konersmann, +41 55 2224827, +41 55 2224844, lars.konersmann@solarenergy.ch

Robert Haberl, +41 55 2224832, +41 55 2224844, Robert.Haberl@solarenergy.ch

Angela Dröscher, +43 316 8737804, +43 316 8737305, angela.droescher@tugraz.at

Elimar Frank, +41 55 2224823, +41 55 2224844, Elimar.Frank@solarenergy.ch

Chris Bales, +46 23 778707, +46 23 778701, cba@du.se

Wolfgang Streicher, +43 316 8737306, +43 316 8737305, w.streicher@tugraz.at

Abstract

A semi-physical model for the simulation of oil, gas and biomass space heating boilers has been parameterized based on measurements on nine different boiler units and simulation results have been compared to results obtained from measurements in steady state and transient operation. Although the agreement between simulated and measured boiler efficiencies was within the range of measurement uncertainties in most cases, model improvements are expected to be possible concerning the heat capacitance modelling in cycling on/off operation as well as influences of start and stop behaviour on the overall efficiency. It is found that electricity consumption during cycling on/off operation of small pellets or oil space heating boilers may have a significant influence on the overall energy balance of these units. This influence increases strongly with decreasing heat load and increasing number of on/off cycles.

Keywords: Simulation and Modelling; Boiler; Biomass; Oil; Gas

Symbols

C_{therm}	effective thermal capacitance, J/K
$\dot{C}$	capacity flow rate, W/K
cp	specific heat, J/kgK
ε	heat exchanger effectiveness, -
E_{el}	electric energy, J
η	efficiency, -
fac	factor, -
fr	fraction, -
GHV	gross (or upper) heating value (reference temperature 25 °C), J/kg
γ_X	mass fraction of the elements (X = C,H,O,S,N) of ash (X = ash) and of water (X = H$_2$O) in the fuel per kg dry fuel, kg/kg
ΔH	enthalpy difference (reference temperature of 25 °C for sensible part and for enthalpy of reaction), J
Δh	specific enthalpy difference (reference temperature of 25 °C for sensible part and for enthalpy of reaction), J/kg
k	coverage factor for uncertainty calculation, -
λ	excess air factor for combustion ($\lambda = 1$ for stoichiometric amount), -
m	mass, kg
$\dot{m}$	mass flow, kg/s
N	counter, -
n	exponent for the dependency of the heat transfer resistance on the mass flow, -
μ	amount of flue gas component per kg of dry fuel burned, kg/kg
NHV	net (or lower) heating value (reference temperature 25 °C), J/kg
O_{min}	minimum oxygen demand per kg dry fuel, kg/kg
$O_{2,fg}^{v,dry}$	volumetric percentage of oxygen in dry flue gas, %
P	power, W
p	pressure, Pa
ppm	volumetric concentration, ppm

pts	measured points
Q	energy, J
$\dot{Q}$	energy (heat) transfer rate, W
q	energy relative to the fuel energy (GHV), -
RH	relative humidity, -
ρ	density, kg/m^3
t	temperature, °C
dT	temperature difference, K
τ	time, s
$\tau_{1/2}$	half time of cooling out in standby, s
u	uncertainty (standard deviation, coverage factor 1)
UA	overall heat transfer coefficient area product, W/K
$\dot{V}$	volume flow rate, m^3/h
V	volume, m³
w	water load of air or flue gas per kg dry gas, kg/kg

Subscripts

air	combustion air
amb	ambient
ash	ashes
avg	average
B	boiler (efficiency)
cc	combustion chamber
C	combustion (efficiency)
CO	carbon monoxide
$chem$	chemical
$cond$	condensate; under condensing conditions
$Ctherm$	thermal capacitance
$cycling$	under cycling (burner on and off) conditions
dp	dew point
$draft$	natural draught
dry	dry heat exchanger surface, dry flue gas
el	electricity
end	at the end of an experiment
$empty$	empty boiler
$evap$	evaporation (enthalpy)
fg	flue gas
$fuel$	fuel
gg	(flue) gas to (combustion air) gas heat exchanger
hot	hot flue gas before heat exchanger (flue gas temperature after adiabatic combustion)
hx	flue gas to water heat exchanger
in	inlet (boiler return line)
inf	after an infinite time
lat	latent
max	maximum
min	minimum
ms	measured

nom	under nominal conditions (of water mass flow and combustion power)
out	outlet (boiler flow line or outlet of flue gas)
OFF	without burner operation (standby)
ON	during burner operation
sat	saturation (water vapour)
sens	sensible
sim	simulated
start	at the start of an experiment or during the start phase of the burner
steady	under steady state conditions
tot	total
vap	vapour
wat	water
wet	wet heat exchanger surface, wet flue gas

Superscripts

dry	dry flue gas
d.b.	dry base; per kg of dry (biomass) fuel
GHV	based on the gross heating value
H	from (chemically bound) hydrogen in dry fuel
H_2O	from water in wet fuel
NHV	based on the net heating value
wet	wet (biomass) fuel
w.b.	wet base (per kg wet fuel)

1   Introduction

A unified model for the simulation of oil, gas, pellets (Pel) and wood chips (Chp) space heating boilers for energy estimating purposes has been presented in a previous article submitted to this journal (Haller et al. 2009), referred to in this article by "Part I". In this follow-up article, results from laboratory measurements performed on nine different space heating boiler units (Table 1) are presented. The investigated boilers were constructed later than year 2000, and all oil and gas boilers investigated were condensing boilers. Steady state measurements have been performed in the range of power modulation, and additional measurements have been performed for the determination of the thermal capacitance and the heat losses during burner standby as well as in cycling burner operation at or below the minimum turndown ratio of combustion power. The measurements have been performed at the Institut für Solartechnik at the University of Applied Sciences Rapperswil (SPF) in Switzerland, the Institute of Thermal Engineering at Graz University of Technology (IWT) in Austria, and in the laboratories of a boiler manufacturer (Man).

Table 1. Overview of tested boilers and test conditions.

Boiler Reference		Pel1	Pel2	Pel3	Pel4[a)]	Chp1	Oil1	Oil2	Gas1	Gas2
Laboratory		SPF	SPF	Man	IWT	Man	SPF	SPF	IWT	SPF
Specifications according to the manufacturer										
$\dot{Q}_{wat,max}$	[kW]	10	10	40	14	150	15	12	14	14
V_{wat}	[l]	59	63	158	800	295	15	35	N/A	3.7
m_{empty}	[kg]	312	406	846	550	1972	58	107	39	45
modulating	[-]	YES	YES	YES	YES	YES	YES	NO	YES	YES
condensing	[-]	NO	NO	NO	NO	NO	YES	YES	YES	YES
Range and numbers of steady state measurements performed										
$\dot{Q}_{wat,out,min}$	[kW]	4	5	13	14	110	6	13	6	3
$\dot{Q}_{wat,out,max}$	[kW]	10	10	38	16	182	15	13	13	14
$t_{wat,in,min}$	[°C]	45	50	55	50	55	25	25	25	25
$t_{wat,in,max}$	[°C]	55	70	65	60	65	60	60	68	60
$t_{wat,out,min}$	[°C]	60	60	74	65	70	31	38	40	28
$t_{wat,out,max}$	[°C]	70	80	84	80	81	82	78	79	78
$\dot{V}_{wat,min}$	[l/h]	190	420	580	750	3'500	300	300	400	300
$\dot{V}_{wat,max}$	[l/h]	960	870	1'780	800	10'000	910	900	1'100	900
pts_{cond}	[-]	0	0	0	0	0	36	11	48	70
pts_{tot}	[-]	11	6	6	3	4	69	19	67	74

pts_{cond} *: number of measured points under condensing (cond) conditions;* pts_{tot} *: total number of measured points;* [a] *pellet burner integrated into a solar heat storage tank; N/A: not available.*

The implementation of the space heating boiler model in a simulation Type for the software TRNSYS (SEL 2006) is referred to as Type 869. Section 2 presents the methods used for measurements on the different boiler units including a discussion about the uncertainties and the process of parameter identification. Results from model calculations are then compared with data obtained from measurements in section 3.

2 Method

2.1 Efficiency definitions

The basic energy balance equation of a space heating boiler unit – according to the sankey diagram of energy flows shown in Part I - may be written as:

$$
\begin{aligned}
& Q_{fuel}^{GHV} + Q_{el,start} \\
& = Q_{ash} + Q_{cc,amb} + Q_{fg,sens} + Q_{fg,lat} + Q_{fg,chem} + Q_{hx,amb} + Q_{draft} + Q_{Ctherm} + Q_{wat}
\end{aligned}
\tag{1}
$$

No standard definition for the term *combustion efficiency* was found in literature. Therefore, the definition used here may differ from definitions found in other sources. In the work presented here, the combustion efficiency shown in Equation (2) is based on the gross heating value (GHV) of the fuel (Q_{fuel}^{GHV}) and flue gas losses, which are calculated from measurements performed on the fuel and air input as well as the flue gas output of the boiler (see also Equations 4 to 6 of Part I):

$$
\eta_C^{GHV} = 1 - \frac{Q_{fg}}{Q_{fuel}^{GHV}} = 1 - \frac{Q_{fg,sens} + Q_{fg,lat} + Q_{fg,chem}}{Q_{fuel}^{GHV}}
\tag{2}
$$

Thus, combustion efficiency equals the fraction of the fuel energy that is transferred to the thermal capacitance of the boiler or lost by the combustion chamber's heat and ash losses:

$$
\eta_C^{GHV} = \frac{Q_{hx} + Q_{cc,amb} + Q_{ash}}{Q_{fuel}^{GHV}}
\tag{3}
$$

For current European state of the art oil and gas boilers, losses due to incomplete combustion (Q_{ash} and $Q_{fg,chem}$) and heat losses of the combustion chamber ($Q_{cc,amb}$) are usually so small that they can be neglected for steady state operation. Thus, simplified combustion efficiency definitions can be found in literature.

The steady state boiler efficiency ($\eta_{B,steady}^{GHV}$) during burner operation is assumed to be always lower than the combustion efficiency due to thermal heat losses through the boiler envelope. These radiation and convection heat losses from hot envelope surfaces to the ambient are a result of the high temperatures in the combustion chamber ($Q_{cc,amb}$) and in the "flue gas to water heat exchanger" (FGWHX) ($Q_{hx,amb}$). Small amounts of chemical heat losses caused by unburned residues in the ashes (Q_{ash}) may be considered, e.g. for solid fuel

boilers. Sensible heat losses with ashes are not separately accounted for in the analysis presented here.

$$\eta_{B,steady}^{GHV} = \eta_C^{GHV} - \frac{Q_{hx,amb} + Q_{cc,amb} + Q_{ash}}{Q_{fuel}^{GHV}} \tag{4}$$

The boiler efficiency η_B^{GHV} may be determined indirectly by measuring the combustion efficiency and subtracting estimated heat and ash losses from this value as shown in Equation (4), or it may be determined directly by the enthalpy gain of the water flow through the boiler (Q_{wat}) divided by the fuel energy input (Q_{fuel}^{GHV}):

$$\eta_B^{GHV} = \frac{Q_{wat}}{Q_{fuel}^{GHV}} \tag{5}$$

If a boiler is operating below its minimum power of continuous burner operation, it will burn fuel intermittently (ON/OFF) and additional losses may occur during OFF times due to unwanted natural draught airflow through the combustion chamber and the FGWHX. Therefore, average boiler efficiency in cycling operation may include an additional loss term accounting for natural draught losses (Q_{draft}):

$$\eta_{B,cycling}^{GHV} = \frac{Q_{wat}}{Q_{fuel}^{GHV}} = 1 - \frac{Q_{fg} + Q_{hx,amb} + Q_{cc,amb} + Q_{ash} + Q_{draft}}{Q_{fuel}^{GHV}} \tag{6}$$

Due to electric fuel heating devices (preheating / ignition) during burner start phases, also electric energy input may become relevant for the boiler's thermal energy balance and increase the useful heat output (Q_{wat}). Therefore, for a fair comparison of the energy consumption of different boilers, also electric energy consumption (E_{el}) of the boiler is included in the boiler efficiency $\eta_{B,el}^{GHV}$:

$$\eta_{B,el}^{GHV} = \frac{Q_{wat}}{Q_{fuel}^{GHV} + E_{el}} \tag{7}$$

In the work presented here, E_{el} includes electricity for the boiler's control, fans used for combustion air or flue gas circulation, stokers used for feeding fuel into the combustion chamber, and the ignition or preheating of fuel. It does not include pumps used for water circulation or any system used to transport wood fuel from a storage room into smaller reservoirs adjacent to the boiler itself. The reason for this is that the electricity consumption of these devices does not depend predominantly on the boiler itself, but on the particularities of each installed system.

In order to do justice to the higher thermodynamic and economic value of electricity, an extended boiler efficiency $\eta_{B,3el}^{GHV}$ is defined:

$$\eta_{B,3el}^{GHV} = \frac{Q_{wat}}{Q_{fuel}^{GHV} + 3 \cdot E_{el}} \tag{8}$$

For the evaluation of influences of operating conditions on boiler efficiencies, the three boiler efficiency definitions shown in Equations (5), (7), and (8) will be used in sections 3.4 and 3.5.

2.2 Fuel characteristics

Oil and biomass fuel samples were collected during every test (except for Gas1) and their heating values as well as their elementary composition ($\gamma_C, \gamma_H, \gamma_N, \gamma_S$) were analysed in external laboratories. For biomass fuels, ash content (γ_{ash}) and moisture content (γ_{H_2O}) were always analysed additionally. Nitrogen and sulphur mass fractions were not always analysed. Oxygen content of oil and biomass fuels was calculated as:

$$\gamma_O = 1 - \gamma_C - \gamma_H - \gamma_N - \gamma_S - \gamma_{ash} \tag{9}$$

For boiler Gas2, consumption proportional samples of natural gas were drawn during the test sequences and the heating value as well as the gas composition were analysed. For boiler Gas1, heating values and natural gas composition were obtained for the measurement periods from the gas supplier. Elementary composition of the natural gas was then calculated with the molecular formulas and the molecular weights of the elements.

The stoichiometric oxygen demand for the combustion was calculated as:

$$O_{min} = 2.6641 \cdot \gamma_C + 7.9366 \cdot \gamma_H + 0.9980 \cdot \gamma_S - \gamma_O \tag{10}$$

2.3 Calculation of excess air and flue gas characteristics

The excess air factor (λ) was calculated based on the measured oxygen content in the dry flue gas at the outlet of the boiler and Equation (11), that is valid under the assumption that only the carbon and hydrogen content of the fuel contribute significantly to the stoichiometric oxygen demand:

$$\lambda = \frac{0.03125 \cdot O_{min} \cdot \left(O_{2,fg}^{v,dry} - 1\right) - O_{2,fg}^{v,dry} \cdot 0.083256 \cdot \gamma_C}{0.14919 \cdot O_{min} \cdot O_{2,fg}^{v,dry} - 0.03125 \cdot O_{min}} \tag{11}$$

Flue gas mass per mass of burned fuel was calculated for steady state conditions from the fuel elementary composition, the water load of the combustion air (w_{air}), and λ. w_{air} was calculated based on the measured temperature (t_{air}) and relative humidity (RH_{air}) as well as the ambient pressure (p_{air}) at the day of the measurement.

The sensible contribution to the enthalpy of the combustion air ($\Delta H_{air,sens}$) and the leaving flue gas ($\Delta H_{fg,sens}$) were calculated with enthalpy functions for each gas component, assuming all water is vaporous. The latent contribution to the enthalpy of the inlet air ($\Delta H_{air,lat}$) and the flue gas ($\Delta H_{fg,lat}$) were calculated with the temperature dependent enthalpy of evaporation ($\Delta h_{evap}(t)$) according to:

$$\Delta H_{air,lat} = w_{air} \cdot m_{air,dry} \cdot \Delta h_{evap}\left(t = 25°C\right) \tag{12}$$

$$\Delta H_{fg,lat} = w_{fg,hot} \cdot m_{fg,dry} \cdot \Delta h_{evap}\left(t = 25°C\right) - m_{cond} \cdot \Delta h_{evap}\left(t_{fg,out}\right) \tag{13}$$

The mass of condensate (m_{cond}) has either been measured directly (Gas1+Gas2), or calculated based on the hydrogen balance of the reaction and the measured relative humidity of the flue gas (Oil1+Oil2). Chemical losses of the flue gas were calculated with Equation (23) of Part I. Combustion efficiency was then calculated based on Equation (2).

Chemical losses with unburned residues in the ash were calculated similarly with the enthalpy of reaction of the oxidation of elementary carbon ($\Delta h_{C \to CO_2} = -32'800 kJ/kg$) and the assumption that all weight loss of the ash in the oven at 815 °C (measured by an external laboratory) is due to the oxidation of carbon.

$$Q_{ash} = -\Delta h_{C \to CO_2} \cdot m_C \tag{14}$$

2.4 Measurements and uncertainty estimation

Measurements on boiler units have been performed in different laboratories (see Table 1). The devices used and their measurement uncertainties were in most cases the same or similar (Table 2). Thus, a general measurement uncertainty estimation is done for all laboratories together, and exceptions from the rule are indicated where the estimated uncertainty for a particular measurement deviates substantially from this general rule. Uncertainty estimations are declared as of type A (based on the measurement data) and of type B (based on prior knowledge) according to the definitions given in the GUM (ISO 1995).

Table 2 shows estimations of uncertainties for values that have been measured during the tests. In some cases, higher uncertainties have been assumed than given by the manufacturer of a measurement device in order to account for differences between the actual position of the sensor and the exact point of interest, or to account for variations of values that have later been taken as averages over a time period. The uncertainties of water volume flow rate and temperature measurements given by the manufacturers have been replaced by the uncertainty of the calibration procedures that were done prior to the measurements.

Fuel composition and heating values were determined by external laboratories. Unfortunately, these did not provide detailed information about the uncertainty of their measurements. Uncertainties assumed for these analysis results are therefore educated guesses (Table 3).

Table 2. Assumed uncertainties (type B estimation) of measured values.

Parameter	methods and devices used	u (k=1)
t_{amb}	Pt100 4w, class A	± 1.0 K [a]
t_{air}	Pt100 4w, class A	± 0.5 K [a]
p_{air} (Gas+Oil)	Fischer Mess- und Regeltechnik, ME 70	± 2 kPa
	Gas1: local meteorological information of ZAMG (2007)	
RH_{air} [b]	Rotronic Hygroclip S and Rotronic HYGROMER I-2000 (u=1.5%)	± 10 % abs.
	Gas1: not measured	
$t_{fg,out}$	Pt100 4w, class A	± 1.5 K [a]
$O_{2,fg}^{v,dry}$	e.g. MRU AirFair VarioPlus Industrial; Testo 350-XL	± 0.2% abs.
ppm_{CO}	e.g. MRU AirFair VarioPlus Industrial; Testo 350-XL	± 5% rel.; min. ± 2 ppm
$RH_{fg,out}$ [b]	Capacitive high humidity level probe with heated sensor. Testo 0636 2142 (u=2.5%)	± 10 % abs.
$t_{wat,in}$	Pt100 4w class A, immersed	± 0.1 K [c]
$t_{wat,out}$	Pt100 4w class A, immersed	± 0.1 K [c]
$\left(t_{wat,out} - t_{wat,in}\right)$	Pt100 4w class A, immersed, simultaneous calibration	± 0.04 K
$\dot{V}_{wat}$	Electromagnetic, e.g. Endress & Hauser Promag P50, PN25 (IWT+Pel3); Krohne IFC 110 (SPF)	± 0.4% [d]
	For boiler Chp1 Ultrasonic, FLUXUS ADM 6725	± 3%
V_{fuel} (Gas)	Actaris (Gas1); Ritter TG20 (Gas2)	± 0.8%
m_{fuel} (Oil)	calibrated scale	± 0.3%
m_{fuel} (Pel)	calibrated scale	± 1.0% [e]
m_{fuel} (Chp)	calibrated scale	± 3.0% [e]
γ_{H_2O} [f]	Drying in oven at 105 °C until constant weight is reached; calibrated scale	± 0.2% abs.
m_{cond} [g]	calibrated balance	± 3% rel.
E_{el}	SPF: 0...500 W: Sineax P530, Camille Bauer	± 1% rel.
	Pel3 + Chp1: Optec DVH 3113, 3/65, Nr. 22004640, accuracy class 2 (DIN IEC 1036)	± 2% rel. [h] + (±1 Wh)
	Pel4: Schell Count EEM12LR-32A, accuracy class 1	± 2% rel. [h] + (±0.5 Wh)

[a] governed by the difference between the actual position of the sensor and the exact place of air intake or bulk flue gas rather than by the uncertainty of the measurement-chain itself; [b] for condensing boilers Oil1, Oil2 and Gas2 only; [c] uncertainty due to calibration device; [d] calibrated with stop-watch and scale; [e] substantially higher than the accuracy of the balance because of uncertainty associated with amount of fuel within fuel supply (stoker) at the beginning and the end of a test-sequence; [f] biomass fuels only; [g] for Gas1 and Gas2 only; [h] governed by the number of pulse signals per measurement period.

Table 3. Assumed uncertainties (type B estimation) of fuel composition measurements.

	$u\left(GHV^{d.b.}\right)$ (rel.)	$u\left(\gamma_C\right)$ (abs.)	$u\left(\gamma_H\right)$ (abs.)	$u\left(\gamma_{ash}\right)$ (abs.)	$u\left(\gamma_S\right)$ (abs.)	$u\left(\gamma_N\right)$ (abs.)
Biomass	1.5%	1.0%	0.2%	0.1%	0.01%	0.01%
Oil	1.0%	1.0%	0.3%	N/A	0.0%	0.01%
Gas	1.0%	1.0%	0.5%	N/A	0.0%	0.05%

N/A: not applicable

The uncertainty of the enthalpy function of flue gas components was calculated as 0.4% by Gaussian error propagation from 0.2% uncertainty for the deviation of the function from tabular data (Baehr, 2005), and an assumed uncertainty of 0.3% for the tabular data itself. The uncertainty of the enthalpy and density functions of water used for the calculation of useful heat was assumed to be negligible. Also, the uncertainties of molecular masses and the uncertainty of the Antoine formula used for the calculation of water vapour pressure were assumed to be negligible.

Type B uncertainties of calculated values were determined with Gaussian error propagation in EES (Klein, 2009). General results are shown in (Table 4).

For biomass boilers, each steady state measurement lasted several hours. For Pel1, Pel2 and Pel4, the boiler efficiency η_B^{GHV} was evaluated for each hour of the measurement separately. Measurement results were only accepted if the standard deviation of the mean of η_B^{GHV} determined for at least three consecutive hours was below 1% (absolute). Type B uncertainty estimation was assumed to include also these random uncertainties. In the case of sensible and latent flue gas losses, the uncertainties in Table 4 are shown as absolute uncertainties of $q_{fg,sens} = Q_{fg,sens}/Q_{fuel}^{GHV}$ and $q_{fg,lat} = Q_{fg,lat}/Q_{fuel}^{GHV}$.

Some interesting results of uncertainty propagation are discussed briefly here. With the assumptions made in Table 2 and Table 3, the uncertainty of water vapour in the flue gas per kg fuel burned is dominated about 50%[1] each by the uncertainty of γ_H and the uncertainty of RH_{air}, for $t_{air} = 25°C$. The uncertainty of the dew point calculation is dominated about 35% each by the uncertainty of RH_{air} and p_{air}. Therefore, not only the exact hydrogen content of the fuel, but also relative humidity and pressure of the ambient (combustion) air should be reported for measurements performed on boiler units under condensing conditions.

---

[1] This percentage is calculated as the ratio of the square of the product of the partial derivative and uncertainty of each measured variable to the square of the uncertainty in the calculated variable

Table 4. Uncertainties of computed values estimated with Gaussian error propagation (type B estimation).

	Pel	Chp	Oil	Gas
$u(\gamma_O)$ (abs.)	1.1%	1.1%	1.1%	1.1%
$u(O_{min})$ (rel.)	4.3%	4.3%	1.7%	1.5%
$u(\lambda)$ (abs.)	0.02 – 0.12[a]	0.02 – 0.12[a]	0.03	0.02
$u(q_{fg,sens})$ (abs.)	0.3–0.7%	0.3–0.7%	0.1%	0.1%
$u(\mu_{H2O,fg})$ (rel.)	--[b]	--[b]	4%	3%
$u(t_{fg,dp})$ (abs)	--[b]	--[b]	0.9 K	0.6 K
$u(RH_{fg,out})$ (abs.)	--[b]	--[b]	--	4-10%
$u(q_{fg,lat})$ (abs)	--[b]	--[b]	0.6 -1.0 %[c]	0.3%
$u(\eta_C^{GHV})$ (abs)	0.3–0.7%	0.3–0.7%	0.1 -1.0 %[c]	0.1-0.3%
$u(Q_{fuel}^{GHV})$ (rel.)	1.8%	3.4%	1.0%	1.3%
$u(Q_{wat})$ (rel.)	0.6%	3.0%	0.6%	0.6%
$u(\eta_B^{GHV})$ (rel.)	1.9%	4.5%	1.2%	1.4%

[a] from 0.02 for $O_{2,fg}^{v,dry}$ = 6% (λ = 1.4) to 0.1 for $O_{2,fg}^{v,dry}$ = 15% (λ = 3.5); [b] not condensing; [c] latent gains were calculated based on measurement of relative humidity of the flue gas, resulting in large uncertainties around the dew point of the flue gas.

The uncertainty of sensible flue gas losses were dominated about 60% by the uncertainty of the fuel composition, and less than 20% by the uncertainty of $t_{fg,out}$. The reason for this is most likely the influence of the fuel composition on the calculated ratio of flue gas mass per fuel mass that has been used instead of flue gas mass flow rate measurements for the calculation of the amount of flue gas that has been produced.

The uncertainty of the chemical flue gas loss calculation $u(Q_{fg,chem})$ is lower than 0.1% of Q_{fuel}^{GHV} for ppm_{CO} <1000 ppm, if it is assumed that no other losses than CO contribute to the chemical losses.

For the estimation of the uncertainty of the determined boiler's thermal capacitance $u(C_{therm})$, Equation (16), it was assumed that the determined temperature difference between the beginning and the end of the cooling out test has an uncertainty of $u(t_{B.start} - t_{B,end}) = \pm 2K$, due to inhomogeneous boiler temperature. Also for the temperature difference between the boiler water or FGWHX and the ambient an uncertainty of ± 2K was assumed. With Gaussian error propagation, $u(C_{therm}) \approx \pm 10\%$, $u(UA_{hx,amb,OFF}) \approx \pm 17\%$, and $u(\tau_{1/2}) \approx \pm 16\%$.

2.5 Boiler parameter identification

2.5.1 General procedure

The methods used for parameter identification are described in the following sections, in the order of their application.

Parameters that were identified from a number of measurements, i.e. all parameters determined from the steady state burner operation measurements, have been identified by the least root mean square error (LRMSE) method, minimizing the function:

$$RMSE = \sqrt{\frac{1}{N} \sum_{i=1}^{N} \left(x_{i,sim} - x_{i,ms} \right)^2} \qquad (15)$$

Where N is the number of measurements, and $x_{i,sim}$ and $x_{i,ms}$ are the simulated (or modelled) variable and the measured variable corresponding to measurement i, respectively.

Results from the parameterization process are shown in Table 6 and discussed in Section 3.

2.5.2 Thermal capacitance and heat losses in standby

The thermal capacitances of the boiler units were determined by a procedure that started with heating the boiler to a uniform temperature ($t_{wat,out} = t_{wat,in} \pm 1K > t_{amb} + 40K$). This was achieved by letting the circulation pump run after burner stop with the return temperature to the boiler at a fixed value (Method A). After a uniform temperature was reached, the boiler was discharged with a return temperature close to the ambient temperature ($t_{wat,in} \approx t_{amb} \approx 20°C$). The thermal capacitance was then determined as the energy balance of the water side during the discharge divided by the temperature difference of the boiler before and after the discharge ($t_{B,start} - t_{B,end}$):

$$C_{therm} = \frac{\sum \dot{V}_{wat} \cdot \rho_{wat} \cdot \left[h_{wat,out} - h_{wat,in} \right] \cdot \Delta\tau}{t_{B,start} - t_{B,end}} \qquad (16)$$

Heat losses during standby were determined by the same procedure with the only difference that the boiler was not discharged immediately after a uniform temperature was reached, but after a certain standby period without pump operation. The heat loss coefficient from the water to the ambient ($UA_{hx,amb,OFF}$) was determined knowing the temperature of the boiler before the standby ($t_{B,start}$) and after the standby ($t_{B,end}$), and the duration of the standby period ($\Delta\tau$) as well as the thermal capacitance of the boiler (C_{therm}) determined before.

$$UA_{hx,amb,OFF} = -\frac{C_{therm}}{\Delta\tau} \cdot LN\left(\frac{t_{B,end} - t_{amb}}{t_{B,start} - t_{amb}} \right) \qquad (17)$$

The boiler temperature t_B is thereby taken as the average of the inlet and outlet temperature. For the determination of $t_{B,end}$, the circulation pump is run

until steady state is reached and $t_{wat,in} = t_{wat,out} \pm 1K$. If energy is withdrawn during the time of this water circulation, this energy Q_{wat} is used to correct the boiler temperature t_B at the end of the standby.

$$t_{B,end} = \frac{t_{wat,in} + t_{wat,out}}{2} + \frac{Q_{wat}}{C_{therm}} \tag{18}$$

Unwanted circulation through the boiler or within the connecting pipes was prevented during standby. A controlled pressure of 10 Pa below ambient was maintained within the exhaust gas duct if the laboratory was equipped with the necessary means. In some cases that will be mentioned explicitly in the following sections, additional tests were performed with a blocked flue gas duct in order to determine the fraction of standby losses that could be attributed to chimney draught.

A half-time of boiler cooling out ($\tau_{1/2}$) was calculated as the time after which the temperature difference between the boiler and the ambient has dropped to half its initial value. This figure is used instead of $UA_{hx,amb,OFF}$ for displaying results of cooling out tests in a more intuitively understandable way. It is interpreted as the time after which half of the energy contained in the thermal capacitance of the boiler will be lost after burner and pump have stopped:

$$\tau_{1/2} = \Delta\tau \cdot LN(1/2) \cdot LN\left(\frac{t_{B,end} - t_{amb}}{t_{B,start} - t_{amb}}\right)^{-1} = -\frac{C_{therm}}{UA_{hx,amb,OFF}} \cdot LN(1/2) \tag{19}$$

In some of the boiler tests the thermal capacitance and the standby heat losses were determined without letting the circulation pump run after the heating up of the boiler (Method B). Results from these tests are therefore not comparable to the results of tests according to method A.

Boiler Pel4 was a pellet burner integrated into a solar thermal energy storage tank (TES). Therefore, a different procedure has been chosen for the determination of heat losses from the heat exchanger (in this case the whole TES) and the combustion chamber. First, the heat losses of the TES where determined for the top, the bottom and three different zones along the vertical axis by a TES heat loss test that followed closely the procedure described in EN12977-3 (2006), using the multiport store simulation model of Drück (2006). Then, the boiler model Type 869 was parameterized without thermal heat losses from the heat exchanger ($UA_{hx,amb} = 0$), and the useful heat output of Type 869 was connected to the electrical auxiliary heating input of the store model. The TES temperature at the height of the integrated burner was taken as the return temperature of the boiler model Type 869, and the return temperature of the heating system was connected to a TES double port at the appropriate height. The simulated flow temperature of the whole burner-storage unit was taken from the TES model double port outlet, and the flow temperature of the boiler model Type 869 remained unused. Then, $fr_{cc,amb}$ was fitted by the same procedure as for the other biomass boilers.

2.5.3 Heat losses during burner operation

Heat losses during burner operation are determined with the boiler parameters $fr_{cc,amb}$, $fr_{cc,ash}$, and $UA_{hx,amb,ON}$ introduced in Equations (11), (12) and (24) of Part I. For condensing gas and oil boiler units $fr_{cc,ash} = 0$ has been assumed. For these boilers, $UA_{hx,amb,ON}$ and $fr_{cc,amb}$ have been fitted simultaneously with the fit objective of the LRMSE method applied to $\dot{Q}_{amb}$ as shown in Equations (20) and (21). For biomass boilers, it was assumed that $UA_{hx,amb,OFF} = UA_{hx,amb,ON}$ and only the fraction of energy lost by the combustion chamber ($fr_{cc,amb} + fr_{cc,ash}$) has been determined by the LRMSE method applied to $\dot{Q}_{amb}$.

$$\dot{Q}_{amb,ms} = \left[\eta_{C,ms}^{GHV} - \eta_{B,ms}^{GHV} \right] \cdot \dot{Q}_{fuel}^{GHV} \tag{20}$$

$$\dot{Q}_{amb,sim} = \left(fr_{cc,amb} + fr_{cc,ash} \right) \cdot \dot{Q}_{fuel}^{GHV} + UA_{hx,amb,ON} \cdot \left[t_{wat,out} - t_{amb} \right] \tag{21}$$

For Pel3, Pel4, and Chp1, ash losses were determined by the collection of ash samples and therefore it was distinguished between $fr_{cc,amb}$ and $fr_{cc,ash}$ for these boilers in Table 6.

2.5.4 Modulation dependent excess air, CO and electricity use

The parameters $\dot{Q}_{fuel,min}^{GHV}$ and $\dot{Q}_{fuel,max}^{GHV}$ were set to the minimum and maximum steady state operation combustion power that were achieved during the steady state combustion tests. Then, the minimum and maximum values for λ, ppm_{CO} and P_{el} where determined by the LRMSE method applied to measured and modelled values of λ, ppm_{CO}, and P_{el}, respectively, using the solver method of a spreadsheet calculation program.

2.5.5 Characterization of the flue gas to water heat transfer

Combustion efficiency ($\eta_{C,ms}^{GHV}$) has been calculated according to Equation (2) based on fuel analysis and measured values performed on the combustion air and the leaving flue gas. Simulated flue gas losses are based on modelling approaches 1 to 3 presented in section 3.3.1 of Part I. All of these modelling approaches use the boiler parameters determined by the procedures described in sections 2.5.3 and 2.5.4 above.

For condensing boilers, $RH_{fg,max}$ was set to the average relative humidity measured (Oil1, Oil2, Gas2) or calculated based on the mass balance of hydrogen (Gas1), using all steady state measurements that achieved significant condensation. Additional parameters for the characterization of the FGWHX were then fitted with TRNSYS Type 869 and the optimization algorithms *Simplex (Nelder and Mead and O'Neill)* and *GPSHookeJeeves* implemented in the software GenOpt (Wetter 2004) with the objective of LRMSE applied to η_C^{GHV}.

2.5.6   Determination of start phase values

Start phase parameters were calculated based on averages of one or more warm start phases. The duration of the start phase (τ_{start}) was taken as the time where increased electricity use and/or significantly different fuel consumption rate could be observed compared to the following stable burner operation. Additional electricity consumption during burner start phase ($Q_{el,start}$) was calculated from the electricity consumption within the start phase, reduced by the electricity consumption of the stable burner operation that followed the start phase. Start phase fuel consumption rates ($\dot{Q}_{fuel,start}^{GHV}$) were calculated in a way that the output of useful heat of a simulation during the corresponding phase matched closely the measured heat output. If no significant start phase could be observed ($\tau_{start} = 0$), the corresponding values were set to zero.

The boiler model also allows for the definition of additional CO emissions during start and stop phases, lumped together into the value of $m_{CO,start}$ that will be added to the emissions of the boiler with every start phase. Based on the restrictions of the testing facilities, additional emissions during start and stop phases of the burner operation could not be quantified. These emissions may be quantified e.g. using flue gas flow rate measurements together with special techniques for the measurement of emissions under transient conditions (e.g. Heinz, 2007; Fiedler & Persson, 2009; Brunner et al. 2008; Nussbaumer et al. 2008).

3   Results

All results of the parameter identification process are listed in Table 6.

3.1   Thermal capacitance and cooling out in standby

The effective thermal capacitance determined with the discharge test described in section 2.5.2 is shown in Figure 1 (white bar), given in terms of effective thermal capacitance in relation to the thermal capacitance of the boiler water alone (100%). These results are compared with alternative ways of calculating the thermal capacitance based on manufacturer's data of water content and empty weight of the boiler (light grey bar) or based on the comparison of cycling simulation results and measurements (dark grey bar). The latter have been determined by matching the effective capacitance in order to firstly decrease the difference between simulated and measured boiler cycling frequency (Pel) and secondly to decrease the difference between the simulated and measured boiler outlet temperatures after the burner stop (Oil).
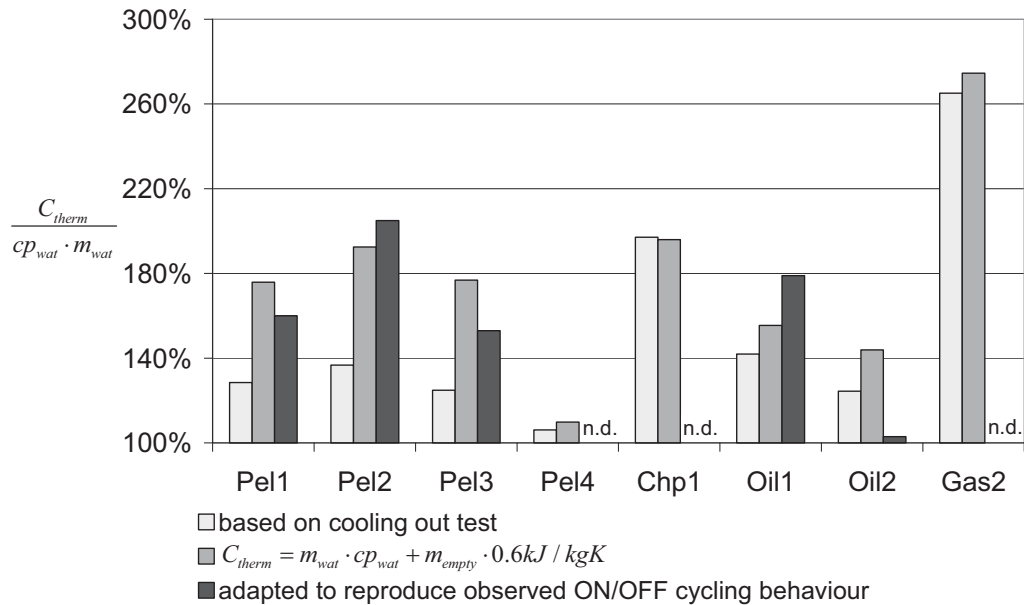
Figure 1. Comparison of thermal capacitances determined with different methods. n.d.: not determined.

The thermal capacitances determined with the discharge test reveal additional capacitance compared to the water volume alone. However, comparison of these values with values adapted for good reproduction of measured cycling frequencies and measured thermal response shows that the method for the determination of the thermal capacitance – or the thermal capacitance model itself – could still be improved. In particular, the boilers Pel1, Pel2, Pel3 and Oil1 show thermal capacitance effects in addition to the one assumed with the thermal capacitance from the discharge test. The estimation of the effective boiler capacitance by adding the capacitance of the empty weight of the boiler with a specific heat of 0.6 kJ/kgK to the capacitance of the water content produces values that are close to the ones determined by the discharge test for most of the observed cases.

Heat losses during standby are shown in Figure 2 in terms of half-times for cooling out of the thermal capacitance. With the exception of boiler Chp1, these values show a clear dependency on the effective thermal capacitance itself.

For boilers Pel4 and Chp1, heat losses during standby where determined once with an open exhaust duct (draught regulator for Chp1, draught controlled to 10 Pa for Pel4), and once with the exhaust duct blocked. Blocking the exhaust duct has the effect of inhibiting natural draught losses. At the same time, envelope losses may increase due to the missing cooling draught air that flows below the envelope surfaces before it enters the combustion chamber (compare Part I, Figure 7). Blocking the exhaust duct had no significant influence on the heat losses for boiler Pel4, and it decreased the heat losses by 10% for boiler Chp1. For boiler Chp1, it also led to an increase of envelope surface temperatures compared to the standby test with the open exhaust duct. Considering the additional heat losses caused by

these increased surface temperatures, up to 25% of the standby heat losses of the test with the unblocked exhaust may have been lost by natural draught through the exhaust duct.
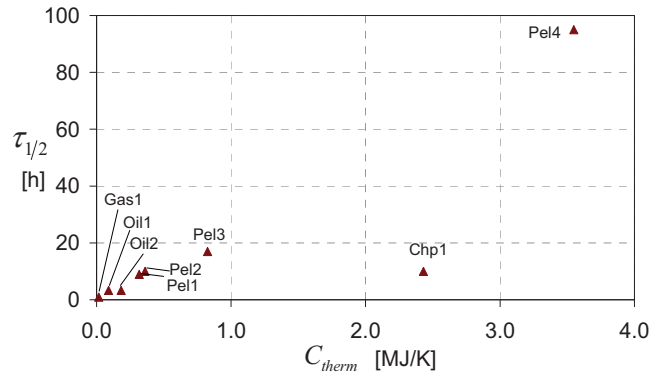
Figure 2. Dependency of the half-time for cooling out in standby on the effective thermal capacitance.

3.2 Excess air, electricity use and CO emissions in steady state

Figure 3 shows the dependency of λ on power modulation for the different boilers. Whereas some boilers (Pel1, Pel3) show an increase of λ up to a factor of two when decreasing power to 40% of its maximum, other boilers (Gas2, Chp1) are able to maintain a constant λ over the whole range of power modulation. Figure 4 shows that the dependency of electricity consumption on power modulation follows the linear model assumptions quite closely.
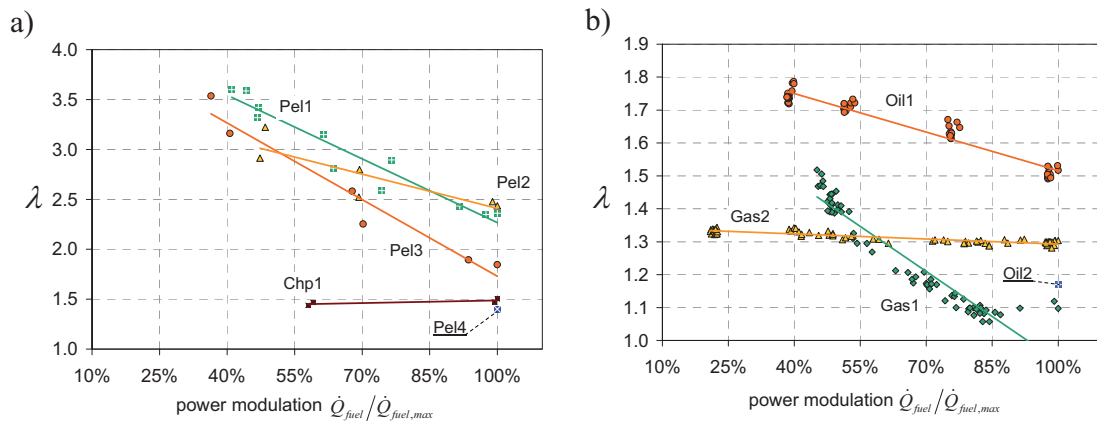
Figure 3. Dependency of the excess air factor on power modulation for biomass boilers (a) and oil and gas boilers (b).
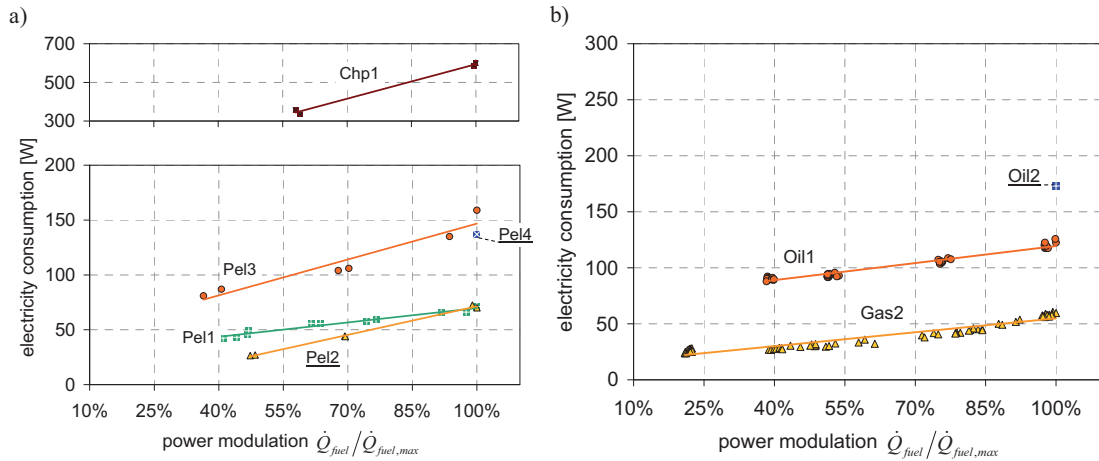
Figure 4. Dependency of electricity use on power modulation for biomass boilers (a) and oil and gas boilers (b).

CO emissions in steady state have only been determined for the biomass boilers. For most of these boilers, CO emissions are considerably higher at part load than at full load (Figure 5). Measured CO emissions of Pel1, Pel2 and Pel3 indicate that the assumption of an exponential dependency on power modulation might eventually be more appropriate than a linear dependency. However, more parameters and measurements will be needed for the characterization of an exponential curve-fit, and the scattering of the measured points is in the same range as the possible improvement by an exponential fit for boilers Pel1 and Pel3. When comparing the emissions of part load and full load operation, it has to be kept in mind that the emissions per delivered useful energy not only depend on the measured concentration of the pollutant in the flue gas, but also on the flue gas to fuel ratio, and thus on λ .

Figure 5. Dependency of CO emissions on power modulation for biomass boilers.

3.3 Steady state combustion efficiency

Simulations have been performed using the empirical delta-T (1), the empirical effectiveness (2), and the effectiveness-NTU approaches (3), described in Part I, section 3.3.1. In addition to this, models 1a and 1b are introduced here based on simplifications of the empirical del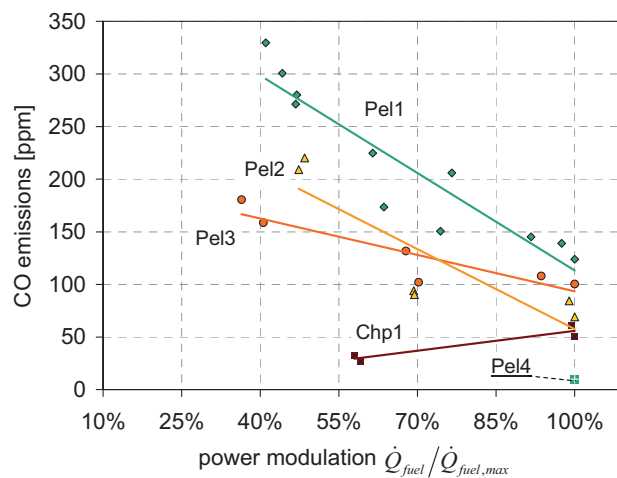ta-T approach. These simplifications where for 1a the disregard of the influence of the water mass flow rate, i.e. $dT_{fg,out} = f\left(\dot{Q}_{fuel}\right)$, and for 1b the disregard of the influence of both, water mass flow rate and power modulation , i.e. $dT_{fg,out} = const$. Apart from 1b, all approaches were able to reproduce the measured data with a RMSE of about 1% or lower, which is in the range or little above the estimated uncertainty of the measurements (Figure 6). Results of the empirical effectiveness approach (model 2 in Part I) showed no significant improvement compared to model 1 and are therefore not shown. A lower RMSE is achieved with model 3 than with model 1a and model 1 for all condensing boilers except of Gas1.
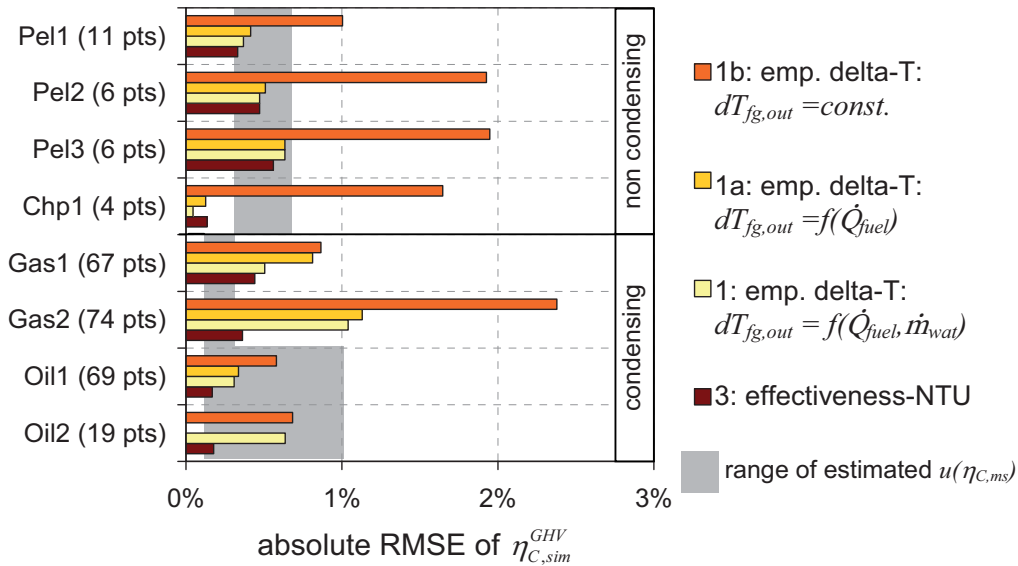
Figure 6. Comparison of the performance of different models for the simulation of combustion efficiency.

Table 5 shows the parameters needed for the simulation of flue gas losses additionally to fuel properties, combustion air properties, λ , and CO emissions. Model 3 does not need more parameters to be identified than model 1a for non condensing boilers – where the RMSE shown in Figure 6 is not significantly lower. However, it may need 3 – 4 parameters more for condensing boilers, where the RMSE is significantly lower for most cases.

Table 5. Parameters for the determination of flue gas losses.

model	cond.	#	Parameters
1a:	no	2	dT_{nom}, dT_{fg}
1a:	yes	3	$RH_{fg,max}$, dT_{nom}, dT_{fg}
3:	no	2[a]	UA_{nom}, $n_{hx,fg}$
3:	yes	6[a,b]	$RH_{fg,max}$, UA_{nom}, $n_{hx,fg}$, $fr_{Rhx,fg}$, $n_{hx,wat}$, fac_{wet}

cond: condensation; #: number of parameters; [a] plus choice of heat exchanger arrangement; [b] plus UA_{gg} in the case of combustion air preheating, assuming a constant $n_{hx,gg}$ =0.8.

A comparison of simulation results from model 1a and model 3 is shown in Figure 7. A more detailed analysis of differences between the two models has been presented for boiler Gas1 and boiler Oil1 by Haller et al. (2009).
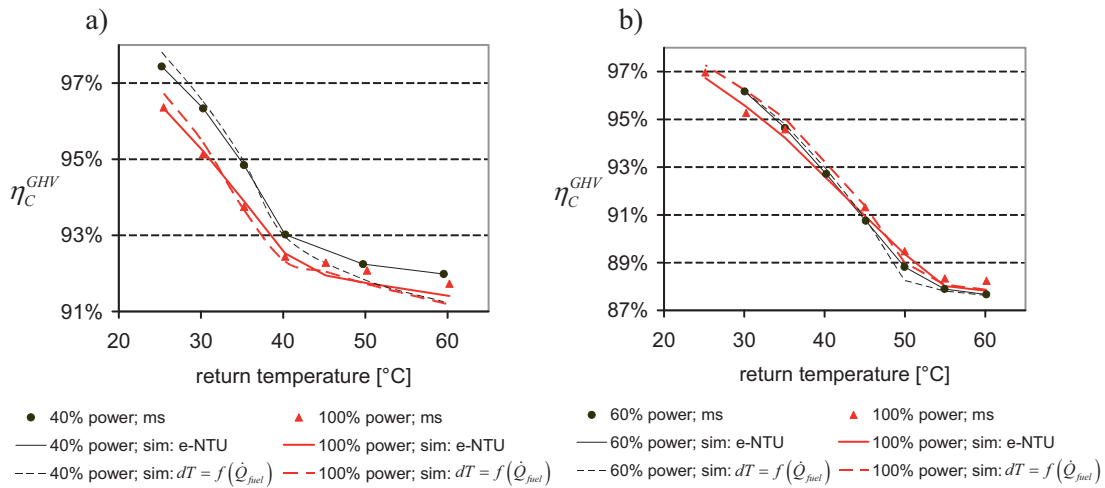
Figure 7. Comparison of measured combustion efficiency with results from two simulation approaches for boiler Oil1 (a) and Gas1 (b). e-NTU: effectiveness-NTU model, $dT = f\left(\dot{Q}_{fuel}\right)$: empirical delta-T model.

3.4   Steady state boiler efficiency

Figure 8 shows measured boiler efficiencies and simulated boiler efficiencies.

Boiler efficiencies of the biomass boilers sometimes – but not always – show a dependency on power modulation. In theory, combustion efficiency may increase with decreasing combustion power due to lower flue gas temperatures that are achieved when the FGWHX is operating at lower power. However, the positive effect of a lower $t_{fg,out}$ is often balanced by the negative effect of increasing λ, as well as by the increase of envelope heat losses relative to the useful heat. Thus, among the biomass boilers, only Chp1 – that maintains a constant λ over its whole range of operation - shows increased boiler efficiency at lower loads. The effect of return temperature on

the boiler efficiency is not pronounced for these boiler units, as they require a minimum return temperature or a minimum boiler water temperature in order to avoid condensation.

For condensing oil and gas boilers however, the return temperature has a far bigger effect on the boiler efficiency than power modulation, particularly when the leaving flue gas temperature drops below the dew point and the enthalpy of condensation is converted into useful heat. The dew point of the flue gas depends both on the fuel – because of different hydrogen content of the fuel – and on the boiler – because of different excess air factors. The maximum return temperature at which condensation occurs additionally depends on the heat transfer characteristics of the FGWHX. It may further be expected that the ambient pressure has an influence on the dew point and on condensation gains, assuming that the pressure at the location of condensation is linked to the ambient pressure. In the presented model, these effects are taken into account based on the Antoine formula for the calculation of water vapour pressure.

3.5   Cycling burner operation efficiency

All biomass boilers and one oil boiler (Oil1) showed a clearly identifiable start phase that lasted more than just a few seconds. Taking into account electricity consumption in the efficiency definition has only little effect for boiler Chp1 and Gas1, but the effect is quite significant e.g. for boiler Pel1 and Oil1, where electric energy accounts for 4% and 7%, respectively, of the total energy input during cycling operation at heat loads of about 10% of maximum load (Table 7). The parameters for start and stop emissions of the boilers have not been determined in this work and do therefore not contribute to the simulated losses.
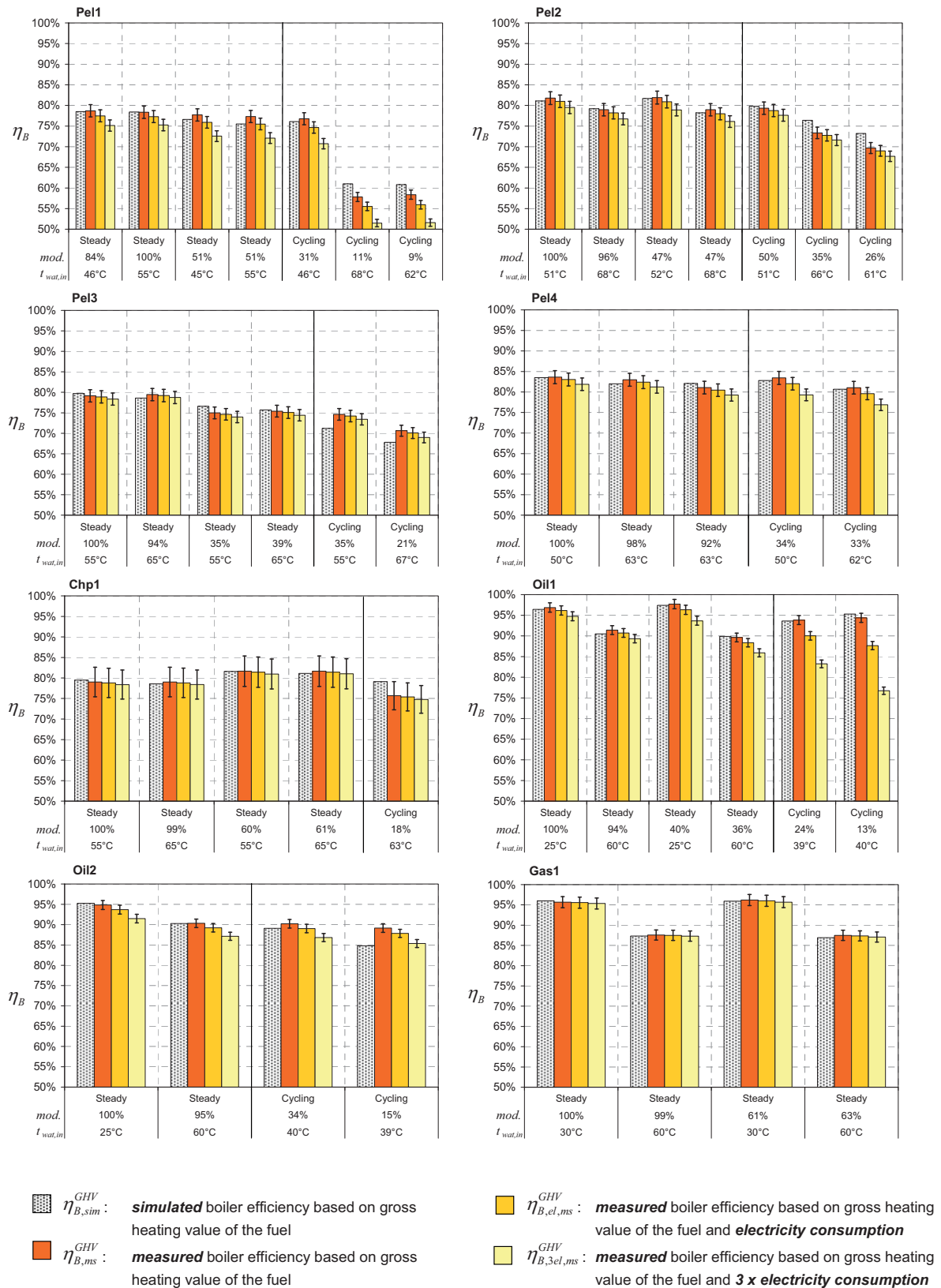
Figure 8. Comparison of measured and simulated boiler efficiencies under steady state and cycling burner operation. mod. : power modulation.

3.6   Boiler cycling details

A test run with an average heating load of 0.87 kW has been performed for pellet boiler Pel1. Figure 9(a) shows that the simulated boiler cycles 25% more frequently than the real boiler if the thermal capacitance determined with the discharge test is used for the model. This deficiency of too frequent cycling can be corrected by increasing the effective thermal capacitance of the boiler by 28% (Figure 9(b)).
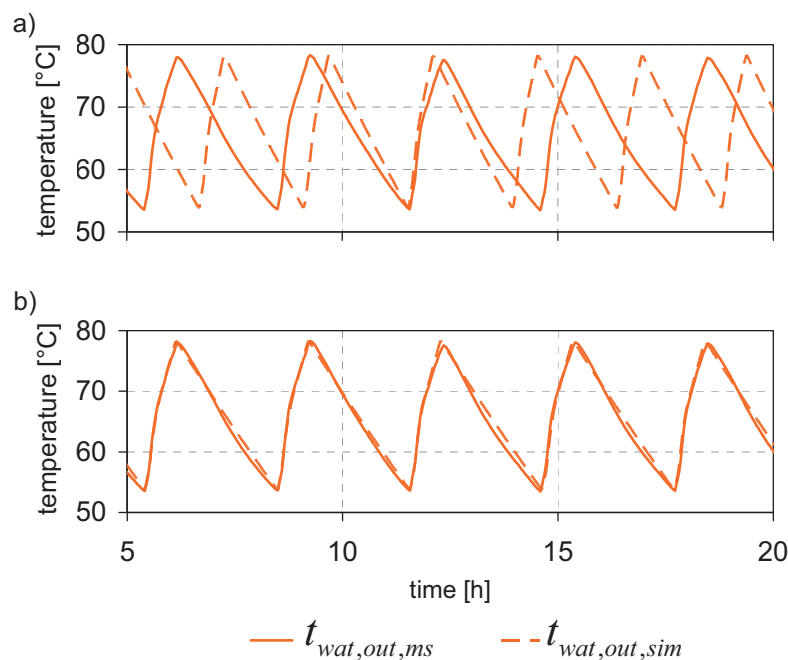
Figure 9. Simulated and measured cycling of pellet boiler Pel1 with boiler's effective thermal capacitance determined by a discharge test (a) and adapted (+28%) to observed cycling behaviour (b).

Figure 10 shows simulated and measured outlet temperatures and heating power in cycling operation. Measured fuel consumption and return temperature have been used as model input data. Fuel consumption has been based on measured weight loss of the pellet storage. It can be expected that in a real pellet boiler, there is a time-delay between the fuel entering the combustion chamber and its actual reaction with the combustion air that produces heat. Therefore, especially at burner start, the measured increase of flow temperature and heating power of the boiler is time-delayed, whereas simulated flow temperature and heating power increase is instantaneous (A) since no time lag is included in the boiler model between fuel feeding and fuel burning. It is also observed that the simulated thermal capacitance of the boiler reacts faster than the real thermal capacitance. Thus, the simulated heating power increases faster and stronger than measured (B) during the start phase and decreases faster and stronger than measured after the burner stop (C). These differences in thermal capacitance modelling can not be corrected by just assuming an increased thermal capacitance of the model.

Due to the nature of the phenomenon, it is likely that more accuracy could be obtained by introducing a separate thermal capacitance for the combustion chamber that reaches higher temperatures during operation than the capacitance of the boiler water and the FGWHX. Thus, after the burning process has stopped, the heat stored in the combustion chamber material continues to be transferred to the FGWHX. Another explanation for the higher $\dot{Q}_{wat,ms}$ than $\dot{Q}_{wat,sim}$ after burner stop could also be that part of the fuel still remains burning in the combustion chamber for a while after the last pellet has been fed.

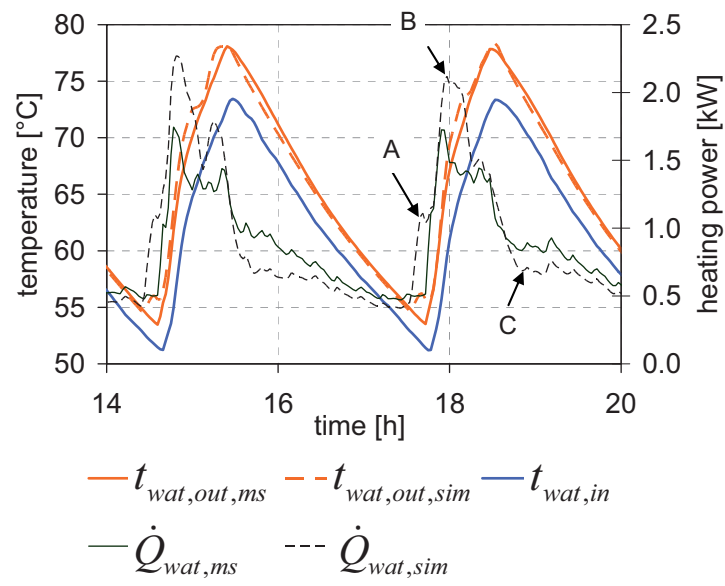Figure 10. Simulated and measured outlet temperature and heating power of pellet boiler Pel1.

Table 6. Identified boiler parameters and root mean square errors (RMSE) of fits.

Parameter	unit	Pel1	Pel2	Pel3	Pel4	Chp1	Oil1	Oil2	Gas1	Gas2
C_{therm}	kJ/K	317 [a]	360 [a]	825 [a]	3550 [a]	2430 [a]	89 [b]	182 [b]	16.7 [a]	4 [b]
$UA_{hx,amb,OFF}$	W/K	6.8 [a,c]	6.8 [a,c]	9.2 [a,d]	N/A [e]	46 [a,d]	5.1 [b,c]	11 [b,c]	3.4 [a,c]	4.9 [b,c]
$\dot{Q}_{fuel,min}^{GHV}$	kW	5.3	5.8	16.7	17.7	127.8	6.0	14.4	6.7	3.1
$\dot{Q}_{fuel,max}^{GHV}$	kW	12.8	12.8	50.0	17.7	222.2	15.0	14.4	14.7	15.6
λ_{min}	-	2.31	2.39	1.64	1.41	1.49	1.54	1.17	1.00	1.29
λ_{max}	-	3.54	3.02	3.41	1.41	1.45	1.76	1.17	1.40	1.33
$RMSE(\lambda)$	-	0.12	0.14	0.14	n.d. [f]	0.01	0.02	0.05 [f]	0.01	0.12
$ppm_{CO,min}$	ppm	120	53	89	10	29	n.d.	n.d.	n.d.	n.d.
$ppm_{CO,max}$	ppm	297	193	169	10	56	n.d.	n.d.	n.d.	n.d.
$RMSE(ppm_{CO})$	ppm	25	31	13	n.d. [f]	5	N/A	N/A	N/A	N/A
$P_{el,min}$	W	44	25	75	137	340	88	173	n.d.	22
$P_{el,max}$	W	69	73	151	137	593	116	173	n.d.	55
$RMSE(P_{el})$	W	2	1.2	7	n.d. [f]	10	2	n.d. [f]	3	2
dT_{nom}	K	67.4	77.2	139	74.5 [g]	104	5.5	23.8	21.2	18.5
$dT_{hx,fg}$	K	-0.48	-0.98	-1.0	N/A [f]	-1.47	-0.09	N/A [f]	-0.09	-0.25
$RH_{fg,max}$	%	N/A [h]	N/A [h]	N/A [h]	N/A [h]	N/A [h]	1.00	0.60	0.57	1.00
$RMSE\left(\eta_C^{GHV}\right)$	% (abs)	0.41	0.51	0.63	N/A	0.13	0.34	0.68	0.81	1.13
fr_{ash}	%	3.3 [i]	0.0 [i]	0.1	0.2	0.2	0.0 [i]	0.0 [i]	0.0 [i]	n.d.
$fr_{cc,amb}$	%			1.3	2.0	2.7				
$UA_{hx,amb,ON}$	W/K	6.8 [k]	6.8 [k]	9.2 [k]	N/A [e]	4.6 [k]	1.83	1.62	1.21	n.d.
$RMSE\left(\eta_B^{GHV}\right)$	% (abs)	0.83	0.46	0.87	0.82	n.d.	0.98	0.46	0.97	n.d.
τ_{start}	h	0.15	0.05	0.05	0.25	1.1	0.14	0	0	0
$\dot{Q}_{fuel,start}^{GHV}$	kW	n.d.	n.d.	31	n.d.	67	0	n.d.	n.d.	n.d.
$E_{el,start}$	Wh	111	5	33.6	36.5	56.5	113	0	0	0

N/A = not applicable; n.d. = not determined; [a] determined with test method A; [b] determined with test method B; [c] controlled exhaust duct draught of 10 Pa; [d] exhaust duct open to ambient with draught regulator, but no active draught control; [e] burner is integrated into solar thermal storage tank with different heat losses at different heights; [f] not modulating; [g] average of 3 measurements (not fitted); [h] not condensing; [i] $fr_{ash} + fr_{cc,amb}$; [k] value taken from cooling out test.

4 DISCUSSION

The uncertainty estimation showed that uncertainties of flue gas loss measurements were significantly lower - in absolute values – than uncertainties of boiler efficiency measurements. The largest uncertainties that could not be reduced in the case of boiler efficiency measurements were those of the heating value of the fuel itself and for biomass and gas boilers also those of the fuel consumption measurements. For the calculation of relative humidity in the flue gas based on the hydrogen balance of the fuel reaction and the condensate mass flow, uncertainties of pressure and relative humidity of the combustion air had a larger effect than expected. Relative humidity of combustion air and ambient pressure are currently not always reported for condensing boiler's performance testing, which could be a problem for the parameterization of the model based on such tests.

The one-node thermal capacitance approach has the advantage that it is simple and that it can be parameterized with a single discharge test or even with manufacturer's data. However, as it has been shown in the previous section, the determination of the effective thermal capacitance, and possibly even the one-node thermal capacitance model itself, could still be improved in order to better reproduce the observed thermal response of biomass boilers. The half-time of cooling out of a boiler in standby has been introduced in order to present cooling losses in an intuitive way. As expected, this half-time of cooling out generally depends on the size, the insulation, and the draught losses of the boiler.

Measured data for λ, CO emissions and electricity consumption showed a good agreement, i.e. the deviation is of the same order of magnitude as the measurement uncertainty, with the model assumption of a linear dependency on the power modulation. However, Type 869 also allows for an exponential relationship between λ and power modulation. An exponential relationship for CO emissions might also be more appropriate for some boilers (Fiedler & Persson, 2009). This is currently not included in the presented model, but it may be calculated based on the model outputs.

Optimization has been used for the determination of flue gas loss parameters based on a large number of experiments (from four for Chp1 to 74 for Gas2). For the empirical approaches, and in the case of non-condensing boilers also for the effectiveness-NTU approach, these parameters can alternatively be calculated with a spreadsheet calculation and a simple solver routine. The number of experiments for the determination of these parameters could be reduced to a set of experiments that covers full load, part load and different return temperatures of the heating system. However, for condensing boilers, the parameters for the effectiveness-NTU approach are difficult to find and might need a larger number of experiments and optimization algorithms such as the ones used in the work presented here.

The determination of steady state heat losses to the ambient during burner operation has been based on differences between measured combustion efficiency and boiler efficiency. However, these differences are often in the same order of magnitude as the uncertainty of the boiler efficiency measurement itself. An often practiced approach is to take standby heat loss

coefficients that have been determined without burner operation and apply them to the burner operation phases. However, as shown in section 3.2.2 of Part I, heat losses during standby may be quite different from those during burner operation. Another approach is to measure surface temperatures during steady state operation and to estimate losses based on models for radiation and convection heat transfer from hot surfaces. This approach can only be recommended if hot air is not leaking out of the envelope. Since the temperature of a boiler envelope surface may vary both with location and also with power modulation, a large number of measurements at different power modulation are required for this procedure.

The effect of cycling burner operation on the boiler efficiency is quite different for different boiler units, and electricity consumption has been shown to be significant at least for some small oil and biomass space heating boilers in cycling operation.

The one-node thermal capacitance model has been shown to overestimate cycling of a pellet boiler by about 25% when the thermal capacitance of a discharge test is used for modelling. This can be counteracted by increasing the value of the effective heat capacitance used for the simulation. Detailed analysis of the time response of a pellet boiler showed that the exact pattern of heat release from the boiler is possibly influenced by heat stored at higher temperatures in the combustion chamber material. An additional thermal capacitance node for the combustion chamber could solve this problem, but this would need additional parameter determination routines and it might not be compatible with the empirical delta-T approach for the calculation of flue gas losses.

Although it would have been desirable to present a model whose parameters can be determined based on standard steady state boiler tests (e.g. EN303-5 for biomass boilers), parameters for the transient behaviour of boilers are impossible to be determined with steady state tests. Therefore, procedures for the determination of the boiler's effective thermal capacitance and start and stop characteristics should be developed and standardized. The data obtained from such procedures will not only help to simulate the energy balance of these boilers more accurately, but it will also allow for a fairer comparison of different heating systems in terms of efficiency, emissions, and functionality. Additional emissions from frequent burner starts and stops have been shown to be substantial, and are sometimes the predominant part of the seasonal emissions of space heating boiler units (Heinz 2007; Fiedler & Persson 2009).

5 Conclusion

A boiler model has been developed that can be used for the simulation of oil, gas and biomass space heating boilers. In combination with a stratified storage tank model, the presented boiler model may also be used for the simulation of a burner integrated into a solar storage tank, a combi-boiler that provides domestic hot water and hot water for space heating within one unit, or boilers with a high degree of stratification.

The presented boiler model's simulation results are in good agreement, i.e. usually within the range of measurement uncertainties, with results observed in steady state and cycling tests performed on the different boiler units.

Different approaches for the modelling of steady state flue gas losses showed a better performance of the effectiveness-NTU approach in the case of condensing boiler units. However, this model requires more parameters and more effort for the parameter identification. For this reason, the simpler delta-T approach with a dependency of delta-T only on power modulation is likely to be the more favourable option in most cases. On the other hand, because of its more physical nature, the effectiveness-NTU approach might be better suited for further developments such as adding thermal capacitance nodes. Furthermore, the choice of the boiler simulation approach depends also on the quantity and quality of available boiler performance data as well as on the aim of the simulation task.

Improvements of the presented model might be possible by addition of a second thermal capacitance node for the combustion chamber and by simplifying the effectiveness-NTU method for condensing boilers. Improvements of efficiency prediction under cycling operation might be achieved by introducing additional start losses and transient calculations for start phase flue gas loss and start phase condensation gains.

For accurate simulation of boiler cycling, data is needed that may currently not be derived from standard test procedures and has to be estimated based on manufacturer's data or additional tests. Cycling operation is very commonly found in small space heating boiler installations and may have a large influence on boiler efficiency, electricity consumption and emissions. Therefore, standard testing procedures for start and stop phase measurements should be developed.

6   Acknowledgements

7   Literature

Baehr, H.D., 2005. *Thermodynamik: Grundlagen und technische Anwendungen*, 12. Auflage, Heidelberg Berlin: Springer. ISBN 3-540-23870-0. (German)

Brunner, T., Bärnthaler, G. & Obernberger, I., 2008. Evaluation of Parameters Determining PM Emissions and Their Chemical Composition in Modern

Residential Biomass Heating Appliances. In: *Proc. of the Int. Conf. World Bioenergy*. Jönköping, Sweden, 59-64.

Drück, H., 2006. *Multiport store model for TRNSYS - Type 340 - V1.99F*.

EN 12977-3:2006-11-01; Entwurf ÖNORM; *Thermische Solaranlagen und ihre Bestandteile - Kundenspezifisch gefertigte Anlagen Teil 3: Leistungsprüfung von Warmwasserspeichern für Solaranlagen*. (German)

EN 303-5:1999; *Heating boilers. Heating boilers with forced draught burners. Heating boilers for solid fuels, hand and automatically fired, nominal heat output of up to 300 kW. Terminology, requirements, testing and marking*.

Fiedler, F. & Persson, T., 2009. Carbon monoxide emissions of combined pellet and solar heating systems. *Applied Energy*, 86(2), 135-143.

Haller, M.Y., Paavilainen, J., Konersmann, L., Haberl, R., Dröscher, A., Frank, E., Bales, C., Streicher, W., 2009. A Unified Model for the Simulation of Oil, Gas, and Biomass Space Heating Boilers for Energy Estimating Purposes - Part I: Model Development. Submitted for publication to Journal of Building Performance Simulation, Nov. 2009.

Haller, M., Haberl, R., Dröscher, A., Konersmann, L., Frank, E., 2009. Vergleich verschiedener Ansätze zur Simulation von Öl-, Gas- und Pellets-Kesseln. In: *19. Symposium Thermische Solarenergie*. Kloster Banz, Bad Staffelstein, Germany. (German)

Heinz, A., 2007. Application of Thermal Energy Storage with Phase Change Materials in Heating Systems. Thesis (PhD). Institute of Thermal Engineering, Graz University of Technology, Austria.

ISO, 1995. *Guide to the expression of uncertainty in measurement (GUM)*, International Organisation for Standardization, Switzerland, ISBN 92-67-10188-9.

Klein, S.A., 2009. *EES - Engineering Equation Solver*, F-Chart Software, 1992-2009, V8.400.

Nussbaumer, T., Doberer, A., Klippel, N., Bühler, R. & Vock, W., 2008. Influence of Ignition and Operation Type on Particle Emissions from Residential Wood Combustion. In *16th European Biomass Conference and Exhibition*. Valencia, Spain.

SEL, TRANSSOLAR, CSTB, TESS, 2006. *TRNSYS 16 - A TRansient SYstem Simulation program*. Solar Energy Research Laboaratory, University of Wisconsin-Madison.

Wetter, M., 2004. *GenOpt, generic optimization program, user manual*.

ZAMG, 2007. Zentralanstalt für Meteorologie und Geodynamik, personal correspondence (email) with Mr. Alfred Ortner on 2007-07-17 and 2007-08-16.

Appendix I

Table 7: Overview over conditions and results achieved for the cycling (on/off) experiments.

boiler		Pel1	Pel1	Pel1	Pel2	Pel2	Pel2	Pel3	Pel3	Pel4	Pel4	Chp1	Oil1	Oil1	Oil2	Oil2
τ	h	15.3	13.9	14.1	16.6	13.0	14.9	7.8	12.3	4.6	3.6	25.0	5.0	6.0	5.0	8.2
$\bar{\dot{Q}}_{wat,ms}$	kW	0.87	1.00	2.92	3.63	2.67	5.21	13.1	7.5	5.33	5.44	27.9	3.71	2.01	4.63	2.05
N_{starts}	h^{-1}	0.33	0.36	0.5	1.27	1.00	0.33	1.54	1.63	1.08	1.10	0.36	1.00	1.17	1.01	0.86
fr_{ON}	%	31	34	50	57	41	61	--	--	59	58	--	35	34	39	20
$\bar{t}_{wat,in}$	°C	62.3	68.1	46.0	65.7	60.8	50.7	54.7	67.4	62.4	49.7	63.4	39.2	39.6	39.5	38.8
Q^{GHV}_{fuel}	kWh	22.85	23.94	53.74	82.19	49.68	96.3	140.0	140.54	30.50	23.61	1053	19.79	12.79	25.43	18.81
$Q_{wat,ms}$	kWh	13.34	13.84	41.26	60.28	34.62	76.4	104.47	99.25	24.72	19.70	797	18.57	12.07	22.94	16.77
$Q_{wat,sim}$	kWh	13.90	14.61	40.91	62.83	36.36	76.8	--	--	24.61	19.56	--	18.49	12.19	22.65	15.96
$E_{el,ms}$	kWh	1.00	0.98	1.53	0.66	0.49	0.71	0.78	1.12	0.55	0.41	4.23	0.84	0.98	0.33	0.28
$E_{el,sim}$	kWh	0.88	0.86	1.22	0.63	0.42	0.62	--	--	0.61	0.51	--	0.79	1.03	0.40	0.36
$\eta^{GHV}_{B,ms}$	%	58.4	57.8	76.8	73.3	69.7	79.3	74.6	70.6	81.1	83.4	75.7	93.8	94.4	90.2	89.1
$\eta^{GHV}_{B,sim}$	%	60.8	61.0	76.1	76.4	73.2	79.8	--	--	80.7	82.8	--	93.6	95.3	89.1	84.8
$\eta^{GHV}_{B,sim} - \eta^{GHV}_{B,ms}$	% abs.	+2.5	+3.2	-0.7	+3.1	+3.5	+0.5	--	--	-0.4	-0.6	--	-0.4	0.9	-1.1	-4.3
GHV/NHV	%	108.6	108.0	107.9	108.0	108.0	108.0	108.6	108.6	108.4	108.4	108.8	106.9	106.9	106.9	106.9

Part III: List of papers not included in this work

Main-Authored

Paper V

Haller, M.Y., 2008. *Thermal Storage for Combined Solar and Pellet Heating Systems*. In: *CeTT Conference on Thermal Storage*, Prague.

Paper VI

Haller, M. & Konersmann, L., 2008. *Energy Efficiency of Combined Pellets and Solar Heating Systems for Single Family Houses*. In: *World Bioenergy 2008*, Jönköping, 103-107.

Paper VII

Haller, M., Konersmann, L. & Dröscher, A., 2008. *Simulation von Öl-, Gas- und Pellet-Kessel in Kombination mit Solaranlagen*. In: *18. OTTI Symposium Thermische Solarenergie*, Bad Staffelstein, 428 – 433.

Paper VIII

Haller, M., Haberl, R., Dröscher, A., Konersmann, L. & Frank, E., 2009. *Vergleich verschiedener Ansätze zur Simulation von Öl-, Gas- und Pellets-Kesseln*. In: *19. OTTI Symposium Thermische Solarenergie*. Bad Staffelstein.

Paper IX

Haller, M., Konersmann, L., Haberl, R., Dröscher, A. & Frank, E., 2009. *Comparison of different approaches for the simulation of boilers using oil, gas, pellets or wood chips*. In: *Proceedings of the 11th IBPSA Conference on Building Simulation*. Glasgow, 732-739.

Paper X

Haller, M.Y., Streicher, W., Andersen, E. & Furbo, S., 2009. *Comparative Analysis of Thermal Energy Storage Stratification Efficiency - a New Method Combines Advantages of Previous Approaches*. In: *EffStock 2009 - The 11th Intl Conference on Thermal Energy Storage for Efficiency*, Stockholm.

Co-Authored Work

XI

Konersmann, L., Haller, M. & Vogelsanger, P., 2007. *PelletSolar - Leistungsanalyse und Optimierung eines Pellet-Solarkombinierten Systems für Heizung und Warmwasser*. Bundesamt für Energie BFE, Bern.

XII

Konersmann, L., Haller, M. & Frank, E., 2008. *PelletSolar – Leistungsanalyse und Optimierung eines Pellet-Solarkombinierten Systems für Heizung und Warmwasser*. In: *18. OTTI Symposium Thermische Solarenergie*, Bad Staffelstein, 298-303.

XIII

Dröscher, A., Ohnewein, P., Haller, M. & Heimrath, R., *Modular Specification of large-scale solar thermal systems for the implementation of an intelligent monitoring system*. In: *Proc. of the Solar World Congress 2009*, Johannesburg, 682-688.

XIV

Heimrath, R. & Haller, M., 2007. *Project Report A2 of Subtask A: The Reference Heating System, the Template Solar System - A Report of IEA SHC Task 32: Advanced Storage Concepts for Solar and Low Energy Buildings*.

"Nobody made a greater mistake than he who did nothing
because he could do only a little."

Edmund Burke